

Functional Nanocoatings Inspired by Natural Polyphenols

Zur Erlangung des akademischen Grades eines
DOKTORS DER NATURWISSENSCHAFTEN
(Dr. rer. nat.)

von der KIT-Fakultät für Chemie und Biowissenschaften
des Karlsruher Instituts für Technologie (KIT)

genehmigte

DISSERTATION

von

Farid Behboodi Sadabad

1. Referent: Priv.-Doz. Dr. Pavel Levkin
 2. Referent: Prof. Dr. Stefan Bräse
- Tag der mündlichen Prüfung: 10 Dezember 2018

Abstract

Development of simple and versatile surface modification strategies is of high importance in science and technology to design functional surfaces with tailored properties such as wettability, adhesion, and bioactivity. Many efforts have been devoted to expand the existing surface modification toolbox including self-assembled monolayer (SAM), functionalized silanes, Langmuir-Blodgett deposition, and layer-by-layer assembly. Another widely used tool that provides spatial and temporal control over the surface modification process are photo-based techniques. Recently, inspired by strong adhesion of natural polyphenols existing in mussel foot proteins (mfp) and the binding ability of plant phenolic compounds to a variety of substrates, substrate-independent coating precursors have been evolved. The main focus of this doctoral thesis is to introduce strategies for photo-induced polymerization, deposition, and patterning of plant polyphenols and to use macrocyclic synthetic polyphenols, known as resorcinarenes, to functionalize the surface of a variety of substrates.

In **Chapter 1**, an introduction is given to describe the recent progress in the field of mussel-inspired substrate-independent nanocoatings. Preparation and adhesion properties of mussel-inspired nanocoatings and the use of low-cost plant phenolic compounds and the building blocks derived from them as precursors for multifunctional universal coatings are realized.

In **Chapter 2**, UV-induced oxidation and polymerization of plant phenolic compounds including tannic acid (TA), caffeic acid (CA), gallic acid (GA), and pyrogallol (PG) at acidic, neutral, and basic pH are described. By decreasing the pH of the polyphenols solution toward acidic condition, autoxidation of polyphenols could be inhibited in the dark environment, while UV irradiating the same solution could trigger polymerization, deposition, and patterning of the plant polyphenols.

In **Chapter 3**, a bio-inspired strategy is described that enabled to retard and inhibit the autoxidation process of a small library of nine polyphenols in basic condition (at pH 8.0). Kinetics of oxidation of phenolic compounds was slowed down by using three natural antioxidants including sodium ascorbate (SA), glutathione (GSH), and uric acid (UA). UV irradiation of polyphenol solutions containing antioxidants, however, could trigger oxidation and polymerization of polyphenols which was used to make micropatterns of different plant

polyphenols on the surface. This strategy enabled to control the oxidation and polymerization process in the presence of antioxidants to form a more uniform polyphenolic nanocoating on the surface.

In **Chapter 4**, modification of the surface of a variety of substrates by simple dip coating into the dilute solution of macrocyclic polyphenols, known as resorcin[4]arenes, is described. On one hand, eight hydroxyl groups on the large rim of these bifunctional resorcin[4]arenes could contribute to the adhesion of these compounds to the substrate serving as multiple anchoring points. On the other hand, the small rim can be decorated with different appending groups to introduce the desired chemical and physical functionalities to the substrate's surface. A resorcin[4]arene possessing four alkenyl appending groups on its small rim (*C*-dec-9-enylresorcin[4]arene) was synthesized and used to modify the surface via a one-step dip coating procedure. Hydrophobic and hydrophilic functional groups were introduced onto the resorcinarene-modified surface via thiol-ene photoclick chemistry.

In **Chapter 5**, different strategies used to control the polymerization and deposition of plant polyphenols are discussed briefly. Using these strategies, a spatiotemporal control over the deposition of phenolic compounds was achieved, that enabled to form more uniform nanocoatings on the surface. A brief summary of resorcinarene-based surface functionalization and an outlook are presented at the end.

Zusammenfassung

Die Entwicklung einfacher und vielseitiger Oberflächenmodifizierungsstrategien ist von großer Relevanz in Wissenschaft und Technologie, um funktionelle Oberflächen mit maßgeschneiderten Eigenschaften, wie Adhäsion, Benetzbarkeit oder Bioaktivität zu konzipieren. Große Bemühungen wurden der Expansion der existierenden Oberflächenmodifizierungstoolbox zur Darstellung funktioneller Oberflächen gewidmet, welche u. a. self-assembled monolayer (SAM), funktionalisierte Silane, Langmuir-Blodgett Abscheidung, und layer-by-layer Abscheidung beinhaltet. Ein weiteres Werkzeug, welches räumliche und zeitliche Kontrolle über den Oberflächenmodifizierungsprozess erlaubt, sind photo-basierte Techniken. Kürzlich wurden, inspiriert von der auf einer Vielzahl von Substraten starken Adhäsion natürlicher in Foot Proteinen von Muscheln (mfp) vorkommender Polyphenole und adhäsiver, pflanzlicher Phenolverbindungen, substratunabhängige Beschichtungsvorläufer entwickelt. Das Hauptaugenmerk dieser Promotionsarbeit ist die Einführung von Strategien zur photo-induzierten Polymerisation, Abscheidung und Oberflächenstrukturierung pflanzlicher Polyphenole. Zudem werden als Resorcinarene bekannte makrocyclische, synthetische Polyphenole genutzt, um die Oberflächen einiger Substrate zu funktionalisieren.

In **Kapitel 1** beschreibt eine Einleitung den aktuellen Fortschritt im Feld Muschel-inspirierter, substratunabhängiger Nanobeschichtungen. Im Anschluss werden die Darstellung und Adhäsionseigenschaften Muschel-inspirierter Nanobeschichtungen und der Einsatz günstiger, pflanzlicher Polyphenole und derer Bausteine als Vorläufer für die Herstellung multifunktionaler, universeller Beschichtungen geschildert.

In **Kapitel 2** wird die UV-induzierte Oxidation und Polymerisierung von pflanzlichen Phenolen wie Tanninsäure (TA), Kaffeesäure (CA), Gallussäure (GA) und Pyrogallol (PG) in saurem, neutralen und basischen Milieu beschrieben. Durch Erniedrigung des pH-Wertes der Polyphenollösung bis hin zu sauren Bedingungen konnte die Autooxidation der Polyphenole unter Lichtausschluss verhindert werden, während aus derselben Lösung durch Bestrahlung mit UV Licht die Polymerisation, Abscheidung und Oberflächenstrukturierung induziert werden konnte.

In **Kapitel 3** wird eine von der Natur inspirierte Strategie beschrieben, welche die Autooxidation einer kleinen Bibliothek von neun Polyphenolen unter basischen Bedingungen (pH 8.0) verzögert und behindert. Durch Nutzung der drei natürlichen Antioxidantien Natriumascorbat (SA), Glutathion (GSH) und Harnsäure (UA) wurde die Oxidation der Phenolverbindungen verlangsamt. Die Bestrahlung der Lösung von Polyphenolen und Antioxidantien mit UV-Licht konnte die Oxidation und Polymerisierung initiieren, was genutzt wurde um Muster im Mikromaßstab von verschiedenen pflanzlichen Polyphenolen auf einer Oberfläche zu erzeugen. Es war möglich die Oxidation und Polymerisation in Anwesenheit von Antioxidantien zu kontrollieren, was einheitlichere Polyphenol Nanobeschichtungen auf der Oberfläche ermöglichte.

In **Kapitel 4** wird die Oberflächenmodifizierung einer Vielzahl von Substraten mittels Tauchbeschichtung unter Verwendung verdünnter Lösungen von makrocyclischen, als Resorcin[4]arene bekannten Polyphenolen beschrieben. Einerseits tragen acht Hydroxylgruppen dieser bifunktionellen Resorcin[4]aren-Molekülen zur Adhäsion bei, da sie als mehrfache Ankerpunkte zur Oberfläche dienen. Andererseits kann der untere Rand mit unterschiedlichen Seitenketten versehen werden, um erwünschte chemische und physikalische Funktionalitäten an der Substratoberfläche einzuführen. Eine Resorcin[4]aren-Verbindung mit vier Alkenyl-Gruppen am unteren Rand (C-dec-9-enylresorcin[4]arene) wurde synthetisiert und in nur einem Schritt zur Oberflächenmodifikation mittels Tauchbeschichtung verwendet. Thiol-En Photoclick-Chemie wurde verwendet, um die mit Resorcin[4]aren modifizierte Oberfläche mit hydrophilen und hydrophoben Gruppen zu funktionalisieren.

In **Kapitel 5** werden verschiedene zur Kontrolle der Polymerisation und Abscheidung von pflanzlichen Polyphenole genutzten Strategien diskutiert. Durch Nutzung dieser Strategien wurde eine räumliche und zeitliche Kontrolle der Abscheidung erzielt, was die Bildung einheitlicherer Nanobeschichtungen auf der Oberfläche ermöglichte. Eine kurze Zusammenfassung Resorcinarene basierter Oberflächenfunktionalisierung wird vorgestellt und ein Ausblick gegeben.

This dissertation is dedicated to my brilliant and outrageously loving and supportive wife, Leila, for her kindness and devotion, and selflessness. And to our exuberant, sweet, and kind-hearted little boy, Adrian, and to my always encouraging, and ever faithful parents.

Acknowledgment

First of all, I am very thankful to my Ph.D. supervisor, Priv.-Doz. Dr. Pavel Levkin, for his consistent attention and full support in the progress of my work and for lots of valuable suggestions and discussions. His guidance and great support were determinant for the accomplishment of the work presented in this thesis.

I would like to thank Prof. Dr. Stefan Bräse (IOC, KIT) and Prof. Dr. Cornelia Lee-Thedieck (IFG, KIT) for being my TAC members and for their valuable scientific suggestions.

I am grateful to Prof. Dr. Philip B. Messersmith for giving me the opportunity to visit his research group at the University of California, Berkeley where I conducted part of my Ph.D. project.

I thank Vanessa Trouillet, and Dr. Alexander Welle for the measurements of X-ray photoelectron spectroscopy (XPS, IAM, KIT) and Time-of-Flight Secondary Ion Mass Spectrometry (ToF-SIMS, IFG, KIT) and helpful discussions at Karlsruhe Institute of Technology (KIT). I thank Prof. Dr. Nicolas Plumeré and his Ph.D. student Huijie Zhang at the Center for Electrochemical Sciences, Ruhr-Universität Bochum for their effort and helpful discussion on the characterization of my samples using electrochemistry techniques. Special thanks to all my colleagues, from whom I learned a lot and got a lot of help. It was great to work with these lovely people. Thanks for the nice working atmosphere.

I want to thank Helmholtz Association's Initiative and Networking Fund (grant VH-NG-621) and the European Research Council starting grant (ERC-2013-StG337077-DropCellArray) for supporting my Ph.D. research and Karlsruhe House of Young Scientist (KHYS) for providing me with the Research Travel Grant (2017) and Networking Grant (2018). The research stay abroad was funded by the Karlsruhe House of Young Scientists (KHYS).

I am especially grateful to my wife and my parents, for their consistent encouragement and support in my academic career.

Publications arising from Ph.D. work

Refereed Publications

- (1) **Farid Behboodi-Sadabad**; Vanessa Trouillet; Alexander Welle; Phillip B. Messersmith; Pavel A. Levkin. Surface Functionalization and Patterning by Multifunctional Resorcinarenes. *Accepted manuscript at ACS Applied Materials & Interfaces* **2018**, DOI: 10.1021/acsami.8b14771.
- (2) Xin Du; Min Wang; Alexander Welle; **Farid Behboodi-Sadabad**; Pavel A. Levkin; Zhongze Gu. Reparable Superhydrophobic Surface with Hidden Reactivity, Its Photofunctionalization and Photopatterning. *Advanced Functional Materials* **2018**, DOI: 10.1002/adfm.201803765.
- (3) **Farid Behboodi-Sadabad**; Huiji Zhang; Vanessa Trouillet; Alexander Welle; Nicolas Plumeré; Pavel A. Levkin. Bioinspired Strategy for Controlled Polymerization and Photopatterning of Plant Polyphenols. *Chemistry of Materials* **2018**, 30, 1937-1946.
- (4) **Farid Behboodi-Sadabad**; Wenxi Lei; Caroline Sobek; Phillip B. Messersmith; Pavel A. Levkin. High Throughput Screening (HTS) of Nature-inspired Polyphenolic Nanocoatings with Tailorable Bioinert and Bio-specific Functions. *Manuscript under preparation*.
- (5) **Farid Behboodi-Sadabad**; Huiji Zhang; Vanessa Trouillet; Alexander Welle; Nicolas Plumeré; Pavel A. Levkin. UV-Triggered Polymerization, Deposition, and Patterning of Plant Phenolic Compounds. *Advanced Functional Materials* **2017**, 27, DOI: 10.1002/adfm.201700127.
- (6) Xin Du; Linxian Li; **Farid Behboodi-Sadabad**; Alexander Welle; Junsheng Li; Stefan Heissler; Huijie Zhang; Nicolas Plumeré; Pavel A. Levkin. Bio-Inspired Strategy for Controlled Dopamine Polymerization in Basic Solutions. *Polymer Chemistry*. **2017**, 8, 2145–2151.

Oral Presentation (with the title of the presented work)

- (1) **Farid Behboodi Sadabad**. From Mussel-Inspired Adhesives to Plant-Derived Phenolic Nanocoatings and Beyond. *BIF-IGS Annual Retreat*, Jun. **2018**, Rothenburg ob der Tauber, Germany.
- (2) **Farid Behboodi-Sadabad**; Pavel A. Levkin. UV-triggered Polymerization and Deposition of Plant Polyphenols. *252nd ACS National Meeting & Exposition*, Aug. **2016**, Philadelphia, Pennsylvania, USA.

Poster Presentations (with the title of the presented work)

- (1) **Farid Behboodi-Sadabad**; Vanessa Trouillet; Alexander Welle; Pavel A. Levkin. Antioxidant Controlled Polymerization and Deposition of Plant Phenolic Compounds. *Dimensional Control of Polymer Materials - From Synthesis to Function*, Sep. **2018**, Karlsruhe, Germany.
- (2) **Farid Behboodi-Sadabad**; Vanessa Trouillet; Alexander Welle; Pavel A. Levkin. Levkin. Controlled UV-induced Deposition and Patterning of Natural Polyphenols. *Biointerfaces International*, Aug. **2018**, Zurich, Switzerland.
- (3) **Farid Behboodi-Sadabad**; Huiji Zhang; Vanessa Trouillet; Alexander Welle; Nicolas Plumeré; Pavel A. Levkin. Multifunctional Plant-derived Polyphenolic Coatings with Tunable Wettability. *2017 MRS Fall Meeting and Exhibit*, Nov. **2017**, Boston, MA, USA.
- (4) **Farid Behboodi-Sadabad**; Huiji Zhang; Vanessa Trouillet; Alexander Welle; Nicolas Plumeré; Pavel A. Levkin. Multifunctional Nanocoatings from plant phenolic compounds, *BIF-IGS Annual Retreat*, Jun. **2017**, Frankfurt am Main, Germany.
- (5) **Farid Behboodi-Sadabad**; Pavel A. Levkin. Photo-patterned Nanocoatings from Plant Polyphenols. *The 644. WE-Heraeus-Seminar "Bio-inspired, Nano- and Microstructured Surfaces: New Functionality by Material and Structure"*, May **2017**, Bad Honnef, Germany.
- (6) **Farid Behboodi-Sadabad**; Huiji Zhang; Vanessa Trouillet; Alexander Welle; Nicolas Plumeré; Pavel A. Levkin. Micropatterning of Multifunctional Plant Phenolic Compounds. *Fifth International Symposium Frontiers in Polymer Science*, May **2017**, Seville, Spain.
- (7) **Farid Behboodi-Sadabad**; Huiji Zhang; Vanessa Trouillet; Alexander Welle; Nicolas Plumeré; Pavel A. Levkin. UV-triggered Polymerization, Deposition, and Patterning of Plant Phenolic Compounds. *5th International Conference on Multifunctional, Hybrid and Nanomaterials*, Mar. **2017**, Lisbon, Portugal.

Other publications

- (1) **Effect of Loading and Surface Modification of Nanoparticles on the Properties of PMMA/Silica Nanocomposites Prepared via In-Situ Free Radical Polymerization.** Salami-Kalajahi, M.; Haddadi-Asl, V.; Rahimi-Razin, S.; Behboodi-Sadabad, F.; Roghani-Mamaqani, H.; Najafi, M. *International Journal of Polymeric Materials and Polymeric Biomaterials* **2013**, 62, 336-344.
- (2) **A study on the properties of PMMA/silica nanocomposites prepared via RAFT polymerization.** Salami-Kalajahi, M.; Haddadi-Asl, V.; Rahimi-Razin, S.; Behboodi-Sadabad, F.; Najafi, M.; Roghani-Mamaqani, H. *Journal of Polymer Research* **2012**, 19, DOI 10.1007/s10965-011-9793-1.
- (3) **Effect of Carbon Nanotubes on the Kinetics of in Situ Polymerization of Methyl Methacrylate.** Salami-Kalajahi, M.; Haddadi-Asl, V.; Behboodi-Sadabad, F.; Rahimi-Razin, S.; Roghani-Mamaqani, H.; Hemmati, M. *Nano* **2012**, 7, DOI: 10.1142/S1793292012500038.
- (4) **Effect of silica nanoparticle loading and surface modification on the kinetics of RAFT polymerization.** Salami-Kalajahi, M.; Haddadi-Asl, V.; Behboodi-Sadabad, F.; Rahimi-Razin, S.; Roghani-Mamaqani, H. *Journal of Polymer Engineering* **2012**, 32, 13-22.
- (5) **Properties of PMMA/Carbon nanotubes nanocomposites prepared by "grafting through" method.** Salami- Kalajahi, M.; Haddadi-Asl, V.; Behboodi-Sadabad, F.; Rahimi-Razin, S.; Roghani-Mamaqani, H. *Polymer Composites* **2012**, 33, 215-224.
- (6) **Matrix-grafted multiwalled carbon nanotubes/poly(methyl methacrylate) nanocomposites synthesized by in situ RAFT polymerization: A kinetic study.** Rahimi-Razin, S.; Haddadi-Asl, V.; Salami-Kalajahi, M.; Behboodi-Sadabad, F.; Roghani-Mamaqani, H. *International Journal of Chemical Kinetics* **2012**, 44, 555-569.
- (7) **Properties of matrix-grafted multi-walled carbon nanotube/poly(methyl methacrylate) nanocomposites synthesized by in situ reversible addition-fragmentation chain transfer polymerization.** Rahimi-Razin, S.; Haddadi-Asl, V.; Salami-Kalajahi, M.; Behboodi-Sadabad, F.; Roghani-Mamaqani, H. *Journal of the Iranian Chemical Society* **2012**, 9, 877-887.
- (8) **Investigating the effect of pristine and modified silica nanoparticles on the kinetics of methyl methacrylate polymerization.** Salami-Kalajahi, M.; Haddadi-Asl, V.; Rahimi-Razin, S.; Behboodi-Sadabad, F.; Roghani-Mamaqani, H.; Hemmati, M. *Chemical Engineering Journal* **2011**, 174, 368-37

Abbreviations

Symbols and Units

°C	degree Celsius
aq	aqueous
e.g.	exempli grātiā (for example)
eq.	equivalents
et al.	et altera (and others)
g	gram
h	hour
Hz	hertz
L	liter
M	molar
min	minutes
N	newton
nm	nanometer
rt	room temperature
s	second
V	volt
W	watt
μm	micrometer

Solvents and Chemicals

•OH	highly reactive hydroxyl radicals
¹ O ₂	singlet oxygen
ACN	acetonitrile
Ag	silver
AgNO ₃	silver nitrate
CDCl ₃	chloroform, deuterated
DI water	de-ionized water
DMPAP	2,2-dimethoxy-2-phenylacetophenone
DMSO	dimethylsulfoxide
EDMA	ethylene dimethacrylate
GSH	glutathione
HCl	hydrochloric acid
HEMA	2-hydroxyethyl methacrylate
KCl	Potassium chloride
ME	2-mercaptoethanol
O ^{2•-}	superoxide radicals

PEG	poly(ethylene glycol)
PFDT	1 <i>H</i> ,1 <i>H</i> ,2 <i>H</i> ,2 <i>H</i> -perfluorodecanethio
Ph	phenyl
ROS	reactive oxygen species
SA	sodium ascorbate
TEA	triethylamine
UA	uric acid

Polyphenols

CA	caffeic acid
catechol	1,2-dihydroxybenzene
CBE	crude extracts of cacao bean
Ctl	catechol
Ctn	catechin
DA	dopamine
DHI	5,6-dihydroxyindole
DOPA	3,4-dihydroxy-L-phenylalanine
ECG	epicatechin gallate
EGC	epigallocatechin
EGCG	epigallocatechin gallate
GA	gallic acid
GTE	green tea extract
HHQ	hydroxyhydroquinone
MAP	mussel adhesive protein
mfp	mussel foot proteins
PDA	polydopamine
PG	pyrogallol
pyrogallol	1,2,3-trihydroxybenzene
RWE	crude extracts of red wine
TA	tannic acid

Substrates

Al	aluminum
Au	gold
GC	glassy carbon
PDMS	poly(dimethylsiloxane)
PE	polyethylene
PMMA	polymethyl methacrylate;
poly(HEMA)	amine-functionalized porous poly(2-hydroxyethyl methacrylate)-co-(ethylene dimethacrylate).

poly(HEMA-EDMA)	poly(2-hydroxyethyl methacrylate)- <i>co</i> -(ethylene dimethacrylate)
PTFE	poly(tetrafluoroethylene)
pyrolyzed photoresist film	PPF
steel	stainless steel;
TiO ₂	titanium dioxide
Zn	zinc

Instruments and techniques

¹ H NMR	Proton nuclear magnetic resonance
AFM	atomic force microscopy
C/O	carbon-to-oxygen ratio
CA (θ)	contact angle
CAH (Δθ)	contact angle hysteresis
CV	cyclic voltammetry
CVD	chemical vapor deposition
DPV	Differential pulse voltammetry
ESI	electrospray Ionization
IR	infrared
LB	Langmuir-Blodgett
LbL	layer-by-layer
MS	mass spectrometer
NMR	nuclear magnetic resonance
PCA	principal component analysis
RMS	mean square roughness
R _q	roughness
SAM	self-assembled monolayer
SEM	scanning electron microscope
ToF-SIMS	time-of-flight secondary ion mass spectrometry
UV	ultraviolet
UV-Vis	ultraviolet-visible
WCA	water contact angle
XPS	X-ray photoelectron spectroscopy

Table of Contents

Abstract	I
Zusammenfassung	III
Acknowledgment	VI
Publications arising from Ph.D. work.....	VII
Other publications.....	IX
Abbreviations.....	XI
1 Chapter 1. Introduction.....	1
1.1 Universal coatings	2
1.2 Mussel-inspired coatings	3
1.2.1 Polydopamine (PDA) formation and deposition.....	4
1.2.2 Mechanism of adhesion of polyphenols to the surface	6
1.2.3 Applications of mussel-inspired materials	9
1.3 Plant polyphenol-inspired coatings	9
1.3.1 Sources and biological function of plant polyphenols	10
1.3.2 Oxidation chemistry of polyphenols	10
1.3.1 Coatings derived from plant polyphenols	11
1.3.2 Post-functionalization of polyphenolic nanocoatings	15
1.4 Surface functionalization via macrocyclic polyphenols.....	16
1.4.1 Calixarenes for surface modification	17
1.4.2 Resorcinarenes for surface modification.....	18
1.4.3 Synthesis of resorcin[4]arenes	20
2 Chapter 2. UV-Triggered Polymerization, Deposition, and Patterning of Plant Phenolic Compounds	23
2.1 Introduction	24

2.2	Results and discussions	25
2.2.1	UV-triggered polymerization of plant polyphenols	30
2.2.2	Electrochemical oxidation of plant phenolic compounds	32
2.2.3	Nanocoatings from plant polyphenols.....	36
2.2.4	Spatiotemporal control of the polymerization and deposition	39
2.2.5	Coatings from polyphenols present in wine, coffee, and tea	42
2.3	Conclusions to chapter 2	43
3	Chapter 3. Bioinspired Strategy for Controlled Polymerization and Photopatterning of Plant Polyphenols	45
3.1	Introduction	46
3.2	Results and discussion	49
3.2.1	Antioxidant-controlled oxidation of plant phenolic compounds	53
3.2.1	Effect of sodium ascorbate and UV light on oxidation of polyphenols	54
3.2.2	On-demand polymerization and deposition of polyphenols	55
3.2.3	Multiple patterns of polyphenols.....	61
3.2.4	Patterning inside microfluidic channels and gradients.....	65
3.3	Conclusions to chapter 3	67
4	Chapter 4. Surface Functionalization and Patterning by Multifunctional Resorcinarenes	68
4.1	Introduction	69
4.2	Results and discussion	72
4.2.1	Coating formation ability of resorcinarenes on different substrates	73
4.2.2	Stability of the resorcinarene layer on the surface	74
4.2.3	Characterization of the surfaces modified with resorcinarenes	77
4.2.4	Post-functionalization of resorcinarene-modified surface	79
4.2.5	Photopatterning of the resorcinarene-modified surface	82

4.2.6	Dynamic wettability behavior of the post-functionalized surfaces	84
4.3	Conclusions to chapter 4	85
5	Chapter 5. Summary and Outlook	87
5.1	Summary of the thesis	88
5.2	Outlook.....	90
6	Chapter 6. Experimental	92
6.1	Experimental details for chapter 2.....	93
6.1.1	Materials.....	93
6.1.1	Characterization	93
6.1.2	UV-irradiation of phenolics solutions.....	94
6.1.3	UV-Vis absorption experiments.....	95
6.1.4	Deoxygenated solutions	95
6.1.5	Samples containing DMSO.....	95
6.1.6	UV-Vis measurement in DI water and deuterium oxide medium.....	95
6.1.7	Electrochemistry.....	96
6.1.8	Deposition of a phenolic layer on the substrate	96
6.1.9	Photopatterning of polyphenols	96
6.1.10	Gradient pattern.....	97
6.1.11	Patterning inside a capillary.....	97
6.1.12	Deposition of polyphenols present in tea, coffee, and wine	98
6.2	Experimental details for chapter 3.....	98
6.2.1	Materials.....	98
6.2.1	Characterization	99
6.2.2	UV Irradiation of phenolic solutions.....	100
6.2.3	UV-vis absorption experiments.....	100

6.2.4	Electrochemistry.....	101
6.2.5	Deposition of polyphenolic layer on the silicon surface	101
6.2.6	Photopatterning of phenolics.....	102
6.2.7	Sequential patterning of polyphenols	102
6.2.8	Gradient pattern.....	103
6.2.9	Patterning inside a capillary	104
6.3	Experimental details for chapter 4.....	105
6.3.1	Materials.....	105
6.3.2	Characterization	105
6.3.3	Synthesis of C-dec-9-enylresorcin[4]arene.....	107
6.3.4	Deposition of the resorcinarene layer on the surface	107
6.3.5	Preparation of amine-functionalized surfaces	107
6.3.6	Post-functionalization of C-dec-9-enylresorcin[4]arene.....	108
6.3.7	Photopatterning on the 3-modified surface	108
7	References.....	109
8	Appendix A: Supplementary information for Chapter 2	124
9	Appendix B: Supplementary information for Chapter 3	140
10	Appendix C: Supplementary information for Chapter 4	153
11	Curriculum Vitae	156

Chapter 1. Introduction

1.1 Universal coatings

Chemical modification of bulk material surfaces plays a central role in modern science and technology. In order to introduce functionalities onto the material surfaces, a toolbox of different methods including layer-by-layer assembly, self-assembled monolayer (SAM) formation, functionalization via silanes, Langmuir-Blodgett deposition, and binding peptides have been used. However, there are still limitations in the widespread practical use of the surface functionalization techniques. Examples include the complex instrumentation required and the limitations of substrate size and shape in Langmuir-Blodgett deposition, the need for multistep procedures in layer-by-layer assembly and surface-binding peptides, and the need for chemical specificity between the precursor and surfaces in the case of alkanethiols on noble metals and silanes on oxides.¹ Lack of spatial and temporal control over the deposition, poor control of layers thickness and regularity and long-term stability are other key limitations of many surface modification techniques. The spatial control of covalently bound functions is also particularly difficult to achieve.²

Universal coatings are a complimentary class of surface functionalization techniques that can be used to modify a wide range of material surfaces with different size and shape, typically without a need for multistep procedures or complex instrumentation. Ideally, such techniques can be used to form substrate-independent coatings on a variety of substrates regardless of the chemical and physical characteristics of the surface.³ To develop universal coatings, several strategies have been used including layer-by-layer (LbL) assembly, laser deposition, surface irradiation, chemical vapor deposition (CVD), the use of blood proteins, spraying fumed silica, spin coating, and electrografting of aryldiazonium salts.³

Alternative substrate-independent coatings that have gained tremendous interest over the last decade are mussel-⁴ and plant polyphenol-inspired^{5,6} nanocoatings. Inspired by the adhesive proteins secreted by mussels for attachment to wet surfaces and the strong interfacial characteristics of plant polyphenols, mussel- and plant polyphenols-inspired coating strategies have been used as a versatile, single step tool for surface modification of multiple classes of organic and inorganic materials including adhesion-resistant materials such as poly(tetrafluoroethylene).^{1,6}

Coatings inspired by plant polyphenol maintain numerous of the advantages of mussel-inspired coatings and could deposit on the surface under the same conditions, but can form colorless and less costly coatings in some cases.⁵

Herein, the preparation and physicochemical properties of mussel-inspired coatings and plant phenolic compounds as precursors for the formation of multifunctional nanocoatings are discussed in **chapter 1**. Coatings based on polyphenols can potentially lead to a lot of useful applications. The ability to control polyphenol nanocoatings spatially and temporally would significantly expand the number of potential applications. In **chapter 2** and **chapter 3**, two strategies are presented that enable the control of polymerization and deposition of plant phenolic compounds spatiotemporally. In **chapter 4**, substrate-independent surface functionalization via macrocyclic polyphenols such as resorcinarenes is reported. A conclusion and outlook of these studies are presented in **chapter 5**.

1.2 Mussel-inspired coatings

Investigations on the strong wet adhesion property of invertebrate mussels to solid surfaces revealed that the robust adhesion of mussels to diverse substrates originates from the presence of 3,4-dihydroxy-L-phenylalanine (DOPA) and lysine-enriched proteins near the plaque-substrate interface. In 2007, oxidative polymerization of dopamine (DA), a mimic of DOPA, was used to form a polydopamine (PDA) coating on various types of inorganic and organic substrates.¹ Polydopamine is also a major pigment of naturally occurring melanin (eumelanin). Polydopamine incorporates functional groups such as catechols, amines, and imines in its chemical structure that can serve as starting points for post-modification with desired molecules and the loading of transition metal ions.⁷

PDA-derived coatings have been used as one of the most powerful tools available for modification of surfaces with a broad range of potential applications in the biomedical, energy, consumer, industrial, military, and other sectors.⁴ A schematic summary of polycatecholamine formation, modification, properties, and applications is shown in Figure 1.1.

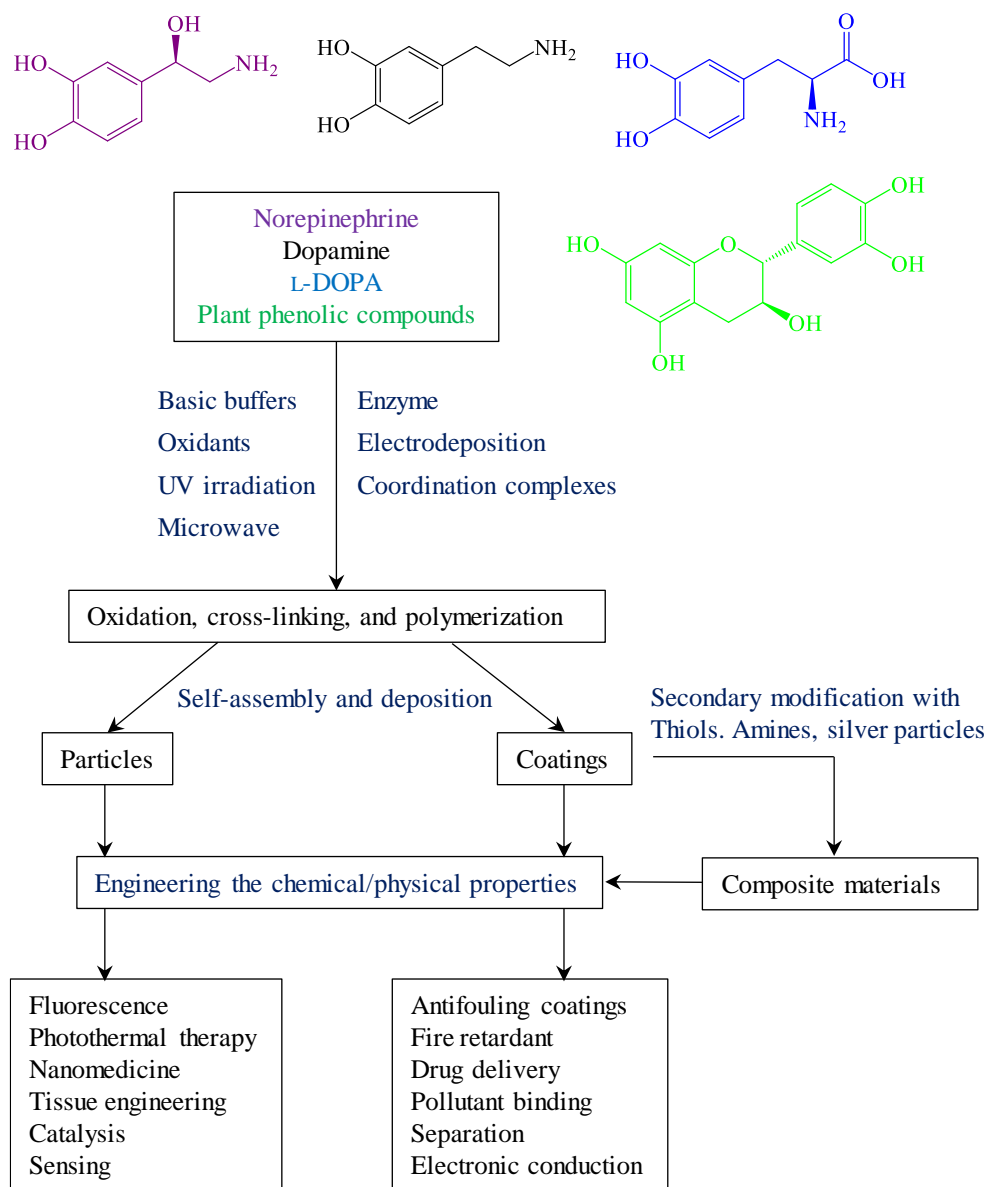


Figure 1.1 Schematic summary of polycatecholamine formation, modification, properties, and applications.

1.2.1 Polydopamine (PDA) formation and deposition

The widespread adoption of PDA originates from its simplicity, low cost, and adaptability in a variety of scientific and applied engineering contexts.⁴ The simplest coating method of PDA is the immersion of the substrate into an aqueous alkaline solution of dopamine for an adjustable

period of time.¹ PDA coating deposits on the surface spontaneously and can be used without further modification or as a primer for secondary coating.⁴

Oxidative polymerization of dopamine triggered by dissolved oxygen at the alkaline pH of the solution is the driving force for PDA coating formation. The details of this process remain an active area of investigation and many features of PDA formation and structure remain unknown.⁴ A brief overview of existing theories of PDA formation and structure is shown in Figure 1.2.⁴

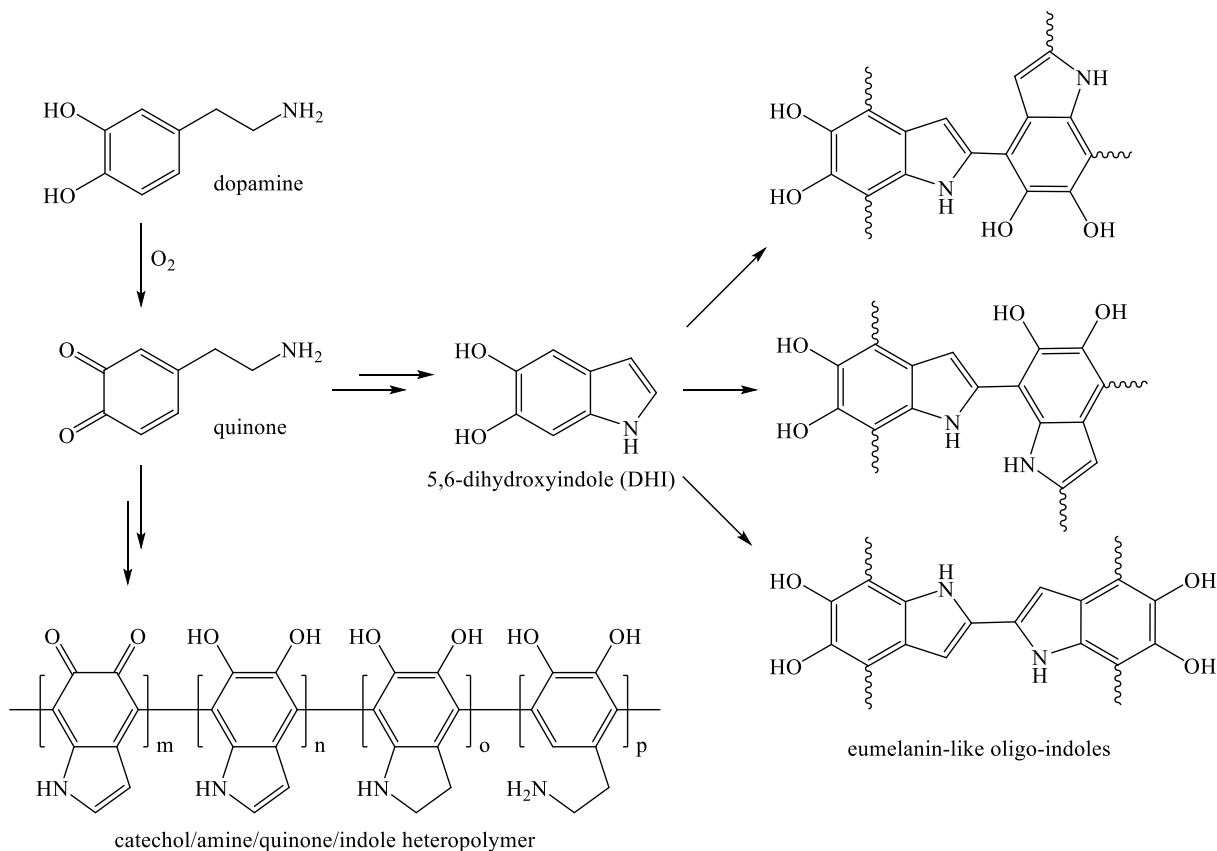


Figure 1.2 Theories of polydopamine structure and formation ranging from noncovalent self-assembly of subunits to form quinhydrone or trimer assemblies to the covalent coupling of subunits to yield a catecholamine/quinone/indole heteropolymer or eumelanin-like oligo-indoles.⁴

The oxidation product of dopamine (dopamine-quinone), undergoes a nucleophilic intramolecular cyclization reaction leading eventually to the formation of 5,6-dihydroxyindole

(DHI).⁴ In some theories PDA is considered noncovalent assemblies of DA and DHI. Other theories hypothesize that DA and DHI polymerize to form a heteropolymer composed of catecholamine, quinone and indole repeat units. Formation of eumelanin-like materials has also been suggested for DA polymerization. However, probably both covalent “polymerization” and “self-assembly” pathways contribute to PDA formation.⁴

Several methods such as UV⁸ and microwave⁹ irradiation as well as using oxidants¹⁰ (such as ammonium peroxodisulfate, sodium periodate, and copper sulfate) have been used to accelerate polymerization and deposition of dopamine (DA) onto the surface of the substrate.

1.2.2 Mechanism of adhesion of polyphenols to the surface

The strong adhesion provided by catechol structure and the “crosslink-network” formed via autoxidation has been widely accepted as the main reasons for PDA attachment on various surfaces.¹¹ Covalent and non-covalent interactions such as hydrogen bonding, π - π stacking and charge transfer interactions play a crucial role in PDA adhesion.¹¹

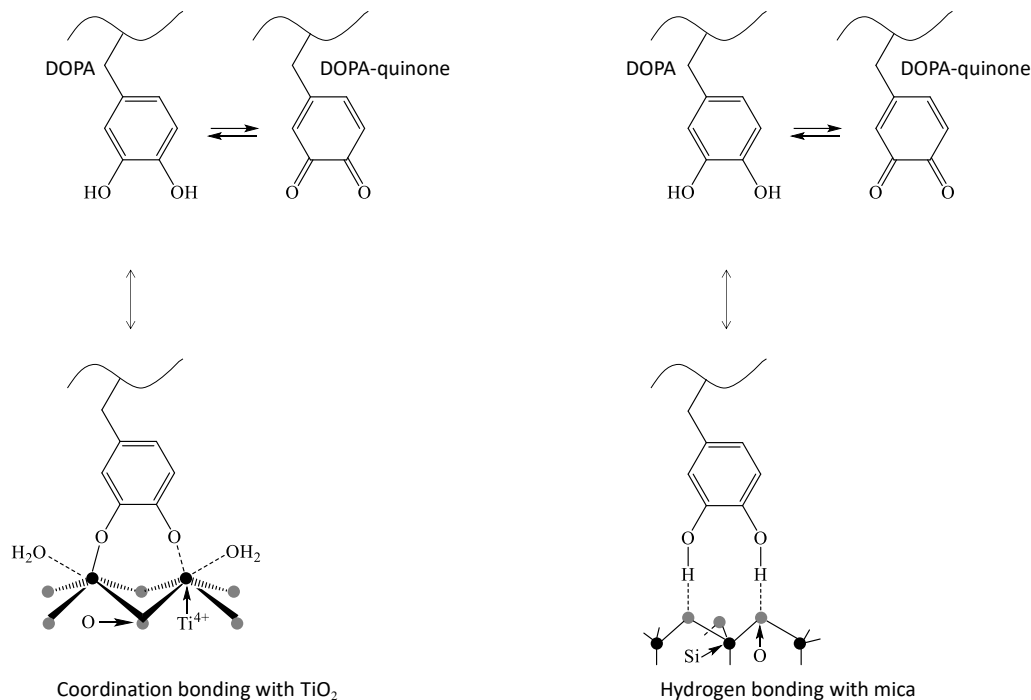


Figure 1.3 Proposed mechanism for the binding of DOPA to TiO₂ and mica surfaces.¹¹

In addition to the previously mentioned possible interactions, other adhesion mechanisms such as changing interactions from hydrogen bonding to coordination with the increase of pH for interaction of the catechol moiety with titanium dioxide (TiO_2) surface, and bidentate hydrogen bonding for interaction of catechol with mica and SiO_2 surfaces have been reported (Figure 1.3).

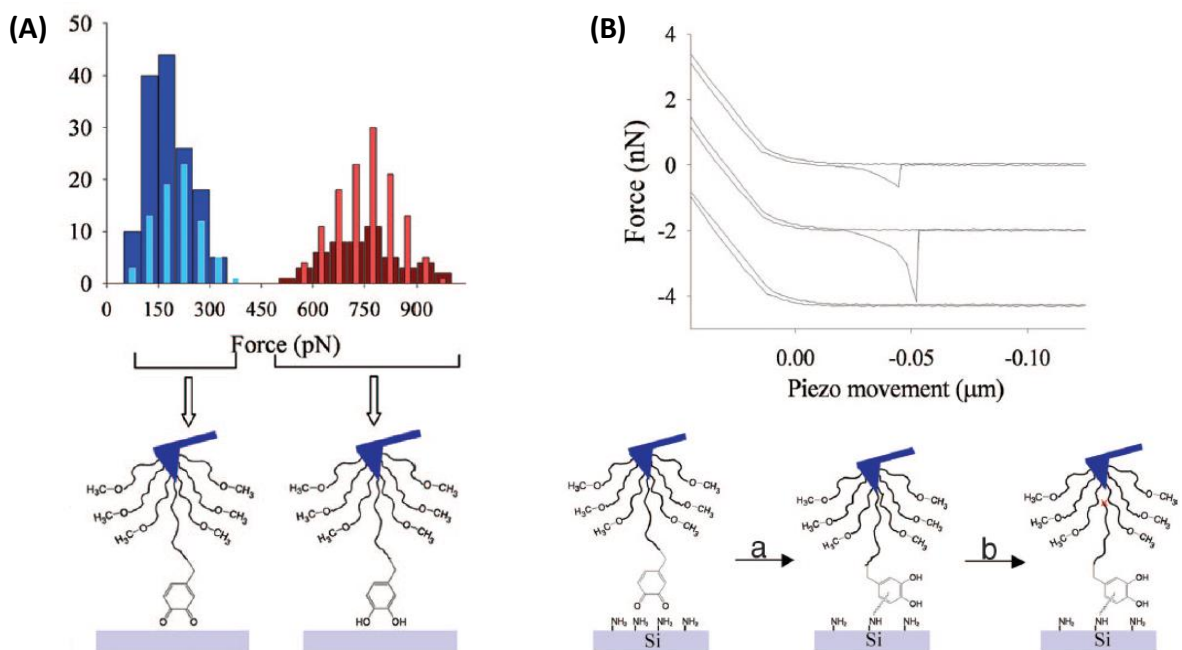


Figure 1.4 Schematic illustration of the interaction of the DOPA (pH 8.3) (A) and DOPA-quinone (pH 9.7) (B) with titanium (Ti) surface and covalent bond formation between DOPA and amines at the organic surface. Modified from Ref.¹² Copyright (2006) National Academy of Sciences.

Messersmith and co-workers¹² reported a reversible coordination when catechol interacts with a titanium (Ti) surface (Figure 1.4A), while an irreversible covalence was reported between catechol and an amino-functionalized surface (Figure 1.4B). Using atomic force microscopy (AFM) measurements, they demonstrated that the oxidation of DOPA, increased adhesion to organic surfaces, while adhesion to Ti surfaces was decreased upon oxidation of DOPA.

Lu et. al.¹³ proposed different possible interactions between the mussel foot proteins (mfp-3 as an example) and different surface types including electrostatic, hydrophobic, cation- π , π - π interactions, hydrogen bonding, and metal complexes (Figure 1.5). Hydrogen bonding between

the phenolic hydroxyl group and hydrogen-bonding acceptors was considered as the primary adhesion, while hydrophobic or π - π interactions played a crucial role in the adhesion of catechol to non-polar polymers such as polyolefins and polystyrene.⁸ However, the mechanism for hydrophobic interaction between catechol and substrates with a low surface energy such as polytetrafluoroethylene and polypropylene remain elusive.¹³

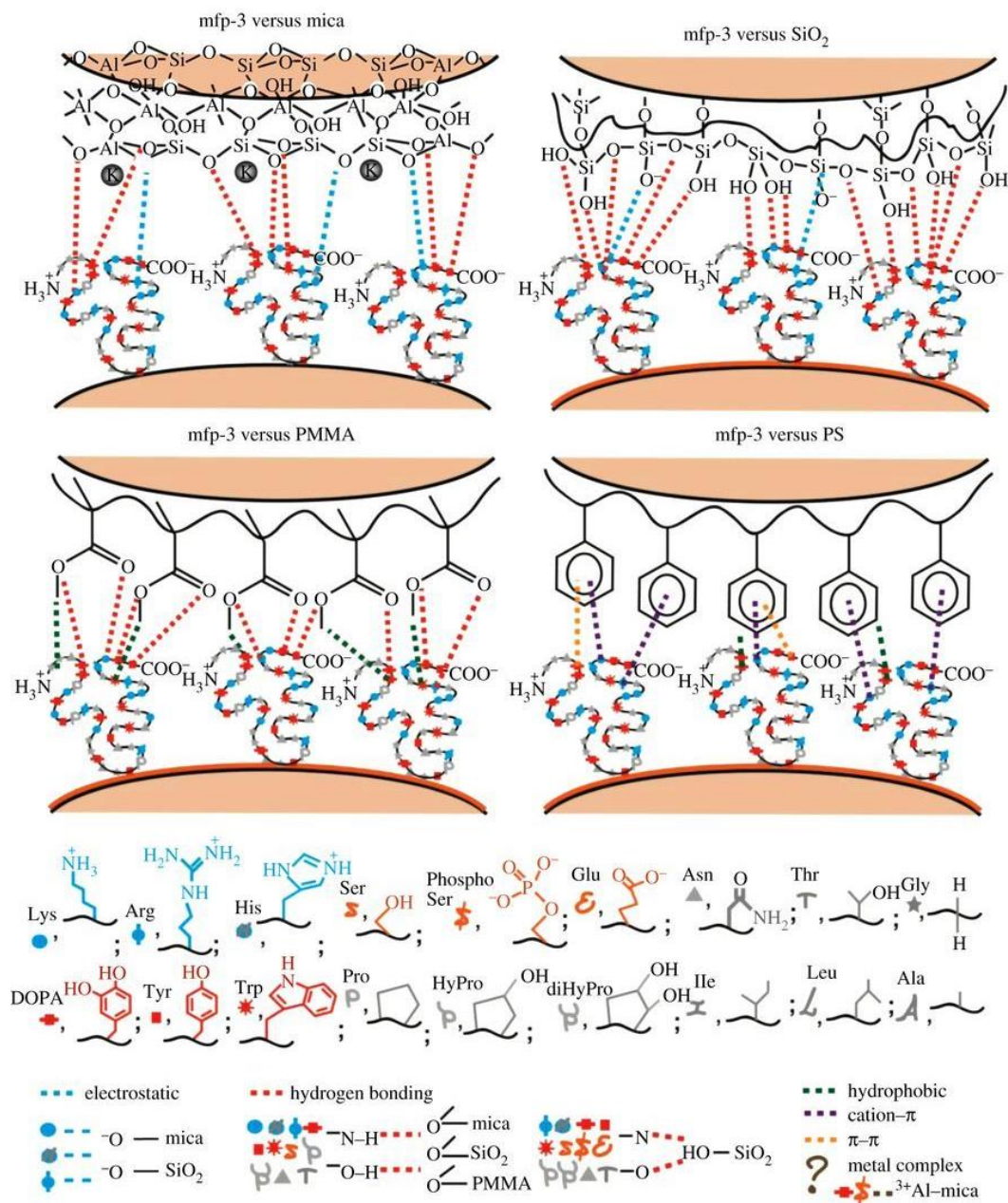


Figure 1.5 A schematic of the likely interactions between the mussel foot proteins (mfp-3 as an example) and different surface types. Adapted from Ref.¹³ © 2012 The Author(s) Published by the Royal Society.

1.2.3 Applications of mussel-inspired materials

Substrate flexibility combined with a variety of ad-layer properties by covalent, coordinate, or noncovalent linkages with other molecules provides polydopamine (PDA) coatings with diverse functional properties. Applications of surface modification with PDA include development of new hydrogels^{14,15} surface coating and chemical functionalization,^{16–18} surfaces with special superwettability,^{10,19} fabrication of nanoparticles,^{20,21} and membrane.¹¹ More applications such as stem and differentiated cell culture, antimicrobial surfaces, scaffold functionalization for tissue engineering, bioimaging, theragnostics, photothermal therapy, nanoparticles and capsules for drug delivery, microfluidics, energy storage devices, immobilization of photocatalysts and photocatalysts, carbonization, oil/water separation, water detoxification, membrane separation technologies, and numerous others that are summarized and reported in review articles.^{4,7,22} It is expected that the scope of PDA research and applications will expand further in the years to come.

1.3 Plant polyphenol-inspired coatings

Plant-derived polyphenols have been used in diverse applications in biology and materials science such as in bio-adhesives, antibacterial coatings, surfaces with reduced biofouling, immobilization of enzymes, drug delivery systems, anticancer drugs, energy storage devices, designing novel antioxidants, self-healing materials, and surface modification of membranes.²³ It has been shown that phenolic compounds, similar to dopamine (DA), can undergo autoxidation and deposition in alkaline pH conditions, in the presence of oxidizing agents or high-redox-potential enzymes.²³ In the following sub-chapter, important bio-physicochemical properties of plant phenolic compounds that make them an attractive class of materials for surface functionalization is described.

1.3.1 Sources and biological function of plant polyphenols

Plant-derived foods such as fruits, vegetables, cereals, chocolate and beverages including tea, coffee, beer, and wine are rich in phenolic compounds and play an important role in the defense system of plants.²⁴ Numerous health benefits of plant phenolics such as antioxidant and anticancer effects and the elimination of the destructive effect of reactive oxygen species in the human body have been demonstrated.²⁴

Plant phenolic compounds are linked to diverse biological functions in plants such as resistance against microbial pathogens, reproduction, structural support, nutrition, antibiotic and antifeeding actions against animal herbivores, pigmentation, and protection against solar radiation (by screening against DNA damaging via UV-B light).^{5,25} Other physical and chemical properties of plant phenolic compounds include radical scavenging, absorption of UV radiation, metal ion complexation, and strong solid-liquid interfacial activity.⁵

1.3.2 Oxidation chemistry of polyphenols

Phenols and phenolate anions are sensitive to oxidation. Phenoxy radicals ($\text{PhO}\bullet$) can be generated by hydrogen abstraction due to the relatively weak bond dissociation energy of the phenolic O-H bond (87-90 kcal/mol).²⁵ Delocalization-stabilized radicals can readily be formed in a one-electron oxidation process of phenolate anions. Such radicals are considered key intermediates in the bio-conversion of simple plant phenolic compounds to more complex phenolic compounds through carbon-carbon and carbon-oxygen radical-coupling events. Some antioxidant properties of plant phenolic compounds rich foods originates from the ability of these compounds to homolytically release a hydrogen atom. Quinones generated from dehydrogenative one-electron oxidation processes of phenolic compounds can behave as electrophilic and/or nucleophilic units (Figure 1.6).²⁵

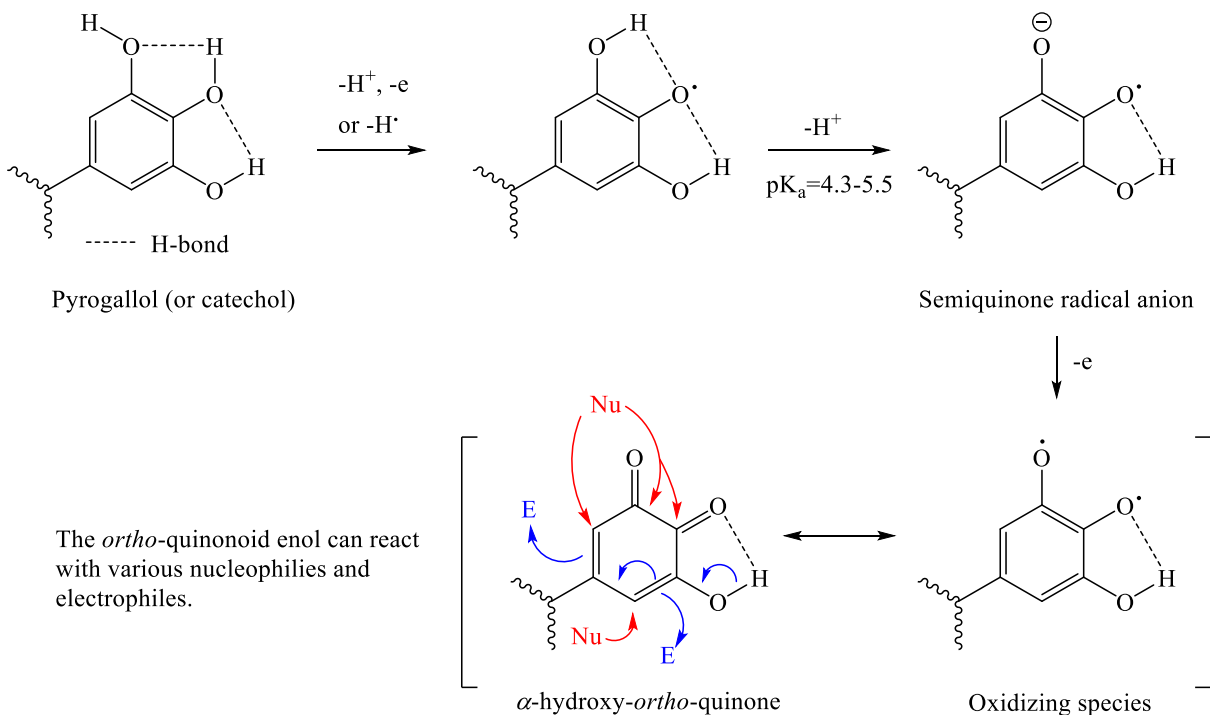


Figure 1.6 Formation of reactive quinonoid species via oxidative dehydrogenation of dihydroxyphenyl (catechol) and trihydroxyphenyl (pyrogallol) moieties of phenols.²⁵

1.3.1 Coatings derived from plant polyphenols

Historically, plant polyphenols have been used in manufacturing of leather (known as vegetable tannins) and as binding agents (lignin).^{5,25} The presence of a high content of dihydroxyphenyl (catechol) and trihydroxyphenyl (pyrogallol) in plant phenolic compounds has been realized to have an important role in their adhesive properties.⁵ One advantage of plant polyphenol-derived coatings is the lower price and transparent precursors compared to coatings derived from dopamine and other catecholamines.⁵ An increased adhesion rate, excellent availability, and good structural diversity are other advantages of plant phenolic compounds.²⁴

Various coating strategies have been developed to modify the surface of a variety of substrates with plant phenolic compounds including deposition induced by a basic solution, oxidizing agents, high-redox potential enzymes, metal-ion complexation, and UV irradiation.²³ All of the mentioned strategies rely on oxidation of catechol or pyrogallol moieties of phenolic compounds into quinones (Figure 1.6).

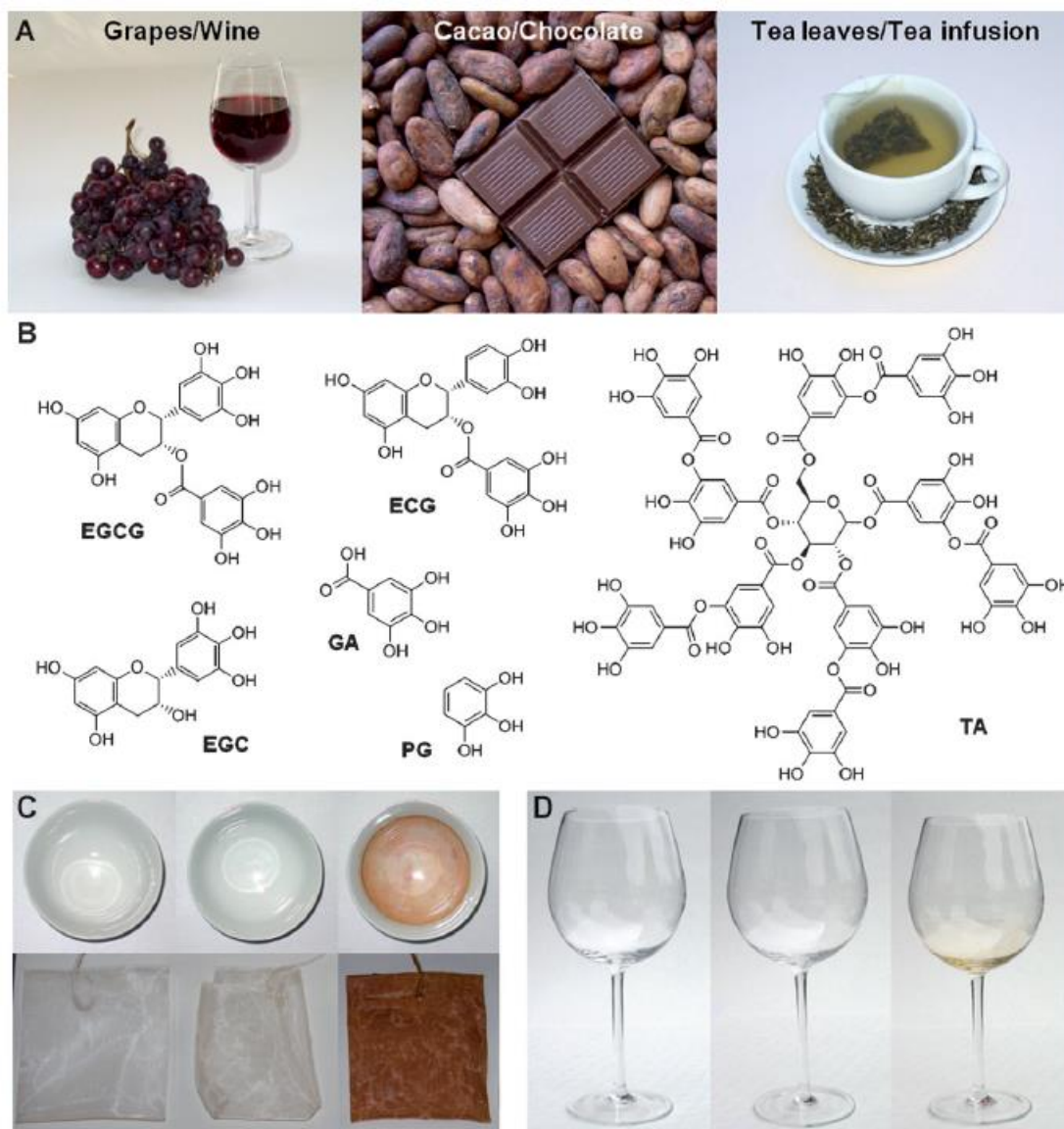


Figure 1.7 Deposition of a thin adherent coating from foods and beverages rich in polyphenols on a surface. (A) Examples of foods and beverages with high polyphenol content (red wine, grapes, chocolate, raw cacao, and green tea leaves). (B) Chemical structures of some plant phenolic compounds, phenolic mimics, and building blocks. (C,D) Deposition of polyphenol coatings on the surfaces that were exposed to tea infusions or red wine. The polyphenols layer was visualized after treatment with an aqueous AgNO_3 solution. Adapted from Ref.⁵

One challenge in the coating formation is the rapid response of plant phenolic compounds and dopamine to oxidation, which limits the control over the kinetics of the oxidation and

deposition process, leading to the formation of weak and inhomogeneous coatings.²³ In order to produce more homogeneous coatings, several strategies have been developed including the use of norepinephrine (a small molecule catecholamine), cyclic catechols, sonication of PDA-coated substrates, and controlling the self-polymerization process of DA by using the $\text{CuSO}_4/\text{H}_2\text{O}_2$ system.²³

Another challenge is to develop a method that enables spatiotemporal control over the deposition of polyphenols. It has been shown that the oxidation kinetics of phenolic polyphenols could be controlled by varying laccase enzyme concentration, the pH of the solution of Fe^{III} ion and polyphenol, and the pH of the coating solution.²³

Sileika et. al.⁵ demonstrated the formation of colorless, multifunctional nanocoatings from phenolic compounds found in foods and beverages and from their building blocks. They demonstrated the spontaneous formation of a thin layer on the surface of a variety of substrates exposed to polyphenol-rich beverages such as tea infusion. Coating formation from crude extracts of red wine (RWE), cacao bean (CBE), and green tea (GTE) was also demonstrated (Figure 1.7).⁵

By immersing various substrates including titanium dioxide (TiO_2), stainless steel and polytetrafluoroethylene (PTFE) in the slightly alkaline solution of pyrogallol (PG), tannic acid (TA) and two phenolic compounds that are known to exist in high concentration in green tea (pure ECG, EGCG), a polyphenolic layer could be formed on the surface. Tannic acid (TA) and pyrogallol (PG) were used to form polyphenol coatings with antibacterial properties against both gram-positive and gram-negative strains of bacteria that at the same time were not toxic to mammalian cells.⁵

Barrett et. al.⁶ investigated the coating formation ability of 19 plant-derived or plant-inspired polyphenolic compounds in an approach that was analogous to polydopamine coatings, by immersing the substrate in the aqueous buffer solution of the polyphenol precursor. They demonstrate that coating deposition for each phenolic compound is dependent on an optimal pH and the coating formation can be significantly affected by subtle changes in deposition conditions.⁶

Jeon et. al.²⁶ used laccase-catalyzed polymerization of plant-derived phenolic compounds to form substrate-independent coatings. Plants use laccase enzymes to synthesize polyphenolic components such as lignins and poly(flavonoid)s from small phenolics such as monolignols and flavonoids.²⁶

Caruso and co-workers²⁷ reported a one-step coating strategy of various substrates using coordination complexes of natural phenolic compounds and Fe^{III} ions. They demonstrated that the film formation was dependent on the adsorption of the phenolic compounds and the pH-dependent multivalent coordination bonding. They observed that the color of the solution of polyphenols and Fe^{III} changed at different pH from colorless at pH values lower than 2, to blue at pH values between 3 to 6, and red at pH values higher than 7. This behavior was attributed to the transition between mono-, bis-, and tris-complex states (Figure 1.8).²⁷

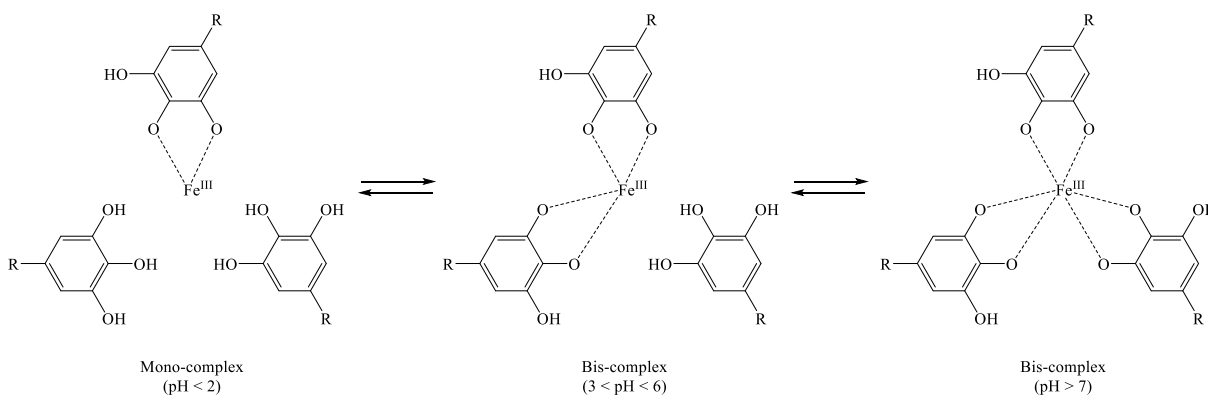


Figure 1.8 The coordination interaction between Fe^{III} ions and tannic acid (TA) is pH-dependent. R is the remainder of the tannic acid molecule.²⁷

Our group^{23,24,28} and other groups^{29,30} used UV irradiation to accelerate polymerization and deposition of phenolic compounds. I²⁴ used UV irradiation to accelerate the oxidation and the following polymerization of plant phenolic compounds including pyrogallol, tannic acid, gallic acid, and caffeic acid at different pH conditions ranging from pH 4 to pH 10. It was demonstrated that by reducing the pH of the phenolic solutions or by storing the solution in a dark environment, the kinetics of the oxidation and polymerization of the phenolic compounds slowed down. On the other hand, increasing the pH value or UV irradiation of the solution could increase the kinetics. This strategy was used to control the polymerization and deposition of the

plant phenolic compounds on the surface and used to make micropatterns on the surface of a variety of substrates. In another study,²³ our group showed that autoxidation of phenolic compounds in basic condition can be inhibited in the presence of natural antioxidants such as sodium ascorbate, glutathione, and uric acid. UV irradiation of the solution, however, could accelerate the kinetics of the polymerization and deposition process. This strategy was used for on-demand polymerization and deposition of plant polyphenols and to form a more homogeneous nanocoatings on the surface. These two strategies enabled a controlled deposition process spatiotemporally which will be discussed in details in **chapter 2** and **chapter 3**.

1.3.2 Post-functionalization of polyphenolic nanocoatings

Catechols and products of their oxidation (quinones), react toward a range of chemical groups, as summarized by Birkedal and co-workers³¹ (Figure 1.9). Common choices for post-functionalization of plant- and mussel-inspired coatings are mainly self-coupling reactions, reactions with nucleophiles (such as amine, thiol, and imidazole groups), and complexation with metal ions. Post-functionalization reactions are affected by several factors including ionic strength, organic reaction partners, pH, and oxidants.³¹

Such post-functionalization strategies have been used to introduce desired functional groups on the surface of polyphenol-modified substrates via different interaction mechanisms. The catechols mainly contribute to non-covalent, strong yet reversible interactions while quinones mainly participate in covalent non-reversible interactions.³¹ For example, quinones react with thiols and amines through Schiff base reactions and Michael-type additions.^{31,32}

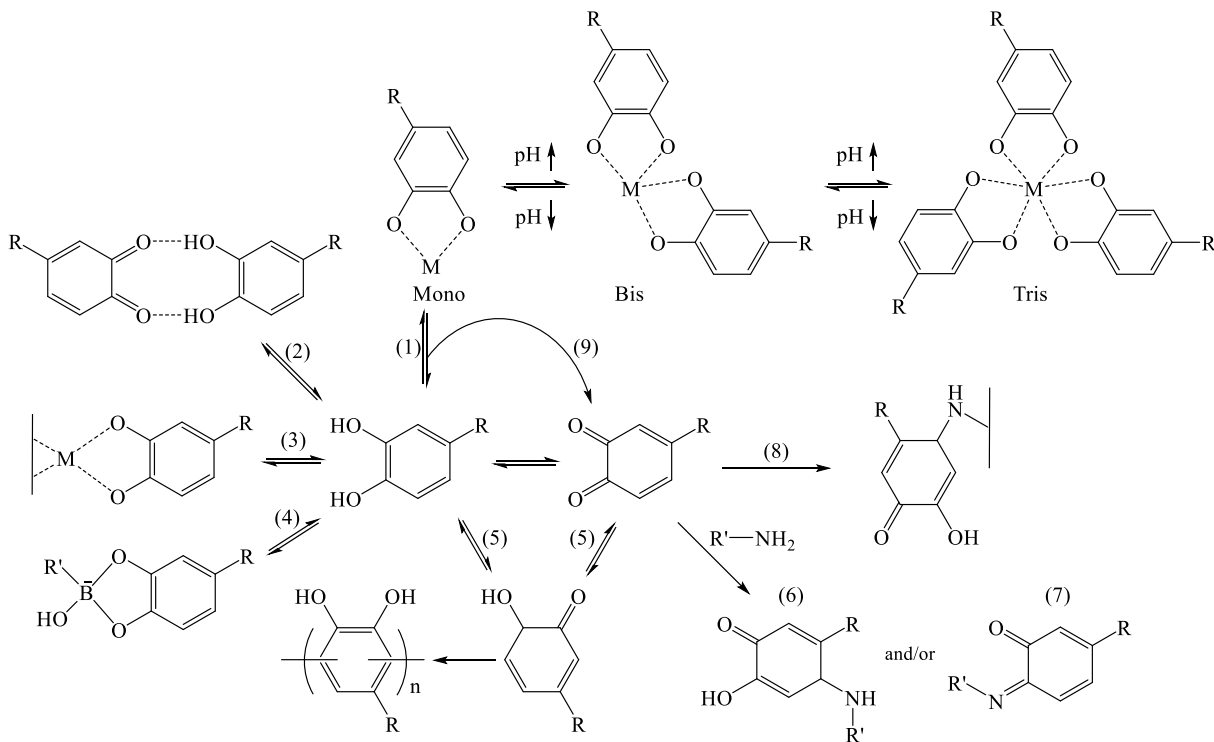


Figure 1.9 Commonly used chemistry of catechols and quinones. 1: formation of a complex with metal ions. 2: participation in hydrogen bonding. 3: Adhesion to the inorganic surface. 4: Boronate-ester complexation. 5: Semiquinone mediated self-coupling. 6: Michael-type addition. 7: Schiff base reaction. 8: Adhesion to an organic surface (amine-functionalized surface as an example). 9: Oxidation of catechol by Fe^{III} .³¹

1.4 Surface functionalization via macrocyclic polyphenols

Most surface functionalization strategies use one attachment point per molecule interacting with the surface.³³ The drawback of this approach is the formation of a weak adlayer on the surface³⁴ or leakage of the modifying species.³³ Therefore, multi-point surface functionalization strategies have been developed to improve these limitations. In the context of mussel- and plant polyphenol-inspired materials, Wei and co-workers³⁵ developed substrate-independent coatings from a mussel-inspired dendritic polymer containing a large number of catechol and amine groups. In another study, Zieger and co-workers,³⁶ inspired by the strong adhesion of catechols to a variety of substrates developed a cyclic catechol material with up to 32 catechol units to form robust coatings on various substrates.

1.4.1 Calixarenes for surface modification

An alternative type of macrocyclic polyphenols that enable multi-anchor points to the surface are resorcinarenes which are resorcinol-derived calixarenes. Gold, silver, silica, and quantum dots have been used as a support for calixarenes.³⁷ Thiol-gold,³⁸ ion-metal coordination,³⁹ amine-graphene oxide,⁴⁰ silane coupling,⁴¹ and platinum catalyzed⁴² binding chemistries have been used to make a layer of resorcinarenes on the surface.

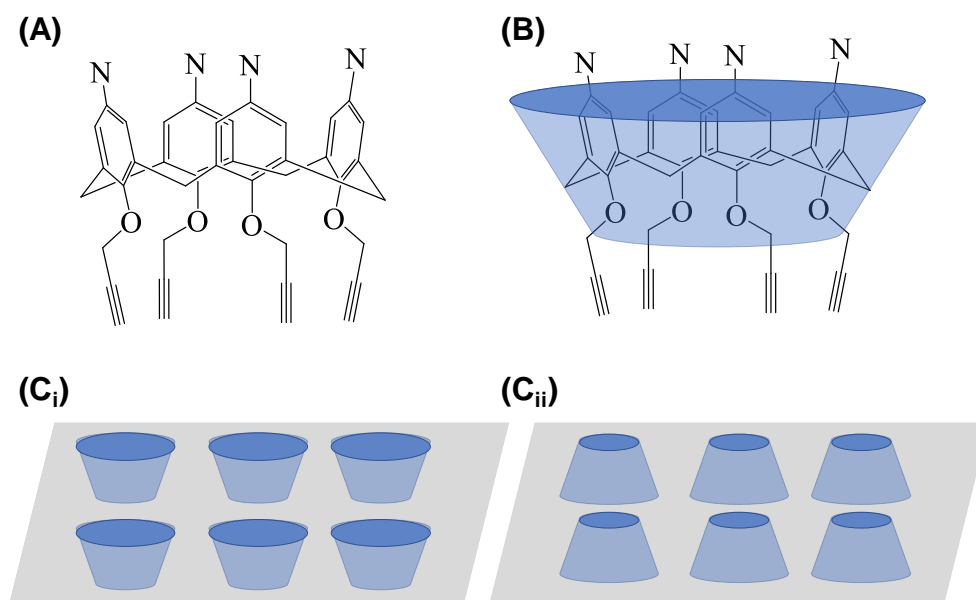


Figure 1.10 Chemical structure of calix[4]arene (“N” are amine or azide functionality) (A). Cone structure of calixarene (B). Immobilized calixarene onto a surface by the lower rim (C_i) or by the upper rim (C_{ii}).³³

Buttress et. al.³³ reported functionalization of the surface using a calix[4]arene having aryldiazonium functionalities on the large rim and alkyne moieties on the small rim (Figure 1.10). Reduction of aryldiazonium or oxidation of alkyne moieties were used to covalently attach this calix[4]arene to the electrode surfaces.

Quan et al.⁴³ immobilized functionalized calix[4]arene on the surface of Si-N₃ via a click reaction for macroscopic chiral recognition by host-guest interactions. First, they modified the silicone surface with 3-(triethoxysilyl)propylamine to fabricate the Si-N₃ containing surface. After immersion of Si-N₃ surface in the solution of calixarene having alkynyl groups on its

lower rim, copper sulfate, and sodium ascorbate for 8h at 75°C, a saturated modification was achieved.

Calix[4]arenes possessing rigid tetrapodants were used by Mattiuzzi et al.^{2,44,45} to functionalize the surface by electrografting of calix[4]arene diazonium salts (Figure 1.11). The unique macroscopic structure of calixarene enabled the formation of a closely packed layer on the surface.²

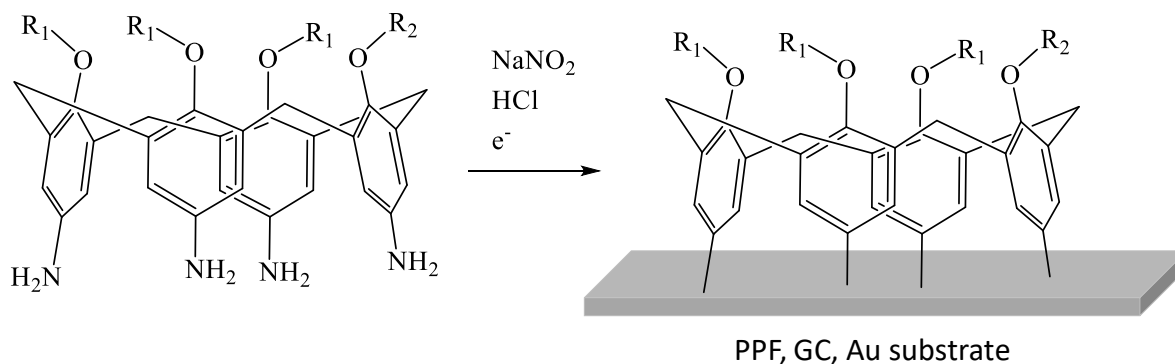


Figure 1.11 Electrografting of calix[4]tetra-anilines to the surface of, pyrolyzed photoresist film (PPF), gold (Au), or glassy carbon (GC).²

1.4.2 Resorcinarenes for surface modification

Resorcinarenes have been incorporated into molecular assemblies via Langmuir-Blodgett layer and lipid bilayers. Van der Waals interactions are considered as driving force of self-assembled monolayers. Many attempts have been made to control the molecular interactions and orientation of the resorcinarenes on the surface in order to achieve selective binding.⁴⁶

Condorelli et al.⁴⁷ used hydrosilylation of double bonds to bind resorcinarene cavitands with decylenic feet (on the lower rim) onto the H-terminated silicon (100) surface. Katz et al.⁴⁸ modified silica surface with chlorosilane to condense calixarene macrocycles onto the surface from the large rim side (Figure 1.12).

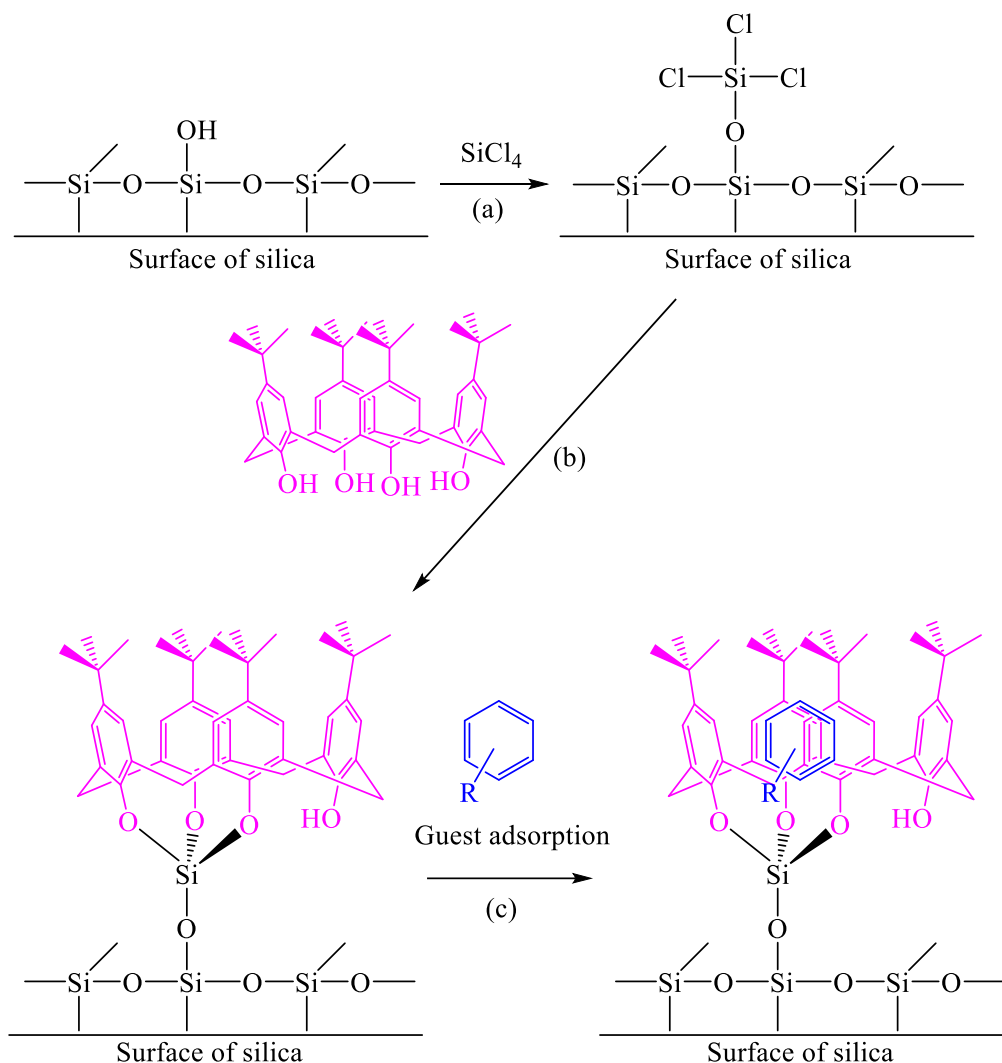


Figure 1.12 Immobilization of *p-tert-butyl-calixarene* on the surface of silica for adsorption of a small-molecule. a) Using silicon tetrachloride to activate the surface of silica. b) Immobilization of calixarene to the surface via a chemical reaction. c) Adsorption of the guest molecule onto the anchored site.⁴⁸

Monolayers on gold and multilayers of resorcinarenes have been reported.⁴⁹ Hassan et al.⁵⁰ used spin coatings and Langmuir-Blodgett (LB) techniques to deposit a thin film of amphiphilic calix[4]resorcinarenes on the surface (Figure 1.13). Such resorcinarenes have been used for selective recognition of organic molecules in the gaseous phase and metal ions in aqueous solutions.⁵⁰

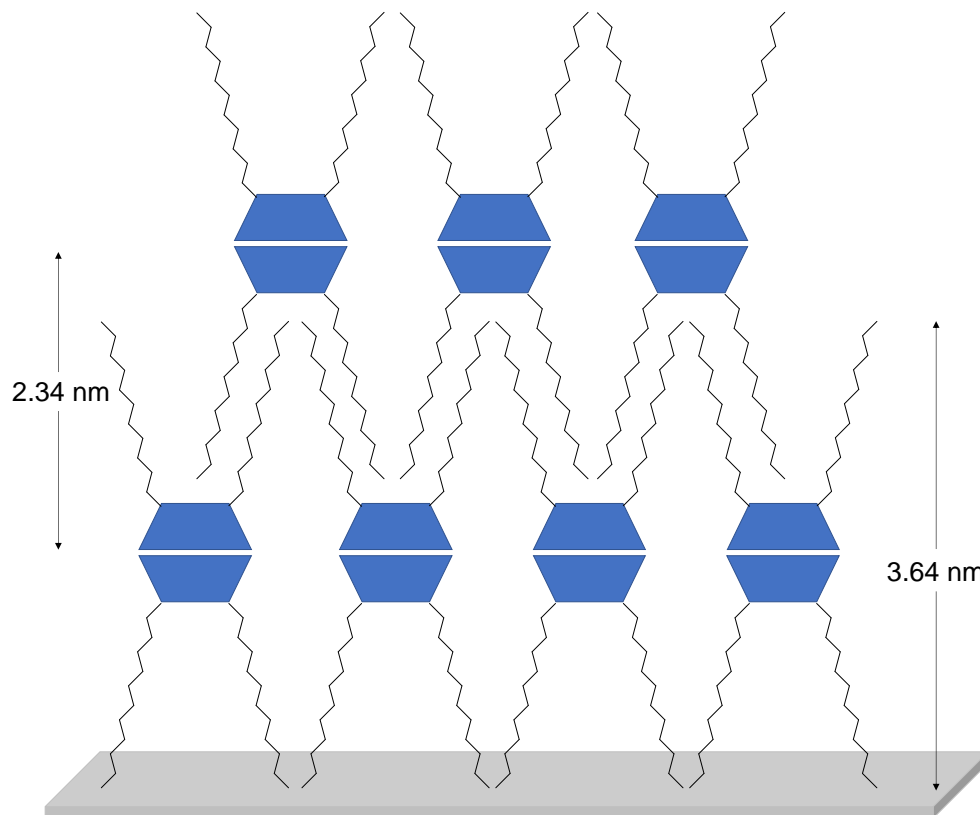


Figure 1.13 Scheme of a multilayer calix[4]resorcinarene film structure formed on the surface as a result of bowl-to-bowl interactions and alkyl chains interdigitation.⁵⁰

1.4.3 Synthesis of resorcin[4]arenes

Resorcin[4]arenes can easily be obtained by the acid catalyzed condensation of resorcinol with various aliphatic or aromatic aldehydes, which occurs by refluxing the reactants in a mixture of ethanol and concentrated hydrochloric acid (HCl) for several hours (Figure 1.14).⁴⁶

Usually, the cyclotetramer crystallizes from the reaction mixture in reasonable to high yields in a simple, one-step, untemplated reaction, although different optimal reaction conditions exist for different aldehydes. Resorcinarenes are versatile molecular platforms that can be secondarily functionalized in order to introduce desired functional groups on the lower or upper rim. Such derivatives could possess different additional properties from the original resorcinarene compound.⁴⁶

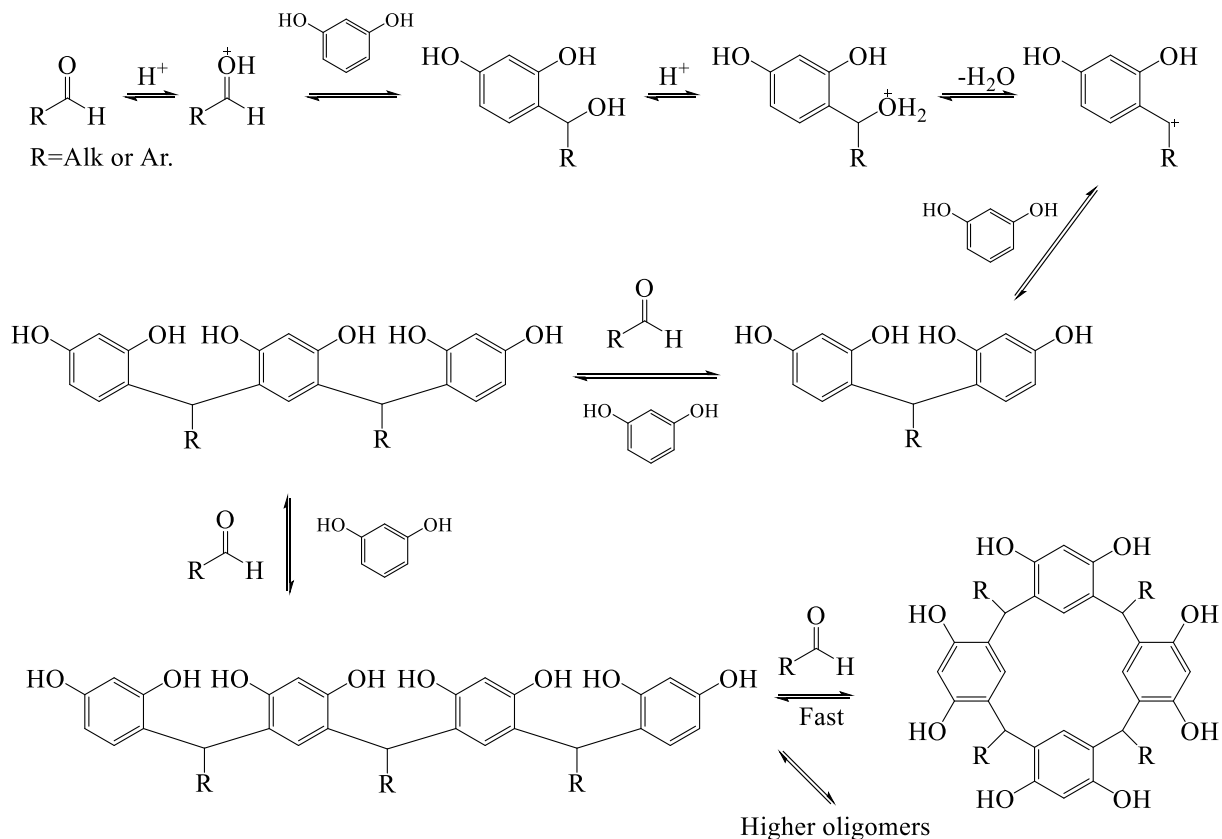


Figure 1.14 The mechanism of the acid-catalyzed condensation reaction that forms calix[4]resorcinarenes. The acid catalyzed condensation of resorcinol with various aliphatic or aromatic aldehydes occurs by refluxing the reactants in a mixture of ethanol and concentrated hydrochloric acid (HCl) for several hours.⁴⁶

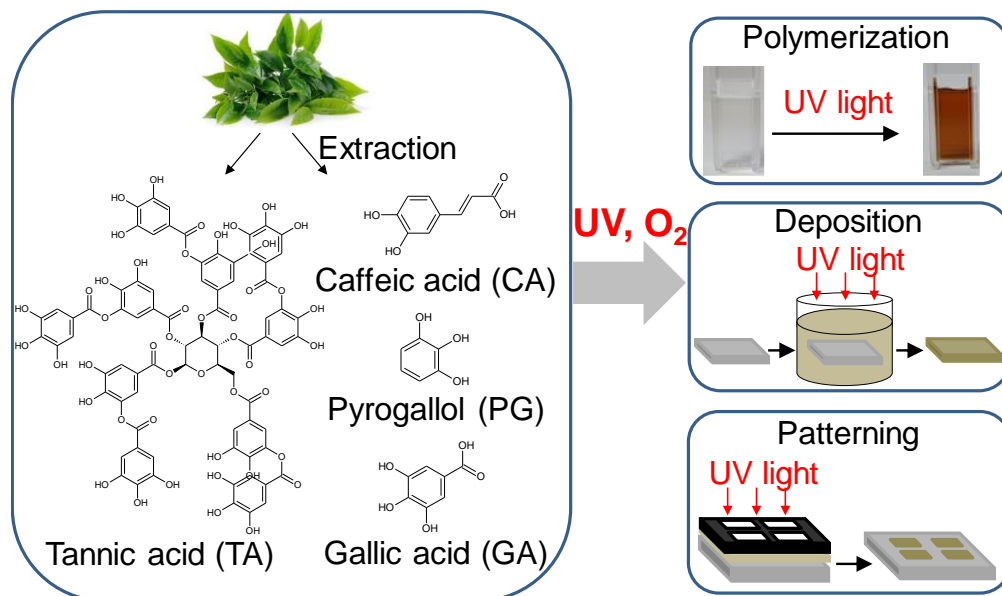
Inspired by the strong adhesion properties of the plant polyphenols to the surface, our group developed a new strategy to modify the surface of a variety of substrates using resorcinarenes. It was demonstrated that resorcinarenes could bind to the surface via interaction of eight hydroxyl groups on the large rim, while the small rim can be decorated with desired functional groups. Deposition of the resorcinarene layer on the surface of a variety of substrates was confirmed by static and dynamic contact angle measurements, atomic force microscopy (AFM), X-ray photoelectron spectroscopy (XPS), and Time-of-Flight Secondary Ion Mass Spectrometry (ToF-SIMS).

This strategy was used in order to introduce alkene moieties on the surface that were used to introduce hydrophobic and hydrophilic functional groups on the surface via a thiol-ene

photoclick chemistry. These post-functionalized substrates were able to repel liquids with both high and low surface tension. High contrast of wettability between the hydrophobic and hydrophilic spots enabled the formation of a drop microarray of water, ethylene glycol, and cyclohexanol on the surface by rolling a drop of liquid on the photopatterned surface.

In **chapter 4**, surface functionalization by deploying bifunctional resorcinarenes is described in more details. Such resorcinarene compounds can adhere to a variety of substrates from their large rim side, while their small rim side can be used for the post-functionalization. The resulting nanocoatings demonstrated strong attachment, homogeneity, and transparency.

Chapter 2. UV-Triggered Polymerization, Deposition, and Patterning of Plant Phenolic Compounds^a



^a This chapter is adapted from the publication below:²⁴

Behboodi-Sadabad, F.; Zhang, H.; Trouillet, V.; Welle, A.; Plumeré, N.; Levkin, P. A. UV-Triggered Polymerization, Deposition, and Patterning of Plant Phenolic Compounds. *Adv. Funct. Mater.* **2017**, *27*, DOI: 10.1002/adfm.201700127.

2.1 Introduction

The ability to control surface properties via functional coatings is fundamentally important in various applications.⁵¹ Recently, mussel adhesive proteins (MAP) and their analogs containing multiple 3,4-dihydroxyphenylalanine (DOPA) moieties inspired many groups to use catechol (1,2-dihydroxyphenyl) containing molecules for surface coating and functionalization,¹⁶⁻¹⁸ nanoparticles fabrication and modification,^{20,21} surfaces with special wettability,^{10,19} and development of new hydrogels^{14,15} and membrane.¹¹ Dopamine (DA) structurally similar to DOPA has been found to form versatile polydopamine nanocoatings on different materials by simple immersion of objects into a dopamine solution under basic conditions,⁶ in the presence of oxidants,¹⁰ and under UV irradiation.⁸

Recently it was shown that different plant-derived phenolic compounds, isolated from various plants and rich in 1,2-dihydroxybenzene (catechol) and 1,2,3-trihydroxybenzene (pyrogallol) moieties, could also form nanocoatings, following polymerization using enzymes,^{26,52} coordination complexes,^{27,53} or using mildly alkaline solutions in the presence of dissolved oxygen.⁵ In comparison to polydopamine, coatings based on plant phenolic compounds were found to possess more rapid adhesion rate, lower cost, excellent availability, and good structural diversity.³ Phenolic compounds, found in various plant-derived foods (for example, fruits, vegetables, cereals, chocolate) and beverages (for example, tea, coffee, beer, wine) are known to be an important part of the defense system of plants.⁵⁴ Plant phenolics show antioxidant and anti-cancer effect.^{54,55} Long-term use of plant phenolics can eliminate destructive effect of undesired reactive oxygen or nitrogen species in the body.⁵⁵ Furthermore, plant phenolics are able to chelate metal ions, interact with surfaces and materials via charge-charge, charge-dipole, and covalent bonds, quench reactive radical species and interact with oxidizing agents, oxidized catechol and pyrogallol moieties enable antimicrobial activity of plant phenolics.^{25,26,56}

Various lithographic techniques such as soft lithography and dip-pen lithography have been developed for surface patterning. Yet, most of the patterning methods are not applicable for the formation of gradients or for the fabrication of patterns inside closed microfluidic channels or on curved surfaces. Creating patterns of functional structures within microfluidic channels or

capillaries is crucial in research areas ranging from micro- and nano-fluidics,⁵⁷[20] analytical chemistry,⁵⁸ drug delivery,⁵⁹ clinical and diagnostics devices⁶⁰ to separation science.⁶¹

Coatings based on polyphenols can potentially lead to a lot of useful applications. However, the ability to control polyphenol nanocoatings spatially and temporally would significantly extend the number of potential applications. Recently, our group showed that dopamine polymerization and deposition could be accelerated by UV irradiation.⁸ In this chapter, the ability of UV irradiation to induce oxidation and polymerization of various plant-derived phenolic compounds has been demonstrated. The effect of UV on plant phenolic compounds was investigated using UV-Vis spectroscopy, ESI-MS and cyclic voltammetry. Various plant-derived phenolic compounds including pyrogallol (PG), tannic acid (TA), caffeic acid (CA), and gallic acid (GA) could be polymerized under UV irradiation. UV-assisted polymerization and deposition of plant phenolic compounds was used to make polyphenol nanocoating on polar and non-polar substrates as well as to create gradients of polyphenol coatings. The ability to use UV-light to trigger polymerization and deposition of phenolic compounds opens the possibility to create polyphenol patterns and gradients within microfluidic channels, which was demonstrated by creating a pattern of PG inside a fused silica capillary. The use of UV-light to accelerate formation of polyphenol nanocoatings opens the possibility for the photolithographic patterning of functional polyphenolic nanocoatings on various substrates, extending the scope of potential applications of plant polyphenols.

2.2 Results and discussions

In order to realize the oxidative effect of UV irradiation, UV-vis spectra of 1,2,3-trihydroxybenzene (pyrogallol, PG), tannic acid (TA), 3,4,5-trihydroxybenzoic acid (gallic acid, GA), 3-(3,4-Dihydroxyphenyl)-2-propenoic acid (caffeic acid, CA) (Figure 2.1), representing some of the most common phenolic compounds derived from plants, in variety of acidic and basic solutions were measured.

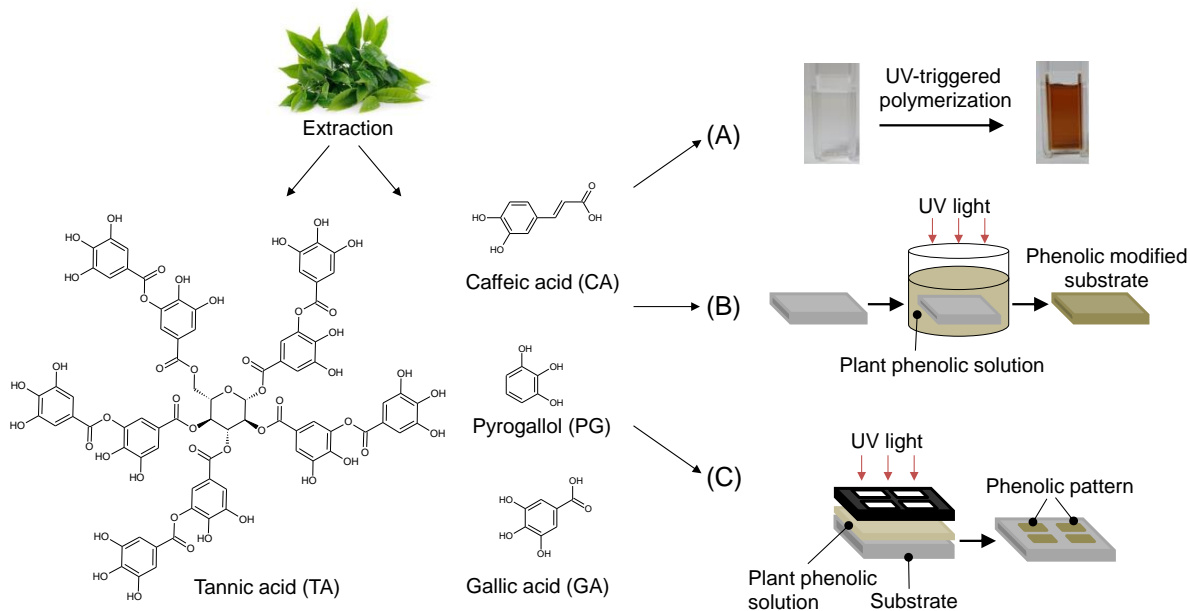


Figure 2.1 Schematic representation of the UV-induced polymerization (A), deposition (B), and patterning (C) of plant-derived phenolics: tannic acid (TA), pyrogallol (PG), gallic acid (GA), and caffeic acid (CA).²⁴

Kinetics and pH dependence of oxidation both in the dark and under UV irradiation (260 nm, 10 mW/cm²), were investigated for each compound at 30 min time intervals for 2 h (Figure 2.2). Our results show that UV irradiation of PG, TA, GA, and CA even under acidic pH leads to a change of color and appearance of the UV absorbance. Figure 2.2A demonstrates the corresponding color change of the PG and TA solutions irradiated with UV light in comparison with those stored in the dark. UV-Vis spectra of irradiated PG (0.2 mg/mL, acetate buffer at pH 5.0) and TA (0.2 mg/mL, phosphate buffer at pH 7.0) solutions shifted to higher absorbance at 350 nm along with increasing UV irradiation time, while absorbance of non-irradiated samples remained unchanged (Figure 2.2B,C).

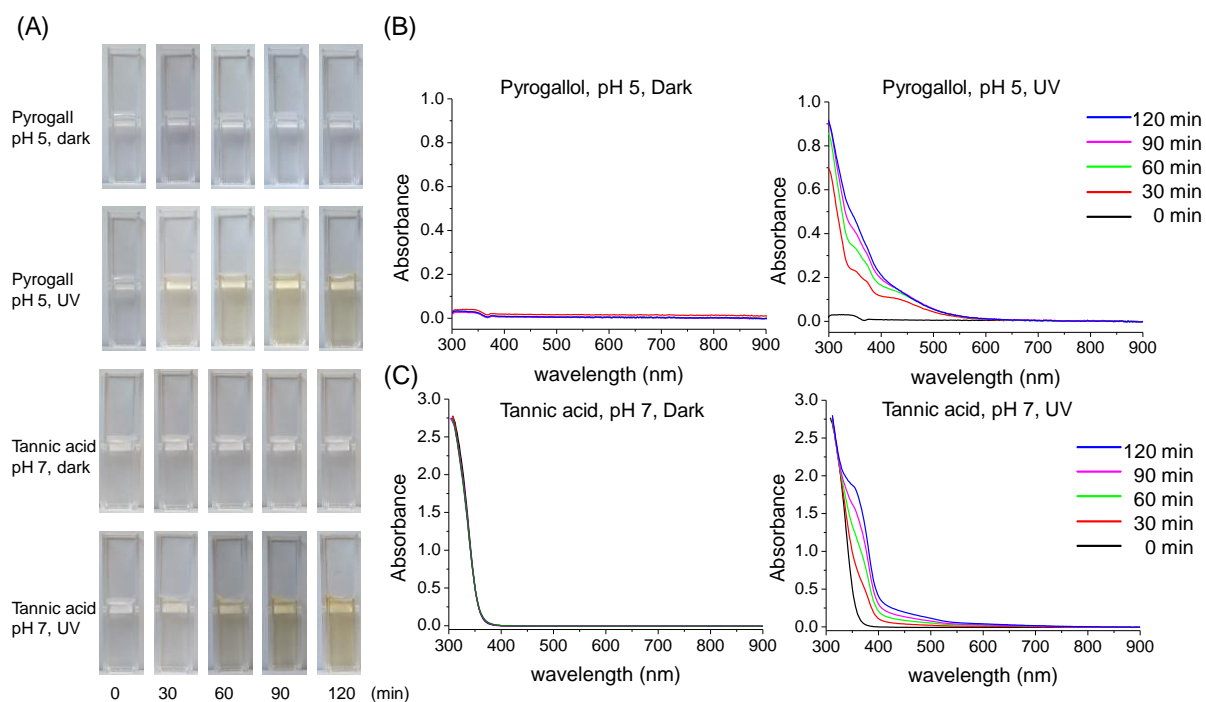


Figure 2.2 UV irradiation of plant-derived phenolics leads to a change of color and increase in absorbance of solutions. The plant-derived concentration of phenolic compounds in each sample is 0.2 mg/mL in a corresponding buffer (100 mM). (A) Photographs of the corresponding solutions after UV irradiation and in the dark. UV-Vis spectra of PG solution in acetate buffer at pH 5.0 (B) and TA in phosphate buffer at pH 7.0 (C) stored in the dark (left) and after UV irradiation (right) measured at different time intervals.²⁴

Increased absorbance of solutions after UV irradiation was also observed for PG, TA, GA, and CA at different pH conditions (both acidic and basic) (Figure 2.4, 2.5, Figure S8.1-7). The increase of absorbance at 350 nm as a function of time for each sample is plotted in Figure 2.3A.

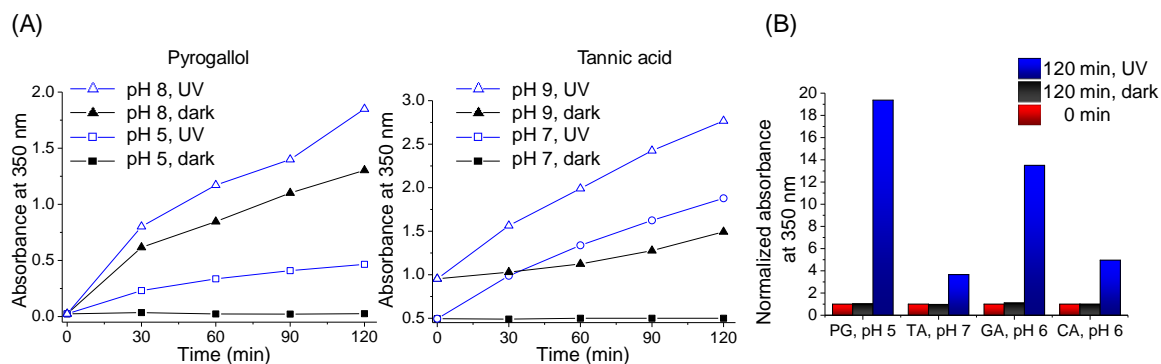


Figure 2.3 (A) Absorbance of the PG (left) and TA (right) solutions at 350 nm as a function of time and pH. (B) Normalized UV absorbance of PG, TA, GA, and CA solutions at 350 nm at 0 h, before and after 2 h of UV irradiation. A significant increase in UV absorbance is observed for phenolics solution after 2 h UV irradiation.²⁴

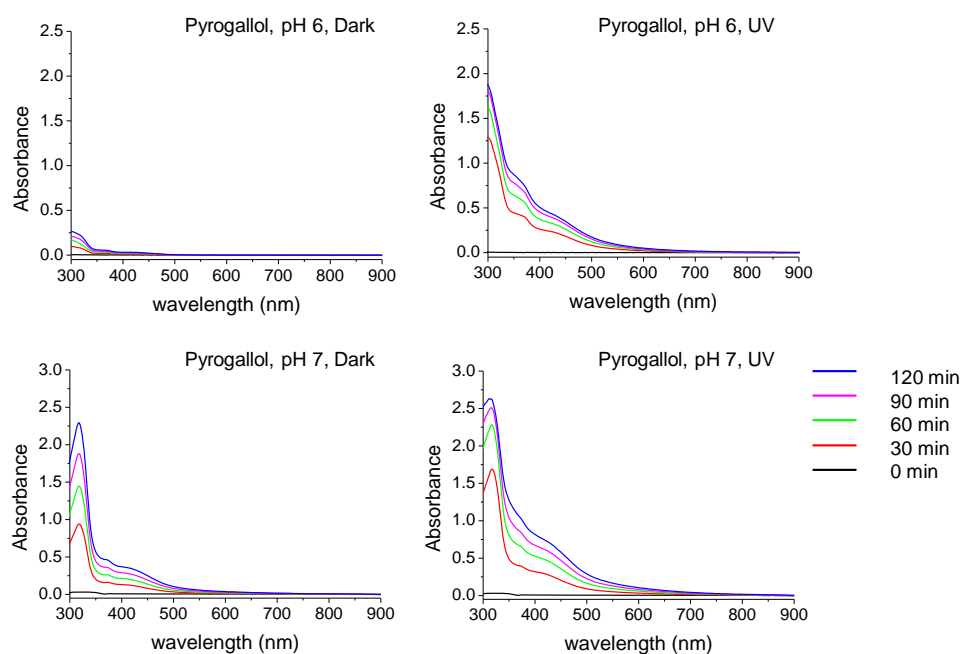


Figure 2.4 UV-Vis spectra of PG solution (0.2 mg/mL) at pH 6.0, and pH 7.0 stored in dark environment (left) and after UV irradiation (right) measured at different time intervals.²⁴

For example, normalized UV absorbance at 350 nm of PG (pH 5.0), TA (pH 7.0), GA (pH 6.0), and CA (pH 6.0) solutions after 2 h of UV irradiation, increased 19.3, 3.6, 13.5, and 4.9,

respectively (Figure 2.3B). However, UV absorbance of these samples stored in the dark for 120 min remained the same (Figure 2.3).

An increase in the kinetics of phenolics oxidation was observed by increasing the pH from 5.0 to 10.0 (Figure S8.1-6). Although increasing the pH of solutions speeds up the oxidation and associated increase of absorbance of the phenolic solutions even in the dark, UV irradiation accelerates this process even more (Figure 2.3 and Figure S8.7 for other phenolics). Darkening of the solution and increase of UV absorbance at 350 nm in oxidative condition usually associated with higher molecular weight species and polymerization of phenolics.

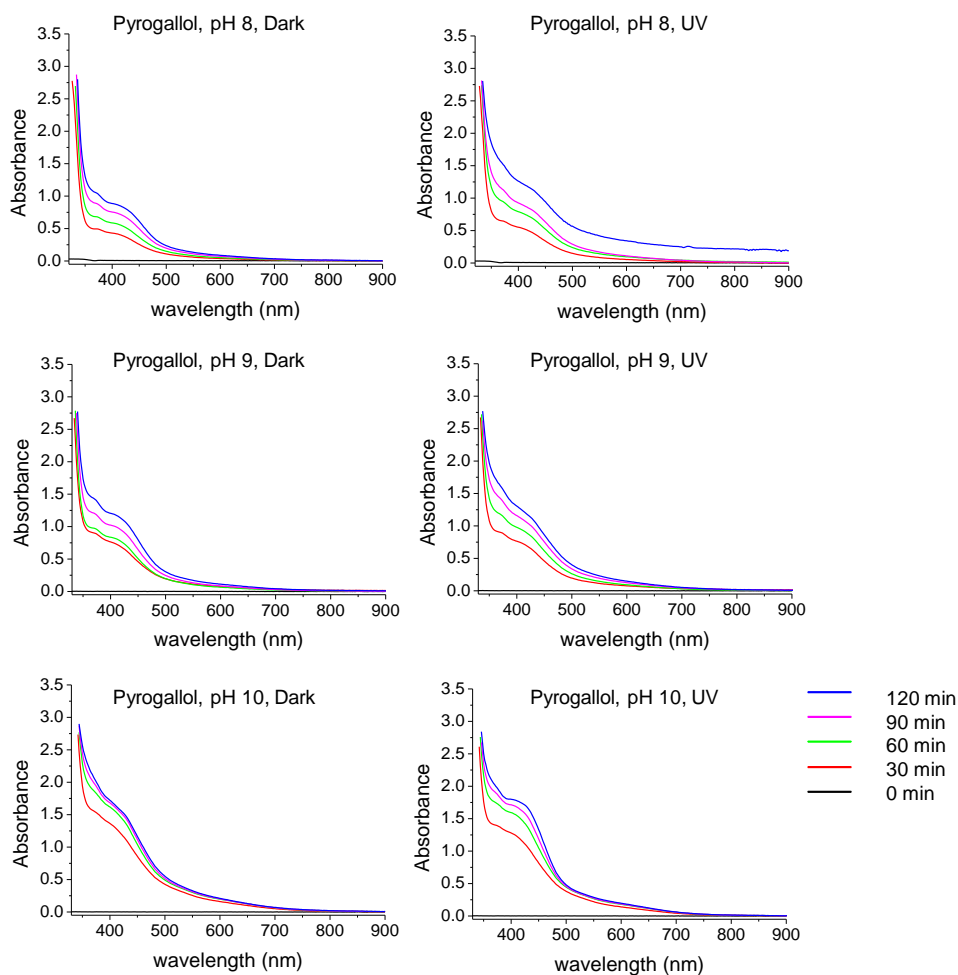


Figure 2.5 UV-Vis spectra of PG solution (0.2 mg/mL) at pH 8.0, pH 9.0, and pH 10.0 stored in dark environment (left) and after UV irradiation (right) measured at different time intervals.²⁴

2.2.1 UV-triggered polymerization of plant polyphenols

In order to prove that UV irradiation triggers polymerization of phenolic compounds, ESI-MS analysis of PG solutions (pH 5.0) either subjected to UV or kept in the dark for 2 h was performed (Figure 2.6). Increase in UV-Vis absorbance at 350 nm of plant phenolics under basic conditions was attributed to quinone formation.²⁶ However, formation of higher molecular weight species through oxidation of catechol and gallol moieties in plant phenolics was also reported.⁶² Our ESI-MS analysis clearly shows the presence of higher molecular-weight species following UV irradiation of PG solution, while no oligomers or polymers were detected in the case of non-irradiated samples (Figure 2.6A). The repeating unit of the observed oligomer is 105.96 m/z, which corresponds to the monomeric unit and oligomer structures depicted in Figure 2.6B. The same repeating unit was previously proposed for the oligomerization of PG under alkaline conditions.

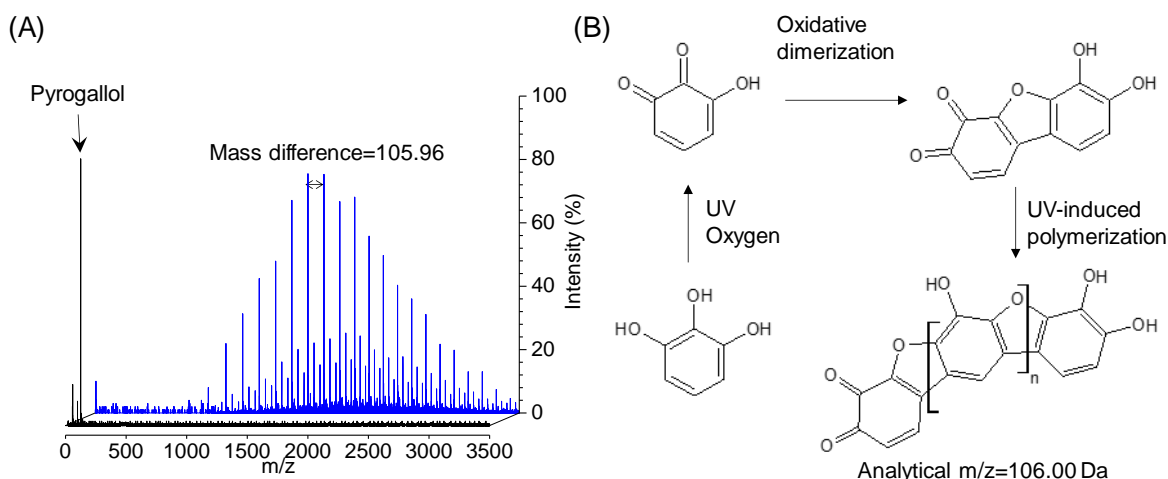


Figure 2.6 (A) ESI-MS spectra (positive mode, data acquired for 30 s) of PG solution in acetate buffer at pH 5.0 in dark and after UV irradiation for 2 h. ESI-MS spectra of UV-irradiated PG polymerization solution clearly shows the presence of higher molecular weight species. (B) Schematic representation of UV-induced polymerization of PG.²⁴

Having shown that UV irradiation can accelerate polymerization of the phenolic compounds, additional experiments were performed in order to investigate the mechanistic aspects of the UV-induced transformation. It is known that reactive oxygen species (ROS), including singlet oxygen ($^1\text{O}_2$), superoxide radicals ($\text{O}_2^{\cdot-}$), or highly reactive hydroxyl radicals ($\cdot\text{OH}$) can be

generated under UV irradiation even in the presence of traces of O₂. Previously our group reported the importance of ROS in the case of UV-induced dopamine polymerization.⁸

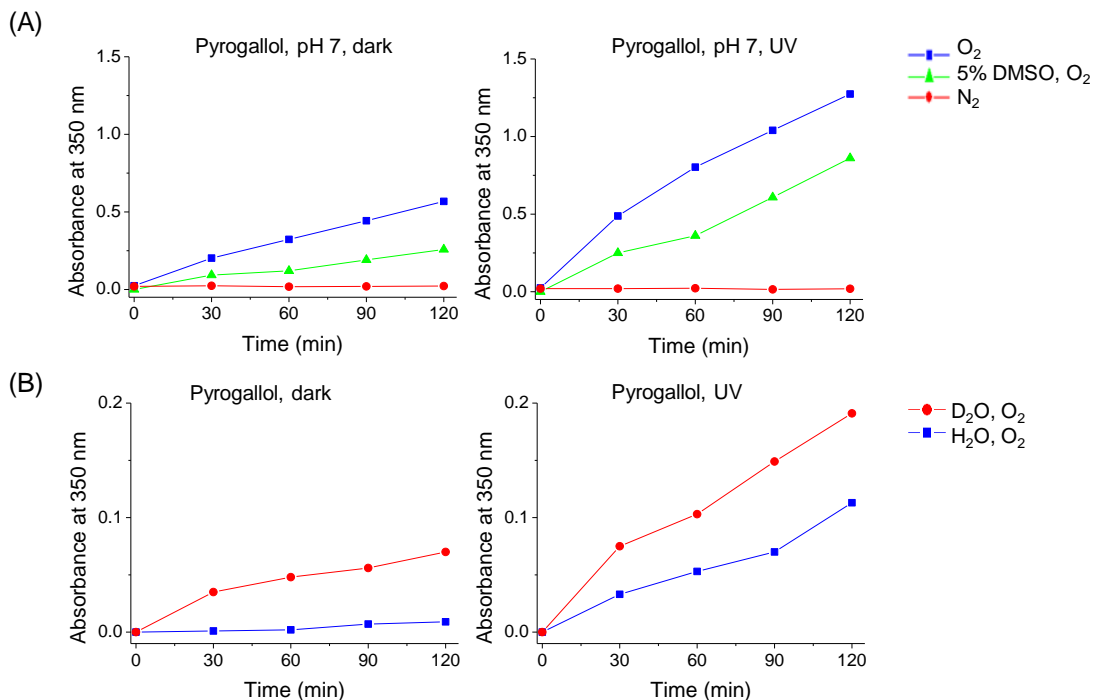


Figure 2.7 (A) UV absorbance at 350 nm of PG solution in phosphate buffer at pH 7.0 (blue), with addition of 5 % vol. DMSO (green), and after deoxygenation with N₂ (red) for solutions kept in dark (left) and under UV irradiation (right). (B) UV absorbance of PG solution at 350 nm in deionized water (blue) and deuterium oxide (red) media stored in dark (left) and under UV irradiation (right).²⁴

In order to investigate the role of oxygen and ROS in the UV-induced polymerization of plant phenolic compounds several experiments were performed (Figure 2.7A,B and Figure S8.8-11). First, PG solution at pH 7.0 was deoxygenated by passing nitrogen for 30 min, followed by UV irradiation. As shown in Figure 2.7A, the UV-absorbance of the deoxygenated solution at 350 nm did not increase even after 2 h of continuous UV irradiation, contrary to the same sample in the presence of oxygen (Figure 2.7A). Interestingly, the same inhibition of the polymerization was observed when the PG solution at pH 7.0 stored in the dark was deoxygenated (Figure 2.7A). In another experiment 5 % vol. of DMSO was added to the reaction solution. DMSO is known to be a hydroxyl radical scavenger.⁶³ UV irradiation of the DMSO-containing PG solution did result in a smaller increase of the absorption at 350 nm in comparison

to the control without DMSO (Figure 2.7A). The same slight inhibition of polymerization in the presence of DMSO was observed in the case of solutions stored in the dark (Figure 2.7A). On the other hand, deuterium oxide is known to be a singlet oxygen half-life prolonger.⁶⁴ Changing the medium from deionized water to deuterium oxide increased the UV absorption of PG solution stored in dark and UV-irradiated PG solution (Figure 2.7B). These observations suggest that UV-triggered polymerization of plant phenolics requires ROS and oxygen. Increasing ROS concentration can increase the rate of the UV-induced polymerization of phenolics, while quenching ROS and deoxygenation of the solution lead to the inhibition of polymerization.

2.2.2 Electrochemical oxidation of plant phenolic compounds

Antioxidant properties and electrochemical behavior of plant phenolics depend on their chemical structure and experimental conditions. The effect of UV irradiation on electrochemical oxidation of plant phenolic compounds using cyclic voltammetry was investigated (Figure 2.8-10 and Figures S8.12-17). PG as well as GA display two anodic peaks corresponding to the oxidation to the semi-quinone and the subsequent oxidation to the quinone form.

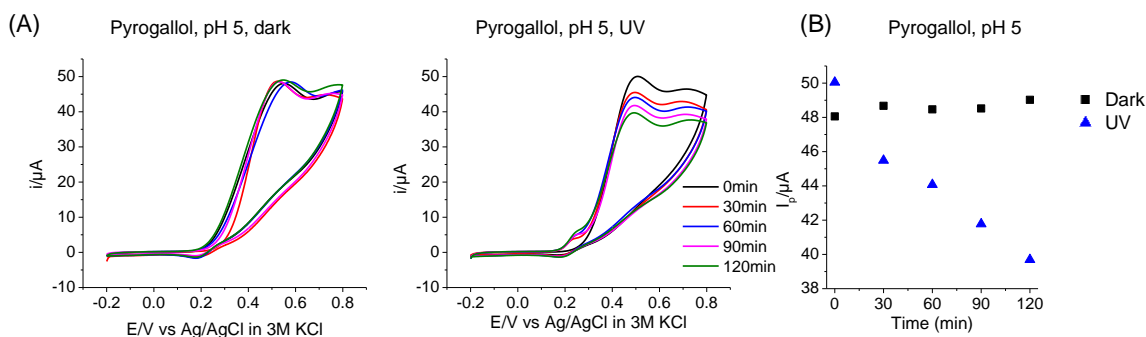


Figure 2.8 Monitoring of PG by cyclic voltammetry (CV). Cyclic voltammograms of PG in acetate buffer at pH 5.0 (A) stored for 2 h in dark (left) and under UV irradiation (right) vs time. Peak currents over time for PG in acetate buffer pH 5.0 (B) stored in dark or under UV irradiation for 2 h. All CVs were measured in 100 mM buffer at a scan rate of 100 mV/s at glassy carbon electrodes with 1.58 mM concentration of PG.²⁴

Monitoring of PG in acetate buffer at pH 5.0 incubated for 2 h in dark environment indicates a slight change in peak current values (Figure 2.8A). However, continuous UV irradiation for 2

h enhanced the oxidation rate of PG and decreased the peak current values by 20 % (Figure 2.8B). Significant decrease in peak current is due to consumption of PG after UV irradiation.

UV irradiation also increased the rate of oxidation of PG in basic pH as indicated by more reduction of peak currents after UV irradiation compared to solutions stored in dark (Figure S8.14,15).

The CV confirmed also irreversible oxidation of TA (Figures S8.14,15). However, in contrast to PG and GA, the anodic peak currents for TA remain mostly constant over time independently of illumination and pH value. TA is composed of 10 quinone moieties, which may predominantly undergo intramolecular reactions. In this case, the total concentration and molecular weights (or diffusion coefficient) of TA and its reaction products would not change significantly, thereby explaining the mostly unchanged oxidation peak current.

Nevertheless, although CV is not sensitive enough to quantitatively monitor the minor fluctuation in peak currents, intermolecular reaction leading to polymeric compounds in analogy to the behavior of GA and PG are also expected to take place.

Caffeic acid in contrast to the other three phenolic compounds, displays a reductive peak in addition to the oxidation peak in the CV at low pH values (Figures S8.16,17). The electrochemical response is attributed to a one electron oxidation to the semiquinone form followed by a second oxidation to the quinone. Both oxidized forms undergo follow up irreversible chemical reactions whereby the semiquinone reaction involves dimerization.

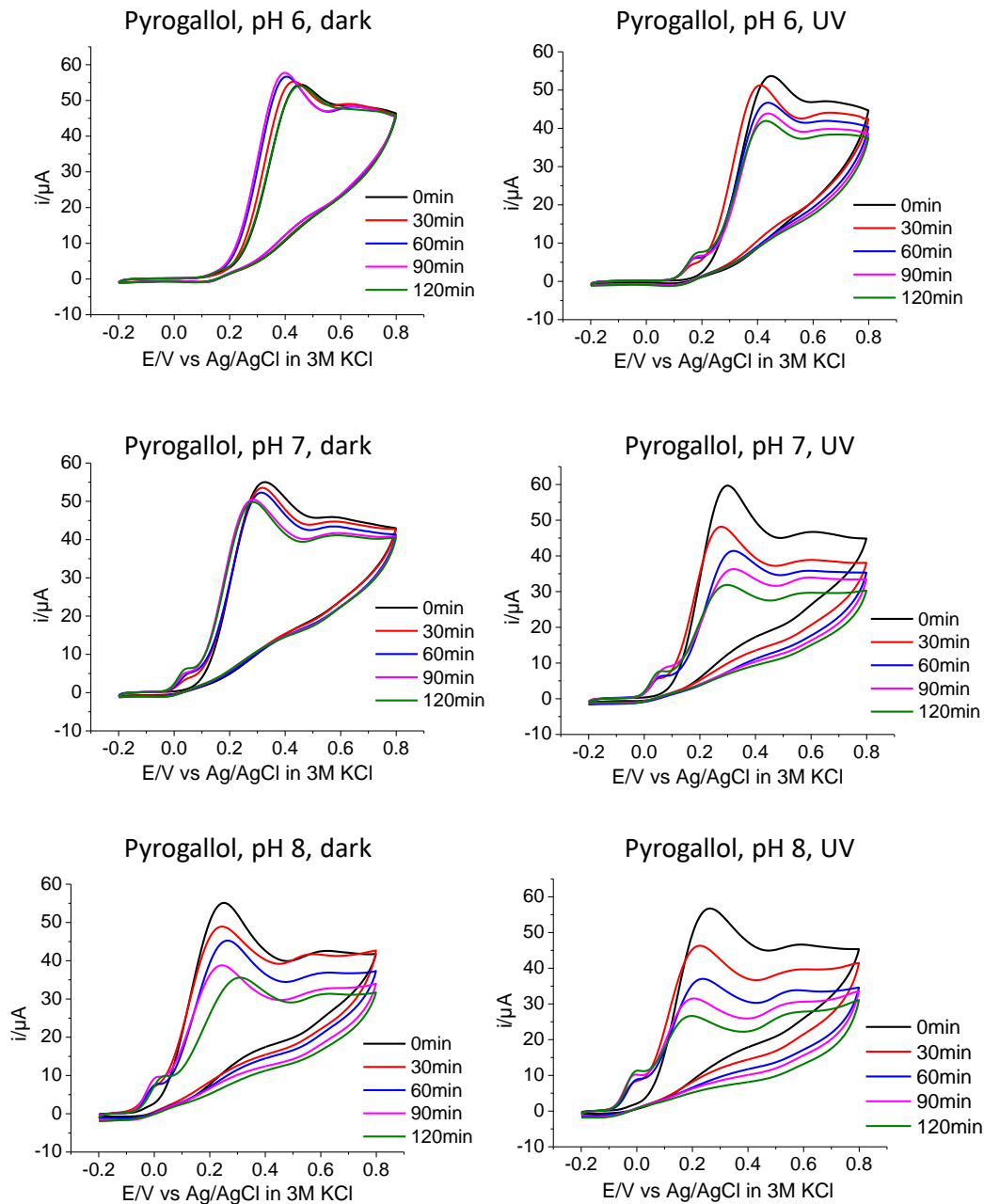


Figure 2.9 Monitoring of PG by cyclic voltammetry (CV). Cyclic voltammograms of PG in buffers at pH 6.0, 7.0, and 8.0 vs time stored for 2 h in dark (left) or under UV irradiation (right). All CVs were measured in 100 mM buffer at a scan rate of 100 mV/s at glassy carbon electrodes with 1.58 mM concentration of plant phenolics.²⁴

In more basic media ($\text{pH} > 8$), an increasingly irreversible behavior, suggests that the oxidation of CA follows a polymerization process. This is confirmed by the decrease in peak

current over time indicating the consumption of the monomeric compounds. The π conjugated systems in CA also induces a different behavior under illumination. While PG, GA and TA undergo light accelerated oxidative polymerization, caffeic acid first undergoes a light induced trans-cis isomerization followed by intramolecular cyclization.

The CVs confirm this behavior with the appearance of a new oxidation wave upon illumination in acidic media. The decrease of the reduction waves reveals the consumption of the caffeic acid (both cis and trans form) over prolonged illumination times. Observations from cyclic voltammetry for all phenolic compounds were in agreement with UV-vis spectroscopic data.

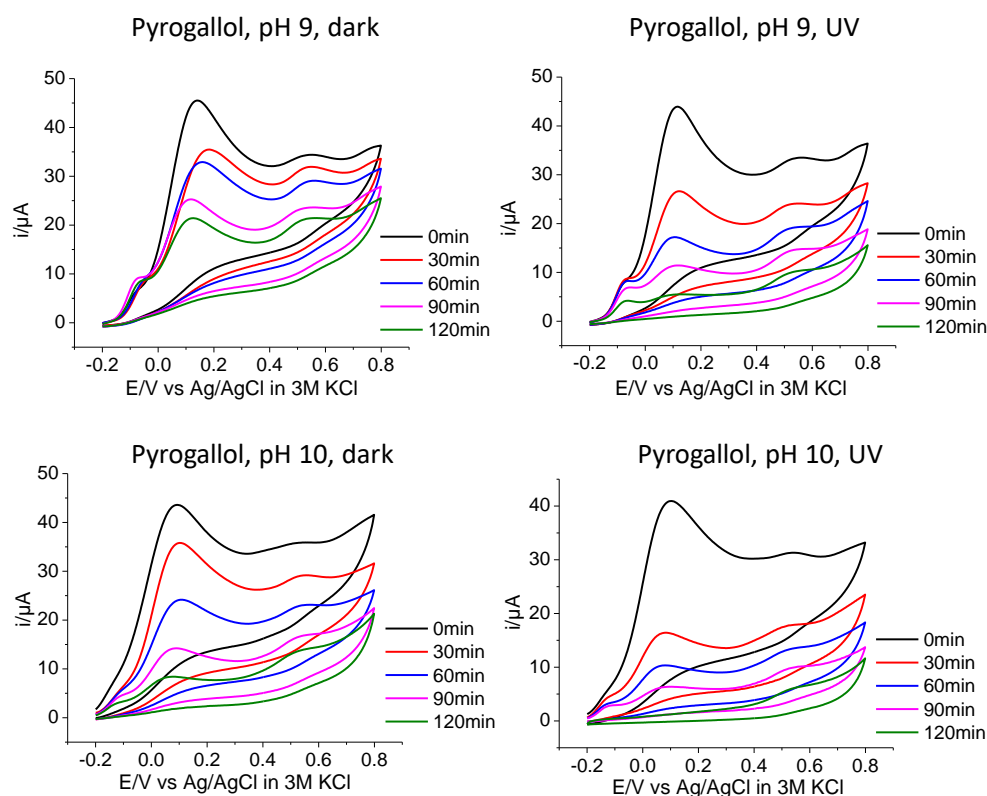


Figure 2.10 Monitoring of PG by cyclic voltammetry (CV). Cyclic voltammograms of PG in buffers at pH 9.0 and 10.0 vs time stored for 2 h in dark (left) or under UV irradiation (right). All CVs were measured in 100 mM buffer at a scan rate of 100 mV/s at glassy carbon electrodes with 1.58 mM concentration of plant phenolics.²⁴

2.2.3 *Nanocoatings from plant polyphenols*

Plant-derived phenolic compounds are able to form functional nanocoatings on various substrates. Messersmith et al.⁵ showed that even phenolic crude extracts from red wine, cacao bean, and green tea could form coatings on different materials. Jeon et al.²⁶ reported the use of laccase enzyme to catalyze polymerization of dopamine, catechin/catechol, ferulic acid/catechol, catechin/syringic acid, and tannic acid/catechol to form functional coatings.

Ejima et al.²⁷ introduced the use of multivalent coordination of TA and Fe^{III} for surface coatings of particulate and planar substrates. All mentioned examples utilized the ability of plant phenolic compounds to spontaneously polymerize either under basic conditions, in the presence of metal ions or enzymes.

In order to investigate the ability to create functional phenolic nanocoatings using UV light as a trigger, polar and non-polar polymeric substrates (PTFE, PE, PMMA) were immersed into a PG solution (10 mM, pH 5.0) and irradiated with UV light for 2 h. Formation of a PG layer onto the surface was visualized by immersing the substrate in AgNO₃ aqueous solution (Figure 2.11).

Substrates modified by PG under UV irradiation turned darker due to the reductive effect of the polyphenol nanocoating and the formation of metallic silver nanoparticles from silver nitrate (Figure 2.11A). The color of unmodified substrates and substrates dipped in PG solution stored in dark remained unchanged (Figure 2.11A).

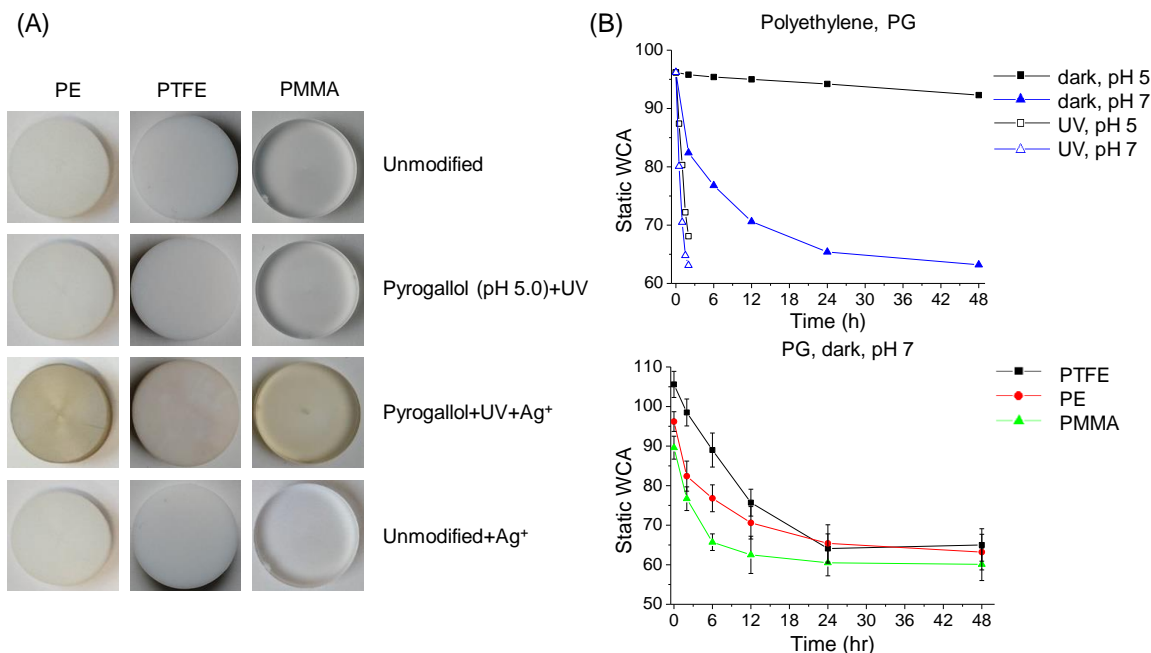


Figure 2.11 Deposition of a plant-derived phenolic coating on PE, PMMA, and PTFE substrates. (A) Photographs of unmodified, PG modified, and AgNO₃-treated substrates. (B) Decrease of the static WCA over time for PE substrate after immersion in 10 mM PG solution (acetate buffer at pH 5.0, phosphate buffer at pH 7.0) stored in dark environment and UV-irradiated substrates for 2 h (top, Figure S8.18C. with error bare). Static WCA reaches to a substrates independent value after immersion of PTFE, PE, and PMMA substrates in 10 mM PG solution (bottom, phosphate buffer at pH 7.0) for 48 h.²⁴

The acceleration of deposition of plant phenolics under UV irradiation is also confirmed by water contact angle measurements (WCA) (Figure 2.11B). Thus, the static WCA of PE substrate immersed in PG solution dropped from 96.2° to 68.1° after 2 h of UV irradiation at pH 5.0, while the static WCA on the same substrate kept in dark did not change after 2 h and decreased only to 92.3° after 48 h. It is known that basic pH accelerates polymerization and deposition of PG. However, even at pH 7.0 static WCA of PE decreased only to 82.4° after 2 h and 24 h of incubation was required to reach the lowest static WCA 63.1° achievable at pH 7.0. Similar static WCAs were measured on PTFE and PMMA substrates after 48 h of incubation the surfaces with PG solution at pH 7.0 in the dark (Figure 2.11B), confirming homogeneous deposition of a PG layer independent of the substrate. UV irradiation of the PE surface for 2 h at pH 5.0 without addition of PG did not result in a decrease of the static WCA (Figure S8.18A). Similar trend was observed for other plant phenolics studied (Figure S8.18B).

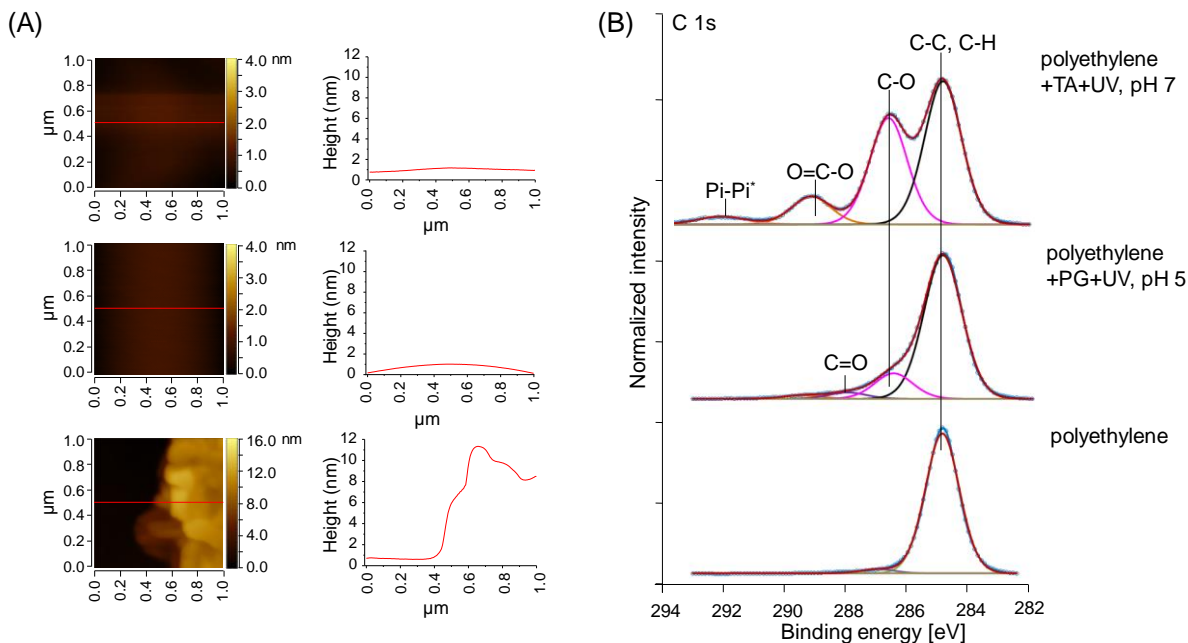


Figure 2.12 (A) AFM image of bare silicon (top), silicon immersed in PG solution in dark (acetate buffer at pH 5.0) (middle) and PG modified silicon wafer (bottom) gently scratched by tweezers. Corresponding diagram of line scan of each sample through the red line is shown below the image. (B) C 1s XP spectra of polyethylene before and after modification with a coating based on PG (acetate buffer at pH 5.0, 2 h UV irradiation) and TA (phosphate buffer at pH 7.0, 2 h UV irradiation). All spectra are normalized to the highest intensity.²⁴

Messersmith et al.⁶ reported thickness of 19 nm and 71.6 nm for a PG based layer on TiO₂ and polycarbonate surfaces, respectively. This measurement was performed after 24 h of incubation in the solution at pH 7. Jeon et al.²⁶ reported thickness of dual-monomer systems of plant phenolics on PET substrates ranging between 90 and 200 nm after 15 h of dipping in polymerization media. Ejima et al.²⁷ reported a thickness of Fe^{III}-TA films on polystyrene templates and gold substrates around 2 and 10 nm respectively within one deposition cycle. It was demonstrated that no polymer deposition happens after 2 h incubation of a silicon wafer in PG solution in acetate buffer at pH 5.0, while a 10±2 nm thick polymer layer as measured by AFM is formed after 2 h UV irradiation (Figure 2.12A). The root mean square deviation of the roughness profile of the silicon wafer incubated for 2 h in the dark (acetate buffer, pH 5.0) changed from 0.128±0.020 nm to 1.195±0.288 nm for the silicon substrate immersed in PG solution and irradiated with UV for 2 h.

In order to investigate the surface chemistry of plant-derived phenolics coated substrates XPS measurements of coated PE substrates immersed in PG and TA solutions (acetate buffer at pH 5.0 and phosphate buffer at pH 7.0 respectively) after 2 h of UV irradiation were conducted. PE substrate immersed in the same buffer after 2 h of UV irradiation was used as the reference substrate. As expected the C 1s XP spectrum from PE shows one main peak at 285.0 eV attributed to C-C, C-H groups (Figure 2.12B). A further peak at 286.6 eV in the C 1s XP spectra of substrates coated with PG and TA appears, corresponding to the presence of C-O groups and proving clearly the deposition of a thin layer of phenolics on the surface. Furthermore, the carboxyl group present in TA can be clearly detected too at 289.0 eV. In addition, the higher intensity ratio C-O/(C-C, C-H) for the TA coating (0.7) as for PG deposition (less than 0.2) leads to conclude that the TA film is thicker than that of the PG film.

2.2.4 Spatiotemporal control of the polymerization and deposition

The ability to use UV light to induce polymerization of various plant-derived phenolic compounds opens the possibility for both spatial and temporal control of the deposition of phenolic nanocoatings on different surfaces. In order to demonstrate this, I irradiated a PTFE substrate covered either with a 125 μm layer of 10 mM PG solution (acetate buffer, pH 5.0) or TA solution (phosphate buffer, pH 7.0) with UV light for 1 h through a quartz photomask (Figure 2.13A). A clear pattern of silver particles or fluorescence was formed on the surface after immersing the substrates either in a silver nitrate aqueous solution or rhodamine-thiol solution, respectively (Figure 2.13, Figure 2.14.A).

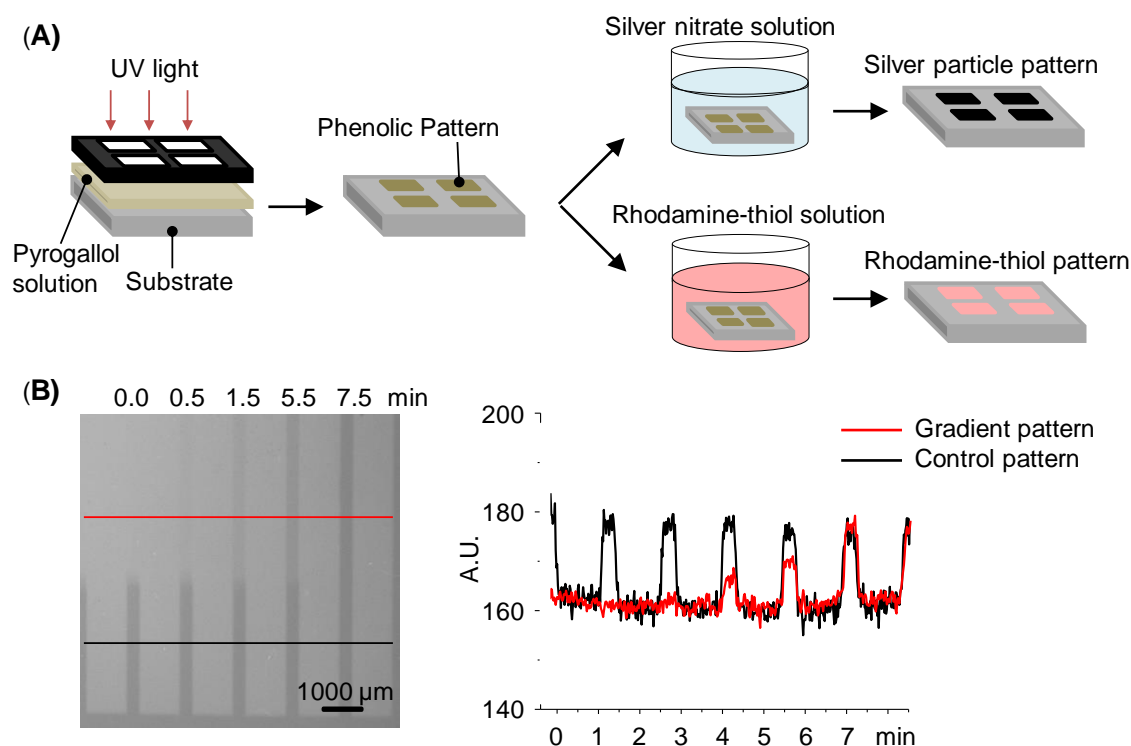


Figure 2.13 (A) Schematic representation of UV patterning of a polypyrogallol layer using a photomask, deposition of silver particles on the pattern and treatment of polypyrogallol pattern with Rhodamine-thiol solution. (B) Gradient phenolic pattern formed on the poly(HEMA-EDMA) surface after UV irradiation of PG solution (0.01 mg/mL, pH 7.0) through a photomask between 0 to 7.5 min, followed by incubation in a silver nitrate aqueous solution for 48 h. Half of the photomask was not covered (irradiated for 7.5 min) to form a control pattern. (right) Corresponding gray values of the image along the red and black lines.²⁴

The formation of a pattern based on PG on PTFE followed by modification with silver particles was confirmed by ToF-SIMS (Figure 2.14B). To demonstrate the unique advantages of UV-assisted polymerization and deposition of plant phenolic compounds, a gradient pattern of PG was formed on the poly(2-hydroxyethyl methacrylate)-*co*-(ethylene dimethacrylate) (poly(HEMA-EDMA) surface.

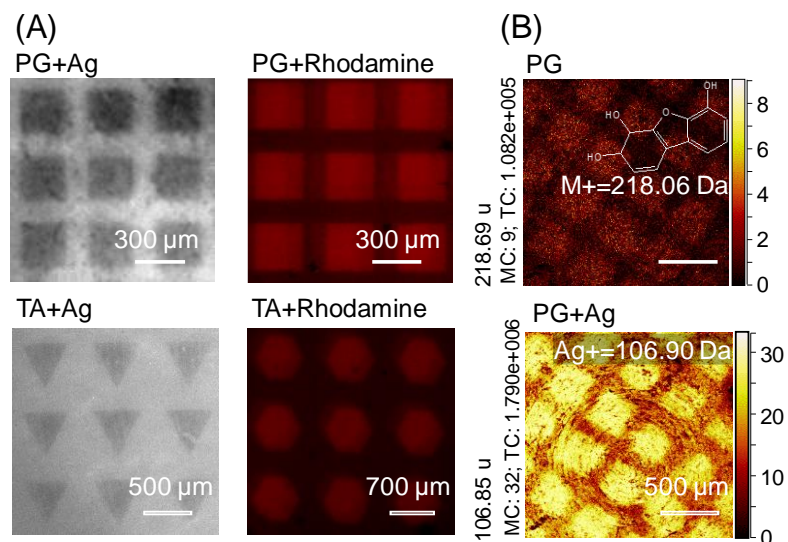


Figure 2.14 (A) Bright-field microscopy image of a silver particle pattern produced on surface of phenolic pattern based on PG (UV, acetate buffer at pH 5.0) or TA (UV, phosphate buffer at pH 7.0) after immersing the substrate in silver nitrate solution for 48 h. Red fluorescence pattern formed by treatment of the phenolic patterns with a rhodamine-thiol solution. (B) ToF-SIMS ion intensity map of a phenolic square pattern (PG, UV, acetate buffer at pH 5.0) on PTFE substrate produced by photopatterning (top), and silver ion intensity map of modified pattern with silver nitrate aqueous solution for 48 h (bottom).²⁴

In order to create a gradient pattern, PG solution (0.01 mg/mL, pH 7.0) was added to the surface, covered by a photomask and by a UV opaque cover. By moving the cover gradually, different regions of the surface were exposed to UV irradiation from 0.0 to 7.5 min generating a gradient of density of the polyphenol coating (Figure 2.13B, Figure 2.15A). To further prove the versatility of this technique, this approach was used to make a pattern of a polyphenol coating inside a microfluidic channel. PG solution (0.01 mg/mL, pH 7.0) was injected into a capillary filled with porous poly(HEMA-EDMA) with a syringe and UV irradiated for 10 min through a photomask (Figure S8.19). Patterned polyphenol coating inside the capillary was further functionalized with silver particles or Rhodamine dye (Figure 2.15B). The observed patterns confirm that multifunctional polyphenolic coating, patterns and gradients can be formed on flat surfaces and on curved interfaces of closed microfluidic channels.

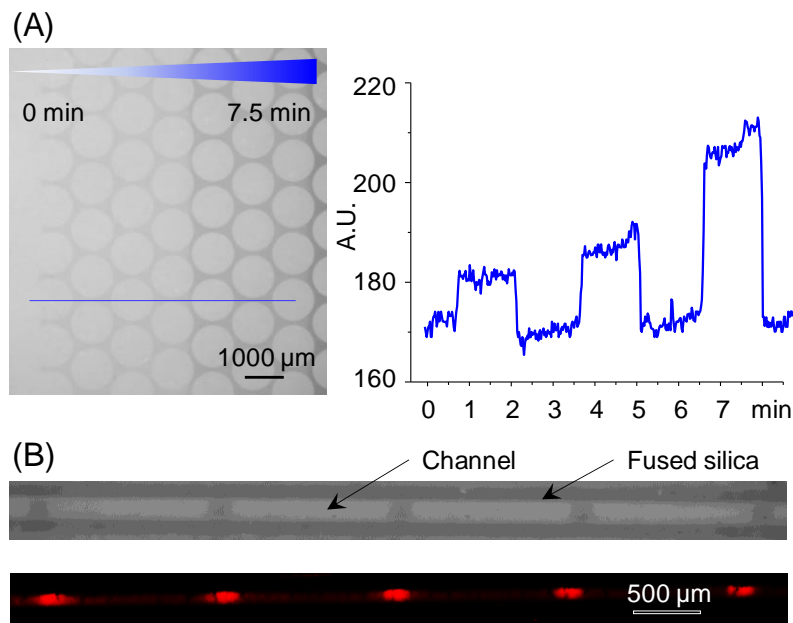


Figure 2.15 (A) Polyphenolic gradient pattern formed by UV irradiation of a poly(HEMA-EDMA) surface in the presence of a PG solution (0.01 mg/mL, pH 7.0). The phenolic pattern was incubated for 48 h in a silver nitrate aqueous solution to obtain a pattern of silver particles. Corresponding gray value vs. UV exposure time along the blue line is shown in the graph (right). (B) Phenolic pattern inside a microfluidic capillary (inner diameter 100 μm). Fused silica capillary filled with a porous polymethacrylate was filled with a pyrogallol solution (0.01 mg/mL, pH 7.0) and irradiated with UV light for 10 min through a photomask. A pattern of silver particles (top) and rhodamine dye (bottom) formed inside the capillary by corresponding post-modification of the polyphenol pattern.²⁴

2.2.5 Coatings from polyphenols present in wine, coffee, and tea

Natural plant phenolic compounds have gained lots of attention due to their antioxidant, antimicrobial, anti-cancer, and anti-inflammatory properties. Plant-derived phenolic compounds are found in various types of beverages and food. Thus, several groups investigated the possibility to create nanocoatings using cocktails of phenolics directly extracted from different beverages.⁵ The advantage of using such mixtures is their availability and low costs. Here it was shown that UV light can also accelerate the polymerization and deposition of phenolic cocktails present in tea, coffee or wine. Figure 2.16 shows the photographs of glass substrate covered with tea, coffee or red wine, after 1 h in the dark and under UV irradiation. The visualization of the coating was performed using a silver nitrate solution. Corresponding

UV-Vis transmittance spectra are depicted in Figure 2.16B. The decrease of transmittance of the coatings after UV irradiation indicates the acceleration of the polymerization and deposition of the phenolics found in these beverages.

Formation of dark layer of silver particles on the glass surface modified with phenolic compounds existing in tea, coffee, and wine after immersion in silver nitrate aqueous solution increased darkness of the glass slides. However, transmittance of glass slides after immersion in tea, coffee, and wine following by immersion in silver nitrate aqueous solution did not change.

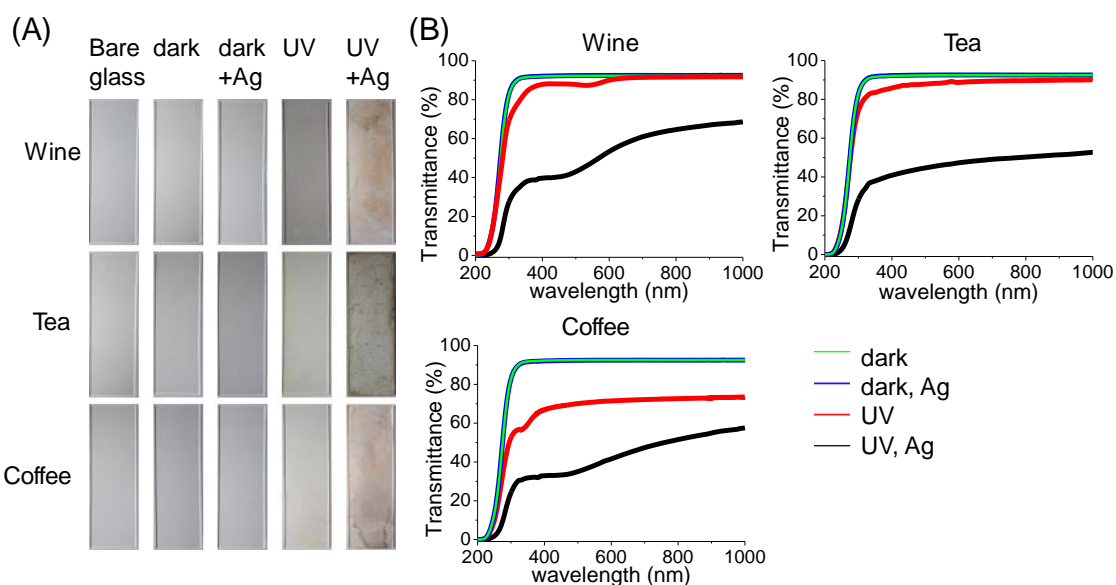


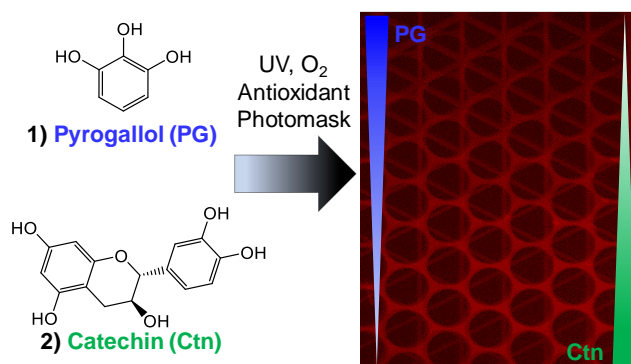
Figure 2.16 Phenolic coatings deposit on surface of glass slides after exposure to wine, tea infusion, and coffee infusion. (A) Photographs of bare glass slides, after 1 h exposure in dark environment, after immersion in silver nitrate aqueous solution for 48 h, and glass slides after 1 h UV irradiation, and 48 h immersion in silver nitrates aqueous solution respectively from left to right. (B) UV-Vis transmittance percentage of glass slides after modification with wine, tea, and coffee in dark and under UV irradiation for 1 h, and after immersion in silver nitrate aqueous solution.²⁴

2.3 Conclusions to chapter 2

In conclusion in this chapter, it was demonstrated that UV irradiation significantly accelerates both polymerization and deposition of various plant-derived phenolic compounds.

The kinetics of oxidative polymerization of plant phenolics depends on the presence of oxygen, ROS and pH of the solution. The pH effect varies for different phenolic compounds. It was shown that increasing ROS concentration in the presence of oxygen or changing the aqueous medium to deuterium oxide solution accelerate the oligomerization of phenolic compounds under UV light, while deoxygenation or addition of ROS scavengers can retard polymerization reaction. This process is general and can be applied to various plant-derived phenolics as demonstrated on pyrogallol, tannic, gallic and caffeic acids as well as natural phenolic compounds present in tea, coffee, and wine. The UV-assisted polymerization and deposition of polyphenols opens the possibility to create patterns and gradients of multifunctional polyphenolic coatings on curved surfaces and inside microfluidic channels in a substrate-independent way. Taking into account the huge diversity, availability and low cost of plant-derived phenolic compounds, this method opens unique opportunities for the spatial and temporal control in the formation of functional plant-derived phenolic nanocoatings and their micropatterns.

Chapter 3. Bioinspired Strategy for Controlled Polymerization and Photopatterning of Plant Polyphenols^a



^a This chapter is adapted from the publication below:²³

Behboodi-Sadabad, F.; Zhang, H.; Trouillet, V.; Welle, A.; Plumeré, N.; Levkin, P. A. Bioinspired Strategy for Controlled Polymerization and Photopatterning of Plant Polyphenols. *Chem. Mater.* **2018**, 30, 1937–1946.

Reprinted (adapted) with permission from (Chem. Mater., 2018, 30 (6), pp 1937–1946, DOI: 10.1021/acs.chemmater.7b04914, Publication Date (Web): February 26, 2018). Copyright (2018) American Chemical Society.

3.1 Introduction

Plant-derived polyphenols were recently introduced for particle and surface modification.^{65,66} Numerous applications in materials science have been already demonstrated including self-healing materials,⁶⁷ surface modification of membranes,⁶⁸ designing novel antioxidants,^{69,70} anticancer drugs,⁷¹ and bioadhesives,⁷² as well as development of drug delivery systems,⁷³ antibacterial coatings and surfaces with reduced biofouling,⁵ energy storage devices,⁷⁴ thin film⁷⁵ and bulk⁷⁶ hybrid functional materials, and immobilization of enzymes.⁷⁷

Phenolic compounds, similar to polycatecholamines such as dopamine (DA), can undergo autoxidation process in the presence of oxidizing agents,⁷³ high-redox-potential enzymes which are suitable for use in oxidative processes,⁷⁸ or in alkaline pH condition.⁶ However, because of the rapid response of phenolic compounds to oxidation, there is a limited control over the kinetics of the oxidation process and spatiotemporal control over the deposition of polyphenols, which leads to the formation of weak and inhomogeneous coatings.³⁶ Formation and deposition of colloidal particles and aggregates have been observed in coatings made of catechol- and pyrogallol-containing compounds.^{36,79} Such colloidal structures on the surface, which cannot be easily avoided in the solution, have been considered as a source of instability and weakness of the anchoring layer and adlayer.³⁶ Several research groups tried to make more homogeneous nanocoatings from polyphenols and DA by using new cyclic catechols,³⁶ norepinephrine (a small molecule catecholamine),⁸⁰ controlling the self-polymerization process of DA by using the $\text{CuSO}_4/\text{H}_2\text{O}_2$ system,¹⁶ and sonication of PDA-coated substrate.⁸¹

Uncontrolled autoxidation and subsequent cross-linking, polymerization, and complexation of catechol and pyrogallol moieties of plant phenolic compounds are dependent on multiple factors, such as pH, buffer strength, concentration, and type of oxidant or enzymes.⁸² Many research groups tried to overcome uncontrolled autoxidation of pyrogallol- and catechol-containing compounds. Qiu et al.⁵² showed that enzyme-induced deposition of tea catechin and chitosan depends on laccase enzyme concentration. Lee et al.⁸³ used sodium periodate, horseradish peroxidase, and mushroom tyrosinase as oxidizing reagents to prepare 3,4-dihydroxyphenylalanine-modified (DOPA-modified) polyethylene glycol (PEG). They observed that the amount of time required for gelation of aqueous PEG-DOPA solution was

dependent on type and concentration of oxidizing agents. Ejima et al.²⁷ showed that multivalent complexation of polyphenols and Fe^{III} ions and film formation are directed by pH value of the solution. Barrett et al.⁶ investigated the effect of pH on polymerization and deposition of a variety of plant phenolic compounds to find the optimum pH condition for nanocoating deposition. Hong et al.⁸⁰ used norepinephrine, a small-molecule catecholamine, in combination with dopamine to achieve a well-controlled coating morphology. Formation of 3,4-dihydroxybenzaldehyde-norepinephrine intermediates is considered as the main mechanism of the controlled oxidation process, leading to formation of a highly smooth nanocoating.

To form multifunctional coatings on the surface, our group²⁴ and other groups^{29,30,84} used UV light to induce oxidation of catechol- and pyrogallol-containing compounds which enabled the control of the kinetics of the polymerization and deposition of these compounds spatiotemporally. Several research groups^{5,6,30,65} including ours²⁴ showed that spontaneous oxidation of plant phenolic compounds can be inhibited by using acidic pH conditions. However, this method may not be applicable to all phenolic compounds because of low solubility of some phenolic compounds at low pH.⁶

Oxidation intermediates of phenolic compounds such as quinones are more stable at mild acidic condition (pH 5.7-6.7), decreasing the rate of cross-linking, polymerization, and metal ion complexation.²⁴ Cross-linking of catechol- or pyrogallol-containing molecules by nucleophiles²⁵ or their binding to tissues and proteins⁸² can be inhibited under acidic conditions.

Therefore, there is a clear need to develop a new strategy to control polymerization and cross-linking of plant phenolic compounds under basic pH. It is generally accepted that reactive oxygen species (ROS) can oxidize catechol and gallol moieties in plant-derived phenolics to generate reactive species such as phenolate ion, phenolic radicals, semiquinone, and quinone. Active quinone groups undergo phenolic coupling or react with nucleophiles such as thiols and amines.⁸⁵

Our group investigated^{24,28} the role of reactive oxygen species [ROS, singlet oxygen (¹O₂), superoxide radical (O^{2-•}) and hydroxyl radical (•OH)] in UV-induced oxidation and polymerization of dopamine and plant phenolic compounds using spectroscopic and electrochemical methods. In human cells many antioxidants, such as sodium ascorbate (SA),

uric acid (UA), and glutathione (GSH), can directly react with ROS or free-radical intermediates induced by ROS (Scheme S9.1) and terminate the ROS-induced damage.⁸⁶

Recently, inspired by the ROS scavenging ability of sodium ascorbate (vitamin C) in the human body, it was demonstrated that dopamine polymerization in basic solution can be inhibited by sodium ascorbate that reduces reactive dopamine quinone and delays dopamine polymerization.²⁸ Several research groups discussed the mechanism of action of the natural antioxidant compounds including SA,⁸⁷ UA,⁸⁸ and GSH.⁸⁹ SA changes to the ascorbate radical by donating an electron to lipid radicals to terminate the lipid peroxidation chain reaction.⁹⁰ The pairs of ascorbate radicals react rapidly to produce one molecule of ascorbate and one molecule of dehydroascorbate.⁹⁰ Uric acid and glutathione are physiological natural antioxidants. Uric acid is the most abundant aqueous antioxidant found in humans.⁹¹ It contributes to as much as two-thirds of all free-radical scavenging activities in the plasma.⁹¹ The oxygen radical scavenging activity of glutathione directly expedites the ROS neutralization and the repair of ROS-induced damage. The presence of the sulfhydryl group in glutathione allows it to serve as an antioxidant.⁹⁰

In this chapter, inspired by the intrinsic function of natural antioxidants to scavenge ROS in plants, animals, and human cells, a method to control the polymerization and surface functionalization by plant-derived phenolic compounds in alkaline conditions (pH 8.0) is presented. The method combines the effect of polymerization inhibition by antioxidants with the ability of UV light to trigger the polymerization of phenolic compounds, enabling spatiotemporal control of the polymerization and deposition of various plant-derived phenolic compounds. It should be noted that phenolic compounds are antioxidants by themselves, which require a stronger reducing agent to inhibit their oxidation at basic pH.

Interestingly, this method leads to more homogeneous polyphenolic films deposited on the surface. UV-induced oxidation and polymerization of pyrogallol (PG), gallic acid (GA), pyrocatechol (CtI), epigallocatechin gallate (EGCG), tannic acid (TA), catechin (Ctn), hydroxyhydroquinone (HHQ), caffeic acid (CA), and morin, some of the most common plant-derived phenolic compounds (Figure 3.1), in the presence of sodium ascorbate (SA), glutathione (GSH), and uric acid (UA) as natural antioxidants were studied.

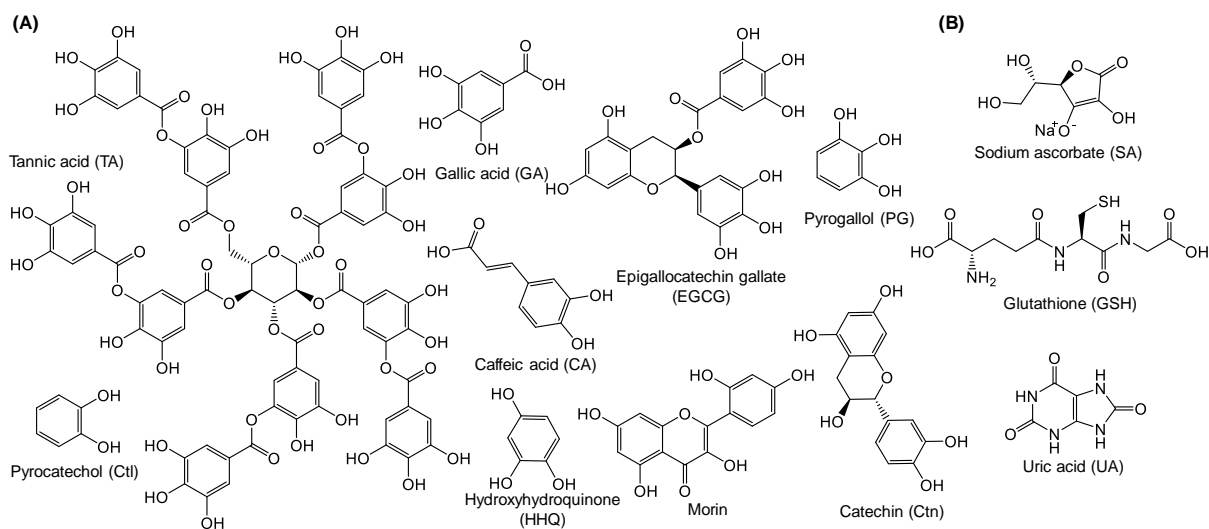


Figure 3.1 Chemical structures of plant-derived natural phenolic compounds commonly used for preparing functional polyphenolic coatings (A) and structures of physiologically important antioxidants (B).

3.2 Results and discussion

To investigate our hypothesis that natural antioxidants can inhibit polymerization and deposition of natural phenolic compounds under basic conditions first UV-vis spectroscopic and differential pulse voltammetric analysis of plant phenolic solutions at pH 8.0 in the presence or absence of antioxidants both in dark and under UV irradiation was performed. UV-vis spectra of PG solution (0.2 mg/mL) with different SA/PG molar ratios from 0:1 up to 1.2:1 were measured in the dark and under UV irradiation (Figure 3.2,3). UV absorbance at 320 nm (at 380 nm for TA) was selected as an indication of quinone formation in the solution to monitor oxidation and polymerization of the phenolic compounds.

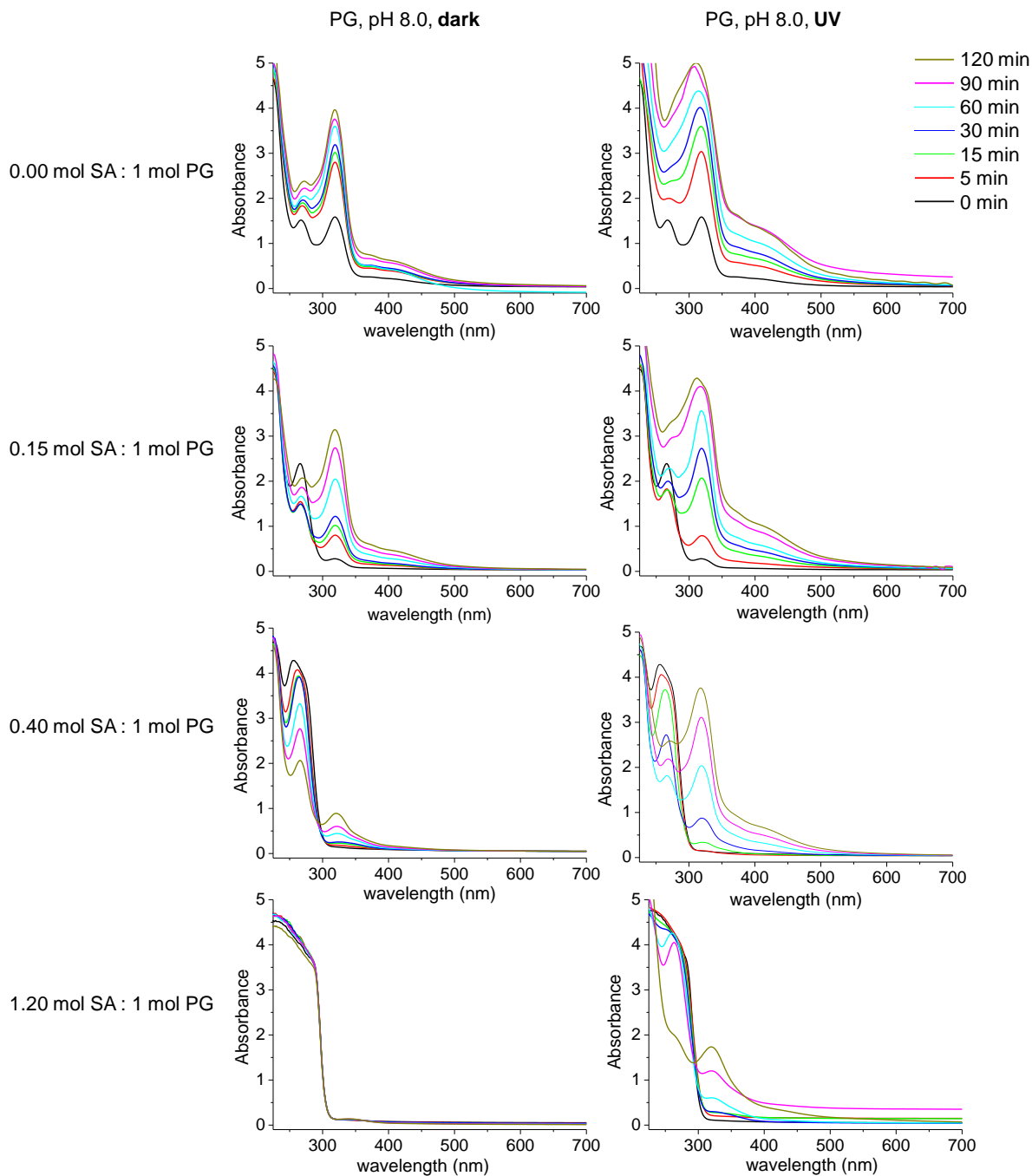


Figure 3.2 UV-vis spectra of PG solution (0.2 mg/mL) at phosphate buffer 5 mmol/L at pH 8.0, stored in dark environment (left) and after UV irradiation (right) containing SA measured at different time intervals.²³

The results demonstrate that oxidation of PG begins immediately at pH 8.0 either in the dark or under UV irradiation. By increasing the amount of SA present in the solution, however, the rate of oxidation of PG decreases for both samples (Figure 3.3).

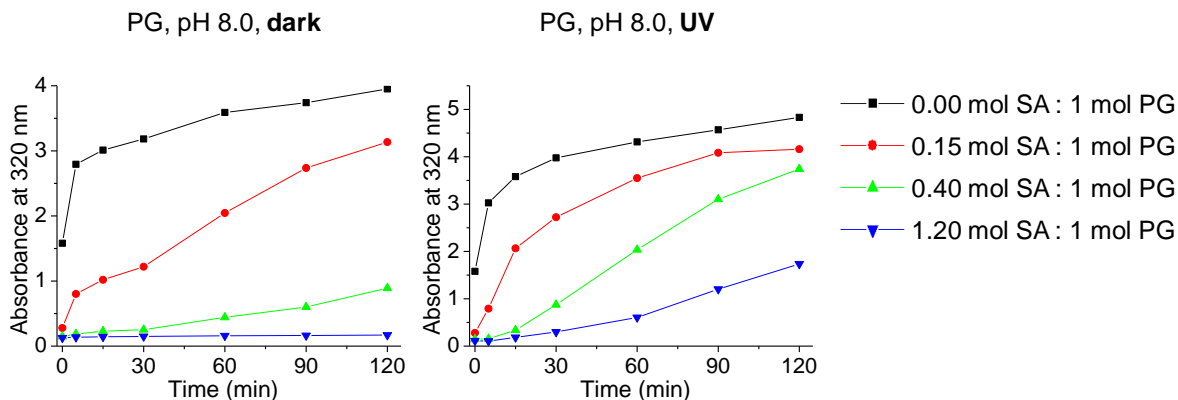


Figure 3.3 Effect of natural antioxidants on PG polymerization with and without UV irradiation. The graphs show UV absorbance of PG solutions (0.2 mg/mL, phosphate buffer 5 mmol/L, pH 8.0) at 320 nm. PG polymerization solution in the dark (left) and under UV irradiation (right) in the presence of SA (with different molar ratios of antioxidants to PG).²³

At the molar ratio as high as 1.2:1 (SA/PG), the oxidation of PG in the dark environment is completely ceased for at least 72 h (Figure 3.4A), while UV irradiation of the sample at 260 nm (6 mW/cm^2) triggered the oxidation and polymerization process, resulting in a 15-fold increase of UV absorbance at 320 nm (from 0.11 to 1.73) already after 2 h (Figure 3.4B). The color of the PG solution stored in dark did not change in the presence of SA/PG 1.2:1 molar ratio. However, color of the same PG solution irradiated with UV light for 2 h and color of the PG solution without SA changed over time (Figure 3.4C).

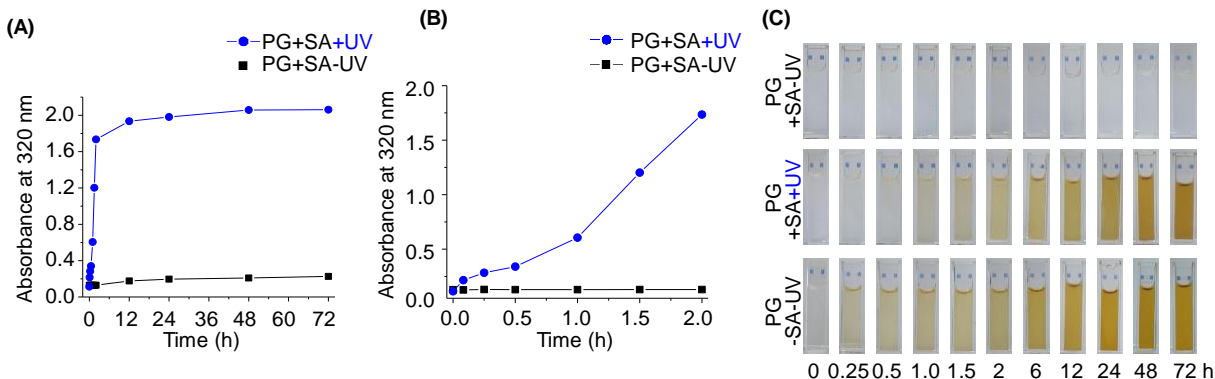


Figure 3.4 (A) Effect of natural antioxidants on PG oxidation in dark and under UV irradiation. The graphs show UV absorbance of PG solutions (0.2 mg/mL of PG in phosphate buffer, 5 mmol/L, pH 8.0) at 320 nm. (A) UV absorbance of PG solution over 72 h stored in the dark or after 2 h of UV irradiation. (B) UV absorbance at 320 nm of PG solution with SA (SA/PG 1.2:1 molar ratio) and without SA in dark and under UV irradiation. (C) Corresponding photographs of each sample.²³

Electrospray ionization time-of-flight mass spectrometry (ESI-TOF) of the pyrogallol solution (pH 8.0, 5 mmol/L, SA/PG molar ratio of 1.2:1) indicated the generation of higher-molecular-weight species after UV irradiation of the solution for 2 h (Figure 3.5A).

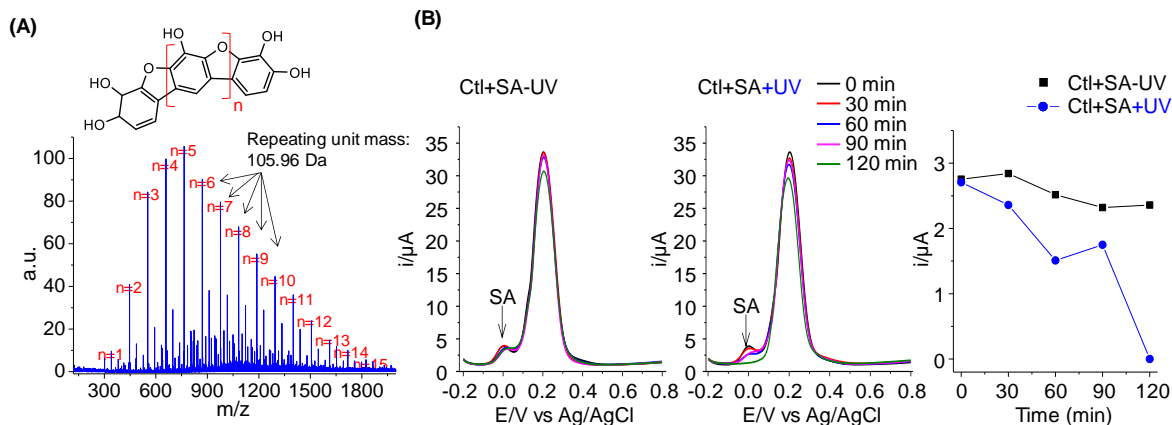


Figure 3.5 (A) ESI-MS spectra (positive mode) of the PG solution (0.2 mg/mL of PG in phosphate buffer, 5 mmol/L, pH 8.0; 1.2:1, SA/PG molar ratio) after UV irradiation for 2 h indicates generation of higher-molecular-weight species with a repeating unit of 105.96 Da. (B) Differential pulse voltammetry (DPV) of Ctl solution (0.2 mg/mL of Ctl in phosphate buffer, 5 mmol/L, pH 8.0; 0.6:1, SA/Ctl molar ratio) with KCl (0.1 mol/L) at activated glassy carbon disk electrodes stored in dark (left) or under UV irradiation (middle) for 2 h. Peak currents for SA oxidation (at 0 V vs Ag/AgCl KCl 3 mol/L) vs time in dark and under UV irradiation (right).²³

A repeating unit with the mass of 105.96 Da was observed in the mass spectra which corresponds to a structure shown in Figure 3.5B.

3.2.1 *Antioxidant-controlled oxidation of plant phenolic compounds*

To show that antioxidant-controlled oxidation of plant phenolic compounds is a general concept, glutathione (GSH) and uric acid (UA) were used to study the kinetics of PG oxidation at pH 8.0 both in dark and under UV irradiation by UV-vis spectroscopy (Figures S9.2-5). Presence of glutathione at GSH/PG 0.8:1 molar ratio could inhibit the oxidation of PG for 2 h (Figure S9.2). However, 2 h of UV irradiation of the same sample caused a 13-fold increase in UV absorbance at 320 nm (from 0.09 to 1.22) (Figure S9.3). A similar effect was observed by using uric acid (UA) as a reducing agent (Figure S9.4). At UA/PG 1.40:1 molar ratio, oxidation of PG was significantly slowed down in dark, while UV irradiation triggered the oxidation of PG, and the UV absorbance of the PG solution increased 6-fold (from 0.55 to 3.45) after UV irradiation (Figure S9.5).

To show that natural antioxidants can be used to effectively control the rate of oxidation of other natural plant-derived phenolic compounds, a library of plant phenolic compounds including gallic acid (GA), pyrocatechol (Ctl), epigallocatechin gallate (EGCG), tannic acid (TA), catechin (Ctn), hydroxyhydroquinone (HHQ), caffeic acid (CA), and morin was investigated. Basic solutions of the phenolic compounds (pH 8.0, 5 mmol/L phosphate buffer) containing different concentrations of SA were analyzed by UV-vis spectroscopy after UV irradiation for 2 h or storage in the dark. Addition of SA to the solutions at pH 8.0 decreased the rate of oxidation both in dark and under UV irradiation (Figures S9.6-13). At SA/phenol molar ratios listed in Table 3.1, oxidation of phenolic compounds is completely stopped for at least 2 h in the dark. However, UV irradiation at these molar ratios could still trigger the oxidation followed by an increase in UV absorbance (Figures S9.6-13). The pH value of the solutions after addition of antioxidants did not change confirming that the inhibition ability of the antioxidants was a result of their ROS scavenging and reducing properties.

Table 3.1 SA:phenol molar ratios at which oxidation of phenolic compounds is completely stopped for at least 2h.

Plant phenolic compound	SA:phenol molar ratio
PG	1.20
GA	0.44
Ctl	0.60
EGCG	2.20
TA	2.15
Ctn	1.50
HHQ	1.90
CA	0.50
Morin	1.50

3.2.1 Effect of sodium ascorbate and UV light on oxidation of polyphenols

To confirm the inhibition effect of SA and the UV acceleration effect on the polymerization of plant phenolic compounds at pH 8.0, electroanalytical methods were used to monitor the change in the SA oxidation peak response as a measure of the SA concentration. We used differential pulse voltammetry (DPV) with specifically activated glassy carbon electrodes to discriminate the respective signals of SA, Ctl, and CA in the SA-phenol mixtures. The SA oxidation in the SA-phenol mixtures appears as a small prepeak or shoulder (at 0 V versus Ag/AgCl) of the larger Ctl or CA oxidation peak at 0.2 and 0.25 V versus Ag/AgCl, respectively (Figure 3.5B, Figure 3.6, and Figure S9.14). Monitoring of SA by means of DPV demonstrates that the oxidation rates of SA increased after UV irradiation of the solution for 2 h (Figure 3.5B). This phenomenon can be attributed to the formation of ROS from dissolved oxygen under UV irradiation, such as singlet oxygen ($^1\text{O}_2$), superoxide radicals ($\text{O}^{2-\bullet}$), or hydroxyl radicals ($\bullet\text{OH}$).

Under UV irradiation, the DPV results of CA display a new peak around 0.35 V versus Ag/AgCl assigned to intermediates of the polymerization processes. In absence of SA, the peak for CA almost fully disappears within only 30 min of irradiation. In the presence of SA, while polymerization intermediates are still detected, the CA peak only decreases moderately within 2 h (Figure S9.14). Overall, the consumption of SA in the SA-phenol mixture and the fast consumption of phenols in the SA-free solutions confirm that the SA functions as a reductant decreasing the rate of phenolic compound oxidation both in dark and under UV irradiation.

Thus, phenolic compounds being natural antioxidants by themselves can be kept in their reduced form in the presence of stronger reducing agents such as SA.

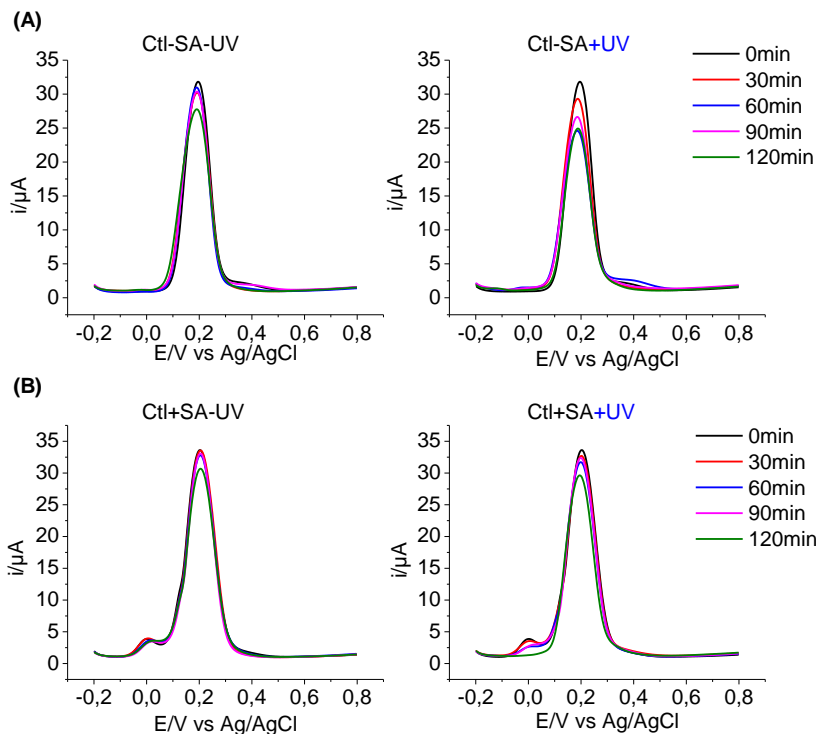


Figure 3.6 Differential pulse voltammetry (DPV) in phosphate buffer (5 mmol/L, pH 8.0) with KCl (0.1 mol/L) at activated glassy carbon disk electrodes for (A) Ctl solution (1.58 mmol/L of Ctl in phosphate buffer, 5 mmol/L, pH 8.0) stored in dark (left) or under UV irradiation (right) for 2h and (B) SA-Ctl solution (1.58 mmol/L of Ctl in phosphate buffer, 5 mmol/L, pH 8.0; 0.6:1, SA:Ctl molar ratio) stored in dark (left) or under UV irradiation (right) for 2h.²³

3.2.2 On-demand polymerization and deposition of polyphenols

UV-vis spectroscopy and electrochemistry results demonstrate the ability of natural antioxidants to effectively inhibit the oxidation of plant phenolic compounds under basic conditions, while UV irradiation can be used for the temporal control of the oxidation and polymerization of polyphenolic compounds. To exemplify this possibility, a PG solution with the GSH additive (GSH/PG molar ratio of 0.8:1; pH 8.0) was used, which does not oxidize for 120 min (Figure 3.7).

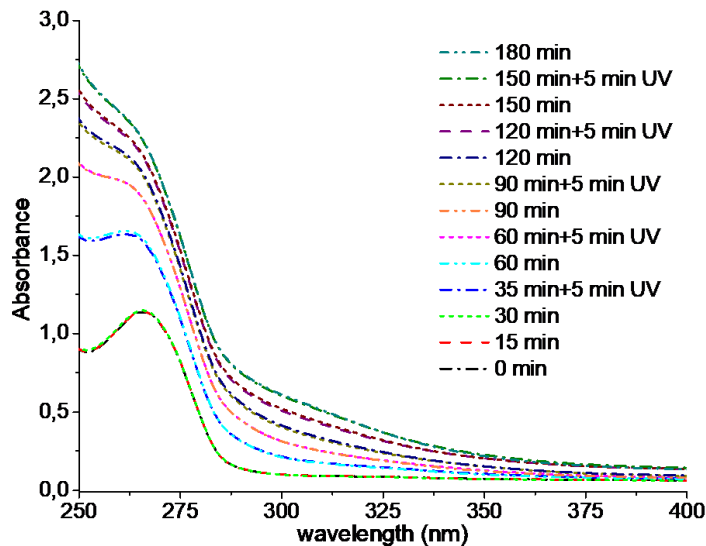


Figure 3.7 On-demand polymerization of PG. UV Absorbance of the PG solution (0.2 mg/mL, phosphate buffer 5 mmol/L, pH 8.0) containing GSH with GSH:PG molar ratio of 0.8:1 at 320 nm as a function of time.²³

However, irradiating the solution for 5 min at any moment triggered the oxidation of PG leading to an immediate increase in the UV absorbance at 320 nm from 0.08 to around 0.15 (Figure 3.8A). In this case, the polymerization of PG does not continue after the UV pulse. However, if the UV irradiation continues, oxidation, polymerization, and deposition of PG steadily continue further as indicated by a gradual increase in UV absorbance at 320 nm (Figure 8.7B). By repeating the UV irradiation for 5 min followed by storing in dark, it was possible to drive the oxidation process of PG to the desired stage at each particular time point for several times (Figure 3.8C), thereby making a stepwise control of the polymerization of PG possible in the presence of antioxidant.

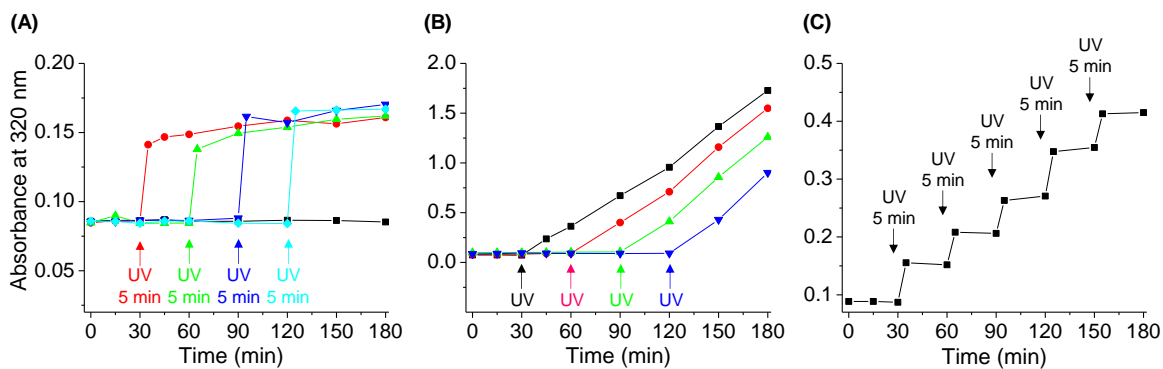


Figure 3.8 On-demand initiation and termination of PG polymerization in the presence of GSH (GSH/PG molar ratio of 0.8:1, phosphate buffer 5 mmol/L, pH 8.0). (A) By UV irradiation of a different GSH-PG solution at different time intervals, PG polymerization can be initiated, and by removing UV light, the polymerization reaction stops again. (B) As long as dormant GSH-PG solution is irradiated with UV light, polymerization initiates and proceeds. (C) Polymerization of PG proceeds stepwise by irradiating the GSH-PG solution for 5 min at different time intervals.²³

In a control experiment, the PG solution without GSH was irradiated with UV pulses for 5 min at 0, 25, and 55 min, and the UV absorbance at 320 nm was measured. In the absence of antioxidant, continuous autoxidation of PG was observed even after the UV pulses (Figure 3.9).

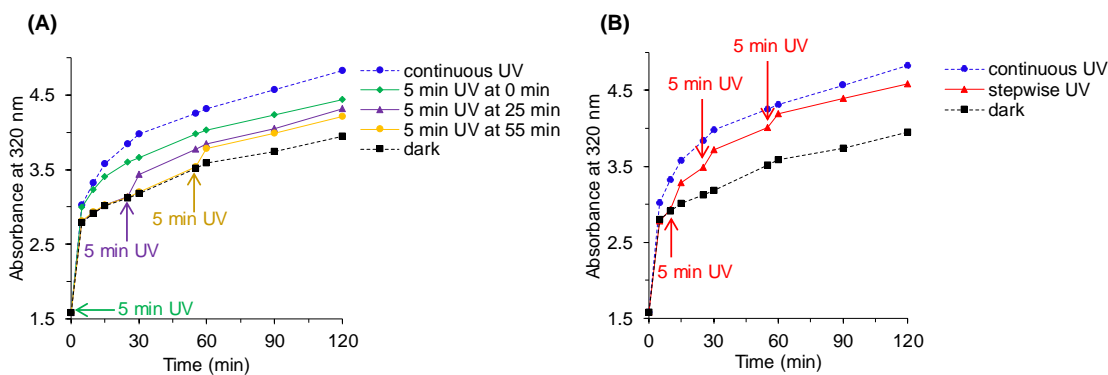


Figure 3.9 Timewise UV irradiation of PG solution (0.2 mg/mL, phosphate buffer 5 mmol/L, pH 8.0) in the absence of antioxidants. UV Absorbance of the PG solution at 320 nm as a function of time recorded after 5 min UV pulse at 0 min, 25 min, and 55 min (A), and after multiple 5 min UV pulse at 10 min, 25 min, and 55 min (B).²³

The formation of polyphenolic layers and its homogeneity on a silicon wafer surface in the presence and absence of SA and with or without UV irradiation was investigated. AFM analysis demonstrated no coating on a surface treated with an SA/PG solution (0.2 mg/mL, 5 mmol/L phosphate buffer, pH 8.0; SA/PG molar ratio 0.4:1) without UV irradiation. The same procedure with 30 min of UV irradiation resulted in the formation of a 4 nm thin coating with 0.98 nm roughness (R_q) (Figure 3.10, Figure S9.15). The polyphenolic layer formed on a silicon wafer in a PG solution without SA and with no UV light was 4 nm thick with R_q roughness 2.33 nm (Figure 3.10, Figure S9.15). The same protocol but with 30 min of UV irradiation results in a 5 nm coating being also highly inhomogeneous with R_q of 3.51 nm (Figure S9.15). Thus, addition of SA into the PG solution resulted in the deposition of a more homogeneous polyphenolic layer, deposition of which could be temporally controlled by UV irradiation.

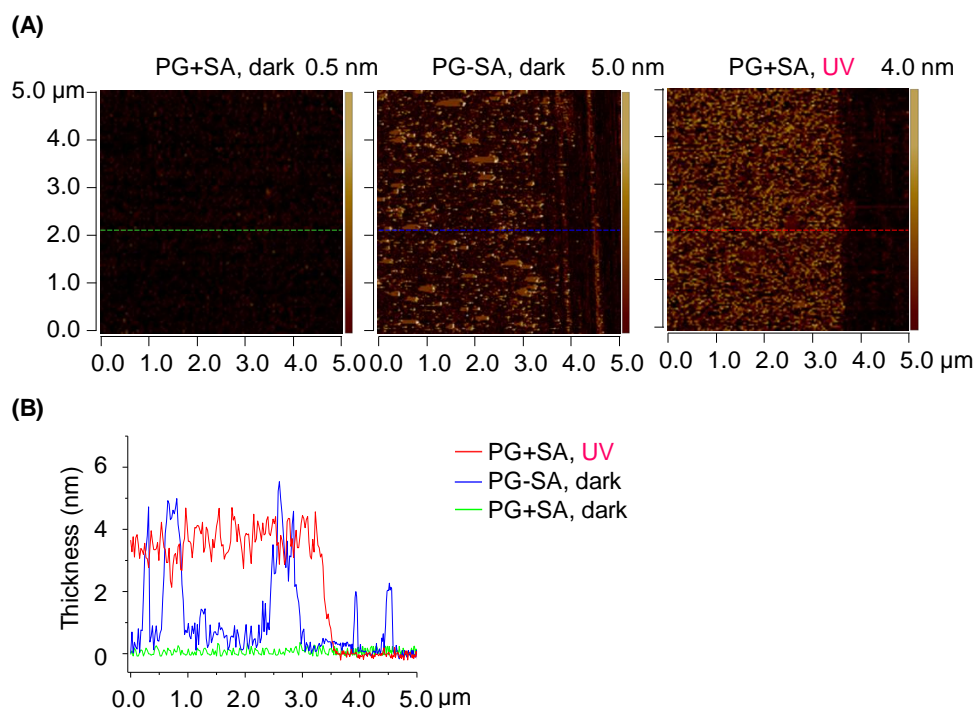


Figure 3.10 (A) AFM on silicon surfaces exposed to PG solution at pH 8.0 (5 mmol/L) with SA in dark (left), without SA in dark (middle), and with SA after 30 min of UV irradiation, gently scratched by tweezers. (B) Surface topographies measured along the dashed lines (graph).²³

Roughness (R_q) of the phenolic nanocoating on the silicon surface was measured for samples without antioxidants stored in dark environment, and for UV-irradiated samples containing SA. A lower value of R_q was observed in Ctl, EGCG, TA, and HHQ samples containing SA compared to the samples without SA (Figure 3.9). However, R_q of Ctn and morin remained almost constant for the samples with and without SA (Figure 3.9). Different roughnesses obtained with or without SA could be due to the difference in the kinetics of oxidation and deposition of each phenolic compound in the presence or absence of SA.

Precipitation or surface adsorption of insoluble higher molecular-weight oligomers and adsorption of colloidal polymer particles, formed from self-assembled polyphenol oligomers in solution, are the main mechanisms for the formation of coatings based on polyphenolic compounds.⁵

Through a change in the oxidation condition from dark to UV-exposed environment, kinetics of the oxidation of phenolic compounds was accelerated as it was seen in UV-vis spectroscopy and electrochemistry analysis. However, the overall oxidation behavior of the phenolic compounds (such as peak shapes and peak positions in UV-vis and electrochemistry graphs) remained almost constant in dark and under UV.

In our previous work,²⁴ similar behavior was observed for different plant phenolic compounds at both acidic and basic solutions. Second, nanoparticle-like aggregates were observed on the surface after coating deposition from phenolic compounds both in dark and under UV (Figures 3.10 and Figure 3.11).

Similar behavior of oxidation and deposition observed in UV-vis spectroscopy, electrochemistry, and AFM images suggests that similar radical intermediates formed during the oxidation process in dark and under UV irradiation.

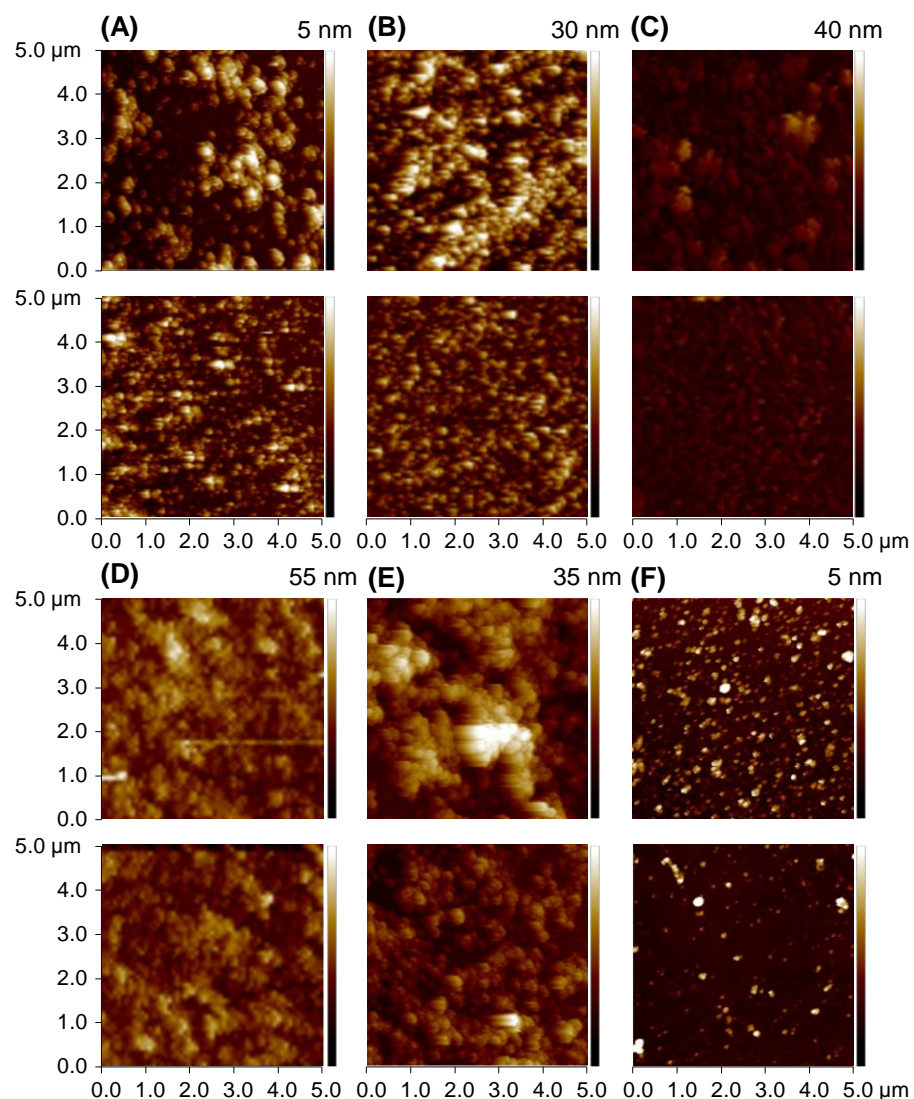
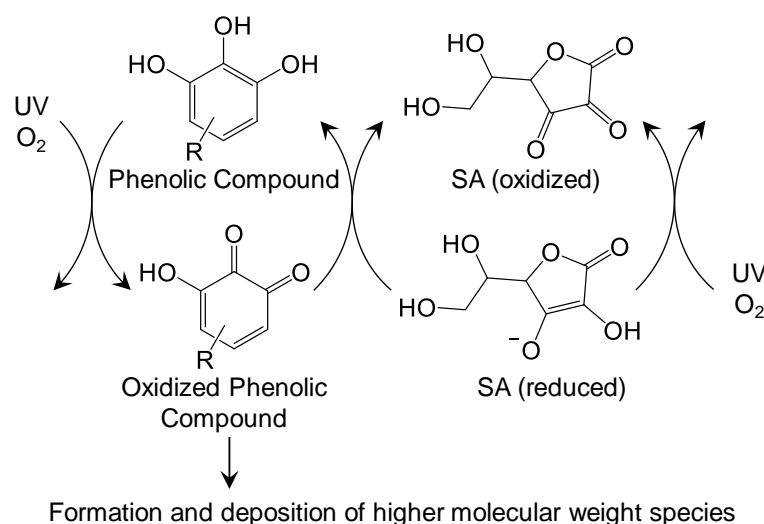


Figure 3.11 AFM images of phenolic layer made on silicon surfaces exposed to phenolic solutions at pH 8.0 without Antioxidant (top image) stored overnight in dark environment, and phenolic solutions containing SA irradiated with UV light for 30 min (bottom image). (A) Ctl, $R_q(\text{top, bottom})=(4.11 \text{ nm}, 3.03 \text{ nm})$. (B) EGCG, $R_q(\text{top, bottom})=(20.1 \text{ nm}, 12.5 \text{ nm})$. (C) TA, $R_q(\text{top, bottom})=(25.2 \text{ nm}, 11.4 \text{ nm})$. (D) Ctn, $R_q(\text{top, bottom})=(38.3 \text{ nm}, 36.5 \text{ nm})$. (E) HHQ, $R_q(\text{top, bottom})=(26.2 \text{ nm}, 15.9 \text{ nm})$. (F) Morin, $R_q(\text{top, bottom})=(3.72 \text{ nm}, 2.83 \text{ nm})$.²³

UV-vis spectroscopy, mass spectrometry, electrochemical analysis, and AFM results indicate that UV irradiation could accelerate polymerization and deposition of plant phenolic compounds, whereas SA is able to inhibit the oxidation of phenols either through direct

scavenging of ROS in the solution or via reducing of quinone moieties of phenols. On one hand, ROS can increase consumption of SA, and on the other hand, ROS accelerates oxidation rate of phenols as was reported before.²⁴

The principle of antioxidant-controlled oxidation of phenolic compounds in the presence of sodium ascorbate (SA) is depicted in Scheme 3.1. Light is uniquely suited for spatiotemporal control of reactions and surface functionalization. The ability to use UV light to trigger polymerization and deposition of structurally diverse natural phenolic compounds, under alkaline conditions where such polymerization and deposition is the fastest, opens endless opportunities for the formation of functional polyphenol patterning, copatterning of different phenolic compounds, and patterning of phenolics inside of closed systems nonaccessible to stamping methods.



Scheme 3.1 Schematic Illustrating Antioxidant-Controlled Oxidation of Plant Phenolic Compounds.²³

3.2.3 Multiple patterns of polyphenols

For evaluation of the ability to pattern phenolic compounds, the poly(2-hydroxyethyl methacrylate)-*co*-(ethylene dimethacrylate) (poly(HEMA-EDMA)) surface was coated with a solution of PG (0.2 mg/mL, phosphate buffer 5 mmol/L, pH 8.0, SA/PG molar ratio 0.4:1), which was covered with a quartz photomask, followed by 10 min of UV irradiation. The surface

was then washed with deionized (DI) water and ethanol followed by drying with N₂. For visualization of the patterns, the surface was immersed in silver nitrate aqueous solution (10 mmol/L) or Rhodamine 110 solution (0.1 g/mL) overnight (Figure 3.12).

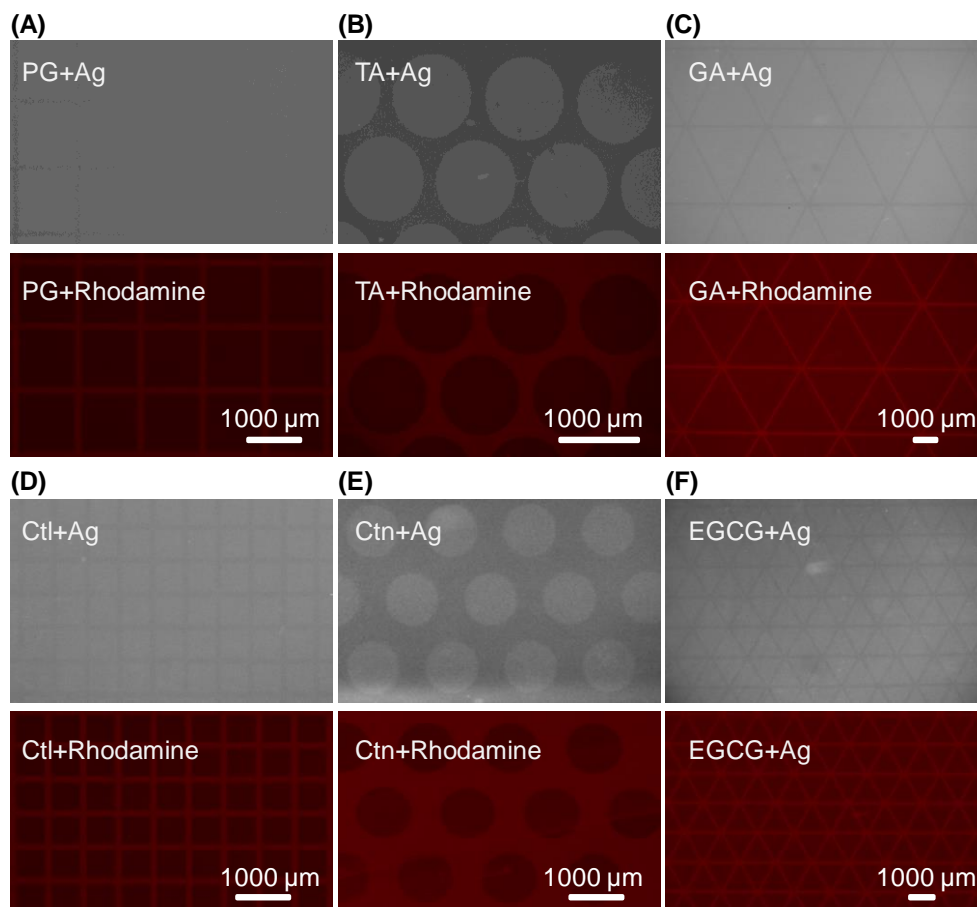


Figure 3.12 Photopatterning of different plant phenolic compounds in the presence of SA in phosphate buffer (5 mmol/L, pH 8.0). (A-F) Micropatterns of PG, TA, GA, Ctl, Ctn, and EGCG on poly(HEMA-EDMA) surfaces by UV irradiating of the phenolic precursor solution containing SA through a photomask for 10 min. The micropatterns were post modified by silver or Rhodamine. The images were obtained by bright field (top) and fluorescence (bottom) microscopy.²³

With this method patterns using various phenolic compounds with features down to 10 μm were created (Figure 3.12A-F). The possibility to create multiple patterns by a sequential wetting of the same surface with different phenolic compound solutions and their UV irradiation for 10 min using a photomask was evaluated (Figure 3.13). The autofluorescence characteristic

of plant phenolic compounds^{92,93} was used to image the patterns. The patterns were visualized by immersing them in silver nitrate aqueous solution overnight (Figure 3.13A,B, bright-field image). Overlaid patterns of different phenolic compounds are shown in Figure 3.13B.

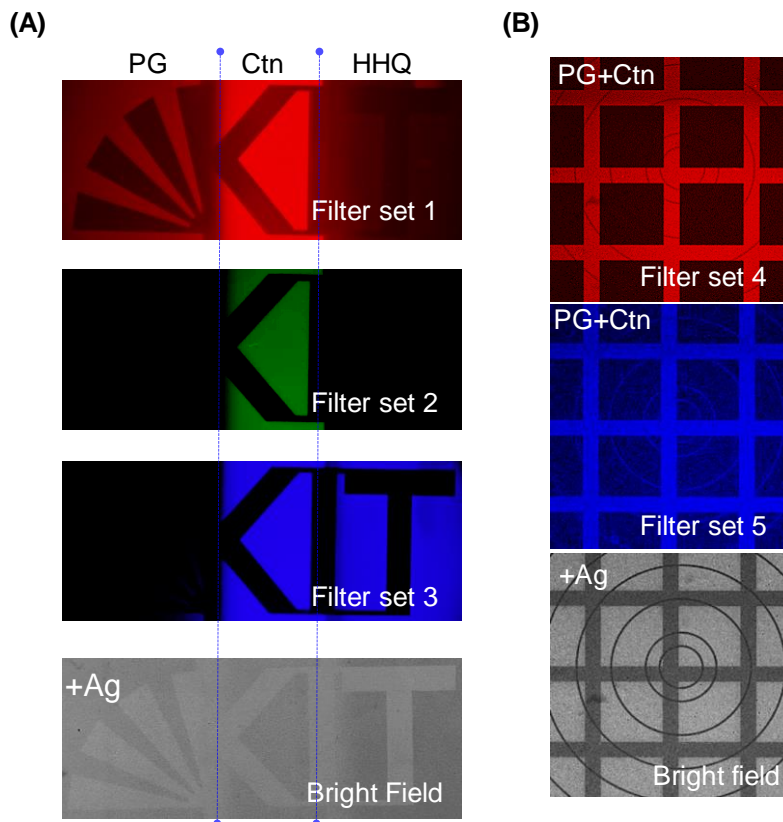


Figure 3.13 Sequential patterning of polyphenols in the presence of SA at pH 8.0 after UV irradiation through a photomask for 10 min. (A) Left part of the KIT logo was prepared using PG solution modified with Rhodamine 110; “K” and “T” letters, middle and right part of the logo, were made using Ctn and HHQ solutions, respectively. Filter sets 1, 2, and 3 were used to visualize the different coatings. Brightfield microscopy images of the “KIT” pattern modified with silver particles (bottom). (B) Overlaid pattern formed on the surface by first UV irradiating PG solution through a photomask with circular patterns, followed by washing and Rhodamine modification. The second pattern was formed on the surface by UV irradiating the Ctn solution through a photomask with square patterns. Fluorescence microscopy images were taken using filter sets 4 and 5. Bright-field microscopy images of the silver-modified pattern (bottom).²³

ToF-SIMS analysis of the patterns indicated deposition of polyphenolic patterns on the surface (Figure 3.14). The results (Figure 3.13,14) demonstrate clear patterns of different

phenolic compounds, indicating the lack of deposition of phenolics in the areas shielded from UV light.

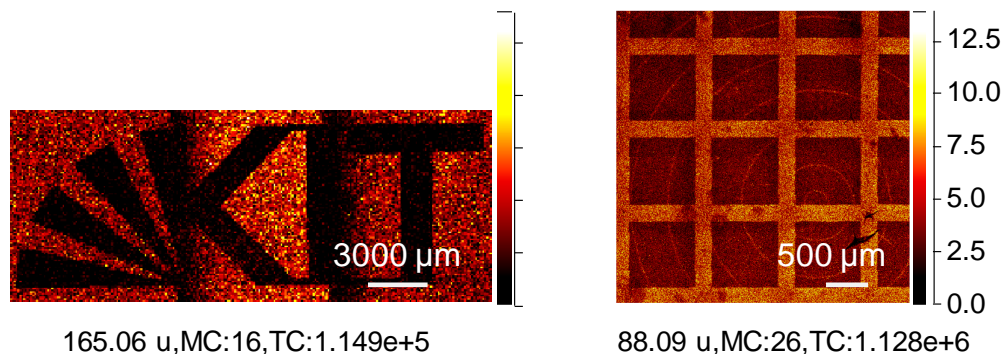


Figure 3.14 ToF-SIMS analysis confirms the deposition and distribution of the phenolic mass fragments on the surface.²³

Bright-field microscopy, fluorescence, and X-ray photoelectron spectroscopy (XPS) analysis (Figure 3.15) clearly indicate the ability to postmodify the polyphenolic micropatterns.

Secondary modification of a phenolic pattern based on PG with silver particles was analyzed by XPS. Since the poly(HEMA-EDMA) surface contains a lot of C-O species, no clear difference in the C 1s spectrum can be observed after coating with different phenolic compounds.

The introduction of silver in the coated regions allows the further detection of the doublet Ag 3d and its mapping on a defined area of a structured sample consisting of lines (polyphenolic coating) and squares (non-coated).

The obtained spectra were analyzed with principal component analysis (Figure 3.15A) in order to improve the differentiation of the different regions. The spin-orbit doublet with Ag 3d_{5/2} at 368.2 eV can be clearly found on the line whereas just a noisy signal is detected in the squares (Figure 3.15B).

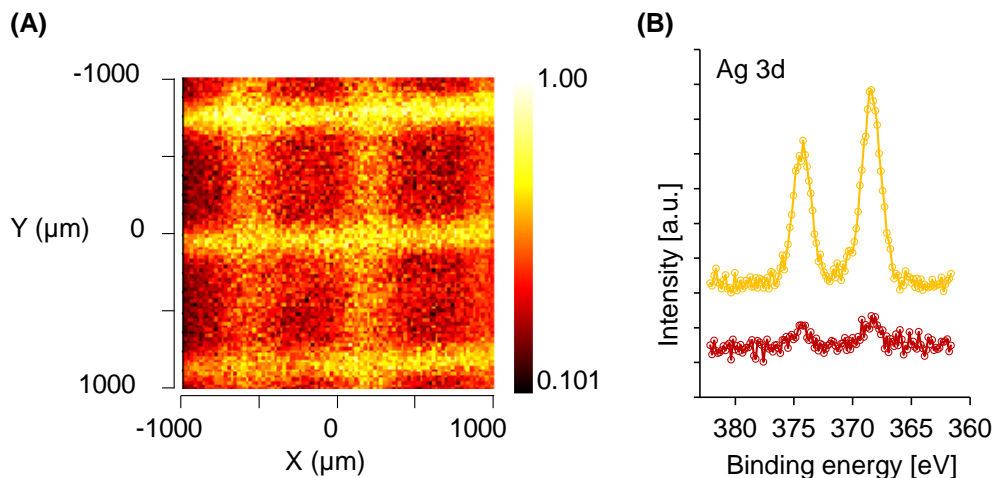


Figure 3.15 XPS Characterization of silver deposition on the phenolic pattern. A phenolic pattern was deposited on the surface by irradiating PG solution (0.2 mg/mL, phosphate buffer 5 mmol/L, pH 8.0) containing SA with SA:PG 0.3:1 molar ratio through a photomask. The pattern was secondary modified with silver particles by immersing in silver nitrate aqueous solution overnight and subsequent washing with water and drying with N₂ (A) Principal Component Analysis of all Ag 3d spectra of the area was carried out. The yellow lines show the presence of Ag whereas the dark squares prove the absence of Ag. (B) Ag 3d XP spectra measured on the line (yellow curve on top) and in the square (red curve on bottom) clearly indicates deposition of silver on the phenolic pattern.²³

3.2.4 Patterning inside microfluidic channels and gradients

Last but not least, the ability to create patterns of phenolic compounds (PG 0.2 mg/mL, phosphate buffer 5 mmol/L, pH 8.0, SA/PG molar ratio 0.4:1, 10 min of UV irradiation through a quartz photomask) inside of microfluidic channels (Figure 3.16A) and formation of gradients of the polyphenolic coatings using a moving mask was demonstrated (Figure 3.16B, Figure 3.17).

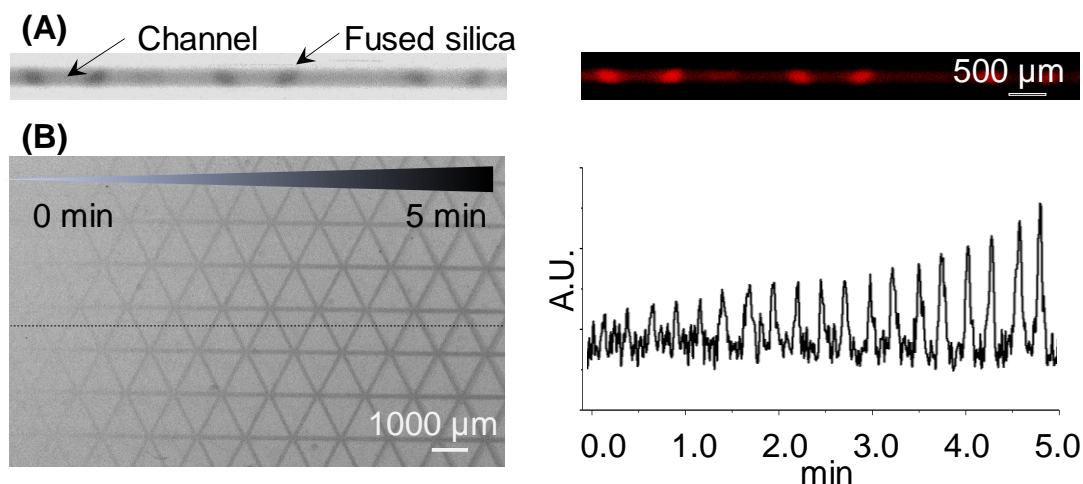


Figure 3.16 Polyphenolic pattern from PG solution (pH 8.0) containing SA (SA/PG molar ratio of 0.4:1) made (A) inside the capillary by UV irradiation through a photomask for 10 min. (B) A gradient polyphenolic pattern was introduced on the flat surface and modified with silver nanoparticles.²³

The phenolic pattern inside the capillary and the gradient patterns were postmodified with silver particles or Rhodamine dye (Figure 3.16). An overlaid gradient polyphenolic pattern was formed on the surface and was modified by silver particles or Rhodamine (Figure 3.17). Such flexibility in the spatiotemporal control of the deposition of different phenolic compounds will be useful in a variety of applications in biotechnology, microfluidics, and surface functionalization.

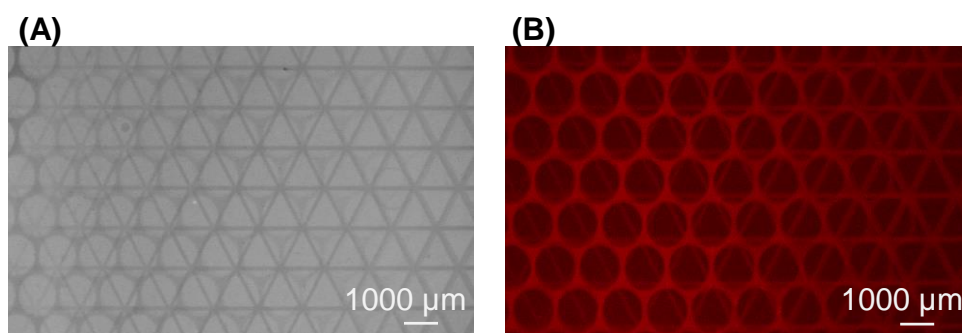
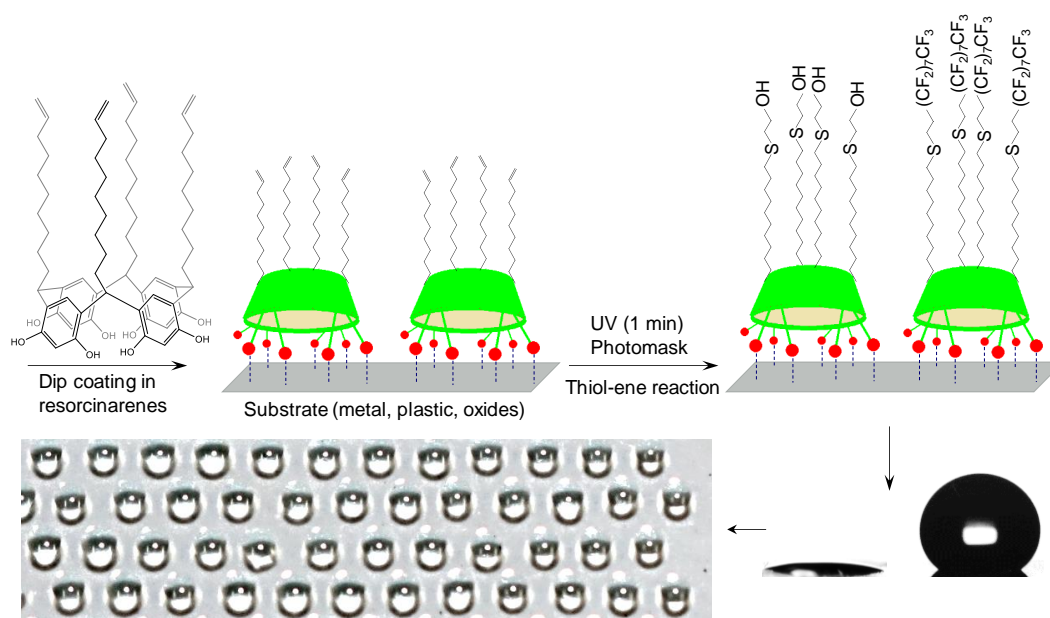


Figure 3.17 Overlaid gradient polyphenolic patterns made on the surface from PG (triangle) and Ctn (hexagonal) solutions. (A) Bright-field and (B) fluorescence microscopy images of the silver- (left) and Rhodamine-modified (right) patterns.²³

3.3 Conclusions to chapter 3

In this chapter, a new strategy to efficiently control the polymerization and deposition of natural plant-derived phenolic compounds under alkaline conditions was introduced, where both polymerization and deposition are most efficient. Natural antioxidants such as sodium ascorbate (SA), glutathione (GSH), and uric acid (UA) were used to inhibit the uncontrolled oxidation of phenolic compounds, while UV light could trigger the oxidation, polymerization, and deposition of polyphenols in a spatiotemporally controlled manner. This general phenomenon was applied to nine plant-derived phenols including pyrogallol, gallic acid, caffeic acid, tannic acid, pyrocatechol, catechin, morin, hydroxyhydroquinone, and epigallocatechin gallate and was demonstrated with three natural antioxidants SA, GSH, and UA. AFM analysis demonstrates that the produced nanocoatings, formed under alkaline and UV-antioxidant controlled conditions, are more homogeneous than those formed without antioxidants and UV light. The applicability of the method to create micropatterns or gradients of polyphenolic coatings, to control the polymerization temporally and stepwise, and to form patterns inside of microfluidic channels and capillaries was shown.

Chapter 4. Surface Functionalization and Patterning by Multifunctional Resorcinarenes^a



^a This chapter is adapted from the publication below:¹¹⁴

Farid Behboodi-Sadabad; Vanessa Trouillet; Alexander Welle; Phillip B. Messersmith; Pavel A. Levkin. Surface Functionalization and Patterning by Multifunctional Resorcinarenes. *Accepted manuscript at ACS Applied Materials & Interfaces* **2018**, DOI: 10.1021/acsami.8b14771.

Reprinted (adapted) with permission from (ACS Appl. Mater. Interfaces, 2018, 10 (45), pp 39268–39278, DOI: 10.1021/acsami.8b14771, Publication Date (Web): October 18, 2018). Copyright (2018) American Chemical Society.

4.1 Introduction

Inspired by the strong solid-liquid interfacial activity of plant polyphenols, various nanocoatings and adhesive precursors have been derived from plant phenolic compounds^{5,23,24,65,94}. Similarly, adhesive coatings based on catecholamines such as dopamine (DA)^{1,4,8,28} have been developed inspired by the key role of marine adhesive polyphenols present in mussel foot proteins.

A substrate-independent coating can be formed on the surface by simple immersion of a substrate into a slightly basic solution of DA or polyphenols. The presence of multiple anchoring points to the surface plays an important role for the strong interaction of polyphenols with the surface via hydrogen bonds, coordination bonds, π - π stacking or hydrophobic interactions.^{34,95} Such nanocoatings have been used for surface modification and development of novel materials for biology,^{51,96} material science,⁶⁵ energy research,^{7,97} and various biomedical applications^{98,99}

However, there are still challenges in the usage of the coatings derived from catecholamines and plant polyphenols that limit applications of such coatings. For instance, several research groups^{36,80,81,100} including ours,²³ tried to reduce nanoparticle-like structure formation in the coatings made from DA or polyphenols. Such aggregates cause high surface roughness, inhomogeneity, and subsequent weakness and instability of the coating.^{16,36,80,81} Multistep post-functionalization^{36,101} is required in order to introduce desired functional groups onto the DA and polyphenolic nanocoating precursors.^{53,102} Examples include post-modification of polydopamine (PDA) layer with hydrophobic molecules or lipid-like molecules such as organic alkanethiols and alkane-phosphates.¹⁰³ Moreover, common choices for secondary functionalization are mainly limited to complexation with metal ions, boronate ester complexation, self-coupling reactions, and reaction with nucleophiles (including amine, imidazole, and thiol groups).^{31,104,105}

Calixarenes represent building blocks for a complementary strategy for surface functionalization. Calixarenes and their derivatives have been used for sensor development,¹⁰⁶ cancer chemotherapy,¹⁰⁷ chemical separations,⁴⁹ molecular recognition,^{108,109} transfection of DNA into cells,¹¹⁰ and other biological applications.¹¹¹ The all-*cis* configuration on a cyclic

tetramer with crown (cone) conformation in calix[4]arenes, which is the thermodynamically most stable isomer,^{42,46,112} provides a three-dimensional structure which can be decorated with desired functional groups on the small or large rim.^{46,113}

In a classical way, surface-reactive head groups on the small rim of the calixarenes were used to covalently bind calixarenes onto the surface.³⁷ Mattiuzzi et al.^{2,44,45} used rigid tetrapodant calix[4]arenes as building blocks to form a monolayer on the surface by electrografting of calix[4]arene diazonium salts on the surface from their large rim side. Multivalency of calixarenes could increase their binding strengths. Using this strategy, a dense and closely packed monolayer of calix[4]arenes was formed on the surface due to the unique macrocyclic structure of the calixarene skeleton which prevents the formation of disorganized multilayers.²

Resorcinarenes are resorcinol-derived calixarenes.⁴⁶ Resorcin[4]arenes can easily be obtained by the acid catalyzed condensation of resorcinol with various aliphatic or aromatic aldehydes, which occurs on refluxing the reactants in a mixture of ethanol and concentrated hydrochloric acid (HCl) for several hours.⁴⁶ Usually, the cyclotetramer crystallizes from the reaction mixture in reasonable to high yields in a simple one-step untemplated reaction, although for different aldehydes different optimal reaction conditions exist.⁴⁶ In the context of surface modification, thiol-gold,³⁸ ion-metal coordination,³⁹ amine-graphene oxide,⁴⁰ silane coupling,⁴¹ and platinum catalyzed⁴² binding chemistries have been used to make a layer of resorcinarenes on surfaces.

In this chapter, I present a one-step strategy for surface functionalization by deploying bifunctional resorcinarenes that can adhere to different substrates including polyethylene (PE), polymethyl methacrylate (PMMA), stainless steel (steel), aluminum (Al), zinc (Zn), amine-functionalized porous poly(2-hydroxyethyl methacrylate)-co-(ethylene dimethacrylate) (poly(HEMA)), amine-functionalized glass, and silicon wafer using their large rim side, while their small rim side can be used for the post-functionalization. The produced nanocoatings demonstrated homogeneity and transparency.

Three different resorcin[4]arenes, compounds **1**, **2**, and **3** (Figure 4.1), were used as building blocks for the functionalization of different substrates. The large rim of resorcinarenes **1**, **2**, and **3** consists of eight hydroxyl groups, serving as multiple anchoring points to the surface, whereas

the small rim is decorated with four methyl, undecyl, or dec-9-enyl legs, respectively. Formation of uniform, aggregate-free, and transparent nanocoatings using all three compounds **1**, **2**, and **3** was demonstrated by apparent water contact angle (WCA) measurement, UV-vis spectroscopy, XPS, and AFM analysis. By varying the choice of “legs” on the small rim, desired functional groups can be directly introduced to the surface. For instance, compound **3** was synthesized with four pendant alkenyl groups at the small rim. UV-induced thiol-ene click chemistry was used to site-selectively post-functionalize the **3**-modified surface with hydrophilic and hydrophobic functional groups, in order to tune the surface wettability against liquids possessing both high and low surface tension. This strategy could expand the choice of multifunctional building blocks for this class of bioinspired nanocoatings from catecholamines and plant phenolic compounds to tailor-made resorcinarenes.

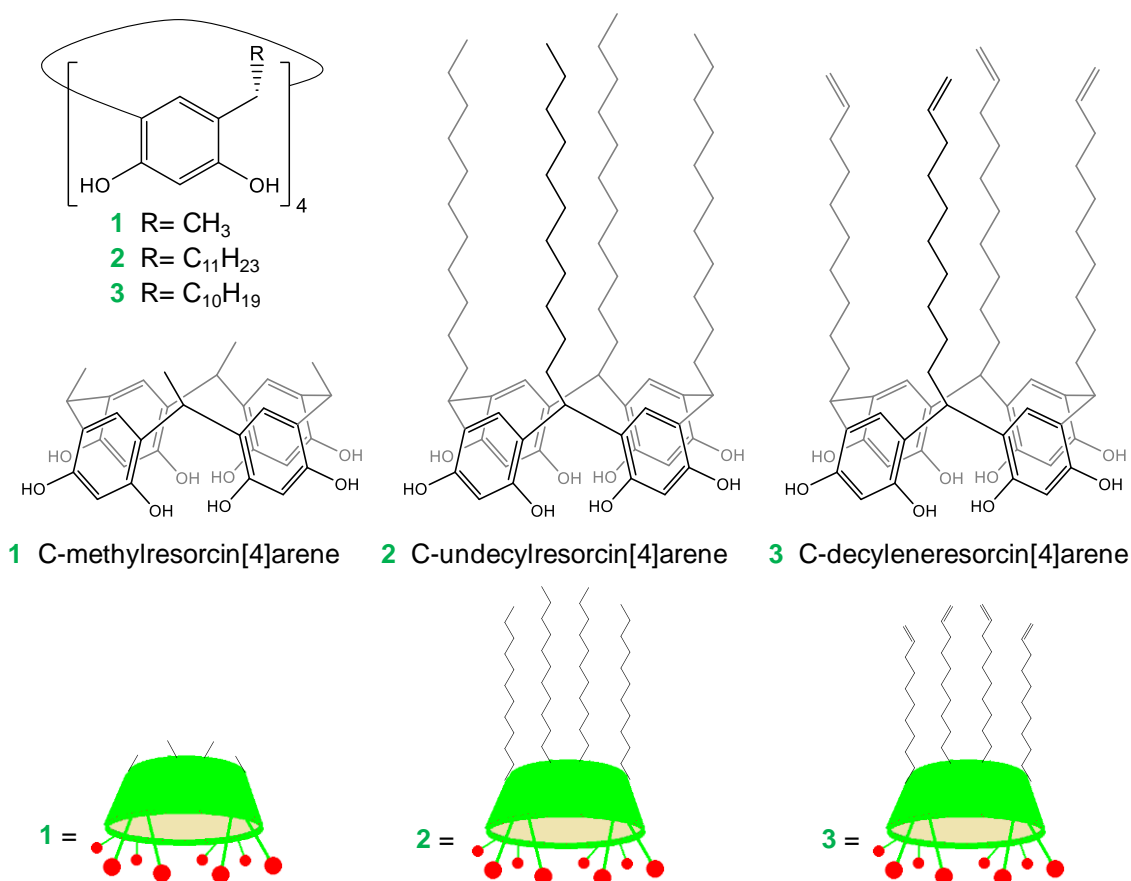
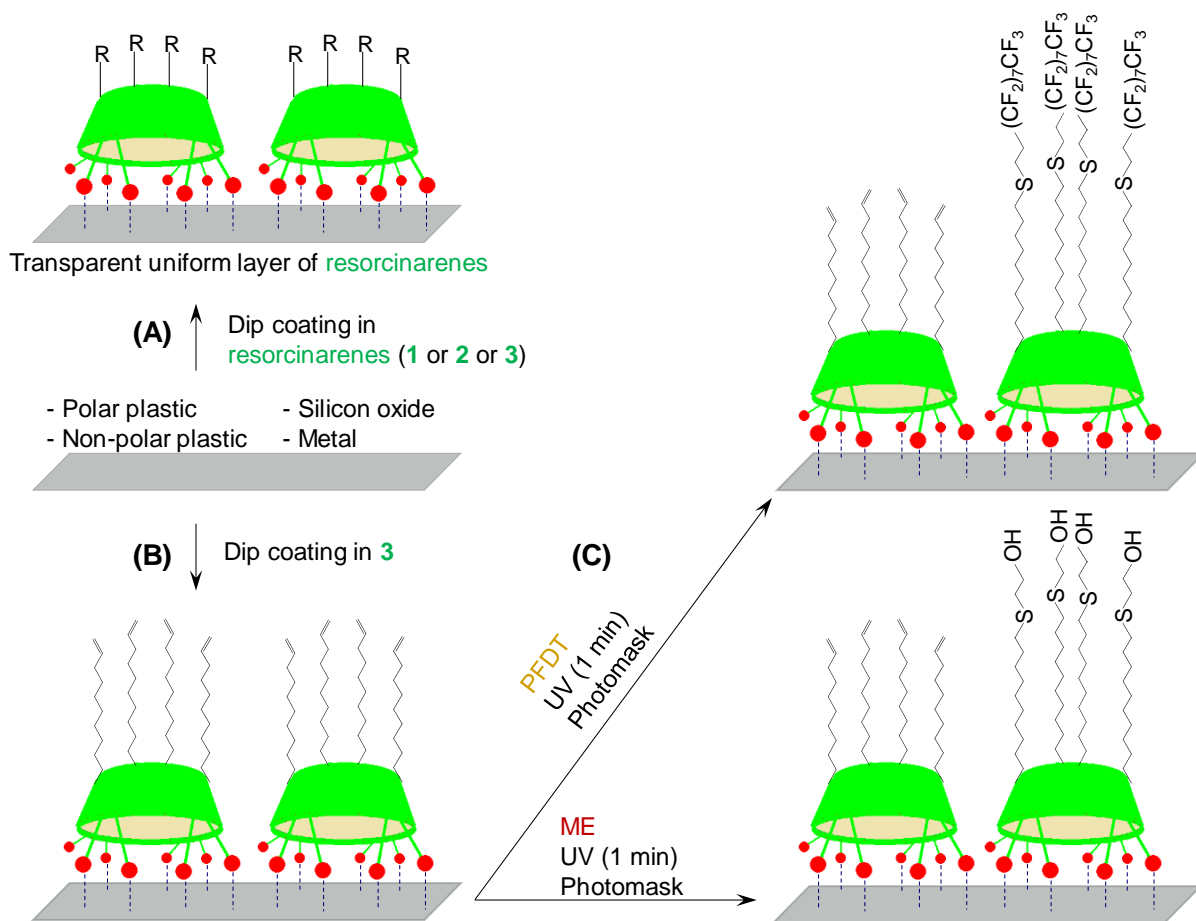


Figure 4.1 Chemical structures of *C*-methylresorcin[4]arene (**1**), *C*-undecylresorcin[4]arene (**2**), and designed *C*-dec-9-enylresorcin[4]arene (**3**) and their schematic representation.¹¹⁴

4.2 Results and discussion

The coating potential of resorcin[4]arenes using two commercially available resorcin[4]arenes, *C*-methylresorcin[4]arene (**1**) and *C*-undecylresorcin[4]arene (**2**) was investigated. In addition, *C*-dec-9-enylresorcin[4]arene (**3**) containing four appending alkenyl groups on its small rim was synthesized according to our previous report (Figure S10.1, Figure S10.2).⁴²



Scheme 4.1 (A) Formation of a uniform and transparent layer of multifunctional resorcin[4]arenes on the surface of a different of substrates by a one-step dip coating technique. (B) Modification of the surface with **3** and subsequent post-functionalization with hydrophilic (2-mercaptoethanol, ME) or hydrophobic (1*H*,1*H*,2*H*,2*H*-perfluorodecanethiol, PFDT) groups via UV-induced thiol-ene click chemistry.¹¹⁴

To investigate coating formation ability of resorcinarenes, different substrates were immersed in a 0.8 mg/mL solution of **1**, **2**, or **3** in an ethanol:tris buffer (10 mM, pH 8.5) mixture, for 24 h at room temperature with gentle agitation (Scheme 4.1A,B). Deposition of a resorcinarene layers on the surface of different substrates including polyethylene (PE), polymethyl methacrylate (PMMA), stainless steel (steel), aluminum (Al), zinc (Zn), amine-functionalized porous poly(2-hydroxyethyl methacrylate)-*co*-(ethylene dimethacrylate) (poly(HEMA)), and silicon wafer was investigated by apparent water contact angle (WCA) measurements, XPS, and AFM analysis. The term poly(HEMA) refers to amine-functionalized porous poly(HEMA) throughout the text and figures.

4.2.1 Coating formation ability of resorcinarenes on different substrates

Apparent WCA and contact angle hysteresis (CAH) on flat PE, PMMA, steel, Al, Zn and rough poly(HEMA) substrates before and after functionalization with **1**, **2** and **3** are shown in Table 4.1. All flat surfaces modified with the same compounds showed similar WCAs indicating successful functionalization and homogeneous coatings. The difference in WCAs in the case of the poly(HEMA) reflects its porous rough surface, which leads to either decrease or increase of the apparent WCA after the modification with either slightly hydrophilic **1** or hydrophobic **2** and **3**, respectively (Figure 4.2A,B).

Table 4.1 Apparent water contact angles (θ) and contact angle hysteresis ($\Delta\theta$) of different substrates before and after modification with **1**, **2**, and **3**.

Substrate	Bare		+1		+2		+3	
	θ	$\Delta\theta$	θ	$\Delta\theta$	θ	$\Delta\theta$	θ	$\Delta\theta$
PE	86±2.1	~57	73±4.2	~60	107±4.3	~52	105±3.2	~51
PMMA	70±2.2	~46	67±4.3	~39	100±3.4	~37	103±4.6	~44
Steel	69±1.9	~33	64±3.9	~35	105±3.8	~39	102±3.9	~34
Al	74±2.2	~42	65±3.6	~38	109±2.9	~36	107±3.8	~34
Zn	75±2.4	~54	64±4.5	~48	108±3.8	~58	106±3.5	~55
Poly(HEMA)	2±1.1	-	15±2.5	~10	138±2.6	~40	137±2.3	~43

Deposition kinetics of the resorcinarenes on the surface was monitored by measuring apparent water contact angle of poly(HEMA) substrate at different time intervals up to 36 h after immersing in the coating solution of **1**, **2**, and **3** (Figure 4.2C). Apparent contact angle reached a constant value of $16^\circ \pm 3$, $138^\circ \pm 3$, $137^\circ \pm 4$ after 24 h of incubation in coating solution of **1**, **2**, and **3**, respectively (Figure 4.2C).

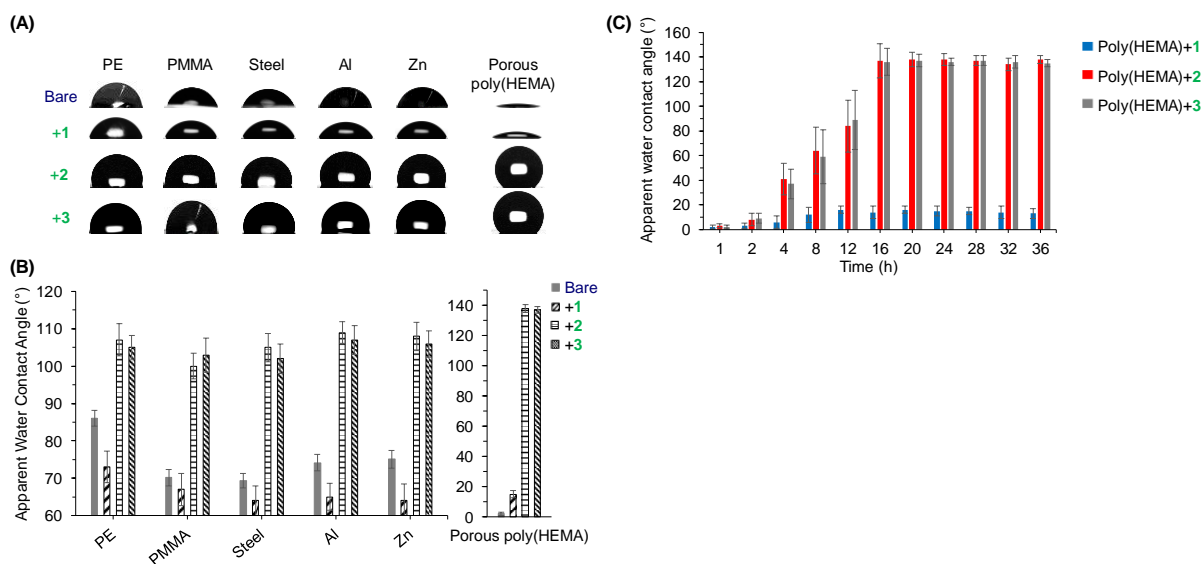


Figure 4.2 Deposition of resorcinarenes (**1,2,3**) on different substrates. (A) Water droplets formed on the surface of PE, PMMA, steel, Al, Zn, and amine-functionalized porous poly(HEMA) substrates before and after modification with **1**, **2**, and **3** and corresponding apparent WCA. (B) (C) Deposition kinetics of **1**, **2**, and **3** on the poly(HEMA) substrate monitored by measuring apparent water contact angle measurements after immersing the substrate in the corresponding coating solutions for different time intervals.¹¹⁴

4.2.2 Stability of the resorcinarene layer on the surface

Stability of the coated layer was investigated by monitoring apparent WCA of PE, steel, and poly(HEMA) substrates coated with **1**, **2**, and **3**, at different time intervals after immersing or sonicating the substrates into a 1:1 ethanol:water mixture for 24 h (Figure 4.3). Apparent WCA of substrates coated with **1**, **2**, and **3** remained constant after immersing in a 1:1 ethanol:water mixture over 24 h, indicating deposition of a relatively stable resorcinarene layer on the surface at the mentioned environment.

Sonication of the solution led to decrease of apparent WCA of the substrates modified with **3** from 105° and 102° of the bare PE and steel substrates to 85° and 70°, respectively, indicating detachment of the resorcinarene layer from the surface within the first 6 h of sonication (Figure 4.3C). Detachment of the resorcinarene from the surface could be due to relatively weak and reversible non-covalent interaction of the polyphenols with the surface.¹² However, **1**, **2**, and **3** formed a much more stable layer on the amine-functionalized porous poly(HEMA), confirmed by no change in apparent WCA even after sonication for 24 h, possibly due to covalent attachment of the phenolic groups of the resorcinarenes to the amino groups on the surface¹² via Michael addition-type reaction or Schiff base formation.^{31,104,105}

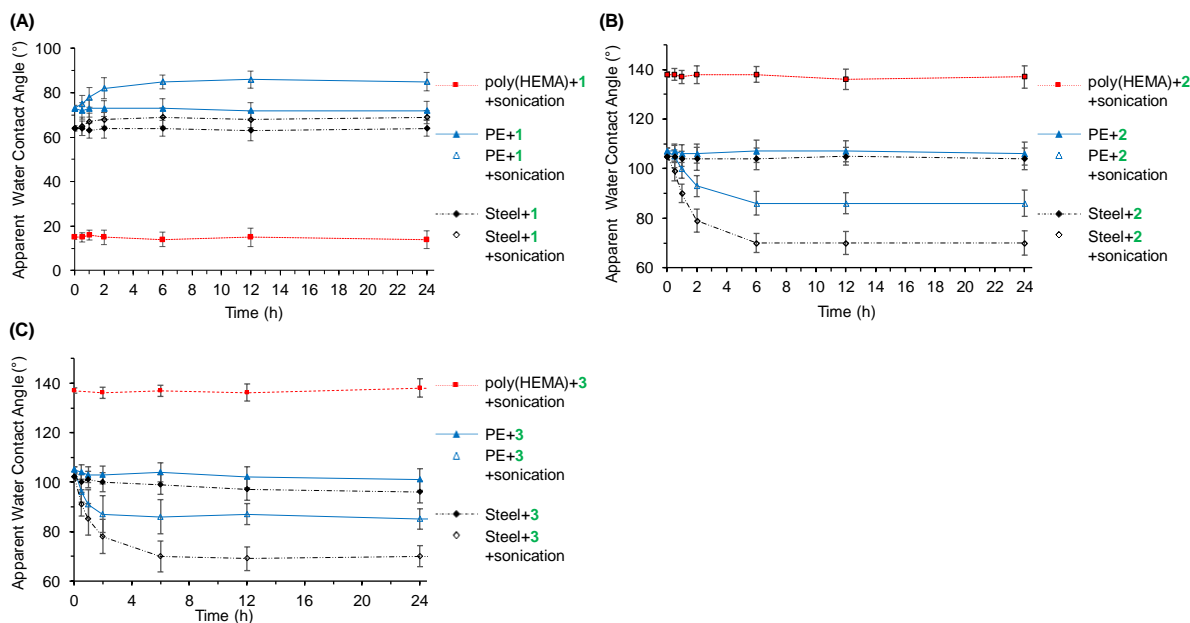


Figure 4.3 Apparent WCA of PE, steel, and poly(HEMA) substrates modified with **1** (A), **2** (B), and **3** (C) after immersion or sonication in ethanol:water 1:1 mixture for 24 h.¹¹⁴

The adhesive strength of the resorcinarene layer of **3** deposited on the steel, PE and (amine-functionalized) glass substrates by monitoring the apparent WCA of the substrates after immersing in aqueous buffer solutions at acidic (pH 3), neutral (pH 7), and basic pH (pH 9) for different time intervals was investigated (Figure 4.4). Apparent WCA of the substrates incubate at neutral pH didn't change after 48 h. However, apparent WCA decreased significantly after 12 h incubation in a basic (steel and PE) or in an acidic solution (amine-functionalized glass)

(Figure 4.4). Significantly higher binding energy of bidentate hydrogen bonds in polyphenols than the binding energy of mono hydrogen bonds has been confirmed theoretically and experimentally.¹¹⁵ Hydrogen bonds could be formed between the hydroxyl groups (as hydrogen donors) on resorcinarene and the oxygen atoms (as hydrogen acceptors) on the (oxidized) PE and steel substrates.¹³ Generation of other types of interaction with the surface in addition to hydrogen bonds could be the reason of the stability of the resorcinarene layer on PE and steel substrates at pH 3, and pH 7 (Figure 4.4A,B).¹³ However, in basic environment (pH 9) resorcinarene layer detached from the surface of PE and steel substrates possibility due to deprotonation of the majority of the hydroxyl groups and their oxidation to quinone moieties²⁵ that leads to a weaker interaction with the PE and steel substrates (Figure 4.4A,B).

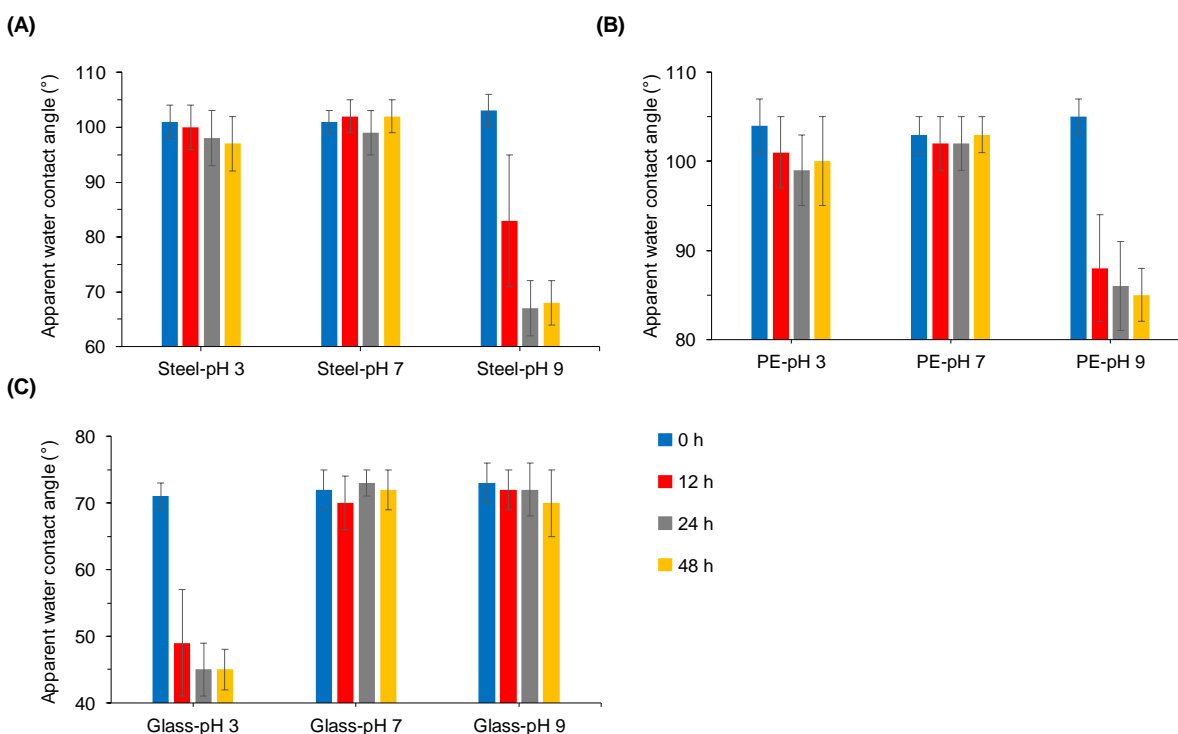


Figure 4.4 Stability of the resorcinarene layer of **3** deposited on the surface of (A) steel, (B) PE, and (C) (amine-functionalized) glass substrates monitored by measuring the apparent water contact angle of the substrates after immersing for different time intervals at aqueous buffer solutions at 100 mM formate (pH 3), phosphate (pH 7), or carbonate-bicarbonate (pH 9) buffers.¹¹⁴

On the other hand, oxidation of hydroxyl groups to quinone moieties at basic pH, could enable covalent binding of the polyphenols to the amine-functionalized surfaces.¹² Apparent contact angle of the **3**-modified (amine-functionalized) glass substrate did not change significantly in natural (pH 7) and basic condition (pH 9), possibly due to covalent interaction with the surface (Figure 4.4C). However, in acidic environment (pH 3), quinone structure is favored over hydroxyl in polyphenols.²⁵ Therefore, the weak surface interaction between resorcinarene layer and amine-functionalized surface observed in acidic pH (Figure 4.4C) could be due to the shift in the chemical equilibria of hydroxyl-quinone toward quinone structure.¹²

Dependency of the adhesion strength and the stability of the substrate-independent polyphenolic nanocoatings on the substrate type, pH of the environment, and phenolic precursor was reported in the literature.^{6,12,13}

4.2.3 *Characterization of the surfaces modified with resorcinarenes*

Deposition of a resorcinarene on the surface was investigated by XPS analysis of the substrates modified with **3**. The strong decrease of the intensity of the characteristic substrate signals proves the modification of the substrate with **3** (Figure 4.5A,B and Figure S10.3).

In the case of PMMA, C 1s at 288.9 eV attributed to O=C-O group was chosen as a marker. For further metal substrates, peaks stemming from the metal itself were observed, namely Fe 2p, Al 2p, and Zn 2p doublets for steel, Al, and Zn substrates, respectively. A decrease of at least 75% of the initial intensity for the bare substrates was observed for all the mentioned peaks, which points out the presence of a new layer on the surface. Furthermore, the carbon concentration increased and more importantly the contribution of the component at 285.0 eV (C-C, C-H) in the C 1s spectra increased after surface modification. This observation supports the deposition of **3** on the surface since this compound contains long alkyl chains.

Surface topography and thickness of the resorcinarene layer deposited on a silicon wafer was analyzed using AFM. A layer free from nanoparticle-like structures was observed on the silicon surface with an average thickness of 1.0 ± 0.15 , 2.1 ± 0.24 , and 1.9 ± 0.18 nm and mean square roughness (RMS) of 0.4, 0.6, 0.5 nm by immersion of the substrate into a coating solution of **1**,

2, and **3**, respectively (Figure 4.5C,D, Figure 4.6). The average thickness of the resorcinarene layer was calculated by subtracting the average height of the scratched area from the average height of the unscratched area. Roughness values were similar to that of the bare substrates ($RMS_{\text{bare Si}}=0.3$ nm, RMS of Si substrates before modification with **1**, **2**, and **3** were 0.3 nm, 0.4 nm, 0.4 nm, respectively) indicating the deposition of a uniform layer on the whole surface.

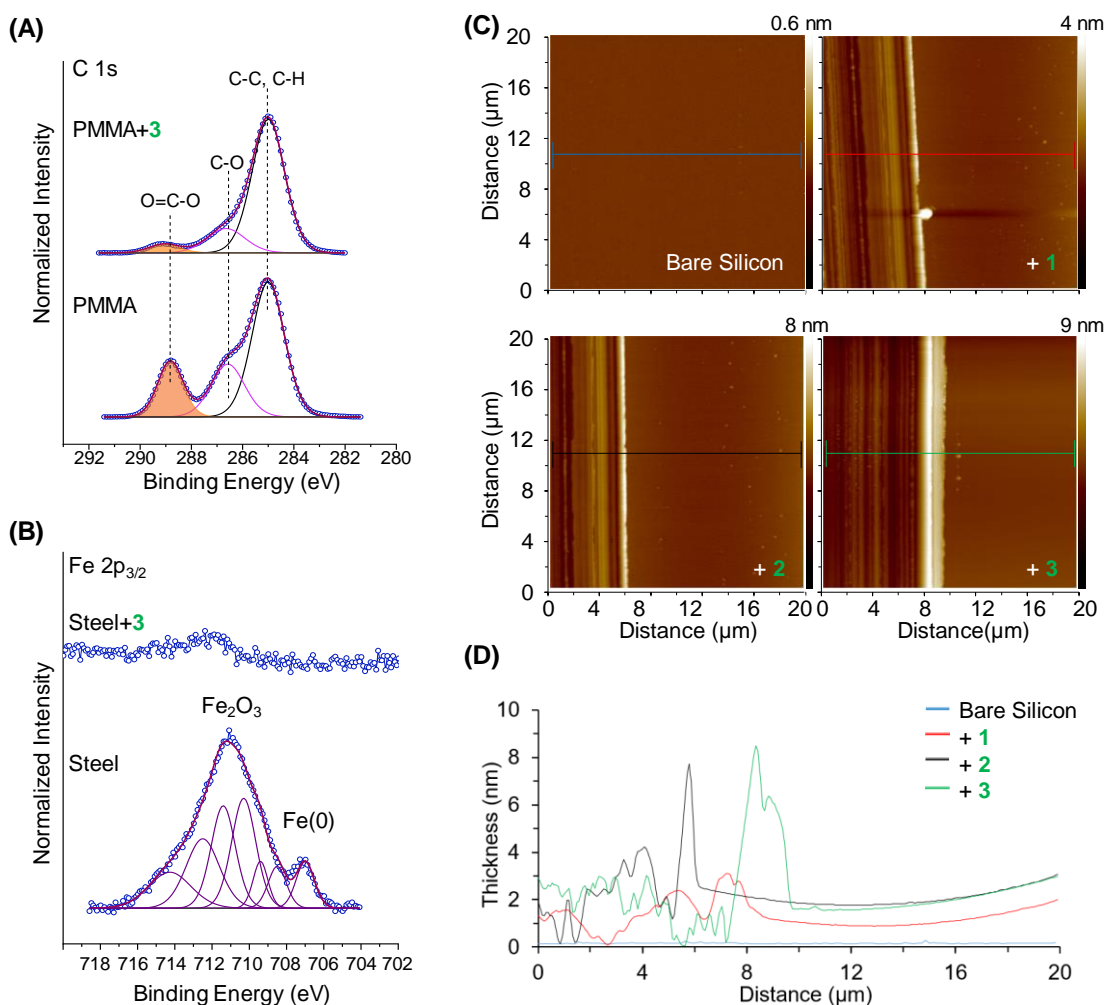


Figure 4.5 Surface modification using resorcinarenes (**1,2,3**). (A) Detailed C 1s and (B) Fe 2p XP spectra of PMMA and steel substrates before and after modification with **3**. (C) AFM height image of bare silicon, silicon after modification with **1**, **2**, and **3** after gentle scratching (on the left side of each sample). (D) Corresponding height profile along the lines.¹¹⁴

These results agree well with the theoretical height values (estimated from MM2 energy minimization using Chem3D software) of ca. 0.8, 1.9, and 1.7 nm for **1**, **2**, and **3**, respectively.

AFM analysis of a smaller area ($5\ \mu\text{m}^2$ squares) of the bare and modified silicon substrates with **1**, **2**, and **3** indicated that a compact uniform layer of resorcinarenes, free from nanoparticle-like structure, formed on the surface (Figure 4.6). The thickness values measured by AFM were in agreement with the thickness values measured by ellipsometry, 0.9 ± 0.12 , 2.3 ± 0.19 , and 2.2 ± 0.21 nm for the silicon substrate coated with **1**, **2**, and **3** respectively.

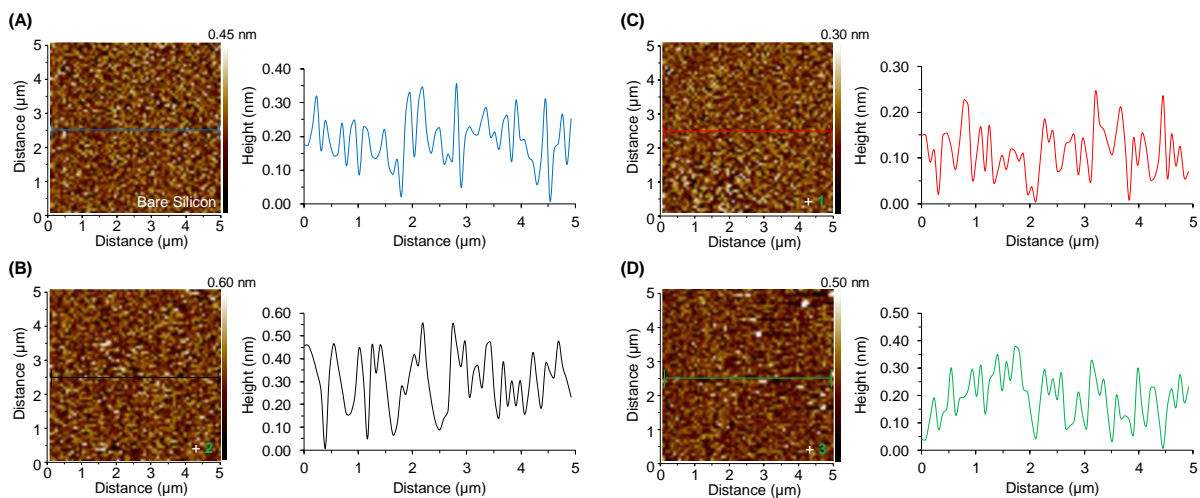


Figure 4.6 AFM height image of the (A) bare, (B) **1**-modified, (C) **2**-modified, and (D) **3**-modified silicon surface. Corresponding height profiles along the lines are shown in the graphs.¹¹⁴

4.2.4 Post-functionalization of resorcinarene-modified surface

In order to investigate the ability to post-functionalize the substrates modified with **3**, UV-induced thiol-ene click chemistry was used to modify dec-9-enyl pendant groups on the small rim of **3** with 2-mercaptoethanol (ME) and *1H,1H,2H,2H*-perfluorodecanethiol (PFDT) (Scheme 1C, Figure 4.7). Hydrophobic PFDT and hydrophilic ME were clicked on the **3**-modified surface by 1 min UV irradiation of PFDT and ME solutions. Apparent WCA measurements of **3**-modified poly(HEMA) and **3**-modified amine-functionalized glass substrates after post-functionalization indicated a high wettability contrast between PFDT- and ME-functionalized surface for liquids possessing both high and low surface tension (Figure 4.7A,B). The term glass refers to amine-functionalized glass throughout the text and figures.

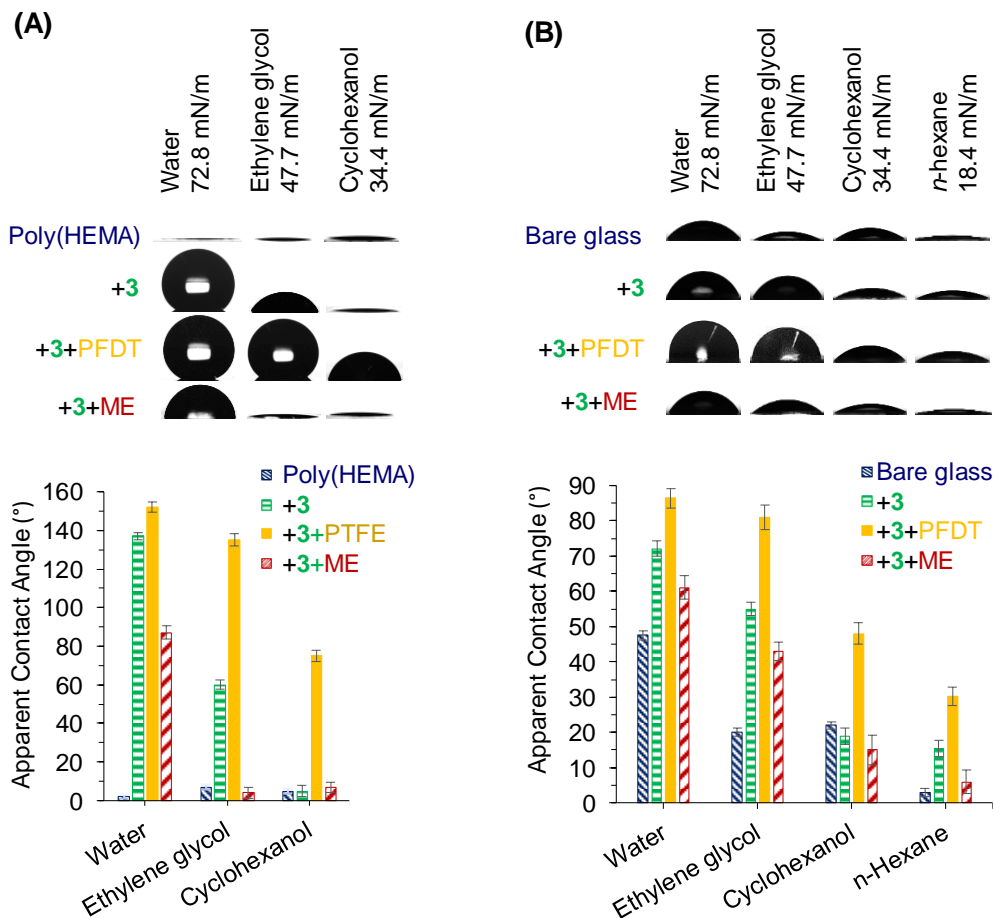


Figure 4.7 Tuning surface wettability by post-functionalization of **3** via UV-induced thiol-ene click chemistry. Droplets of solvents with different surface tensions formed on the surface of poly(HEMA) (A) and glass (B) after modification with **1**, **2**, and **3**, and after post-functionalization of **3**-modified surface with 1H,1H,2H,2H-perfluorodecanethiol (PFDT) and 2-mercaptoethanol (ME) via UV-induced thiol-ene click chemistry. Corresponding apparent contact angles are shown in the graphs.¹¹⁴

Apparent WCA of poly(HEMA) substrate increased from 2° to 137°, 152°, and 87° after modification with **3**, and post-functionalization with PFDT and ME respectively (Figure 4.7A). Due to the combined micro- and nanoporosity of the poly(HEMA),¹¹⁶ apparent WCA reached 152° after post-functionalization with PFDT. Water droplets rolled off the PFDT-functionalized surface (tilting angle 8°), while water droplets were pinned onto the ME-functionalized surface.

3-modified poly(HEMA) substrate post-functionalized with PFDT was able to repel liquids with lower surface tension such as ethylene glycol (surface tension 47.7 mN/m) and cyclohexanol (surface tension 34.4 mN/m). However, surfaces post-functionalized with ME became again completely wettable for ethylene glycol and cyclohexanol (Figure 4.7A).

Apparent WCA of glass substrate increased from 47° to 72°, 86°, and 61° after modification with **3**, and post-functionalization with PFDT and ME respectively (Figure 4.7B). **3**-modified glass after post-functionalization with PFDT was able to repel liquids with lower surface tension than water (surface tension=72.8 mN/m) including ethylene glycol (surface tension 47.7 mN/m), cyclohexanol (surface tension=34.4 mN/m), and *n*-hexane (surface tension 18.4 mN/m) (Figure 4.7B).

By post-functionalization of the **3**-modified glass surface with ME, the contact angle of water, ethylene glycol, cyclohexanol, and *n*-hexane decreased from 72°, 55°, 19°, and 15° for the **3**-modified glass to 61°, 43°, 15°, and 6° for ME-functionalized surface. Small differences observed in the contact angles after post-functionalization with PFDT and ME (Figure 4.7A,B) could be due to the chemical structure of compound **3**, which contains a large relatively hydrophobic macrocycle (of four benzene rings) with four hydrophobic long alkenyl chains. Thus, post-functionalization of **3** with hydrophilic hydroxy groups (from ME) leads to a decrease of the surface energy but not a drastic one. Apparent WCA measurements, on one hand, confirmed post-functionalization of the substrates modified with **3** via thiol-ene click reaction, and on the other hand, demonstrated the ability to tune the surface wettability for a variety of liquids.

The transparency of resorcinarene layer formed on the glass surface was investigated by measuring UV-vis spectra before and after modification of the surface with **3** and post-functionalization with PFDT and ME. UV-vis spectra indicated that glass remains transparent after deposition of the resorcinarene layer and the subsequent post-functionalization (Figure 4.8A).

Stability of resorcinarene layer of **3** was investigated by measuring apparent WCA at different time intervals after sonication in a 1:1 ethanol:water mixture for 24 h. Apparent WCA of **3**-modified substrates remained constant before and after post-functionalization via thiol-ene

photoclick reaction further confirming deposition of a more stable resorcinarene layer on the surface (Figure 4.8B).

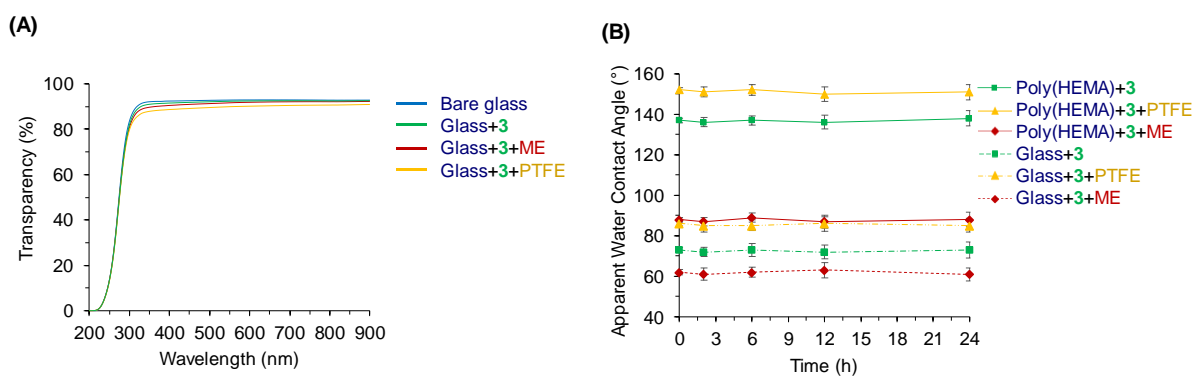
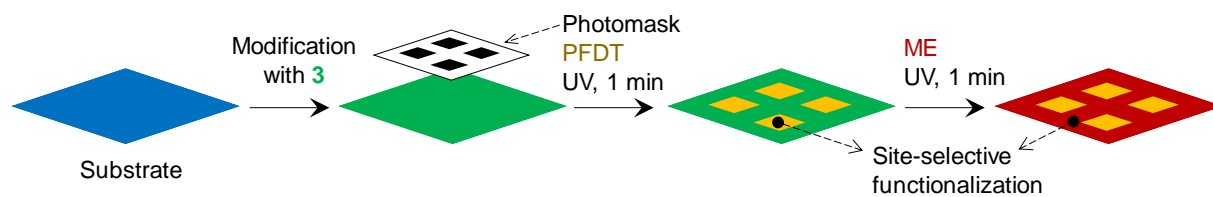


Figure 4.8 (A) Transparency (%) of bare glass, **3**-modified glass, and after clicking PFDT and ME. (B) Apparent WCA of **3**-modified porous poly(HEMA) and glass substrates before and after thiol-ene reaction after sonication in ethanol:water 1:1 mixture for 24 h.¹¹⁴

4.2.5 Photopatterning of the resorcinarene-modified surface

Thiol-ene photo-click chemistry is a versatile one-step procedure for spatial and temporal controlled coupling of thiol and alkene-functionalized compounds and has been used widely in materials science.¹¹⁷



Scheme 4.2 (A) Schematic representation of site-selective functionalization of **3**-modified glass surface with PFDT or ME via UV-induced thiol-ene click chemistry.¹¹⁴

A layer of **3** contains alkenyl groups formed on the glass surface by immersing the substrate into the coating solution of **3** (0.8 mg/mL, in a 1:1 ethanol:tris buffer (10 mM, pH 8.5)). By UV irradiating through a photomask in the presence of PFDT and ME, it was possible to control the post-functionalization of alkenyl groups spatially (Scheme 4.2). For instance, to make a

micropattern of hydrophilic spots within hydrophobic borders on the **3**-modified substrate, a solution of PFDT was filled in between the surface and a photomask followed by 1 min UV irradiation through a photomask, followed by washing and drying. Finally, a solution of ME was filled into the setup and irradiated with UV light for 1 min to introduce hydroxyl groups on the alkenyl chains of **3**, followed by washing and drying (Scheme 4.2).

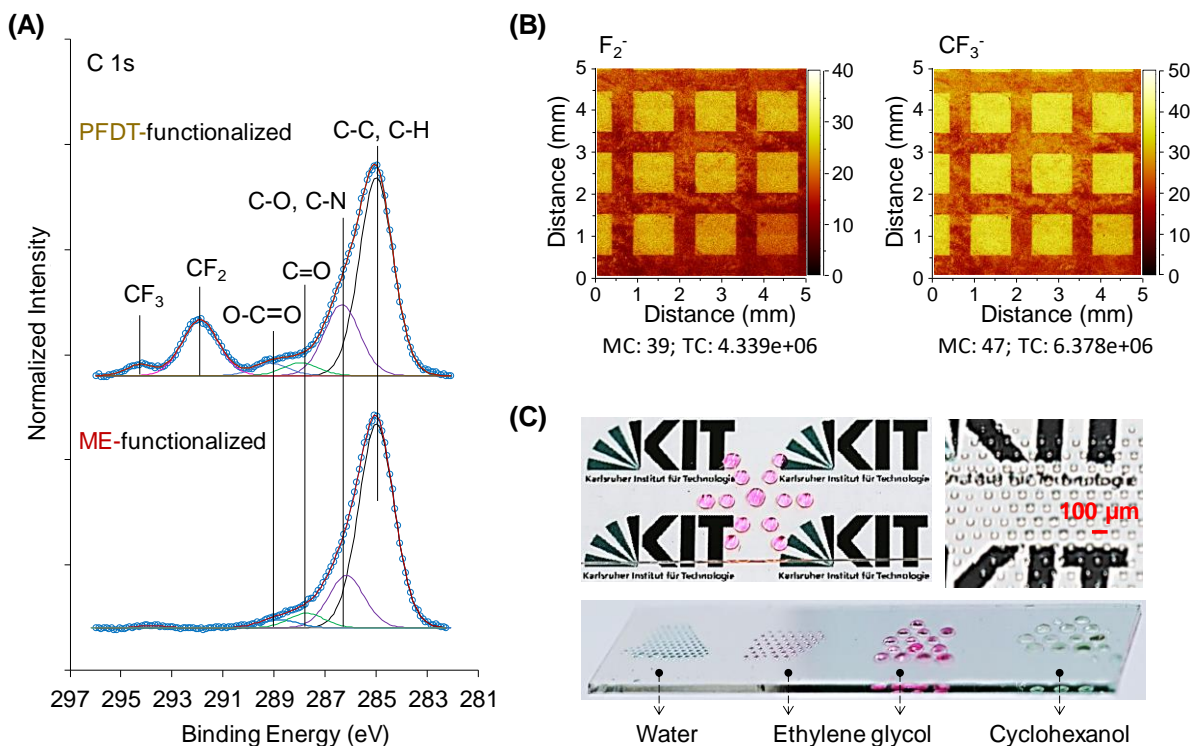


Figure 4.9 Photopatterning of the glass surface modified with **3** and formation of droplet microarray. (A) C 1s XPS spectra of the **3**-modified surface after post-functionalization with PFDT (top) and ME (bottom), indicating the formation of $-\text{CF}_2$ and $-\text{CF}_3$ functional groups on the surface after functionalization with PFDT. (B) ToF-SIMS F_2^- and CF_2^- ion intensity maps of **3**-modified surface post-functionalized with PFDT (squares) and ME (borders). (C) Droplet microarray of dyed water, ethylene glycol, and cyclohexanol formed on **3**-modified glass slide after the micropatterning.¹¹⁴

Micropatterning of the **3**-modified surface with PFDT and ME was confirmed by XPS and ToF-SIMS (Figure 4.9A,B). XPS chemical mapping was first conducted in order to identify the position of the chemically different areas (Figure 4.10).

Afterward, high energy resolution spectra could be recorded at well-defined locations evidenced by the mapping (Figure 4.9A). Two peaks at 291.9 eV and 294.1 eV in the C 1s spectrum and the corresponding F 1s signal at 689.0 eV proved¹¹⁸ the presence of -CF₂ and -CF₃ functional groups in the PFDT-functionalized regions next to ME-functionalized regions. In another micropatterning experiment, ToF-SIMS analysis confirmed the presence of the mass fragments corresponding to F₂⁻ and CF₃⁻ in the regions modified with PFDT (Figure 4.9B).

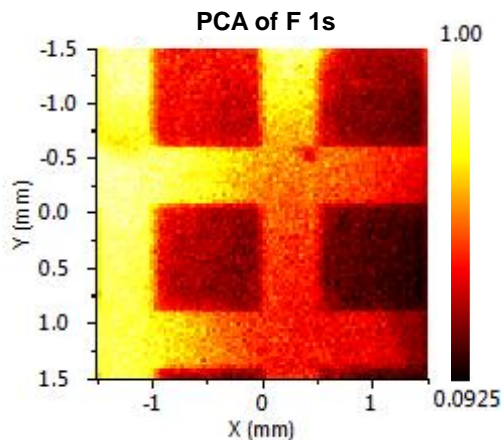


Figure 4.10 Principal component analysis (PCA) of F 1s / XPS mapping of the **3**-modified surface after post-functionalization with PFDT (borders) and ME (squares).¹¹⁴

4.2.6 *Dynamic wettability behavior of the post-functionalized surfaces*

In order to investigate the dynamic wetting behavior of the surface, advancing and receding contact angles of water, ethylene glycol, and cyclohexanol on glass substrate were measured before and after modification with **3**, and post-functionalization with PFDT and ME (Figure 4.11).

The results of static and dynamic contact angle measurements indicated that although static apparent contact angles did not change a lot after the post-functionalization with PFDT or ME, the contact angle hysteresis values showed much larger difference confirming a successful post-functionalization (Figure 4.11). These observations further confirmed the hypotheses that a resorcinarene layer containing bulk hydrophobic groups was deposited on all the surfaces.

Due to the high contrast of wettability between PFDT- and ME-functionalized regions (Figure 4.7A,B, Figure 4.11), droplet microarrays could be spontaneously formed on the transparent micropatterned surface by rolling a droplet of liquid, including water, ethylene glycol, or cyclohexanol on the micropatterned surface (Figure 9C).¹¹⁹

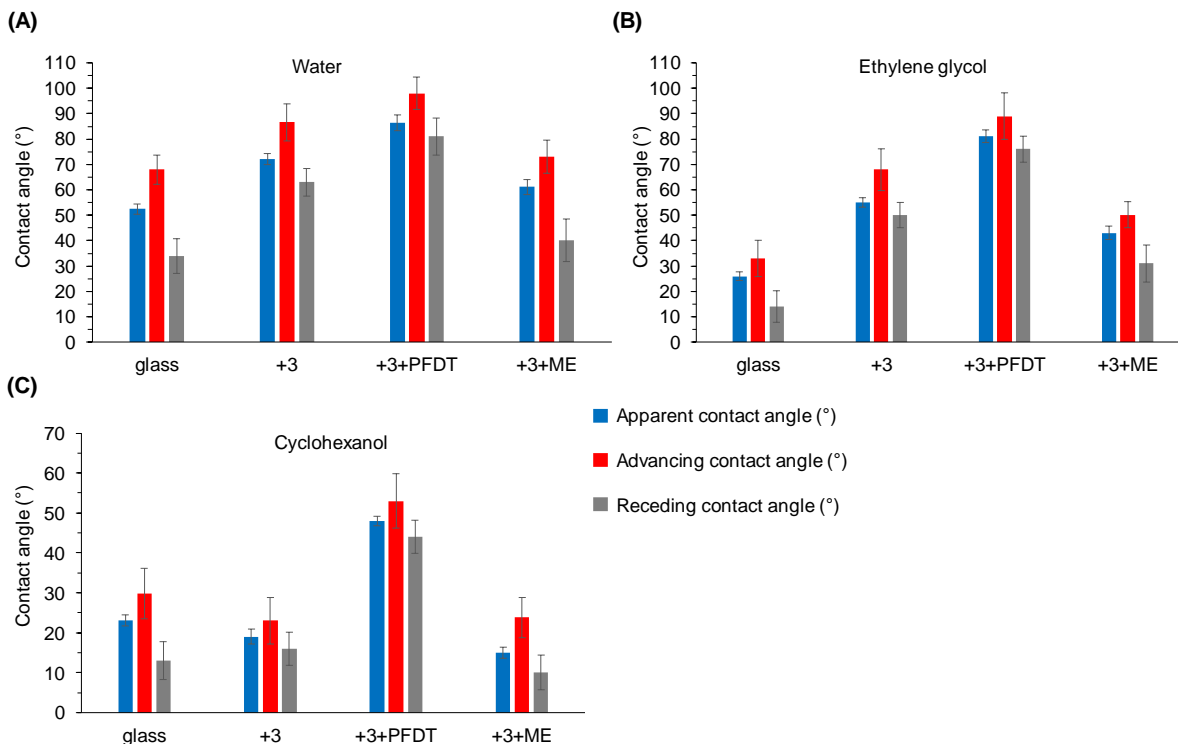


Figure 4.11 Apparent static, advancing, and receding contact angles of (A) water, (B) ethylene glycol, (C) cyclohexanol on (amine-functionalized) glass, before and after modification with **3**, and after post-functionalization with PTFE or ME.¹¹⁴

4.3 Conclusions to chapter 4

In this chapter, inspired by strong adhesive properties of natural polyphenols found in plant polyphenols, a new strategy was developed to use resorcinarenes as building blocks for surface functionalization. Resorcinarenes can be synthesized in a simple one-step reaction and provide eight hydroxyl groups on the large rim that serve as multiple anchor points to PE, PMMA, steel, Al, Zn, (amine-functionalized) poly(HEMA), (amine-functionalized) glass, and silicon wafer substrates, while the small rim can be decorated with desired functional groups.

Three resorcin[4]arenes, compound **1**, **2**, and **3**, were used to make transparent uniform layers on the surface of plastic, metals, and silicon oxides by a single-step dip coating of the substrates in the corresponding solutions of resorcinarenes. Investigation of the stability of the resorcinarene layer on the surface indicated that the extent of stability of the resorcinarene layer on the surface was dependent on the substrate type and the pH values. Variation of the stability may be attributed to the different interaction mechanism of the polyphenols with different substrates. The most stable layer of resorcinarene was formed on amine-functionalized substrates possibly due to covalent attachment of resorcinarene to the surface.

Compound **3** decorated with alkenyl appendages on the small rim enabled post-functionalization of the surface via thiol-ene photo click chemistry. The **3**-modified glass was post-functionalized with hydrophobic or hydrophilic functional groups by UV irradiating the substrate through a photomask for 1 min in the presence of PFDT or ME. Droplet microarray of liquids with either high or low surface tension was formed on the surface of the micropatterned glass substrate by rolling a drop of the liquid over the surface.

This strategy could expand the choice of building blocks for this class of bioinspired nanocoatings from catecholamines and plant phenolic compounds to tailor-made multifunctional resorcinarenes with a wide range of potential applications in chemistry, biology, and material science.

Chapter 5. Summary and Outlook

5.1 Summary of the thesis

Plant phenolic compounds and macrocyclic polyphenols offer a wide range of choice for coating precursors to modify a variety of substrates. Desired physical and chemical properties of the surface can be achieved by modification with polyphenols and/or subsequent post-functionalization. A literature review on substrate-independent coating strategies and their advantages and limitations with the focus on polyphenolic coatings was given in **chapter 1**.

Phenolic compounds can undergo autoxidation in alkaline pH conditions. However, due to the rapid oxidation of phenolic compounds, there is a limited kinetic and spatiotemporal control over the deposition of polyphenols, which leads to the formation of weak and inhomogeneous nanocoatings. Two strategies were developed to control the kinetics of the oxidation, followed by polymerization and deposition of phenolic compounds including pyrogallol, gallic acid, pyrocatechol, tannic acid, catechin, and caffeic acid, some of the most common plant-derived phenolic compounds. In the first approach (**chapter 2**), it was demonstrated that reducing the pH of the solution to a slightly acidic condition slows down autoxidation kinetics, allowing the use of UV-induced photooxidation to control the deposition of polyphenolic compounds. In the second approach (**chapter 3**), inspired by the role of natural antioxidants in the human body to scavenge free radicals, antioxidants such as sodium ascorbate developed to inhibit the autoxidation of plant phenolic compounds in basic conditions. UV-light was used to induce on-demand oxidation of natural polyphenols in both strategies which enabled spatiotemporal control over the polymerization and deposition of polyphenols. UV-vis spectroscopy and cyclic voltammetry analysis indicated that the kinetics of the oxidation of polyphenols slows down by reducing the pH or by adding sodium ascorbate to the solution of phenolic compounds, while UV irradiation can trigger and accelerate the oxidation process on demand. AFM analysis indicated formation of more homogeneous nanocoatings in the presence of sodium ascorbate on the surface. Fluorescence microscopy, XPS and ToF-SIMS confirmed formation of nanocoatings and micropatterns of polyphenols on polar and non-polar substrates. These two strategies were used to create micropatterns or gradients of polyphenolic coatings, to control the polymerization temporally and in a stepwise manner, and to form patterns inside of microfluidic channels and capillaries, opening the way to well-defined 2D coatings based on

natural polyphenols and introducing a new simple path to the fabrication of bioinspired functional materials with potential applications in a wide range of fields.

In **chapter 4**, resorcin[4]arenes were used to modify the surface of a variety of metal and non-metal substrates. The surface modification was achieved by dip coating the substrates into the dilute solution of these macrocyclic polyphenols. Resorcin[4]arenes can interact with the surface the eight hydroxyl groups which serve as multiple anchoring points. Decorating the lower rim with desired appending groups enables the surface properties to be tuned. Deposition of a uniform, stable and transparent layer of resorcinarenes on the surface was confirmed by water contact angle measurements, UV-vis spectroscopy, atomic force microscopy (AFM), and X-ray photoelectron spectroscopy (XPS). A stable layer of resorcinarene was formed on amine-functionalized substrates possibly due to the covalent attachment of resorcinarene to the surface. A resorcinarene compound possessing four alkenyl groups at its lower rim was used to modify the surface, followed by site-selective post-functionalization via thiol-ene photoclick chemistry in order to introduce hydrophilic and hydrophobic micropatterns on the surface. Photopatterning was confirmed by XPS and time-of-flight secondary ion mass spectrometry (ToF-SIMS). A droplet microarray of liquids with either high or low surface tension was formed on the surface of the micropatterned glass substrate by rolling a drop of the liquid over the surface. This strategy could expand the choice of building blocks for this class of bioinspired nanocoatings from catecholamines and plant phenolic compounds to tailor-made multifunctional resorcinarenes.

5.2 Outlook

Plant polyphenol-inspired materials offer a diverse range of building blocks that can be used to design a wide variety of functional materials and tune the final material properties.

A promising area of further research in the field of plant polyphenol-inspired materials and coatings, would be the screening of a library of phenolic compounds and their combinations in order to strategically design multi-component phenolic materials. Investigation of properties of such libraries and combinations of polyphenols enables the engineering of surface properties such as antibacterial, antioxidant, and anticancer properties, which may lead to unexpected results. For example, antibacterial properties of tannic acid-based coatings have been investigated. However, properties of hundreds of other phenolic compounds have not been realized. Such studies may provide more insight into the structure-function relationship and the synergistic effects of polyphenols.

One approach could be combining polyphenols with strong antibacterial properties with other compounds possessing strong coating formation abilities. Identification of combinations of phenolic compounds that lead to antibacterial coatings that are non-toxic to mammalian cells would be attractive. Blending polyphenols with antibiotics or silver to discover new types of therapies would be another attractive topic.

Engineering material properties can be expanded to polyphenolic extracts of foods and beverages. Some of these extracts, for example extracts from green tea, are known to have herbal health benefits. In chapter 2, the coating formation ability of plant-sourced phenolic compounds from tea, wine, and coffee was demonstrated. This green approach can be used to develop environmentally-friendly approaches of surface functionalization.

Investigation of the degradation kinetics of phenolic coatings at different pH conditions can enable the design of a controlled-release mechanism of cargos that bind to phenolic coatings and materials. Degradation kinetics of the coatings or nanoparticles made of a combination of phenolic compounds could be different from individual compounds. Investigating these behaviors could lead to developing dual responsive nanocoatings and nanoparticles that can release two different cargos at two different pH range.

In chapter 4, I demonstrated that resorcinarenes are capable to bind to the surface of a variety of substrates. A promising extension of this concept would be using resorcinarenes to develop surface modification strategies with the ability to form specific host-guest interactions. Comprehensive research has been devoted to derivatize resorcinarenes to provide a wide range of choices for developing resorcinarene based host-guest system on the surface of a variety of substrates.

There are other attractive topics in the field of plant polyphenol-inspired materials that can be further investigated, such as expanding polyphenolic materials from 2D to 3D structure, tuning electrical conductivity by blending phenolic compounds and different metals, and improving mechanical properties of polyphenolic materials.

Polydopamine-based materials have been investigated widely in a variety of applications. Established concepts from dopamine-based materials can be employed into the plant polyphenol-inspired research to generate new ideas for different applications. For example, oxidizing agents or microwave irradiation have been used to accelerated the polymerization and deposition of dopamine. Such strategies can be applied to polyphenolic compounds as well. Plant polyphenol-inspired materials offer a wide range of diversity of chemical and physical properties compared to dopamine and other catecholamines.

Chapter 6. Experimental

6.1 Experimental details for chapter 2^a

6.1.1 Materials

Tannic acid (TA, 1701.19 g/mol, solid brown powder) was purchased from Sigma-Aldrich (Germany). All other (poly)phenols analogs, including, pyrogallol (PG, 126.11 g/mol, solid white powder), caffeic acid (CA, 170.12 g/mol, solid yellow powder), gallic acid (GA, 180.16 g/mol, solid powder) were purchased from Sigma (Germany). 2-Hydroxyethyl methacrylate (HEMA), ethylene dimethacrylate (EDMA) were purchased from Sigma-Aldrich (Germany).

Poly(tetrafluoroethylene) (PTFE), poly(methyl methacrylate) (PMMA), and poly(ethylene) (PE), glass slides, and silicon wafer substrates were cleaned by sonication in, deionized (DI) water, 2-propanol, and 0.1 M HCl for 10 min, washed with DI water, and dried with nitrogen gas. PMMA, PTFE, PE substrates were kindly provided by Institute of Toxicology and Genetics (ITG). Silver nitrate and all the other chemicals were purchased from Sigma-Aldrich (Germany) and used without further purification. High-purity DI water with a resistivity of 18.2 M Ω .cm was obtained from an inline Millipore water purification system. Acetone and the other solvents were obtained from Merck KGaA (Germany). Flexible UV transparent fused silica capillary tubing (TSU100375 model) was purchased from Polymicro Technologies (Germany).

All buffers were made at 100 mM concentration. The following buffers were used: acetate (pH 4, pH 5, pH 6), phosphate (pH 7, pH 8), and carbonate-bicarbonate (pH 9, pH 10). Sodium chloride (600 mM) was added to buffers in deposition and patterning process.

6.1.1 Characterization

UV-Vis spectroscopy was performed with an Epoch 2 microplate spectrophotometer (BioTech). UV-Vis transmittance of glass slides was measured with a Lambda 35 UV-Vis Spectrometer (PerkinElmer). A UK 1115 digital camera from EHD imaging (Germany) was used to take images of the water droplet on the surface under ambient conditions. ImageJ

^a This sub-chapter is adapted from Ref.²⁴

software with a Dropsnake plugin was used to measure the static water contact angle. The brightfield and fluorescence images were taken using a Leica DFC360 microscope (Germany). Mass analysis was performed using an electrospray ionization mass spectrometry (ESI-MS) (Bruker ESI-TOF in INT, KIT).

XPS measurements were performed using a K-Alpha+ XPS spectrometer (ThermoFisher Scientific, East Grinstead, UK). All coatings were analyzed using a microfocused, monochromated Al K α X-ray source (400 μ m spot size). The K-Alpha charge compensation system was employed during analysis, using electrons of 8 eV energy, and low-energy argon ions to prevent any localized charge build-up. The spectra were fitted with one or more Voigt profiles (BE uncertainty: ± 0.2 eV) and Scofield sensitivity factors were applied for quantification. All spectra were referenced to the C 1s peak (C-C, C-H) at 285.0 eV binding energy controlled by means of the well-known photoelectron peaks of metallic Cu, Ag, and Au, respectively.

The distributions of phenolic mass fragments and silver ions on the surface were investigated with a time of flight secondary ion mass spectrometry (ToF-SIMS) (ION TOF Inc., Münster, Germany), IFG, KIT. Atomic force microscopy was performed on a Dimension Icon AFM (Bruker) in standard tapping mode in air, INT, KIT. Cantilevers used were of type HQ:NSC15/AI BS (MikroMasch) with a nominal force constant of 40 N/m and a resonance frequency of 325 kHz.

6.1.2 UV-irradiation of phenolics solutions

An OAI model 30 deep-UV collimated light source (San Jose, CA, USA) fitted with a 500 W HgXe lamp was used for UV irradiation. The lamp was calibrated to 10 mW/cm² at 260 nm with the OAI 306 UV power meter. Reaction solutions were transferred into a glass vial and irradiated under UV lamp for 2 h (stirred at room temperature, ambient atmosphere).

6.1.3 UV-Vis absorption experiments

Phenolic compound solution (0.2 mg/mL) in buffers at different pH (100 mM) were stored in dark environment (dark samples) and were irradiated under UV (UV samples) for 2 h. The UV-Vis absorbance (300-900 nm) of the dark and UV samples measured at different time points (0, 30, 60, 90 and 120 min, buffer as the reference) using a Biotek Epoch 2 spectrophotometer.

6.1.4 Deoxygenated solutions

In order to keep the low oxygen-containing conditions, nitrogen gas was passed through the PG solution for 30 min in a quartz vial equipped with a septum. After purging nitrogen solution, the vial was irradiated for 2 h with the same UV light used for other solutions. The same procedure was used to prepare solution in a dark environment.

6.1.5 Samples containing DMSO

Buffer solutions (pH 7.0 non-purged solutions were used) containing 5 volume % DMSO were added to the PG solutions (0.2 mg/mL) and samples were irradiated with UV or kept in the dark for 2 h. UV-Vis absorption spectra were recorded at 0 min, 30 min, 60 min, 90 min, and 120 min.

6.1.6 UV-Vis measurement in DI water and deuterium oxide medium

PG solution (0.2 mg/mL) in DI water was subjected to UV irradiation or kept in dark environment for 2 h, and UV-Vis absorption spectra were recorded at 0 min, 30 min, 60 min, 90 min, and 120 min. The same procedure was used to measure UV-Vis spectra of PG solution (0.2 mg/mL) in deuterium oxide.

6.1.7 *Electrochemistry*

All electrochemical measurements were performed with a Reference 600 potentiostat (Gamry Instruments, Warminster, PA) in a three-electrode cell with a coiled Pt wire as the counter electrode, a Ag/AgCl (3 M KCl) reference electrode and a glassy carbon disk electrode (3 mm in diameter) was employed as a working electrode. The phenolic compounds (1.58 mM) were dissolved in buffer (100 mM) at different pH values (vide supra). Cyclic voltammograms were scanned from -0.2 V to 1 V for gallic acid and -0.2 V to 0.8 V for the other phenolic compounds at a scan rate of 100 mV/s. The glassy carbon electrode was polished before each cycle with 0.3 μm alumina slurry and rinsed thoroughly with DI water to remove adsorbed polymeric species resulting from the previous measurements. A neoLab-UV Inspection Lamp Type 6 with 14 mW/cm^2 was used for UV irradiation and positioned at a distance of 0.5 cm of a quartz cuvette containing the solution of the phenolic compound. The cyclic voltammograms were recorded at different time points (0, 30, 60, 90 and 120 min).

6.1.8 *Deposition of a phenolic layer on the substrate*

Clean substrates were immersed in buffered solutions of 10 mM precursor for 2 h, 6 h, 12 h, 24 h 48 h in dark room at room temperature. Modified samples were then rinsed thoroughly with DI water and dried with nitrogen gas. Same conditions used to modify substrate with precursor under UV irradiation for 2 h. Coatings were visualized by immersing samples in 10 mM AgNO_3 for 48 h, followed by rinsing thoroughly with DI water, and drying with N_2 gas.

6.1.9 *Photopatterning of polyphenols*

For patterning on the substrate, a photomask was fixed on top of the substrate. After filling the 10 mM phenolic solution (pH 5.0 for PG and pH 7.0 for TA), the sample was UV irradiated for 1 h. Then photomask was removed and the sample was rinsed with DI water and dried with N_2 . For the secondary modification by AgNO_3 , the patterned substrates were immersed into a 10 mM AgNO_3 aqueous solution for 48 h, followed by washing with DI water and drying with

N₂. For the secondary modification by Rhodamine-SH (Rhodamine B was modified with cysteamine as described in our previous report¹²⁰ to yield a rhodamine-thiol), the patterned substrates were immersed in a mixture containing 3 mL of DI water, 10 mg of the dye and 70 μ L of triethylamine for 24 h, then the substrate was carefully washed with DI water and dried with N₂.

6.1.10 Gradient pattern

In order to make a polyphenolic gradient pattern, poly(HEMA-EDMA) modified substrate (detail of nano-porous poly(HEMA-EDMA) could be found in our previous report¹¹⁶), was fed into the patterning setup described before, and filled with PG solution (0.01 mg/mL, pH 7.0, phosphate buffer). A black cardboard cover was used to cover the photomask. To make a gradient pattern of polyphenol, different regions of the surface were exposed to UV light from 0.0 to 7.5 min by moving the cardboard gradually.

6.1.11 Patterning inside a capillary

First, capillaries were modified with porous poly(HEMA-EDMA). Briefly, capillaries were filled with a sodium hydroxide solution (1 mol/L) for 1 h, followed by rinsing with DI water, then filling with an HCl solution (1 mol/L) for 30 min, then washing with DI water and drying with pumping air inside the capillary. The activated glass surface was functionalized with 20 % vol. 3-(trimethoxysilyl)propyl methacrylate in ethanol for 30 min followed by washing with ethanol. The polymerization mixture (HEMA 24 % wt., EDMA 16 % wt., 1-decanol 45.5 % wt., cyclohexanol 14.5 % wt., 2,2-dimethoxy-2-phenylacetophenone (DMPAP) 1 % wt. with respect to monomers) was injected into the modified capillary using a syringe. Capillary filled with the polymerization mixture was placed under the UV lamp and irradiated with UV light for 15 min (The lamp was calibrated to 10 mW/cm² at 260 nm with the OAI 306 UV power meter.) followed by washing with ethanol. Porous polymer was formed inside the capillary. In order to make a polyphenolic pattern inside the capillary, PG solution (0.01 mg/mL, pH 7.0, phosphate) was injected into the capillary using a syringe. Capillary filled with the PG solution was placed

under a photomask and irradiated with UV light (10 mW/cm² at 260 nm) for 10 min followed by washing with DI water and acetone. For secondary modification with silver particles and fluorescent dye, aqueous solution of silver nitrate (10 mM) or Rhodamine 110 chloride solution (0.2 mg/mL in 10 mM phosphate buffer at pH 8.0) were injected into the capillaries and reacted overnight, followed by washing with DI water and acetone and drying with air.

6.1.12 Deposition of polyphenols present in tea, coffee, and wine

Green tea bags (TEEKANNE Grüner TEE) and 20 g coffee powder (Bellarom espresso coffee) were steeped for 10 min in 100 mL DI water at 80°C and left to be cooled to room temperature following by filtration with paper filter. 50 mL of tea infusion, coffee infusion, wine (VIÑA DEL ASADOR® Rioja DOCa) transferred to petri dish and a cleaned glass slide was dipped into beverages solution. After 1 h in dark environment or 1 h UV irradiation with the described setup glass slides were rinsed with DI water. In order to visualize the phenolic coating glass slides placed in 10 mM AgNO₃ aqueous solution for 48 h followed by rinsing with DI. Photographing and UV-Vis spectroscopy of glass slides were performed before and after each step.

6.2 Experimental details for chapter 3^a

6.2.1 Materials

Materials. Pyrogallol (PG), gallic acid (GA), pyrocatechol (Ctl), epigallocatechin gallate (EGCG), tannic acid (TA), catechin (Ctn), hydroxyhydroquinone (HHQ), caffeic acid (CA), and morin were purchased from Sigma-Aldrich. L-Ascorbic acid sodium salt and uric acid were purchased from Alfa Aesar. Glutathione (reduced) was purchased from Amresco (Germany). Silver nitrate, Rhodamine 110 chloride, and all the other chemicals were purchased from Sigma-Aldrich and used without further purification. 2-Hydroxyethylmethacrylate (HEMA), ethylene

^a This sub-chapter is adapted from Ref.²³

dimethacrylate (EDMA) were purchased from Sigma-Aldrich. Nexterion B glass slides obtained from Schott AG and silicon wafers (CZ-Si-wafer 4 in.) from MicroChem GmbH were used. Glass slides and silicon wafer substrates were cleaned by sonication in deionized (DI) water, 2-propanol, and 0.1 M HCl for 5 min, washed with DI water, and dried with nitrogen gas. Flexible UV-transparent fused silica capillary tubing (TSU100375 model) was purchased from Polymicro Technologies. High-purity DI water with a resistivity of 18.2 M Ω cm was obtained from an in-line Millipore water purification system. Acetone and the other solvents were obtained from Merck KGaA. Phosphate buffers were made at 5 mmol/L concentration at pH 8.0. The final pH value adjusted by using a METTLER TOLEDO digital pH meter.

6.2.1 Characterization

Characterization. UV-vis spectroscopy was performed with a Lambda 35 UV-vis spectrometer (PerkinElmer). The bright-field and fluorescence images were taken using a Leica DFC360 microscope and Keyence BZ-9000 microscope. ImageJ software was used to measure gray value. Mass analysis was performed using an ESI-MS (Bruker ESI-TOF in INT, KIT) instrument in positive mode. Atomic force microscopy (AFM) was performed on a Dimension Icon AFM (Bruker) in standard tapping mode in air, INT, KIT. Cantilevers used were of type HQ:NSC15/AI BS (MikroMasch) with a nominal force constant of 40 N/m and a resonance frequency of 325 kHz. The distributions of phenolic mass fragments on the surface were investigated with time-of-flight secondary ion mass spectrometry (ToF-SIMS) (ION TOF Inc.), IFG, KIT. XPS measurements were performed using a K-Alpha+ XPS spectrometer (ThermoFisher Scientific, East Grinstead, UK), IAM, KIT. Data acquisition and processing using the Thermo Advantage software are described elsewhere.¹²¹ All coatings were analyzed using a microfocused, monochromated Al K α X-ray source (400 μ m spot size). The KAlpha charge compensation system was employed during analysis, using electrons of 8 eV energy, and low-energy argon ions to prevent any localized charge build-up. The spectra were fitted with one or more Voigt profiles (BE uncertainty: + 0.2 eV), and Scofield sensitivity factors were applied for quantification.¹²² All spectra were referenced to the C 1s peak (C-C, C-H) at 285.0 eV binding energy controlled by means of the well-known photoelectron peaks of metallic

Cu, Ag, and Au, respectively. The K-alpha+ snapmap option was used to image an area of 2×2 mm with an X-ray spot of 200 μm (5 iterations were run to reach a better statistic).

6.2.2 *UV Irradiation of phenolic solutions*

UV Irradiation of Phenolic Solutions. An OAI model 30 deep-UV collimated light source (San Jose, CA) fitted with a 500 W HgXe lamp was used for UV irradiation. The lamp was calibrated to 6 mW/cm^2 at 260 nm with the OAI 306 UV power meter. Reaction solutions were transferred into a quartz cuvette and irradiated under UV lamp for 2 h (unless stated otherwise) at room temperature, ambient atmosphere.

6.2.3 *UV-vis absorption experiments*

UV-vis absorption experiments. A 2 mL phenolic compound solution (0.2 mg/mL, unless stated otherwise) in the phosphate buffers at pH 8.0 (5 mmol/L) was stored in dark environment (dark samples) and irradiated under UV (UV samples) in quartz cuvettes for the desired time. The UV-vis absorbance (230-700 nm) of the dark and UV samples was measured at different time points (0, 5, 15, 30, 45, 60, 90, and 120 min; buffer as the reference) using a Lambda 35 UV-vis spectrometer (PerkinElmer). For sample stored for a longer time, 2 mL of the solution was added into a quartz cuvette and sealed for each time point. UV-vis spectra were measured after 6, 12, 24, 48, and 72 h. Morin solution was prepared at 0.05 mg/mL in the phosphate buffer at pH 8.0 (5 mmol/L). For samples contacting antioxidants, the desired amount of the antioxidant was added to the buffer solution, and then the phenol was added to this solution. Because of the solubility issue of UA, PG solutions containing UA were prepared at 0.1 mg/mL in a 2.5 mmol/L phosphate buffer at pH 8.0.

For on-demand polymerization experiments, PG solution (0.2 mg/mL, phosphate buffer pH 8.0, 5 mmol/L, with GSH/PG molar ratio of 0.8:1 or without antioxidant) was kept in the dark for 30, 60, 90, 120, 150, and 180 min before recording the solution's UV-vis absorption spectra. After UV irradiation for 5 min at 30, 60, 90, and 120 min the solution was placed in the dark,

and the solution's UV-vis spectrum was recorded every 30 min for 3 h. Similar experiments were done on PG solutions with 5 min of UV irradiation at different time points (30, 60, 90, 120, and 150 min), and the UV-vis spectra of the solutions were recorded every 30 min. In another set of experiments, the solution was stored in dark and continuously irradiated with UV light at different time points, and the UV-vis spectra were recorded every 30 min for 3 h.

6.2.4 *Electrochemistry*

Electrochemistry. All electrochemical measurements were performed with a Reference 600 potentiostat (Gamry Instruments, Warminster, PA) in a three-electrode cell with a coiled Pt wire as the counter electrode, and an Ag/AgCl (3 mol/L KCl) reference electrode.

The working electrodes were a specifically activated glassy carbon disk electrode (3 mm in diameter) prepared as described in the literature.¹²³ The electrodes were polished with 0.3 μm alumina slurry and activated before each measurement. The phenolic compounds (1.58 mmol/L) were dissolved in phosphate buffer (5 mmol/L) at pH 8.0. A neoLab-UV inspection lamp Type 6 with 14 mW/cm^2 was used for UV irradiation and positioned at a distance of 0.5 cm from a quartz cuvette containing the solution of the phenolic compound. The differential pulse voltammetry (DPV) was measured from -0.2 to 0.8 V with 25 mV pulse size, and the frequency is 5 Hz. The low buffer concentration does not provide sufficient ionic strength for the DPV measurements. Therefore, 0.1 mol/L KCl was added to the solution before measurement.

6.2.5 *Deposition of polyphenolic layer on the silicon surface*

Deposition of the Polyphenolic Layer on the Silicon Surface. Sodium chloride (60 mmol/L) was added to the phosphate buffers (5 mmol/L) in the deposition and micropatterning process to increase the ionic strength of the solution. Clean silicon substrates were immersed in buffered solutions of 0.2 mg/mL PG with SA (SA/PG molar ratio 0.4:1) or without SA for 30 min in dark room or under UV irradiation at room temperature. Modified samples were then rinsed thoroughly with DI water and ethanol and dried with nitrogen gas followed by a gentle scratch

with one tip of a pair of tweezers. Similarly, a phenolic layer was deposited on the surface of silicon by immersing the silicon surface in a 0.2 mg/mL (0.05 mg/mL for morin) phenolic solution of Ctl, EGCG, TA, Ctn, HHQ, and morin containing SA at SA/phenol molar ratios of 0.15, 0.70, 0.85, 0.4, 1.50, and 0.30:1, respectively, and the samples were stored overnight in dark. The same conditions were used to make a phenolic layer on the silicon surface under UV irradiation for 30 min.

6.2.6 Photopatterning of phenolics

Photopatterning of Phenolics. For patterning on the substrate, a photomask was fixed on top of the poly(HEMA-EDMA) substrate using a setup described in our previous report.²⁴ Details of nanoporous poly(HEMA-EDMA) preparation could be found in our report.¹¹⁶ A 0.2 mg/mL phenolic solution of PG, GA, Ctl, EGCG, TA, Ctn, and HHQ containing SA at SA/phenol molar ratios of 0.4, 0.1, 0.15, 0.70, 0.85, 0.4, and 1.50:1, respectively, was filled in between the photomask and the substrate, and the sample was UV irradiated for 10 min. Then, the photomask was removed, and the sample was rinsed with DI water and ethanol and dried with N₂. For the secondary modification by AgNO₃, the patterned substrates were immersed into a 10 mmol/L AgNO₃ aqueous solution overnight, followed by washing with water and drying with N₂. For the secondary modification by Rhodamine 110, the patterned substrates were immersed in an ethanol/phosphate buffer (pH 8.0, 5 mmol/L) 1:1 mixture containing 0.1 g/mL of dye overnight; then, the substrate was carefully washed with deionized water and ethanol and dried with N₂.

6.2.7 Sequential patterning of polyphenols

Sequential Patterning of Polyphenols. For the preparation of the “KIT” pattern of three different polyphenols, first, the left part of the KIT logo was deposited on the surface of poly(HEMA-EDMA) by irradiating the PG solution (0.2 mg/mL, phosphate buffer 5 mmol/L, pH 8.0) containing SA/PG 0.4:1 molar ratio through a photomask, followed by washing the substrate with water and ethanol and secondary modification with Rhodamine 110 by incubation in dye solution overnight as explained before. Then, the “K” and “T” letters, the middle and

right part of the logo, were deposited on the surface by UV irradiation of Ctn and HHQ solutions (0.2 mg/mL, phosphate buffer 5 mmol/L, pH 8.0) containing SA/phenol 0.4, 1.5:1 molar ratio through the photomask for 10 min, respectively, followed by washing after each step. Three different filter sets [filter set 1 (DsRED), excitation filter 510-560 nm, emission filter 590-650 nm; filter set 2 (GFP plants), excitation filter 450-490 nm, emission filter 500-550 nm; filter set 3 (CFP), excitation filter 426-446 nm, emission filter 460-500 nm] were used to visualize each phenolic pattern. The “KIT” pattern was modified with silver particles by immersing it in a silver nitrate 10 mmol/L aqueous solution overnight.

An overlaid pattern of polyphenols was made on the poly(HEMAEDMA) surface first by irradiation of PG solution (0.2 mg/mL, phosphate buffer 5 mmol/L, pH 8.0) containing SA with SA/PG 0.4:1 molar ratio and subsequent secondary modification with Rhodamine 110 as described before. The second pattern was formed by irradiation of Ctn solution (0.2 mg/mL, phosphate buffer 5 mmol/L, pH 8.0) containing SA with SA/PG 0.4:1 molar ratio followed by washing with water and ethanol after each step. Two different filter sets filter set 4 (TexasRed), excitation filter 522-602 nm, emission filter 584-664 nm; filter set 5 (DAPI-BP), excitation filter 327-427 nm, emission filter 387-507 nm] were used to visualize each phenolic pattern.

6.2.8 *Gradient pattern*

Gradient Pattern. For a gradient of the polyphenolic pattern, poly(HEMA-EDMA)-modified substrate was fed into the patterning setup described before, and filled with PG solution (0.2 mg/mL, phosphate buffer 5 mmol/L, pH 8.0) containing SA with SA/PG 0.4:1 molar ratio. A black cardboard cover was used to cover the photomask.

For a gradient pattern of polyphenol, the cardboard was pulled off the photomask gradually within 5 min. Gradient patterns of polyphenols were modified with silver particles as described before. For overlaid gradient patterns, after deposition of the first pattern (triangle) by 5 min of UV irradiation of PG solution through a photomask and modification with Rhodamine as describe before, the second gradient pattern (hexagonal) was deposited on the same substrate by UV irradiation of Ctn solution through a photomask for another 5 min as describe before. The black cardboard was pulled off in the opposite direction (from right to left for PG and from

left to right for Ctn) to make a contrast of patterns on two different sides. The substrate was immersed overnight in 10 mmol/L aqueous silver nitrate solution or Rhodamine dye solution for modification with silver or Rhodamine.

6.2.9 *Patterning inside a capillary*

Patterning Inside a Capillary. First, capillaries were modified with porous poly(HEMA-EDMA) according to our previous report.²⁴ Briefly, capillaries were filled with a sodium hydroxide solution (1 mol/L) for 1 h, followed by rinsing with DI water, then filling with an HCl solution (1 mol/L) for 30 min, then washing with DI water and drying with pumping air inside the capillary. The activated glass surface was functionalized with 20 vol % 3-(trimethoxysilyl)propyl methacrylate in ethanol for 30 min followed by washing with ethanol. The polymerization mixture (HEMA 24 wt %, EDMA 16 wt %, 1-decanol 45.5 wt %, cyclohexanol 14.5 wt %, 2,2-dimethoxy-2-phenylacetophenone 1 wt % with respect to monomers) was injected into the modified capillary using a syringe. The capillary filled with the polymerization mixture was placed under the UV lamp and irradiated with UV light for 15 min (the lamp was calibrated to 6 mW/cm² at 260 nm with the OAI 306 UV power meter) followed by washing with ethanol. A porous polymer was formed inside the capillary. For a polyphenolic pattern inside the capillary, PG solution was injected into the capillary using a syringe. The capillary filled with the PG (0.2 mg/mL, phosphate buffer 5 mmol/L, pH 8.0) containing SA with SA/PG 0.4:1 molar ratio was placed under a photomask and irradiated with UV light (6 mW/cm² at 260 nm) for 10 min followed by washing with DI water and acetone. For secondary modification with silver particles and fluorescent dye, an aqueous solution of silver nitrate or Rhodamine 110 chloride solution described before was injected into the capillaries and reacted overnight, followed by washing with DI water and acetone and drying with air.

6.3 Experimental details for chapter 4^a

6.3.1 *Materials*

C-methylcalix[4]resorcinarene (**1**) and C-undecylcalix[4]resorcinarene monohydrate (**2**) resorcinol, 10-undecenal were purchased from Sigma-Aldrich (China, Switzerland, Germany, India, respectively). 2-Hydroxyethyl methacrylate (HEMA) and ethylene dimethacrylate (EDMA) were purchased from Sigma-Aldrich (Germany) and purified through a short column filled with basic aluminum oxide to get rid of the inhibitors. All the other chemicals were purchased from Sigma-Aldrich (Germany) and used without further purification. Formate (pH 3), phosphate (pH 7), and carbonate–bicarbonate (pH 9) buffers were prepared at 100 mM concentration.

Nexterion B glass slides were obtained from Schott AG (Mainz, Germany) and silicon wafers (CZ-Si-wafer 4 inch) from MicroChem GmbH (Berlin, Germany) were used. Polyethylene (PE), polymethyl methacrylate (PMMA), stainless steel (steel), aluminum (Al), zinc copper alloy (Zn) substrates were kindly provided by Institute of Toxicology and Genetics (ITG) at the KIT. Bare glass slides and silicon wafer substrates were cleaned by sonication for 10 min in, deionized (DI) water, 2-propanol, and acetone and dried with nitrogen gas. DI water, 2-propanol, and ethanol were used to clean other substrates by 10 min sonication followed by drying with nitrogen gas. High-purity DI water with a resistivity of 18.2 MΩ cm was obtained from an inline Millipore water purification system. Acetone and the other solvents were obtained from Merck KGaA (Germany). Tris buffers were made at 10 mM concentration at pH 8.5. The final pH value adjusted by using a Mettler Toledo digital pH meter (China).

6.3.2 *Characterization*

Mass spectrometry was performed using an ESI-MS (Bruker ESI-TOF, Institute of Nanotechnology (INT), KIT) in positive mode. ¹H NMR spectra were recorded on a DRX-500

^a This sub-chapter is adapted from Ref.¹¹⁴

(500 MHz) (Bruker, Germany), and chemical shifts were reported in ppm using residual solvent peaks as internal standards. The UV–vis absorbance (200–900 nm) of the bare and coated glass slides was measured using a Lambda 35 UV–vis spectrometer (PerkinElmer, Germany). Apparent contact angle of different liquids (~4 μL) on bare and modified substrates was measured using a Drop Shape Analyzer model DSA25S (Krüss, Hamburg, Germany). Advancing contact angles were obtained by measuring the contact angle while the liquid was slowly added (at a rate of 0.1 $\mu\text{L/s}$) from a ~4 μL droplet to 12 μL in contact with the sample and a micrometer syringe. Receding contact angles were obtained with liquid slowly retracting (at a rate of 0.1 $\mu\text{L/s}$) from a ~12 μL droplet to 4 μL . Atomic force microscopy (AFM) was performed on a Dimension Icon AFM (Bruker, Karlsruhe, Germany) in standard tapping mode in air (INT, KIT). Cantilevers used were of type HQ:NSC15/AI BS (MikroMasch) with a nominal force constant of 40 N m^{-1} and a resonance frequency of 325 kHz. The thickness of the resorcinarene layer on silicon substrates was measured using spectroscopic ellipsometry in dry state (M44, Woollam Co., Inc., Lincoln NE, USA). The ellipsometry measurements were performed at an angle of incidence of 75° in the spectral region of 370–900 nm. Ellipsometric parameters were fitted using a Cauchy model. ToF-SIMS experiments were performed on a TOF-SIMS 5 machine (ION-TOF GmbH, Münster, Germany) at the Institute of Functional Interfaces, KIT. XPS measurements were performed using a K-Alpha+ XPS spectrometer (ThermoFisher Scientific, East Grinstead, UK), IAM, KIT. Data acquisition and processing using the Thermo Advantage software is described elsewhere.¹²¹ All coatings were analyzed using a micro-focused, monochromated Al $K\alpha$ X-ray source (400 μm spot size). The K-Alpha+ charge compensation system was employed during analysis, using electrons of 8 eV energy, and low-energy argon ions to prevent any localized charge build-up. The spectra were fitted with one or more Voigt profiles (BE uncertainty: $\pm 0.2\text{eV}$) and Scofield sensitivity factors were applied for quantification.¹²² All spectra were referenced to the C 1s peak (C-C, C-H) at 285.0 eV binding energy controlled by means of the well-known photoelectron peaks of metallic Cu, Ag, and Au, respectively. The K-alpha+ snapmap option was used to image an area of 3×3 mm with an X-ray spot of 50 μm . (8 iterations were run in order to reach a better statistic).

6.3.3 *Synthesis of C-dec-9-enylresorcin[4]arene*

Compound **3** was synthesized by the acid catalyzed condensation of resorcinol with 10-undecenal by heating the reactants to reflux in a mixture of ethanol at 60°C for 16 hours according to our previous report.⁴² Briefly, 12 N hydrochloric acid (32 mL) was added to a solution of 10-undecenal (33.6 g, 0.2 mol) and resorcinol (22.0 g, 0.2 mol) in ethanol (200 mL) over 10 min at 0°C. The red oil that formed after stirring the mixture for 16 h at 60°C was poured into well-stirred deionized water (600 mL). The orange precipitate was filtered off and washed thoroughly with hot deionized water followed by drying. The solid product was dissolved in acetonitrile (ACN) at 40°C and kept at room temperature for 3 h. By decanting the solution, the precipitated dark oil was removed. The yellow resulting solution was concentrated around by one-third and cooled to 0°C. The solvent was decanted after precipitation of another part of the dark oil. This procedure was repeated until no more dark precipitation was formed. The solvent was removed under reduced pressure to afford about 10 g (22%) of **3**. Nuclear magnetic resonance (NMR) and mass spectrometry (ESI-MS) analysis were used to characterize compound **3**. ¹H NMR (500 MHz, CDCl₃) of **3** is shown in Figure S9.1. ESI-MS (positive mode, *m/z*): [M+Na]⁺_{theor.}=1063.6991, [M+Na]⁺_{exp.}=1063.7035 (Figure S9.2).

6.3.4 *Deposition of the resorcinarene layer on the surface*

Cleaned substrates were immersed in a 0.8 mg/mL solution of **1**, **2**, or **3** in a 1:1, 3:1, or 1:1 ethanol:tris buffer (10 mM, pH 8.5) mixture, respectively, for 24 h at room temperature with a gentle agitation. Resorcinarene modified samples were then rinsed thoroughly with DI water and ethanol and dried with nitrogen gas.

6.3.5 *Preparation of amine-functionalized surfaces*

Cleaned glass-plates were immersed in 1 M NaOH for 1 h and afterward washed with deionized water followed by immersing them in 1 M HCl for 30 min, washing with deionized water and drying with a nitrogen gun. Bare glass plates were immersed into 50 mL of ethanol

containing 20 % vol. (3-aminopropyl)triethoxysilane. Then, the solution was stirred at RT for 5 min. The substrates were washed with ethanol and dried with nitrogen gas. Details of the preparation of amine-functionalized nanoporous poly(HEMA) could be found in our reports.^{116,124}

6.3.6 *Post-functionalization of C-dec-9-enylresorcin[4]arene*

Amine-functionalized glass or amine-functionalized porous poly(HEMA) substrates were modified with **3** according to the deposition process described above. **3**-modified substrates were wetted with ethyl acetate solution of 20 vol% of *1H,1H,2H,2H*-perfluorodecanethiol (PFDT), covered by a quartz slide, and irradiated by 5.0 mW/cm² 260 nm UV light for 1 min. After removing the quartz slide, the glass was washed with ethanol and dried with nitrogen gas. For post-functionalization with 2-mercaptoethanol (ME), the **3**-modified substrates were wetted with ethanol-water (1:1) solution containing 10 wt% of ME, covered by a quartz slide, and irradiated by UV light for 1 min. The substrates were washed extensively with ethanol and dried.

6.3.7 *Photopatterning on the 3-modified surface*

The same procedure as used for post-functionalization was employed for photopatterning, however, instead of quartz slide a quartz chromium photomask was used to UV irradiate PFDT solution for 1 min. After removing the photomask, the substrate was washed with ethanol and dried. The resulting substrate was wetted again with ethanol-water (1:1) solution containing 10 wt% of ME, covered by a quartz slide, and irradiated by UV light for 1 min. The substrate was washed extensively with ethanol and dried. For ToF-SIMS analysis, the **3**-modified glass was first post-functionalized with ME by UV irradiating the ME solution through a photomask, followed by washing and subsequent post-functionalization with PFDT as described above. A droplet microarray formed on the micropatterned surface spontaneously by rolling a colored droplet of the liquid on the surface. Food dyes were used to give color to the liquids forming droplet microarray.

References

- (1) Lee, H.; Dellatore, S. M.; Miller, W. M.; Messersmith, P. B. Mussel-Inspired Surface Chemistry for Multifunctional Coatings. *Science* **2007**, *318*, 426-430.
- (2) Mattiuzzi, A.; Jabin, I.; Mangeney, C.; Roux, C.; Reinaud, O.; Santos, L.; Bergamini, J.-F.; Hapiot, P.; Lagrost, C. Electrografting of Calix [4]Arenediazonium Salts to Form Versatile Robust Platforms for Spatially Controlled Surface Functionalization. *Nat. Commun.* **2012**, *3*, DOI:10.1038/ncomms2121.
- (3) Wei, Q.; Haag, R. Universal Polymer Coatings and Their Representative Biomedical Applications. *Mater. Horiz.* **2015**, *2*, 567–577.
- (4) Ryu, J. H.; Messersmith, P. B.; Lee, H. Polydopamine Surface Chemistry: A Decade of Discovery. *ACS Appl. Mater. Interfaces* **2018**, *10*, 7523–7540.
- (5) Sileika, T. S.; Barrett, D. G.; Zhang, R.; Lau, K. H. A.; Messersmith, P. B. Colorless Multifunctional Coatings Inspired by Polyphenols Found in Tea, Chocolate, and Wine. *Angew. Chem., Int. Ed.* **2013**, *52*, 10766–10770.
- (6) Barrett, D. G.; Sileika, T. S.; Messersmith, P. B. Molecular Diversity in Phenolic and Polyphenolic Precursors of Tannin-Inspired Nanocoatings. *Chem. Commun.* **2014**, *50*, 7265–7268.
- (7) Liu, Y. L.; Ai, K. L.; Lu, L. H. Polydopamine and Its Derivative Materials: Synthesis and Promising Applications in Energy, Environmental, and Biomedical Fields. *Chem. Rev.* **2014**, *114*, 5057–5115.
- (8) Du, X.; Li, L. X.; Li, J. S.; Yang, C. W.; Frenkel, N.; Welle, A.; Heissler, S.; Nefedov, A.; Grunze, M.; Levkin, P. A. Uv-Triggered Dopamine Polymerization: Control of Polymerization, Surface Coating, and Photopatterning. *Adv. Mater.* **2014**, *26*, 8029-8033.
- (9) Lee, M.; Lee, S.-H. H.; Oh, I.-K. K.; Lee, H. Microwave-Accelerated Rapid, Chemical Oxidant-Free, Material-Independent Surface Chemistry of Poly(Dopamine). *Small* **2017**, *13*, 1–6.
- (10) Ponzio, F.; Barthes, J.; Bour, J.; Michel, M.; Bertani, P.; Hemmerle, J.; d'Ischia, M.; Ball, V. Oxidant Control of Polydopamine Surface Chemistry in Acids: A Mechanism-Based

- Entry to Superhydrophilic-Superoleophobic Coatings. *Chem. Mater.* **2016**, *28*, 4697–4705.
- (11) Yang, H.-C. C. H.-C.; Luo, J. Q.; Lv, Y.; Shen, P.; Xu, Z.-K. Z.-K. K. Surface Engineering of Polymer Membranes via Mussel-Inspired Chemistry. *J. Membr. Sci.* **2015**, *483*, 42–59.
- (12) Lee, H.; Scherer, N. F.; Messersmith, P. B. Single-Molecule Mechanics of Mussel Adhesion. *Proc. Natl. Acad. Sci. U. S. A.* **2006**, *103*, 12999–13003.
- (13) Lu, Q. Y.; Danner, E.; Waite, J. H.; Israelachvili, J. N.; Zeng, H. B.; Hwang, D. S. Adhesion of Mussel Foot Proteins to Different Substrate Surfaces. *J. R. Soc., Interface* **2013**, *10*, DOI: 10.1098/rsif.2012.0759.
- (14) Zhang, Q. M.; Serpe, M. J. Versatile Method for Coating Surfaces with Functional and Responsive Polymer-Based Films. *ACS Appl. Mater. Interfaces* **2015**, *7*, 27547–27553.
- (15) Holten-Andersen, N.; Harrington, M. J.; Birkedal, H.; Lee, B. P.; Messersmith, P. B.; Lee, K. Y. C.; Waite, J. H. PH-Induced Metal-Ligand Cross-Links Inspired by Mussel Yield Self-Healing Polymer Networks with near-Covalent Elastic Moduli. *Proc. Natl. Acad. Sci. U. S. A.* **2011**, *108*, 2651–2655.
- (16) Zhang, C.; Ou, Y.; Lei, W.-X. X.; Wan, L.-S. S.; Ji, J.; Xu, Z.-K. K. CuSO₄/H₂O₂-Induced Rapid Deposition of Polydopamine Coatings with High Uniformity and Enhanced Stability. *Angew. Chem., Int. Ed.* **2016**, *55*, 3054–3057.
- (17) Perrot, D.; Croutxé-Barghorn, C.; Allonas, X. Towards Mussel-like on-Demand Coatings: Light-Triggered Polymerization of Dopamine through a Photoinduced PH Jump. *Polym. Chem.* **2016**, *7*, 2635–2638.
- (18) Knorr, D. B.; Tran, N. T.; Gaskell, K. J.; Orlicki, J. A.; Woicik, J. C.; Jaye, C.; Fischer, D. A.; Lenhart, J. L. Synthesis and Characterization of Aminopropyltriethoxysilane-Polydopamine Coatings. *Langmuir* **2016**, *32*, 4370–4381.
- (19) Wang, Z.; Xu, Y.; Liu, Y.; Shao, L. A Novel Mussel-Inspired Strategy toward Superhydrophobic Surfaces for Self-Driven Crude Oil Spill Cleanup. *J. Mater. Chem. A*

- 2015**, *3*, 12171–12178.
- (20) Zheng, X.; Chen, F.; Zhang, J.; Cai, K. Silica-Assisted Incorporation of Polydopamine into the Framework of Porous Nanocarriers by a Facile One-Pot Synthesis. *J. Mater. Chem. B* **2016**, *4*, 2435–2443.
- (21) Song, Y.; Ye, G.; Lu, Y.; Chen, J.; Wang, J.; Matyjaszewski, K. Surface-Initiated ARGET ATRP of Poly(Glycidyl Methacrylate) from Carbon Nanotubes via Bioinspired Catechol Chemistry for Efficient Adsorption of Uranium Ions. *ACS Macro Lett.* **2016**, *5*, 382–386.
- (22) Sedo, J.; Saiz-Poseu, J.; Busque, F.; Ruiz-Molina, D. Catechol-Based Biomimetic Functional Materials. *Adv. Mater.* **2013**, *25*, 653–701.
- (23) Behboodi-Sadabad, F.; Zhang, H.; Trouillet, V.; Welle, A.; Plumeré, N.; Levkin, P. A. Bioinspired Strategy for Controlled Polymerization and Photopatterning of Plant Polyphenols. *Chem. Mater.* **2018**, *30*, 1937–1946.
- (24) Behboodi-Sadabad, F.; Zhang, H.; Trouillet, V.; Welle, A.; Plumeré, N.; Levkin, P. A. P. A. UV-Triggered Polymerization, Deposition, and Patterning of Plant Phenolic Compounds. *Adv. Funct. Mater.* **2017**, *27*, DOI: 10.1002/adfm.201700127.
- (25) Quideau, S.; Deffieux, D.; Douat-Casassus, C.; Pouysegu, L.; Pouységu, L. Plant Polyphenols: Chemical Properties, Biological Activities, and Synthesis. *Angew. Chem., Int. Ed.* **2011**, *50*, 586–621.
- (26) Jeon, J.-R. J.-R. R.; Kim, J.-H. J.-H. H.; Chang, Y.-S. S. Y.-S. Enzymatic Polymerization of Plant-Derived Phenols for Material-Independent and Multifunctional Coating. *J. Mater. Chem. B* **2013**, *1*, 6501–6509.
- (27) Ejima, H.; Richardson, J. J.; Liang, K.; Best, J. P.; van Koeverden, M. P.; Such, G. K.; Cui, J. W.; Caruso, F. One-Step Assembly of Coordination Complexes for Versatile Film and Particle Engineering. *Science* **2013**, *341*, 154–157.
- (28) Du, X.; Li, L.; Behboodi-Sadabad, F.; Welle, A.; Li, J.; Heissler, S.; Zhang, H.; Plumere, N.; Levkin, P. A. P. A.; Plumeré, N.; Levkin, P. A. P. A. *Polym. Chem.* **2017**, *8*, 2145–

- 2151.
- (29) Yuan, Z.; Zhao, Y.; Yang, W.; Hu, Y.; Cai, K.; Liu, P.; Ding, H. Fabrication of Antibacterial Surface via UV-Inducing Dopamine Polymerization Combined with Co-Deposition Ag Nanoparticles. *Mater. Lett.* **2016**, *183*, 85–89.
- (30) Bai, G. Q.; Ma, S. H.; Qie, R. T.; Liu, Z. Q.; Shi, Y. L.; Li, C. H.; Wang, R. J.; Guo, X. H.; Zhou, F.; Jia, X. UV-Triggered Surface-Initiated Polymerization from Colorless Green Tea Polyphenol-Coated Surfaces. *Macromol. Rapid Commun.* **2016**, *37*, 1256–1261.
- (31) Krogsgaard, M.; Nue, V.; Birkedal, H. Mussel-Inspired Materials: Self-Healing through Coordination Chemistry. *Chem. - Eur. J.* **2016**, *22*, 844–857.
- (32) Krogsgaard, M.; Andersen, A.; Birkedal, H. Gels and Threads: Mussel-Inspired One-Pot Route to Advanced Responsive Materials. *Chem. Commun.* **2014**, *50*, 13278–13281.
- (33) Buttress, J. P.; Day, D. P.; Courtney, J. M.; Lawrence, E. J.; Hughes, D. L.; Blagg, R. J.; Crossley, A.; Matthews, S. E.; Redshaw, C.; Bulman Page, P. C.; Wildgoose, G. G. “Janus” Calixarenes: Double-Sided Molecular Linkers for Facile, Multianchor Point, Multifunctional, Surface Modification. *Langmuir* **2016**, *32*, 7806–7813.
- (34) Schlaich, C.; Wei, Q.; Haag, R. Mussel-Inspired Polyglycerol Coatings with Controlled Wettability: From Superhydrophilic to Superhydrophobic Surface Coatings. *Langmuir* **2017**, *33*, 9508–9520.
- (35) Wei, Q.; Achazi, K.; Liebe, H.; Schulz, A.; Noeske, P.-L. M. L. M.; Grunwald, I.; Haag, R. Mussel-Inspired Dendritic Polymers as Universal Multifunctional Coatings. *Angew. Chem., Int. Ed.* **2014**, *53*, 11650–11655.
- (36) Zieger, M. M.; Pop-Georgievski, O.; De Los Santos Pereira, A.; Verveniotis, E.; Preuss, C. M.; Zorn, M.; Reck, B.; Goldmann, A. S.; Rodriguez-Emmenegger, C.; Barner-Kowollik, C.; Pereira, A. D.; Verveniotis, E.; Preuss, C. M.; Zorn, M.; Reck, B.; Goldmann, A. S.; Rodriguez-Emmenegger, C.; Barner-Kowollik, C. Ultrathin Monomolecular Films and Robust Assemblies Based on Cyclic Catechols. *Langmuir* **2017**, *33*, 670–679.

- (37) Kim, H. J.; Lee, M. H.; Mutihac, L.; Vicens, J.; Kim, J. S. Host-Guest Sensing by Calixarenes on the Surfaces. *Chem. Soc. Rev.* **2012**, *41*, 1173–1190.
- (38) Balasubramanian, R.; Kwon, Y. G.; Wei, A. Encapsulation and Functionalization of Nanoparticles in Crosslinked Resorcinarene Shells. *J. Mater. Chem.* **2007**, *17*, 105–112.
- (39) Xiong, D.; Li, H. Colorimetric Detection of Pesticides Based on Calixarene Modified Silver Nanoparticles in Water. *Nanotechnology* **2008**, *19*, 465502, doi: 10.1088/0957-4484/19/46/465502.
- (40) Zhou, J.; Chen, M.; Diao, G. W. Assembling Gold and Platinum Nanoparticles on Resorcinarene Modified Graphene and Their Electrochemical Applications. *J. Mater. Chem. A* **2013**, *1*, 2278–2285.
- (41) Ruderisch, A.; Iwanek, W.; Pfeiffer, J.; Fischer, G.; Albert, K.; Schurig, V. Synthesis and Characterization of a Novel Resorcinarene-Based Stationary Phase Bearing Polar Headgroups for Use in Reversed-Phase High-Performance Liquid Chromatography. *J. Chromatogr. A* **2005**, *1095*, 40–49.
- (42) Levkin, P. A.; Ruderisch, A.; Schurig, V. Combining the Enantioselectivity of a Cyclodextrin and a Diamide Selector in a Mixed Binary Gas-Chromatographic Chiral Stationary Phase. *Chirality* **2006**, *18*, 49–63.
- (43) Li, H.; Quan, J.; Nie, G.; Xue, H.; Luo, L.; Zhang, R. Macroscopic Chiral Recognition by Calix[4]Arene-Based Host-Guest Interaction. *Chem. - Eur. J.* **2018**, *24*, 15502-15506.
- (44) Santos, L.; Mattiuzzi, A.; Jabin, I.; Vandencastele, N.; Reniers, F.; Reinaud, O.; Hapiot, P.; Lhenry, S.; Leroux, Y.; Lagrost, C. One-Pot Electrografting of Mixed Monolayers with Controlled Composition. *J. Phys. Chem. C* **2014**, *118*, 15919–15928.
- (45) De Leener, G.; Evoung-Evoung, F.; Lascaux, A.; Mertens, J.; Porras-Gutierrez, A. G.; Le Poul, N.; Lagrost, C.; Over, D.; Leroux, Y. R.; Reniers, F.; Hapiot, P.; Le Mest, Y.; Jabin, I.; Reinaud, O. Immobilization of Monolayers Incorporating Cu Funnel Complexes onto Gold Electrodes. Application to the Selective Electrochemical Recognition of Primary Alkylamines in Water. *J. Am. Chem. Soc.* **2016**, *138*, 12841–12853.

- (46) Jain, V. K.; Kanaiya, P. H. Chemistry of Calix 4 Resorcinarenes. *Russ. Chem. Rev.* **2011**, *80*, 75–102.
- (47) Condorelli, G. G.; Motta, A.; Favazza, M.; Fragala, I. L.; Busi, M.; Menozzi, E.; Dalcanale, E.; Cristofolini, L. Grafting Cavitands on the Si(100) Surface. *Langmuir* **2006**, *22*, 11126–11133.
- (48) Katz, A.; Da Costa, P.; Lam, A. C. P.; Notestein, J. M. The First Single-Step Immobilization of a Calix-[4]-Arene onto the Surface of Silica. *Chem. Mater.* **2002**, *14*, 3364–3368.
- (49) Li, N.; Harrison, R. G.; Lamb, J. D. Application of Resorcinarene Derivatives in Chemical Separations. *J. Inclusion Phenom. Macrocyclic Chem.* **2014**, *78*, 39–60.
- (50) Hassan, A. K. Thin Films of Calix-4-Resorcinarene Deposited by Spin Coating and Langmuir – Blodgett Techniques : Determination of Film Parameters by Surface Plasmon Resonance. *Mater. Sci.* **1999**, *8-9*, 251–255.
- (51) Ye, Q.; Zhou, F.; Liu, W. M. Bioinspired Catecholic Chemistry for Surface Modification. *Chem. Soc. Rev.* **2011**, *40*, 4244–4258.
- (52) Qiu, W.-Z.; Zhong, Q.-Z.; Du, Y.; Lv, Y.; Xu, Z.-K. Enzyme-Triggered Coatings of Tea Catechins/Chitosan for Nanofiltration Membranes with High Performance. *Green Chem.* **2016**, *18*, 6205–6208.
- (53) Huang, S. Y.; Zhang, Y.; Shi, J. F.; Huang, W. P. Superhydrophobic Particles Derived from Nature-Inspired Polyphenol Chemistry for Liquid Marble Formation and Oil Spills Treatment. *ACS Sustainable Chem. Eng.* **2016**, *4*, 676–681.
- (54) Dai, J.; Mumper, R. J. Plant Phenolics: Extraction, Analysis and Their Antioxidant and Anticancer Properties. *Molecules* **2010**, *15*, 7313–7352.
- (55) Pandey, K. B.; Rizvi, S. I. Plant Polyphenols as Dietary Antioxidants in Human Health and Disease. *Oxid. Med. Cell. Longevity* **2009**, *2*, 270–278.
- (56) Cowan, M. M. Plant Products as Antimicrobial Agents. *Clin. Microbiol. Rev.* **1999**, *12*, 564–582.

- (57) Mark, D.; Haeberle, S.; Roth, G.; Von Stetten, F.; Zengerle, R. Microfluidic Lab-on-a-Chip Platforms: Requirements, Characteristics and Applications. *Chem. Soc. Rev.* **2010**, *39*, 1153–1182.
- (58) Kawamura, K.; Yasuda, T.; Hatanaka, T.; Hamahiga, K.; Matsuda, N.; Ueshima, M.; Nakai, K. In Situ UV–VIS Spectrophotometry within the Second Time Scale as a Research Tool for Solid-State Catalyst and Liquid-Phase Reactions at High Temperatures: Its Application to the Formation of HMF from Glucose and Cellulose. *Chem. Eng. J.* **2017**, *307*, 1066–1075.
- (59) Hitzbleck, M.; Gervais, L.; Delamarche, E. Controlled Release of Reagents in Capillary-Driven Microfluidics Using Reagent Integrators. *Lab Chip* **2011**, *11*, 2680–2685.
- (60) Lenicek Krleza, J.; Dorotic, A.; Grzunov, A.; Maradin, M. Capillary Blood Sampling: National Recommendations on Behalf of the Croatian Society of Medical Biochemistry and Laboratory Medicine. *Biochem. Med.* **2015**, *25*, 335–358.
- (61) Zhu, Z.; Lu, J. J.; Liu, S. Protein Separation by Capillary Gel Electrophoresis: A Review. *Anal. Chim. Acta* **2012**, *709*, 21–31.
- (62) Balasundram, N.; Sundram, K.; Samman, S. Phenolic Compounds in Plants and Agri-Industrial by-Products: Antioxidant Activity, Occurrence, and Potential Uses. *Food Chem.* **2006**, *99*, 191–203.
- (63) Zhihua, Z.; Goldstein, B. D.; Witz, G. Iron-Stimulated Ring-Opening of Benzene in a Mouse Liver Microsomal System. Mechanistic Studies and Formation of a New Metabolite. *Biochem. Pharmacol.* **1995**, *50*, 1607–1617.
- (64) Yang, J.-L.; Wang, L.-C.; Chang, C.-Y.; Liu, T.-Y. Singlet Oxygen Is the Major Species Participating in the Induction of DNA Strand Breakage and 8-Hydroxydeoxyguanosine Adduct by Lead Acetate. *Environ. Mol. Mutagen.* **1999**, *33*, 194–201.
- (65) Ejima, H.; Richardson, J. J.; Caruso, F. Metal-Phenolic Networks as a Versatile Platform to Engineer Nanomaterials and Biointerfaces. *Nano Today* **2017**, *12*, 136–148.
- (66) Lee, J. S.; Lee, J. S.; Lee, M. S.; An, S.; Yang, K.; Lee, K.; Yang, H. S.; Lee, H.; Cho,

- S.-W. Plant Flavonoid-Mediated Multifunctional Surface Modification Chemistry: Catechin Coating for Enhanced Osteogenesis of Human Stem Cells. *Chem. Mater.* **2017**, *29*, 4375–4384.
- (67) Wang, Y.; Park, J. P.; Hong, S. H.; Lee, H. Biologically Inspired Materials Exhibiting Repeatable Regeneration with Self-Sealing Capabilities without External Stimuli or Catalysts. *Adv. Mater.* **2016**, *28*, 9961–9968.
- (68) Zhang, X.; Lv, Y.; Yang, H.-C.; Du, Y.; Xu, Z.-K. Polyphenol Coating as an Interlayer for Thin-Film Composite Membranes with Enhanced Nanofiltration Performance. *ACS Appl. Mater. Interfaces* **2016**, *8*, 32512–32519.
- (69) Tang, C.; Amin, D.; Messersmith, P. B.; Anthony, J. E.; Prud'homme, R. K. Polymer Directed Self-Assembly of PH-Responsive Antioxidant Nanoparticles. *Langmuir* **2015**, *31*, 3612–3620.
- (70) Zhan, K.; Ejima, H.; Yoshie, N. Antioxidant and Adsorption Properties of Bioinspired Phenolic Polymers: A Comparative Study of Catechol and Gallol. *ACS Sustain. Chem. Eng.* **2016**, *4*, 3857–3863.
- (71) Lu, Y.-C.; Luo, P.-C.; Huang, C.-W.; Leu, Y.-L.; Wang, T.-H.; Wei, K.-C.; Wang, H.-E.; Ma, Y.-H. Augmented Cellular Uptake of Nanoparticles Using Tea Catechins: Effect of Surface Modification on Nanoparticle-Cell Interaction. *Nanoscale* **2014**, *6*, 10297–10306.
- (72) Shin, M.; Kim, K.; Shim, W.; Yang, J. W.; Lee, H. Tannic Acid as a Degradable Mucoadhesive Compound. *ACS Biomater. Sci. Eng.* **2016**, *2*, 687–696.
- (73) Yao, X.; Zheng, X.; Zhang, J.; Cai, K. Oxidation-Induced Surface Deposition of Tannic Acid: Towards Molecular Gates on Porous Nanocarriers for Acid-Responsive Drug Delivery. *RSC Adv.* **2016**, *6*, 76473–76481.
- (74) Das, C.; Chatterjee, S.; Kumaraswamy, G.; Krishnamoorthy, K. Elastic Compressible Energy Storage Devices from Ice Templated Polymer Gels Treated with Polyphenols. *J. Phys. Chem. C* **2017**, *121*, 3270–3278.

- (75) Rahim, M. A.; Kempe, K.; Müllner, M.; Ejima, H.; Ju, Y.; Van Koeverden, M. P.; Suma, T.; Braunger, J. A.; Leeming, M. G.; Abrahams, B. F.; Caruso, F. Surface-Confined Amorphous Films from Metal-Coordinated Simple Phenolic Ligands. *Chem. Mater.* **2015**, *27*, 5825–5832.
- (76) Rahim, M. A.; Björnmalm, M.; Suma, T.; Faria, M.; Ju, Y.; Kempe, K.; Müllner, M.; Ejima, H.; Stickland, A. D.; Caruso, F. Metal–Phenolic Supramolecular Gelation. *Angew. Chem., Int. Ed.* **2016**, *55*, 13803–13807.
- (77) Zhang, S. H.; Jiang, Z. Y.; Wang, X. L.; Yang, C.; Shi, J. F. Facile Method To Prepare Microcapsules Inspired by Polyphenol Chemistry for Efficient Enzyme Immobilization. *ACS Appl. Mater. Interfaces* **2015**, *7*, 19570–19578.
- (78) Dhand, C.; Harini, S.; Venkatesh, M.; Dwivedi, N.; Ng, A.; Liu, S.; Verma, N. K.; Ramakrishna, S.; Beuerman, R. W.; Loh, X. J.; Lakshminarayanan, R. Multifunctional Polyphenols- and Catecholamines-Based Self-Defensive Films for Health Care Applications. *ACS Appl. Mater. Interfaces* **2016**, *8*, 1220–1232.
- (79) Lim, C.; Huang, J.; Kim, S.; Lee, H.; Zeng, H.; Hwang, D. S. Nanomechanics of Poly(Catecholamine) Coatings in Aqueous Solutions. *Angew. Chem., Int. Ed.* **2016**, *55*, 3342–3346.
- (80) Hong, S.; Kim, J.; Na, Y. S.; Park, J.; Kim, S.; Singha, K.; Im, G.-I. G.-I.; Han, D.-K. D.-K.; Kim, W. J.; Lee, H. Poly(Norepinephrine): Ultrasooth Material-Independent Surface Chemistry and Nanodepot for Nitric Oxide. *Angew. Chem., Int. Ed.* **2013**, *52*, 9187–9191.
- (81) Cho, J. H.; Katsumata, R.; Zhou, S. X.; Kim, C. Bin; Dulaney, A. R.; Janes, D. W.; Ellison, C. J. Ultrasooth Polydopamine Modified Surfaces for Block Copolymer Nanopatterning on Flexible Substrates. *ACS Appl. Mater. Interfaces* **2016**, *8*, 7456–7463.
- (82) Kord Forooshani, P.; Lee, B. P. Recent Approaches in Designing Bioadhesive Materials Inspired by Mussel Adhesive Protein. *J. Polym. Sci., Part A: Polym. Chem.* **2017**, *55*, 9–33.
- (83) Lee, B. P.; Dalsin, J. L.; Messersmith, P. B. Synthesis and Gelation of DOPA-Modified

- Poly(Ethylene Glycol) Hydrogels. *Biomacromolecules* **2002**, *3*, 1038–1047.
- (84) Wang, L.; Shi, Y.; Chen, S.; Wang, W.; Tian, M.; Ning, N.; Zhang, L. Highly Efficient Mussel-like Inspired Modification of Aramid Fibers by UV-Accelerated Catechol/Polyamine Deposition Followed Chemical Grafting for High-Performance Polymer Composites. *Chem. Eng. J.* **2017**, *314*, 583–593.
- (85) Waterhouse, A. L.; Laurie, V. F. Oxidation of Wine Phenolics: A Critical Evaluation and Hypotheses. *Am. J. Enol. Vitic.* **2006**, *57*, 306–313.
- (86) Lü, J.; Lin, P. H.; Yao, Q.; Chen, C. Chemical and Molecular Mechanisms of Antioxidants: Experimental Approaches and Model Systems. *J. Cell. Mol. Med.* **2010**, *14*, 840–860.
- (87) Szultka, M.; Buszewska-Forajta, M.; Kaliszan, R.; Buszewski, B. Determination of Ascorbic Acid and Its Degradation Products by High-Performance Liquid Chromatography-Triple Quadrupole Mass Spectrometry. *Electrophoresis* **2014**, *35*, 585–592.
- (88) Stinefelt, B.; Leonard, S. S.; Blemings, K. P.; Shi, X.; Klandorf, H. Free Radical Scavenging, DNA Protection, and Inhibition of Lipid Peroxidation Mediated by Uric Acid. *Ann. Clin. Lab. Sci.* **2005**, *35*, 37–45.
- (89) Galano, A.; Alvarez-Idaboy, J. R. Glutathione: Mechanism and Kinetics of Its Non-Enzymatic Defense Action against Free Radicals. *RSC Adv.* **2011**, *1*, 1763–1771.
- (90) Nimse, S. B.; Pal, D. Free Radicals, Natural Antioxidants, and Their Reaction Mechanisms. *RSC Adv.* **2015**, *5*, 27986–28006.
- (91) Waring, W. S. Uric Acid: An Important Antioxidant in Acute Ischaemic Stroke. *QJM - Mon. J. Assoc. Physicians India* **2002**, *95*, 691–693.
- (92) Roshchina, V. V. Vital Autofluorescence: Application to the Study of Plant Living Cells. *Int. J. Spectrosc.* **2012**, *2012*, 1–14.
- (93) Talamond, P.; Verdeil, J.-L.; Conéjéro, G. Secondary Metabolite Localization by Autofluorescence in Living Plant Cells. *Molecules* **2015**, *20*, 5024–5037.

- (94) Rahim, M. A.; Björnmalm, M.; Bertleff-Zieschang, N.; Besford, Q.; Mettu, S.; Suma, T.; Faria, M.; Caruso, F. Rust-Mediated Continuous Assembly of Metal–Phenolic Networks. *Adv. Mater.* **2017**, *29*, DOI: 10.1002/adma.201606717.
- (95) Yu, L. X.; Cheng, C.; Ren, Q. D.; Schlaich, C.; Noeske, P. L. M.; Li, W. Z.; Wei, Q.; Haag, R. Bioinspired Universal Monolayer Coatings by Combining Concepts from Blood Protein Adsorption and Mussel Adhesion. *ACS Appl. Mater. Interfaces* **2017**, *9*, 6624–6633.
- (96) Ding, Y. H.; Floren, M.; Tan, W. Mussel-Inspired Polydopamine for Bio-Surface Functionalization. *Biosurface and Biotribology* **2016**, *2*, 121–136.
- (97) Jeong, Y. K.; Park, S. H.; Choi, J. W. Mussel-Inspired Coating and Adhesion for Rechargeable Batteries: A Review. *ACS Appl. Mater. Interfaces* **2017**, *10*, 7562–7573.
- (98) Kaushik, N. K.; Kaushik, N.; Pardeshi, S.; Sharma, J. G.; Lee, S. H.; Choi, E. H. Biomedical and Clinical Importance of Mussel-Inspired Polymers and Materials. *Mar. Drugs* **2015**, *13*, 6792–6817.
- (99) Ryu, J. H.; Hong, S.; Lee, H. Bio-Inspired Adhesive Catechol-Conjugated Chitosan for Biomedical Applications: A Mini Review. *Acta Biomater.* **2015**, *27*, 101–115.
- (100) Zhang, C.; Lv, Y.; Qin, W. Z.; He, A.; Xu, Z. K. Polydopamine Coatings with Nanopores for Versatile Molecular Separation. *ACS Appl. Mater. Interfaces* **2017**, *9*, 14437–14444.
- (101) Ge, H.; Kong, Y.; Pan, Y.; Deng, L.; Shou, D.; Lu, Q. Polydopamine Core Half-Polyamidoamine Dendrimers Based Drug-Delivery Platform and Characterization by Electrochemical Impedance Spectroscopy. *J. Electrochem. Soc.* **2015**, *162*, G87–G93.
- (102) Faure, E.; Falentin-Daudre, C.; Jerome, C.; Lyskawa, J.; Fournier, D.; Woisel, P.; Detrembleur, C. Catechols as Versatile Platforms in Polymer Chemistry. *Prog. Polym. Sci.* **2013**, *38*, 236–270.
- (103) You, I.; Jeon, H.; Lee, K.; Do, M.; Seo, Y. C.; Lee, H. H. A.; Lee, H. H. A. Polydopamine Coating in Organic Solvent for Material-Independent Immobilization of Water-Insoluble Molecules and Avoidance of Substrate Hydrolysis. *J. Ind. Eng. Chem.* **2017**, *46*, 379–

385.

- (104) Barclay, T. G.; Hegab, H. M.; Clarke, S. R.; Ginic-Markovic, M. Versatile Surface Modification Using Polydopamine and Related Polycatecholamines: Chemistry, Structure, and Applications. *Adv. Mater. Interfaces* **2017**, *4*, DOI: 10.1002/admi.201601192.
- (105) Yang, J.; Stuart, M. A. C.; Kamperman, M. Jack of All Trades: Versatile Catechol Crosslinking Mechanisms. *Chem. Soc. Rev.* **2014**, *43*, 8271–8298.
- (106) Mokhtari, B.; Pourabdollah, K. Application of Calixarenes in Development of Sensors. *Asian J. Chem.* **2013**, *25*, 1–12.
- (107) Yousaf, A.; Hamid, S. A.; Bunnori, N. M. Applications of Calixarenes in Cancer Chemotherapy. *Drug Des., Dev. Ther.* **2015**, *9*, 2831–2838.
- (108) Zhang, F.; Sun, Y.; Tian, D.; Shin, W. S.; Kim, J. S.; Li, H. Selective Molecular Recognition on Calixarene-Functionalized 3D Surfaces. *Chem. Commun.* **2016**, *52*, 12685–12693.
- (109) Joseph, R.; Rao, C. P. Ion and Molecular Recognition by Lower Rim 1,3-Di-Conjugates of Calix[4]Arene as Receptors. *Chem. Rev.* **2011**, *111*, 4658–4702.
- (110) Samanta, K.; Ranade, D. S.; Upadhyay, A.; Kulkarni, P. P.; Rao, C. P. A Bimodal, Cationic, and Water-Soluble Calix[4]Arene Conjugate: Design, Synthesis, Characterization, and Transfection of Red Fluorescent Protein Encoded Plasmid in Cancer Cells. *ACS Appl. Mater. Interfaces* **2017**, *9*, 5109–5117.
- (111) Nimse, S. B.; Kim, T. Biological Applications of Functionalized Calixarenes. *Chem. Soc. Rev.* **2013**, *42*, 366–386.
- (112) Böhmer, V. Calixarenes, Macrocycles with (Almost) Unlimited Possibilities. *Angew. Chem., Int. Ed.* **1995**, *34*, 713–745.
- (113) Tauran, Y.; Coleman, A. W.; Perret, F.; Kim, B. Cellular and in Vivo Biological Activities of the Calix [n] Arenes. *Curr. Org. Chem.* **2015**, *19*, 2250–2270.
- (114) Behboodi-Sadabad, F.; Trouillet, V.; Welle, A.; Messersmith, P. B.; Levkin, P. A.

- Surface Functionalization and Patterning by Multifunctional Resorcinarenes. *ACS Appl. Mater. Interfaces* **2018**, 10, 39268–39278.
- (115) Yu, J.; Kan, Y.; Rapp, M.; Danner, E.; Wei, W.; Das, S.; Miller, D. R.; Chen, Y.; Waite, J. H.; Israelachvili, J. N. Adaptive Hydrophobic and Hydrophilic Interactions of Mussel Foot Proteins with Organic Thin Films. *Proc. Natl. Acad. Sci. U. S. A.* **2013**, 110, 15680–15685.
- (116) Geyer, F. L.; Ueda, E.; Liebel, U.; Grau, N.; Levkin, P. A. Superhydrophobic-Superhydrophilic Micropatterning: Towards Genome-on-a-Chip Cell Microarrays. *Angew. Chem., Int. Ed.* **2011**, 50, 8424–8427.
- (117) Xi, W. X.; Scott, T. F.; Kloxin, C. J.; Bowman, C. N. Click Chemistry in Materials Science. *Adv. Funct. Mater.* **2014**, 24, 2572–2590.
- (118) Reshetenko, T. V.; St-Pierre, J.; Artyushkova, K.; Rocheleau, R.; Atanassov, P.; Bender, G.; Ulsh, M. Multianalytical Study of the PTFE Content Local Variation of the PEMFC Gas Diffusion Layer. *J. Electrochem. Soc.* **2013**, 160, F1305–F1315.
- (119) Feng, W. Q.; Li, L. X.; Du, X.; Welle, A.; Levkin, P. A. Single-Step Fabrication of High-Density Microdroplet Arrays of Low-Surface-Tension Liquids. *Adv. Mater.* **2016**, 28, 3202–3208.
- (120) Li, L.; Li, J.; Du, X.; Welle, A.; Grunze, M.; Trapp, O.; Levkin, P. A. Direct UV-Induced Functionalization of Surface Hydroxy Groups by Thiol-OI Chemistry. *Angew. Chem., Int. Ed.* **2014**, 53, 3835–3839.
- (121) Parry, K. L.; Shard, A. G.; Short, R. D.; White, R. G.; Whittle, J. D.; Wright, A. ARXPS Characterisation of Plasma Polymerised Surface Chemical Gradients. *Surf. Interface Anal.* **2006**, 38, 1497–1504.
- (122) Scofield, J. H. Hartree-Slater Subshell Photoionization Cross-Sections at 1254 and 1487 EV. *J. Electron Spectrosc. Relat. Phenom.* **1976**, 8, 129–137.
- (123) Thiagarajan, S.; Tsai, T.-H.; Chen, S.-M. Easy Modification of Glassy Carbon Electrode for Simultaneous Determination of Ascorbic Acid, Dopamine and Uric Acid. *Biosens.*

Bioelectron. **2009**, *24*, 2712–2715.

- (124) Feng, W. Q.; Li, L. X.; Ueda, E.; Li, J. S.; Heissler, S.; Welle, A.; Trapp, O.; Levkin, P. A. Surface Patterning via Thiol-Yne Click Chemistry: An Extremely Fast and Versatile Approach to Superhydrophilic-Superhydrophobic Micropatterns. *Adv. Mater. Interfaces* **2014**, *1*, DOI: 10.1002/admi.201400269.

Appendix A: Supplementary information for Chapter 2^a

^a This chapter is adapted from Ref.²⁴

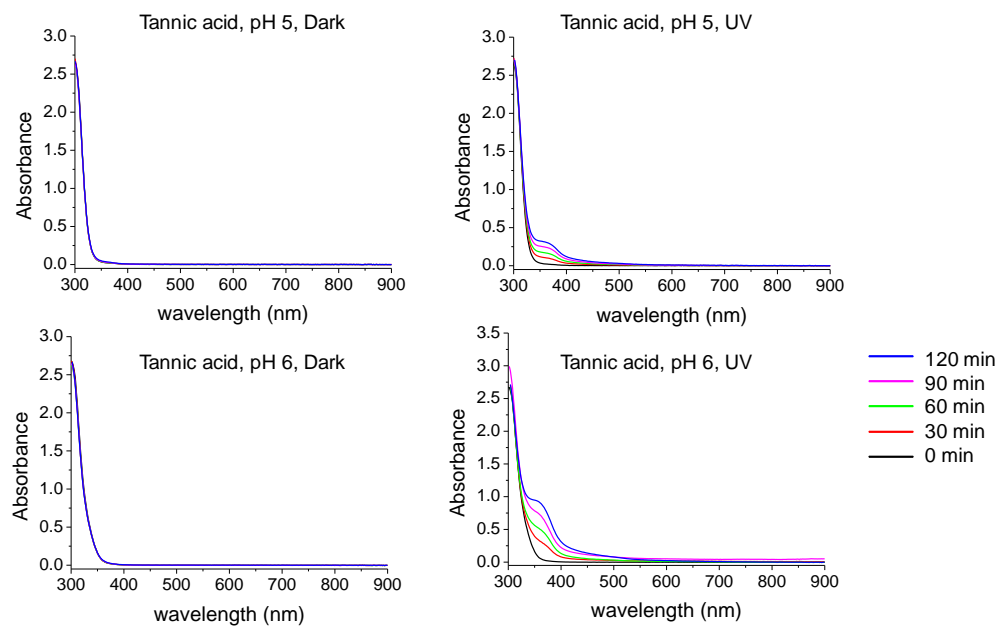


Figure S 8.1 UV-Vis spectra of TA solution (0.2 mg/mL) at pH 5.0, and pH 6.0 stored in dark environment (left) and after UV irradiation (right) measured at different time intervals.²⁴

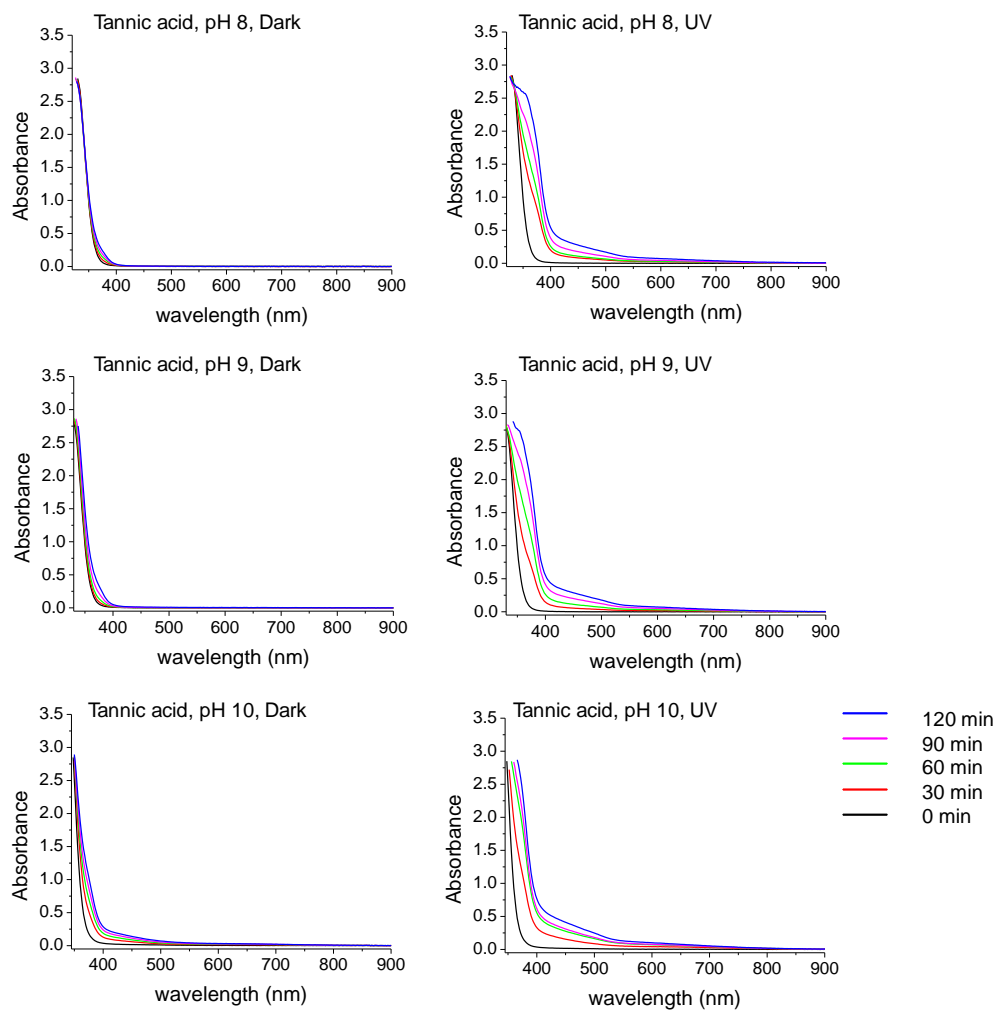


Figure S 8.2 UV-VIS spectra of TA solution (0.2 mg/mL) at pH 8.0, pH 9.0, and pH 10.0 stored in dark environment (left) and after UV irradiation (right) measured at different time intervals.²⁴

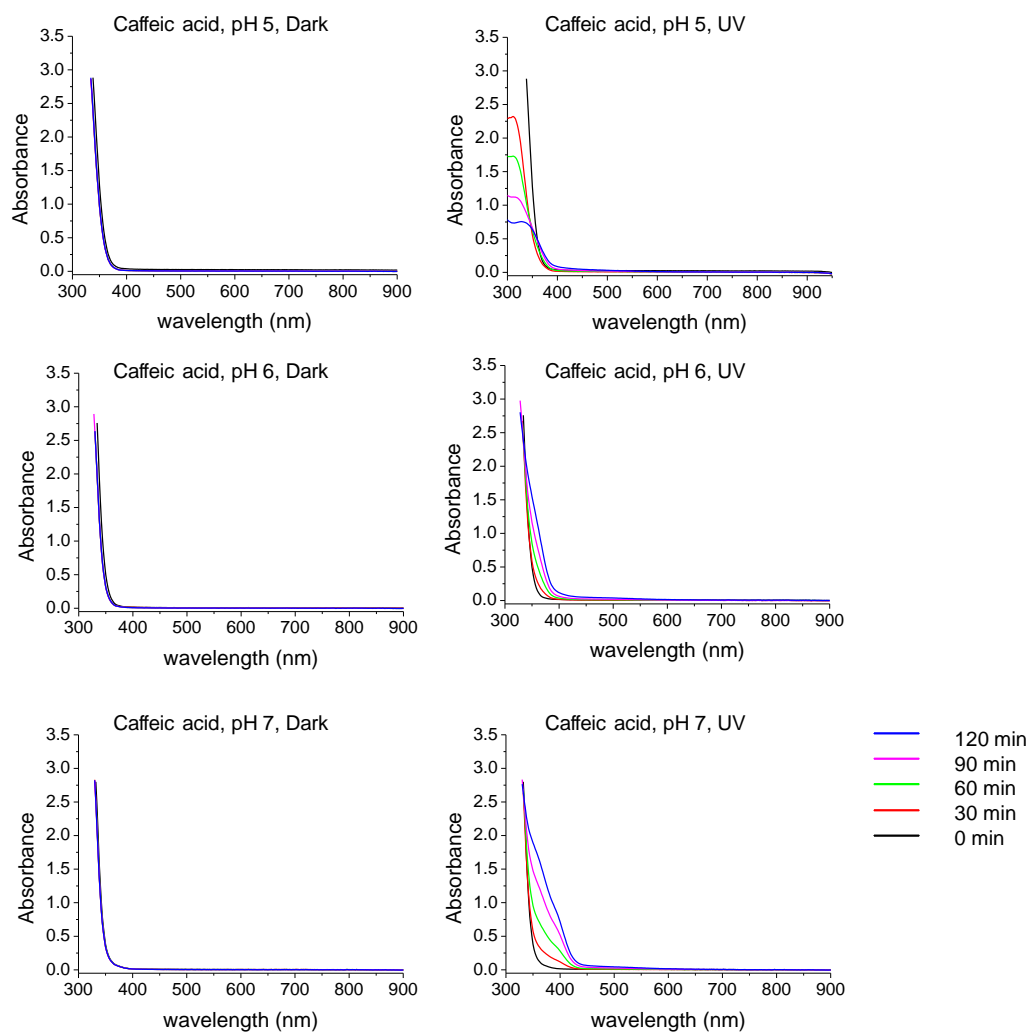


Figure S 8.3 UV-VIS spectra of CA solution (0.2 mg/mL) at pH 5.0, pH 6.0, and pH 7.0 stored in dark environment (left) and after UV irradiation (right) measured at different time intervals.²⁴

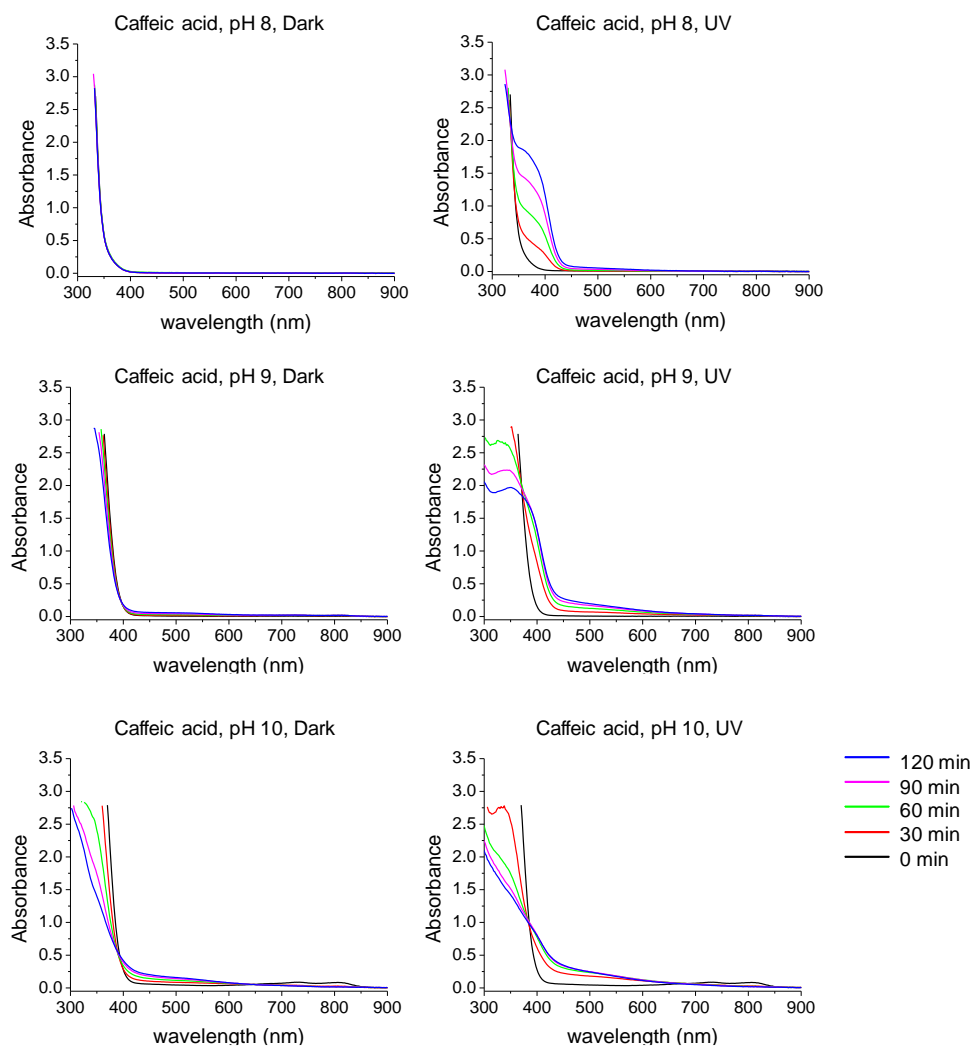


Figure S 8.4 UV-VIS spectra of CA solution (0.2 mg/mL) at pH 8.0, pH 9.0, and pH 10 stored in dark environment (left) and after UV irradiation (right) measured at different time intervals.²⁴

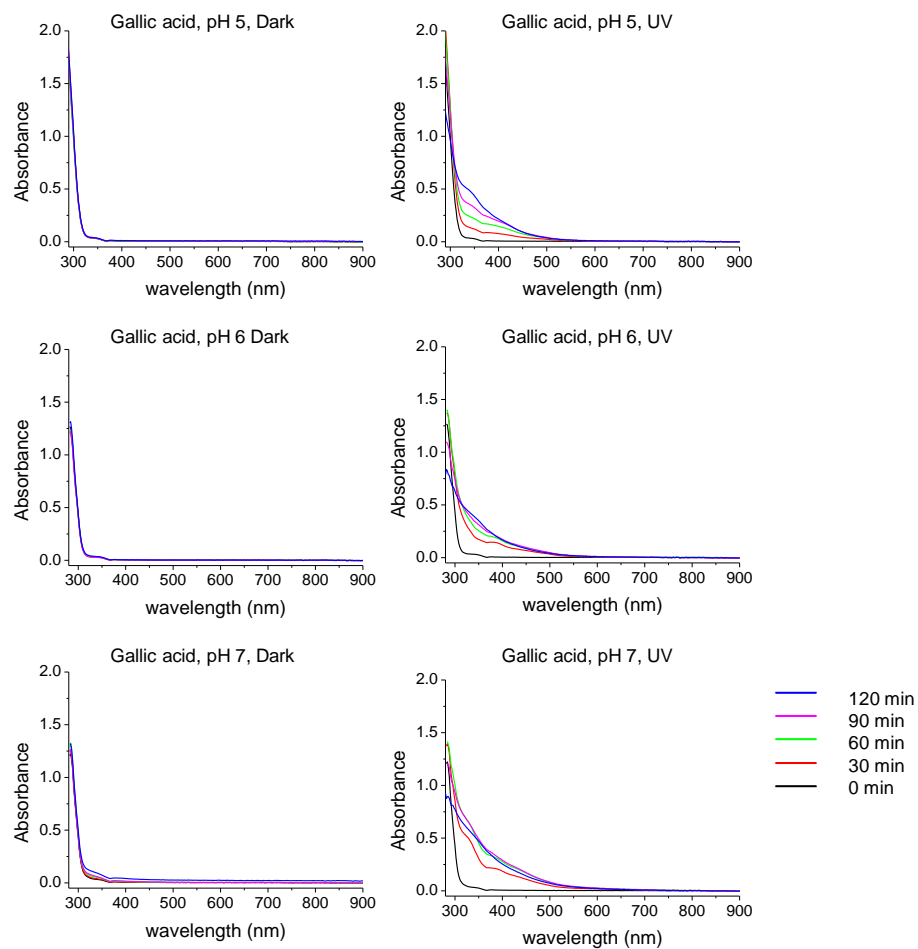


Figure S 8.5 UV-Vis spectra of GA solution (0.2 mg/mL) at pH 5.0, pH 6.0, and pH 7.0 stored in dark environment (left) and after UV irradiation (right) measured at different time intervals.²⁴

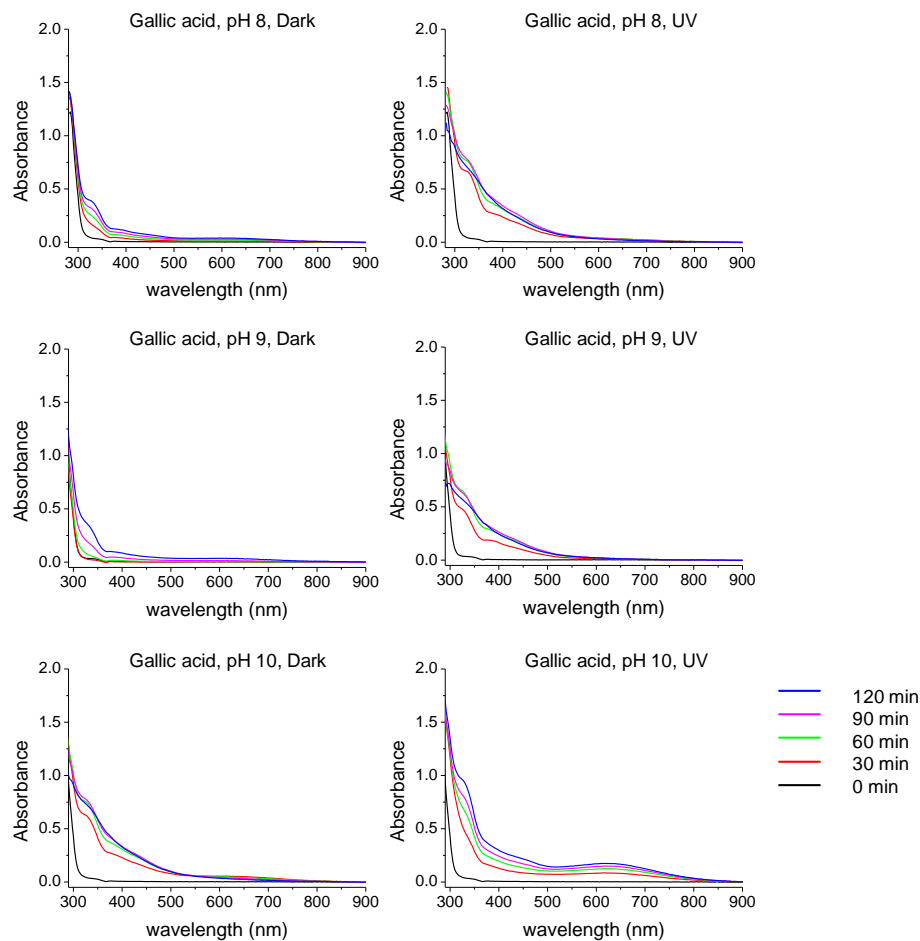


Figure S 8.6 UV-VIS spectra of GA solution (0.2 mg/mL) at pH 8.0, pH 9.0, and pH 10.0 stored in dark environment (left) and after UV irradiation (right) measured at different time intervals.²⁴

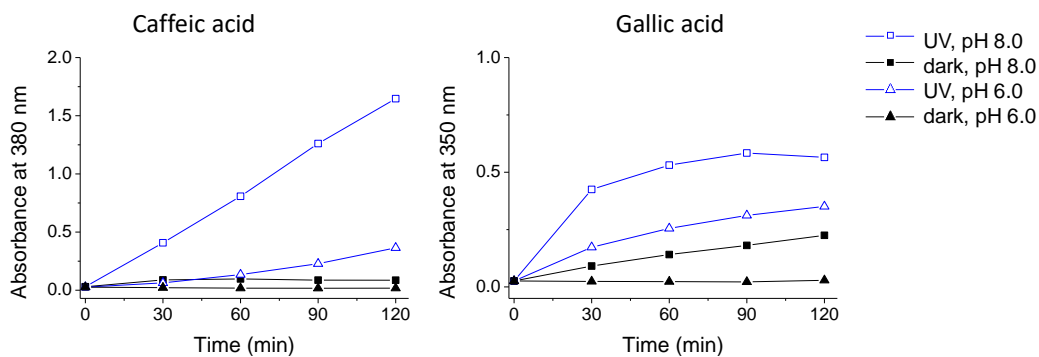


Figure S 8.7 UV Absorbance of the CA at 380 nm (left) and GA at 350 nm (right) as a function of time and pH.²⁴

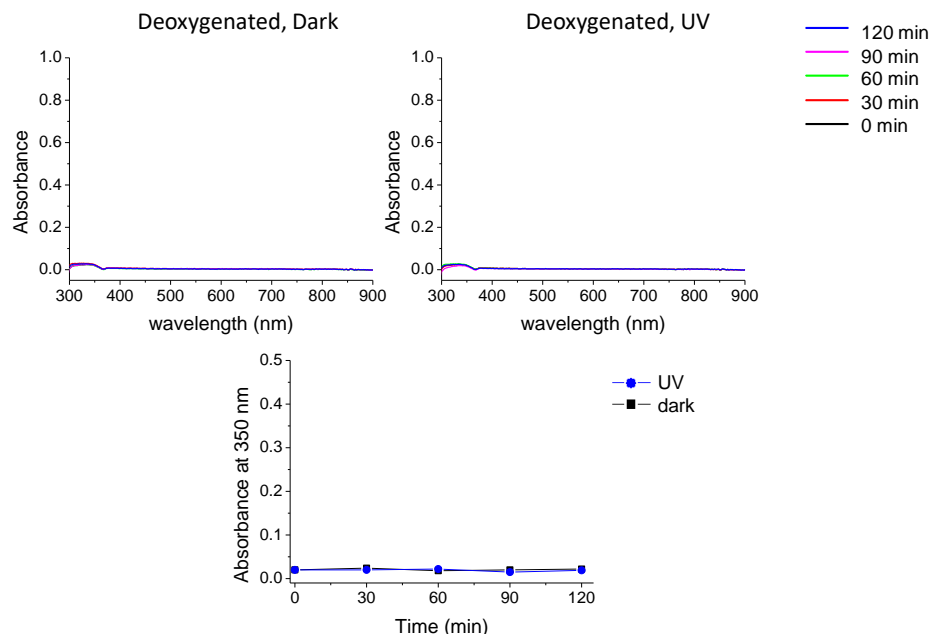


Figure S 8.8 UV-Vis spectra of PG solution (0.2 mg/mL) at pH 7.0 after 30 min purging nitrogen into the solution. Solution stored in dark environment (left) and after UV irradiation (right) measured at different time intervals. Absorbance of the PG solution at 350 nm (bottom) as a function of time and pH.²⁴

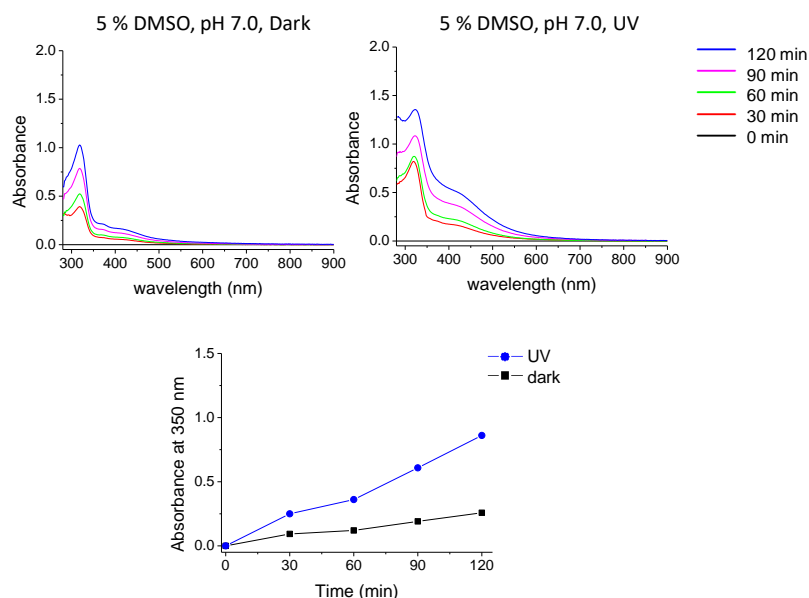


Figure S 8.9 UV-VIS spectra of PG solution (0.2 mg/mL) at pH 7.0 after adding 5 % DMSO to the solution. Solution stored in dark environment (left) and after UV irradiation (right) measured at different time intervals. Absorbance of the pyrogallol solution at 350 nm (bottom) as a function of time and pH.²⁴

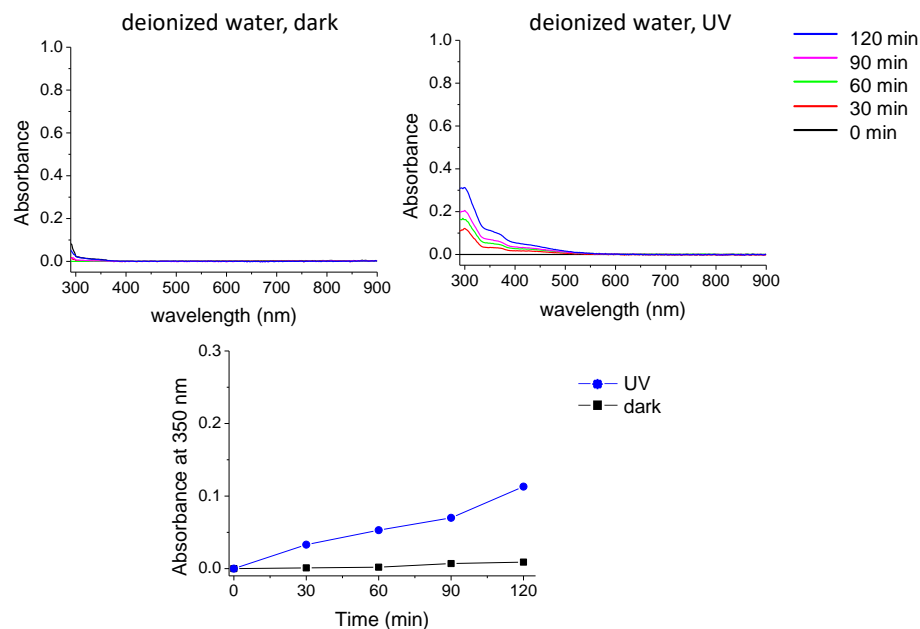


Figure S 8.10 UV-Vis spectra of PG solution (0.2 mg/mL) in deionized water. Solution stored in dark environment (left) and after UV irradiation (right) measured at different time intervals. Absorbance of the PG solution at 350 nm (bottom) as a function of time and pH.²⁴

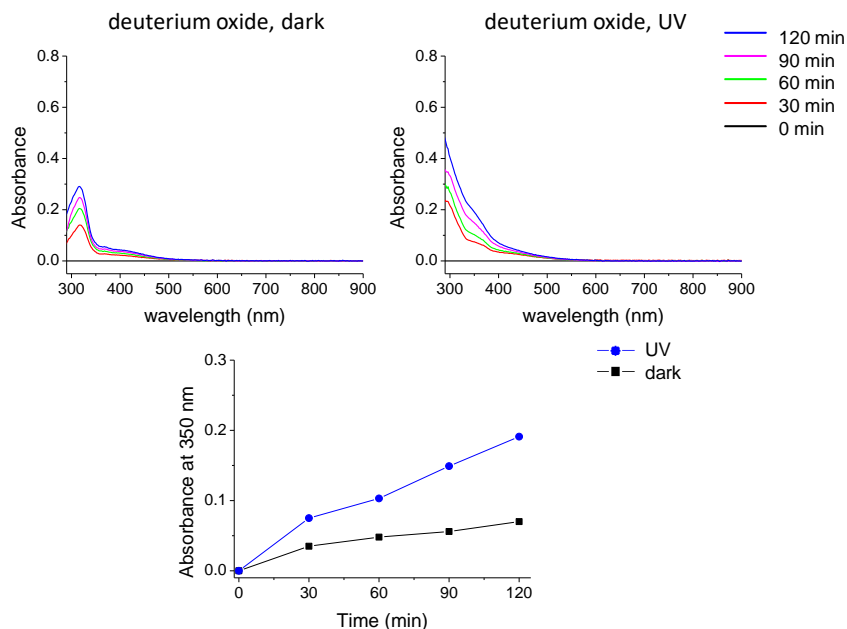


Figure S 8.11 UV-VIS spectra of PG solution (0.2 mg/mL) in deuterium oxide. Solution stored in dark environment (left) and after UV irradiation (right) measured at different time intervals. Absorbance of the PG solution at 350 nm (bottom) as a function of time and pH.²⁴

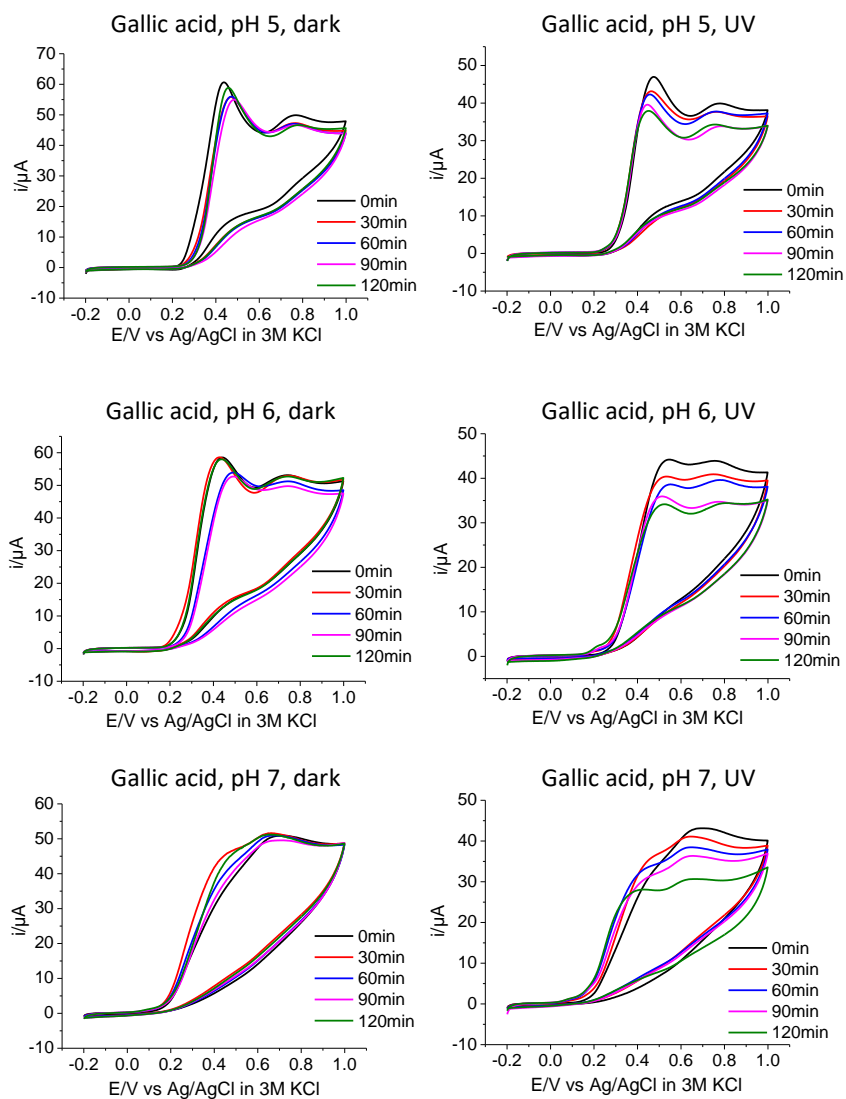


Figure S 8.12 Monitoring of GA by cyclic voltammetry (CV). Cyclic voltammograms of GA in buffers at pH 5.0, 6.0, and 7.0 vs time stored for 2 h in dark (left) or under UV irradiation (right). All CVs were measured in 100 mM buffer at a scan rate of 100 mV/s at glassy carbon electrodes with 1.58 mM concentration of plant phenolics.²⁴

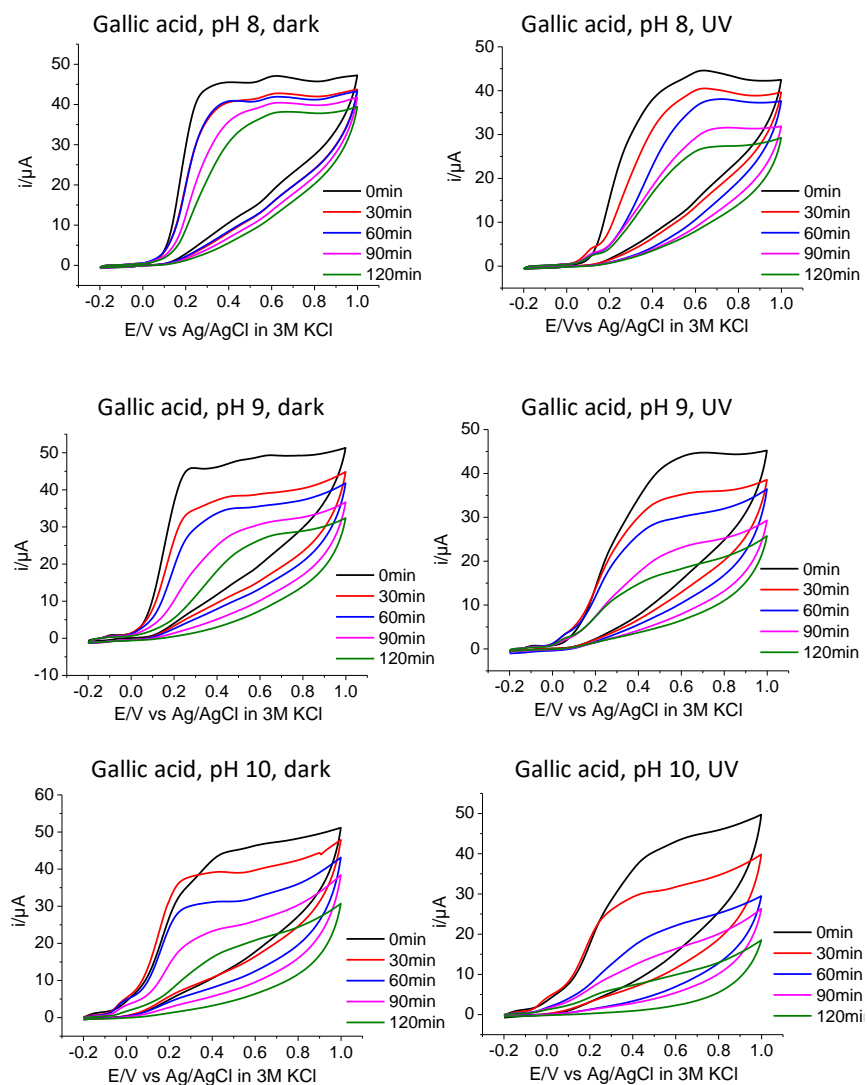


Figure S 8.13 Monitoring of GA by cyclic voltammetry (CV). Cyclic voltammograms of GA in buffers at pH 8.0, 9.0 and 10.0 vs time stored for 2 h in dark (left) or under UV irradiation (right). All CVs were measured in 100 mM buffer at a scan rate of 100 mV/s at glassy carbon electrodes with 1.58 mM concentration of plant phenolics.²⁴

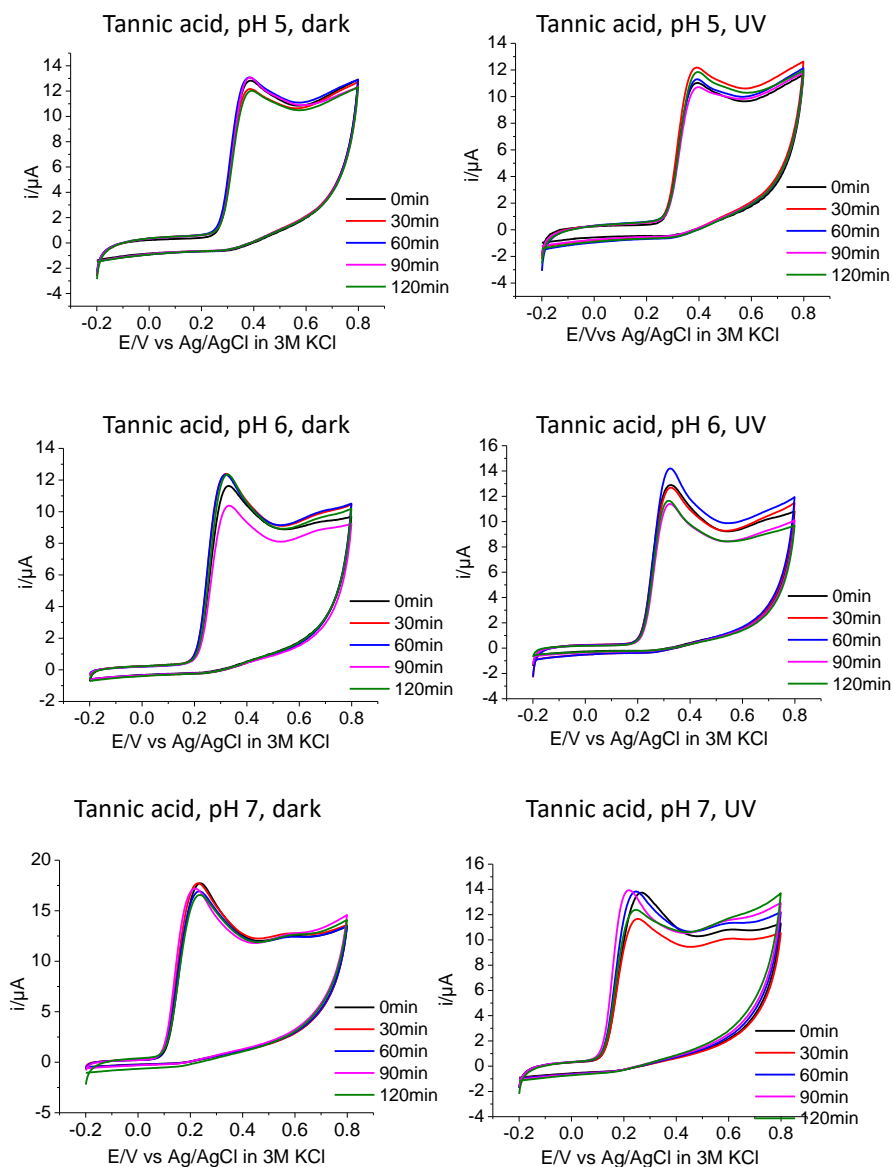


Figure S 8.14 Monitoring of TA by cyclic voltammetry (CV). Cyclic voltammograms of TA in buffers at pH 5.0, 6.0, and 7.0 vs time stored for 2 h in dark (left) or under UV irradiation (right). All CVs were measured in 100 mM buffer at a scan rate of 100 mV/s at glassy carbon electrodes with 1.58 mM concentration of plant phenolics.²⁴

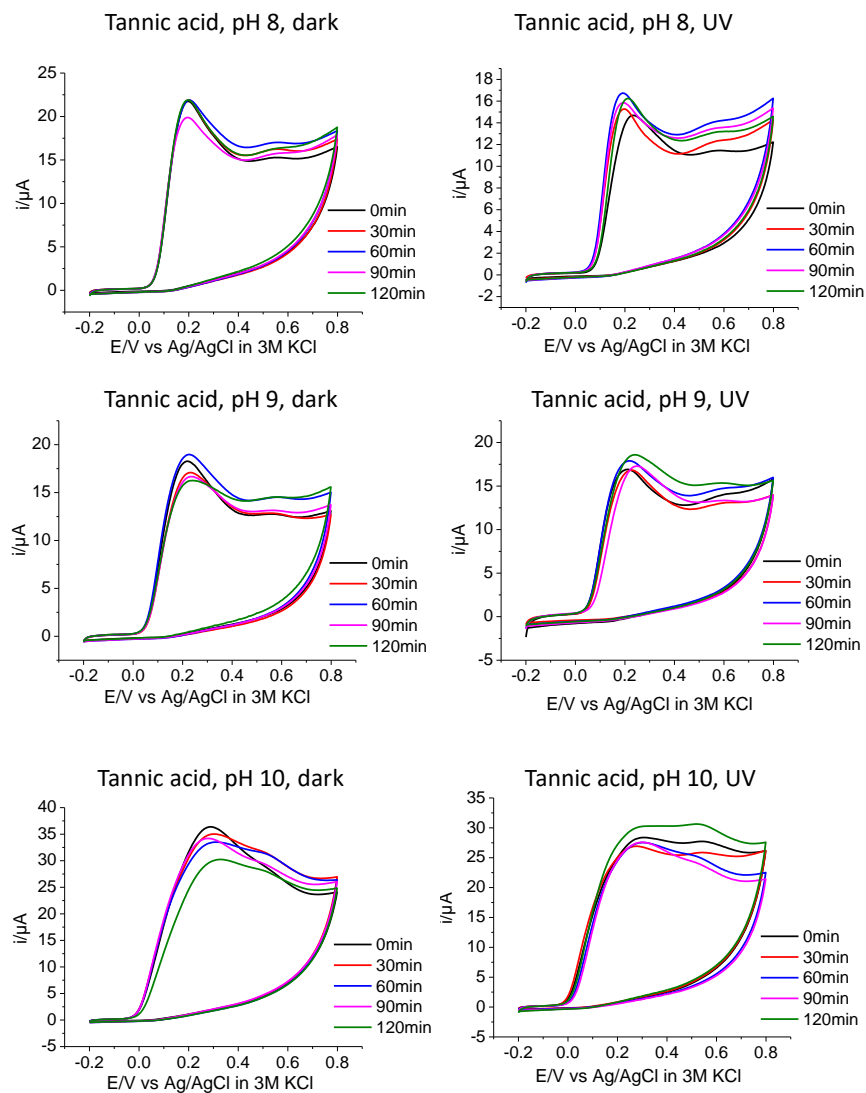


Figure S 8.15 Monitoring of TA by cyclic voltammetry (CV). Cyclic voltammograms of TA in buffers at pH 8.0, 9.0 and 10.0 vs time stored for 2 h in dark (left) or under UV irradiation (right). All CVs were measured in 100 mM buffer at a scan rate of 100 mV/s at glassy carbon electrodes with 1.58 mM concentration of plant phenolics.²⁴

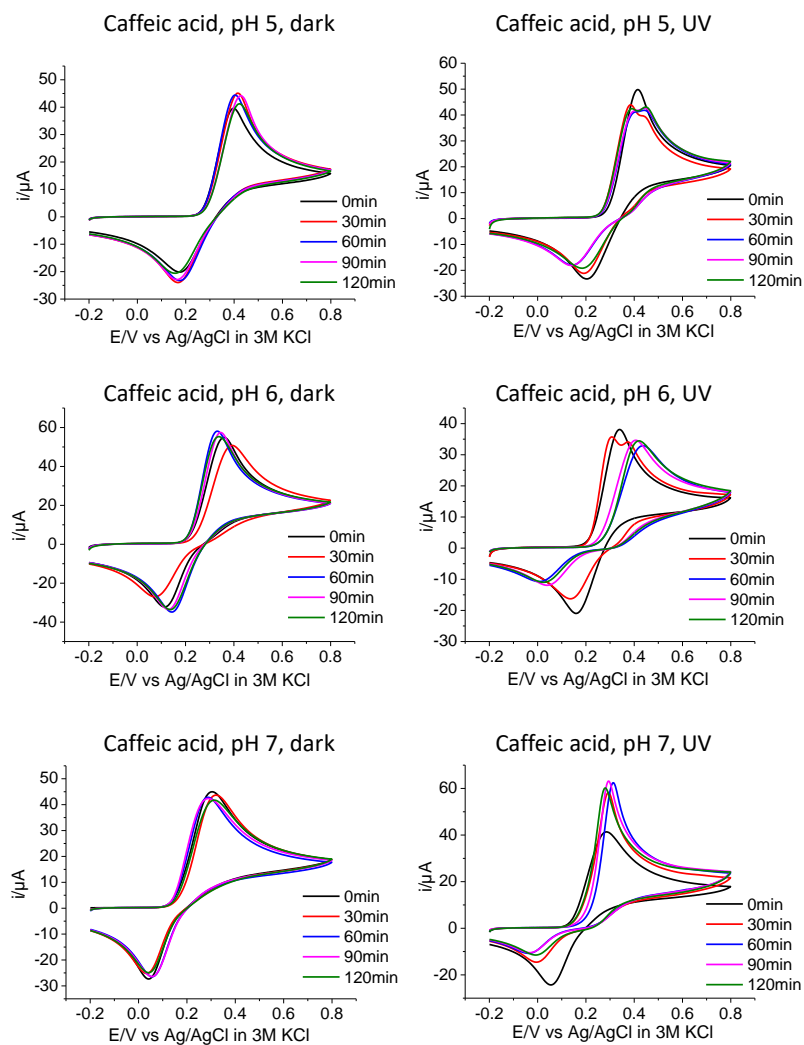


Figure S 8.16 Monitoring of CA by cyclic voltammetry (CV). Cyclic voltammograms of CA in buffers at pH 5.0, 6.0, and 7.0 vs time stored for 2 h in dark (left) or under UV irradiation (right). All CVs were measured in 100 mM buffer at a scan rate of 100 mV/s at glassy carbon electrodes with 1.58 mM concentration of plant phenolics.²⁴

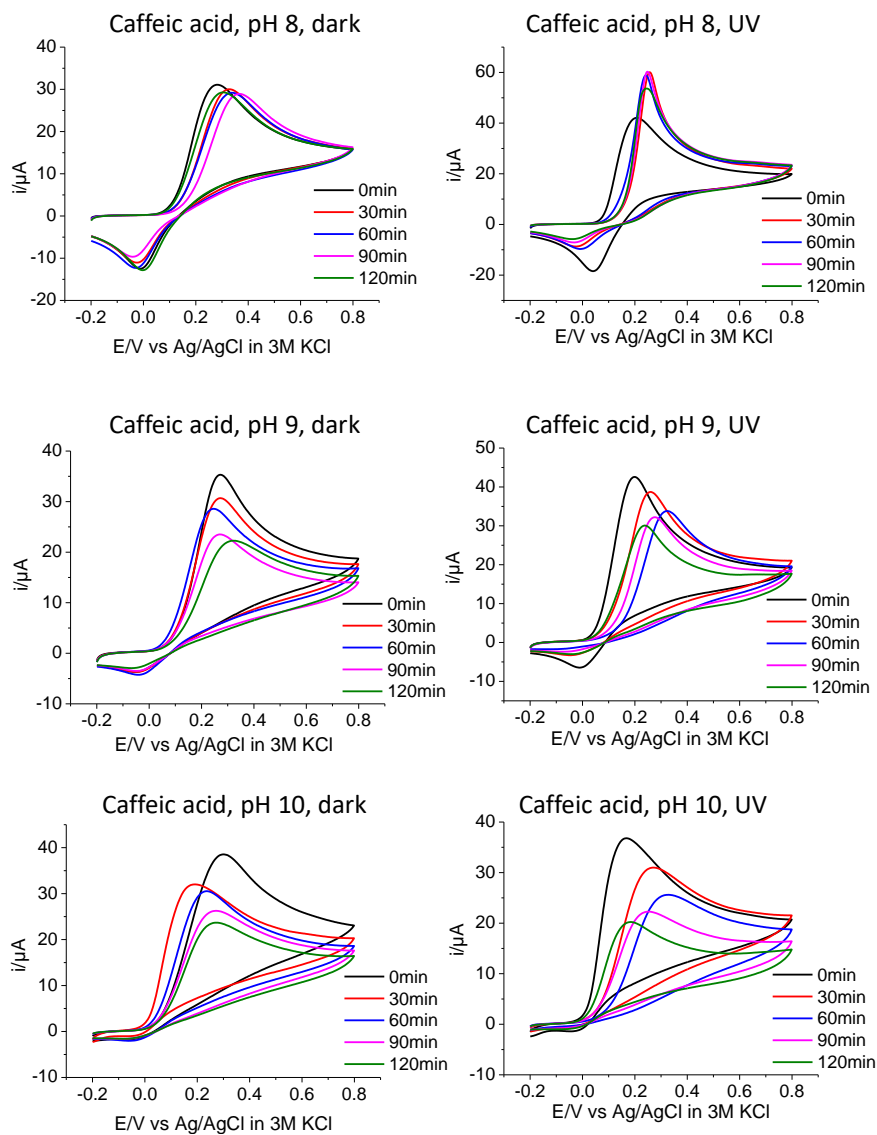


Figure S 8.17 Monitoring of CA by cyclic voltammetry (CV). Cyclic voltammograms of CA in buffers at pH 8.0, 9.0, and 10.0 vs time stored for 2 h in dark (left) or under UV irradiation (right). All CVs were measured in 100 mM buffer at a scan rate of 100 mV/s at glassy carbon electrodes with 1.58 mM concentration of plant phenolics.²⁴

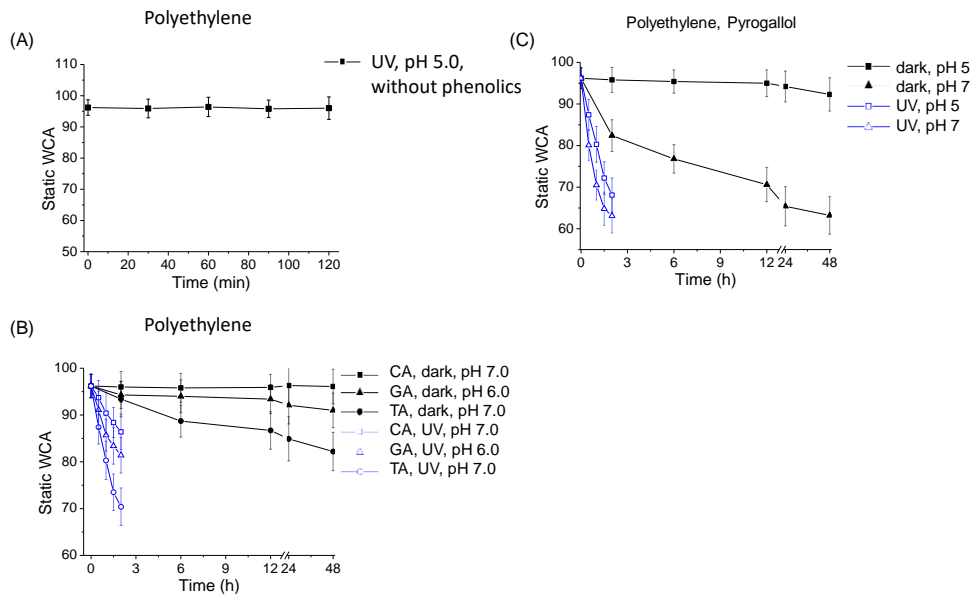


Figure S 8.18 A) Static water contact angle of polyethylene substrate immersed in buffer solution (100 mM, pH 5.0) after 2 h of UV irradiation, measured in 30 min interval. B) Decrease of the static water contact angle (WCA) over time for polyethylene substrates after immersion in TA (pH 7.0), GA (pH 6.0), and CA (pH 7.0) solution (10 mM) stored in dark environment and UV-irradiated substrates for 2 h. C) Decrease of the static WCA over time for PE substrate after immersion in 10 mM pyrogallol solution (acetate buffer at pH 5.0, phosphate buffer at pH 7.0) stored in dark environment and UV-irradiated substrates for 2 h.²⁴

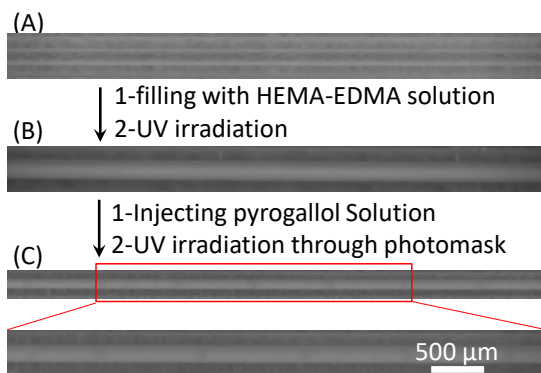


Figure S 8.19 Phenolic pattern inside the capillary tube. (A) Bare capillary tube. (B) HEMA-EDMA polymerization mixture injected inside the capillary, then irradiated with UV light for 15 min to produce a porous structure. (C) Capillary tube filled with pyrogallol solution (0.01 g/mL, pH 7.0) irradiated with UV light for 10 min through a photomask.²⁴

Appendix B: Supplementary information for Chapter 3^a

^a This chapter is adapted from Ref.²³

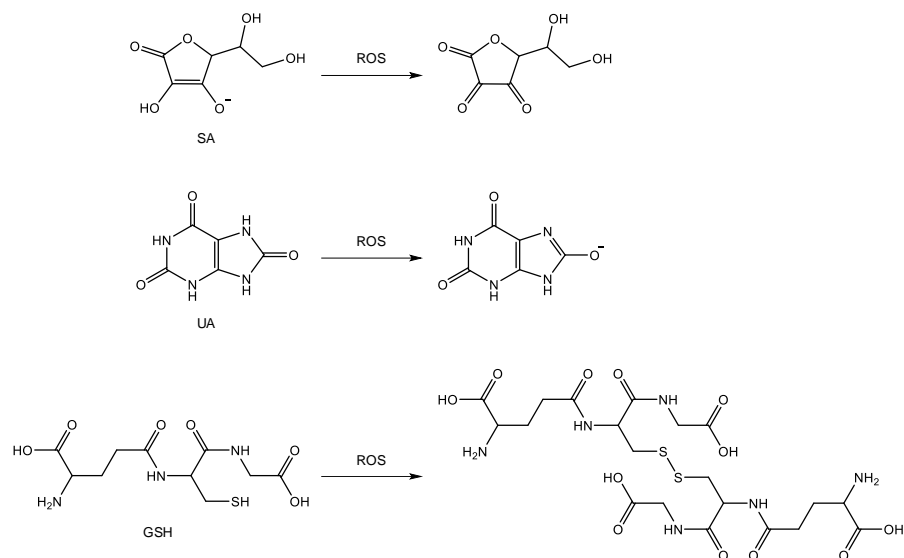


Figure S 9.1 Oxidation products of sodium ascorbate (SA), uric acid (UA), and glutathione (GSH) in the presence of oxygen and radical derivatives of oxygen (ROS).²³

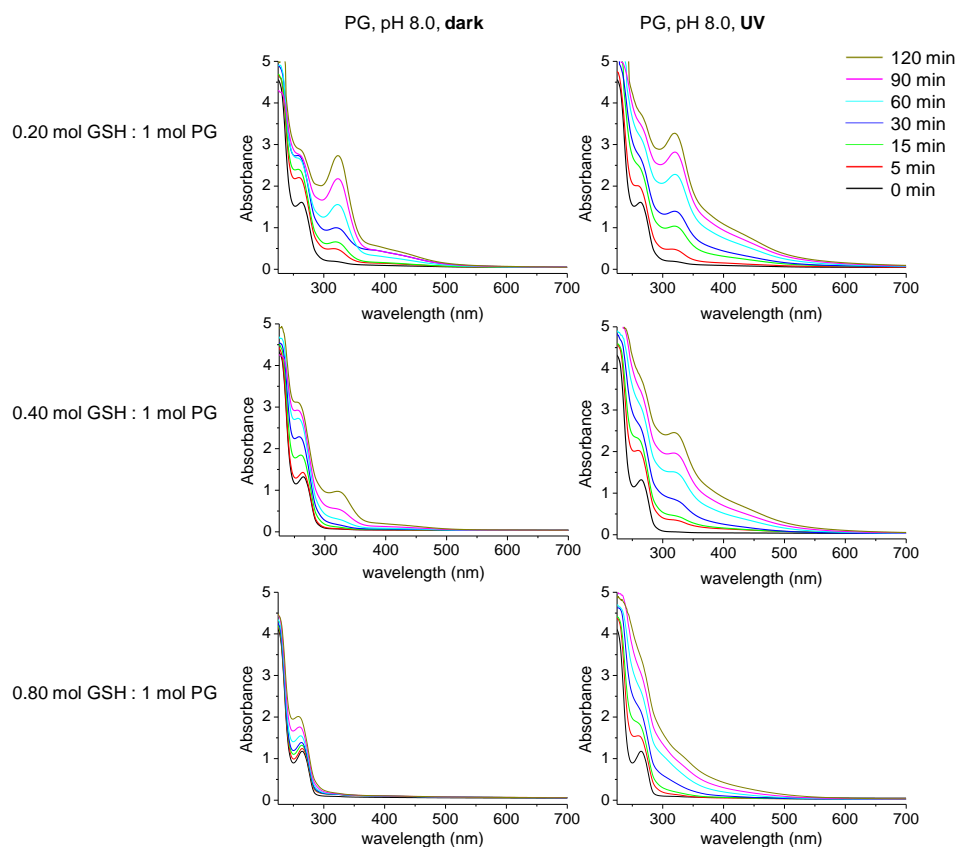


Figure S 9.2 UV-vis spectra of PG solution (0.2 mg/mL) at phosphate buffer 5 mmol/L at pH 8.0, stored in dark environment (left) and after UV irradiation (right) containing GSH measured at different time intervals.²³

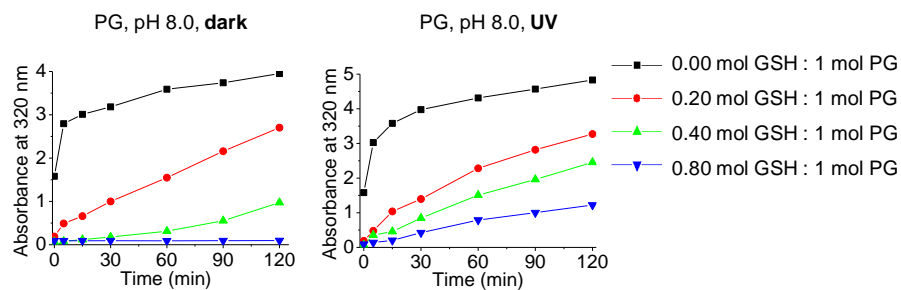


Figure S 9.3 Effect of natural antioxidants on PG polymerization with and without UV irradiation. The graphs show UV absorbance of PG solutions (0.2 mg/mL, phosphate buffer 5 mmol/L, pH 8.0) at 320 nm. PG polymerization solution in the dark (left) and under UV irradiation (right) in the presence of GSH (with different molar ratios of antioxidants to PG).²³

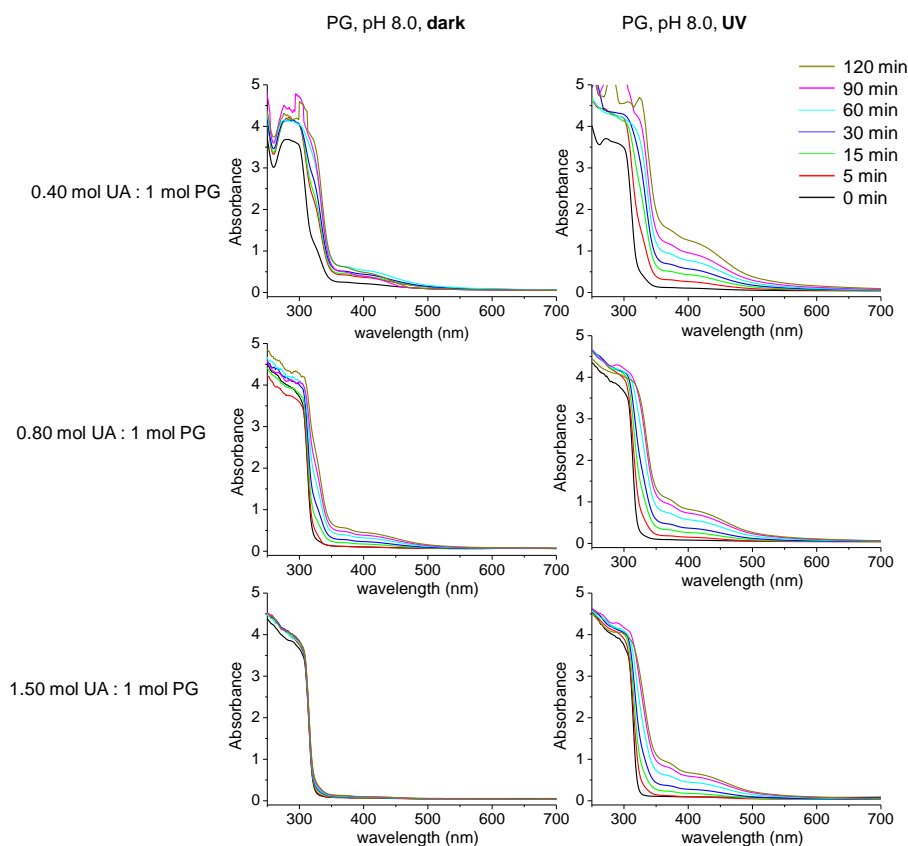


Figure S 9.4 UV-vis spectra of PG solution (0.2 mg/mL) at phosphate buffer 5 mmol/L at pH 8.0, stored in dark environment (left) and after UV irradiation (right) containing UA measured at different time intervals.²³

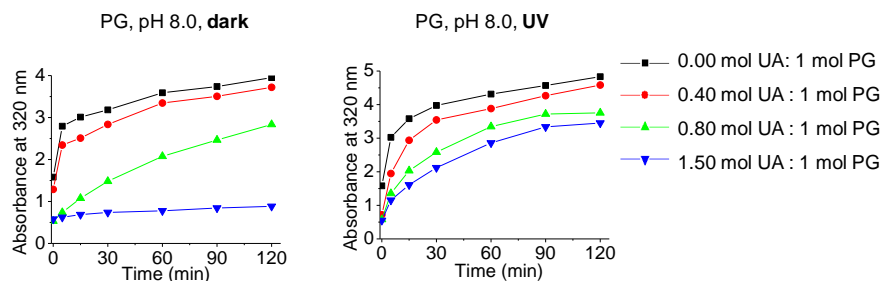


Figure S 9.5 Effect of natural antioxidants on PG polymerization with and without UV irradiation. The graphs show UV absorbance of PG solutions (0.2 mg/mL, phosphate buffer 5 mmol/L, pH 8.0) at 320 nm. PG polymerization solution in the dark (left) and under UV irradiation (right) in the presence of UA (with different molar ratios of antioxidants to PG).²³

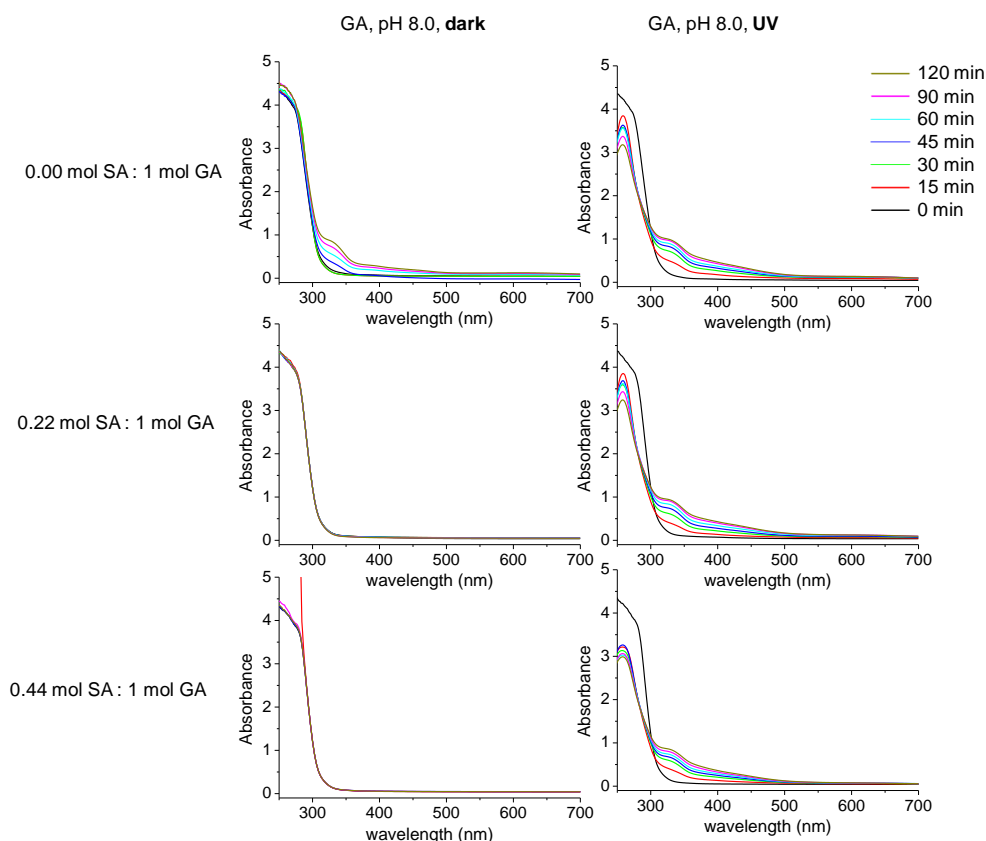


Figure S 9.6 UV-vis spectra of GA solution (0.2 mg/mL) at phosphate buffer 5 mmol/L at pH 8.0, stored in dark environment (left) and after UV irradiation (right) containing SA measured at different time intervals.²³

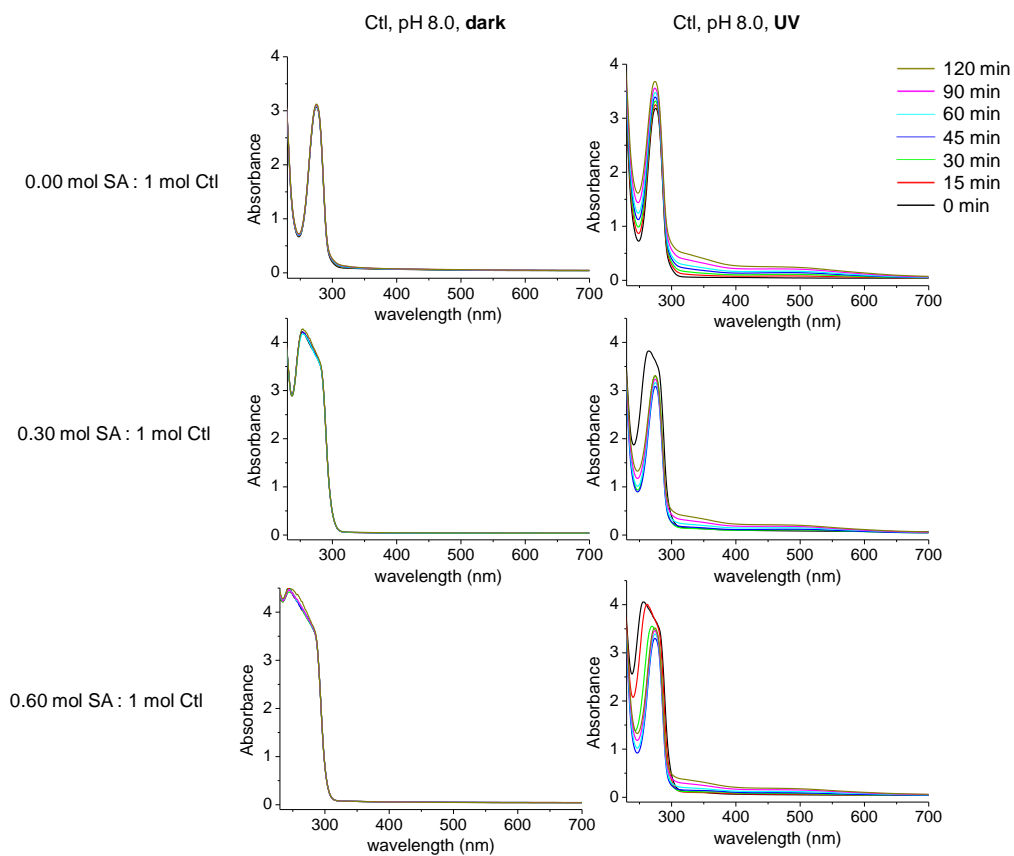


Figure S 9.7 UV-vis spectra of Ctl solution (0.2 mg/mL) at phosphate buffer 5 mmol/L at pH 8.0, stored in dark environment (left) and after UV irradiation (right) containing SA measured at different time intervals.²³

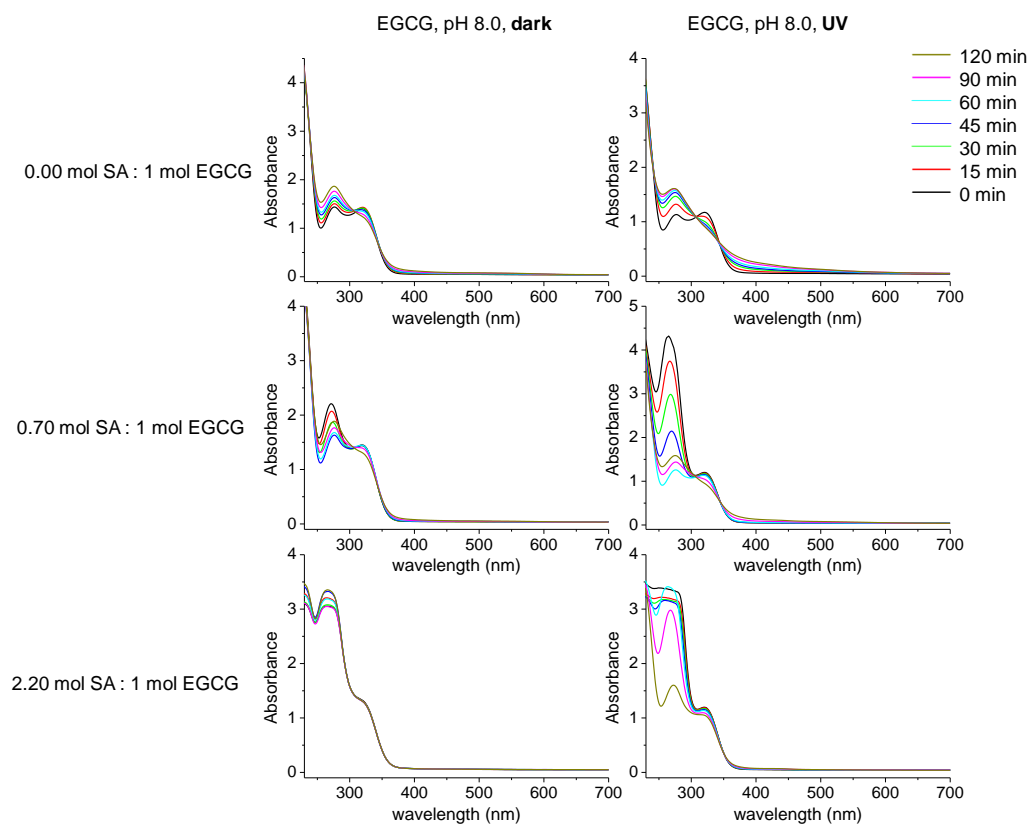


Figure S 9.8 UV-vis spectra of EGCG solution (0.2 mg/mL) at phosphate buffer 5 mmol/L at pH 8.0, stored in dark environment (left) and after UV irradiation (right) containing SA measured at different time intervals.²³

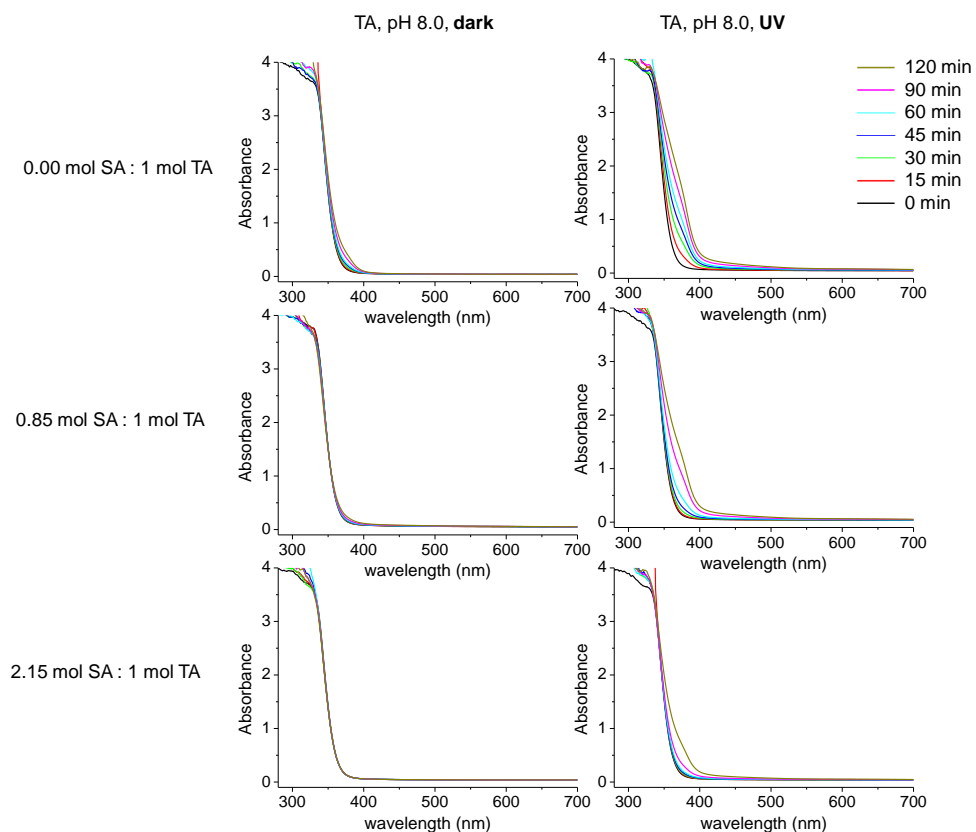


Figure S 9.9 UV-vis spectra of TA solution (0.2 mg/mL) at phosphate buffer 5 mmol/L at pH 8.0, stored in dark environment (left) and after UV irradiation (right) containing SA measured at different time intervals.²³

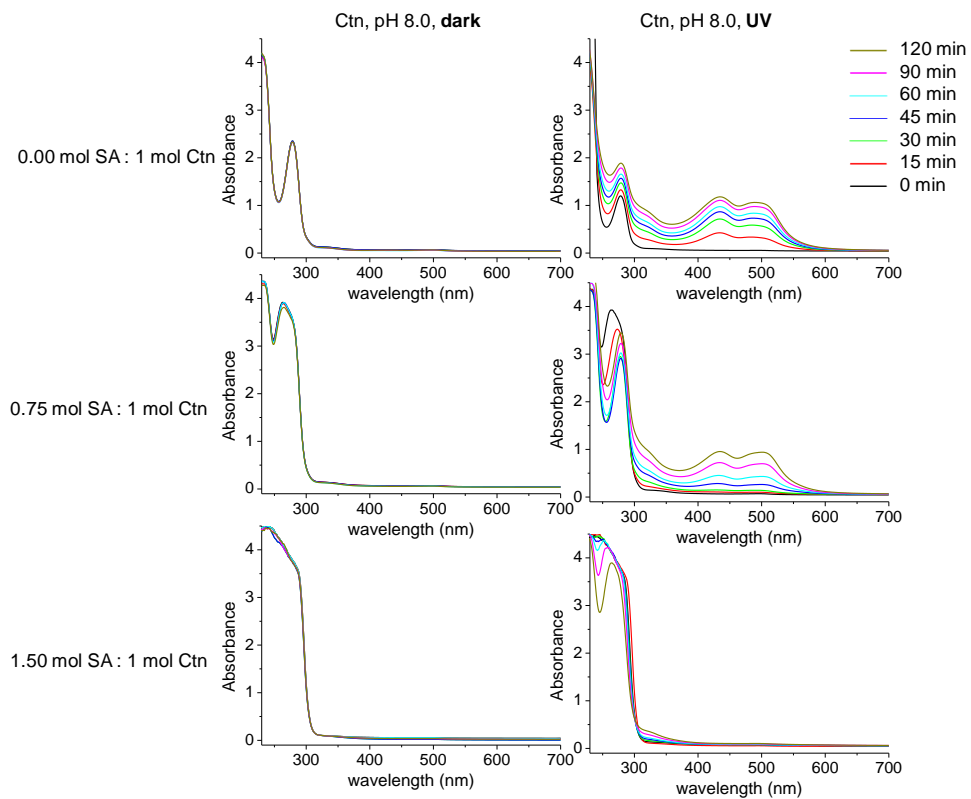


Figure S 9.10 UV-vis spectra of Ctn solution (0.2 mg/mL) at phosphate buffer 5 mmol/L at pH 8.0, stored in dark environment (left) and after UV irradiation (right) containing SA measured at different time intervals.²³

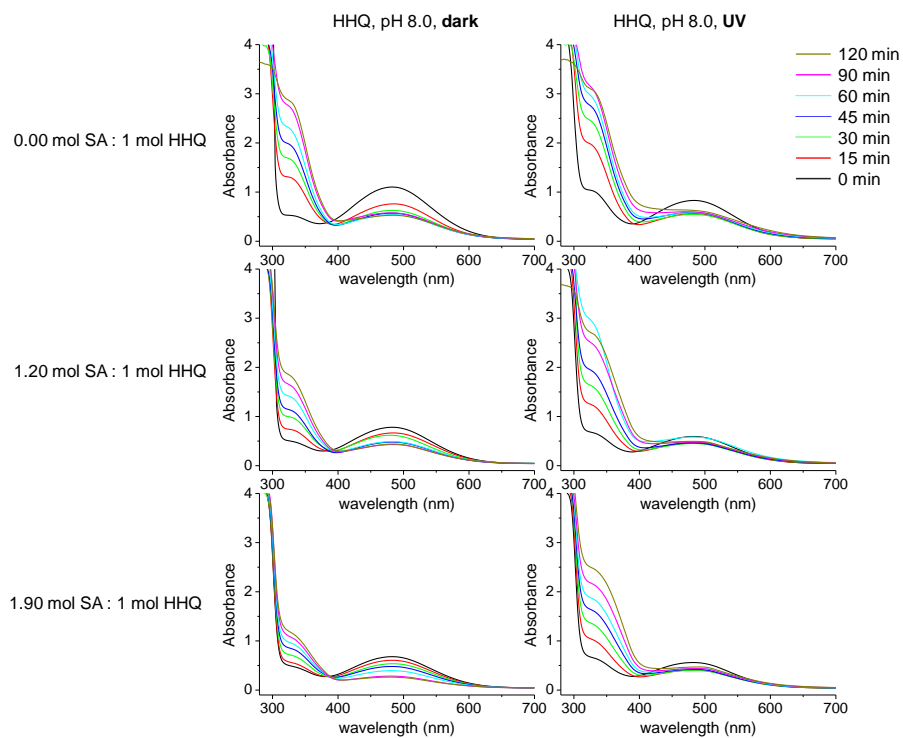


Figure S 9.11 UV-vis spectra of HHQ solution (0.2 mg/mL) at phosphate buffer 5 mmol/L at pH 8.0, stored in dark environment (left) and after UV irradiation (right) containing SA measured at different time intervals.²³

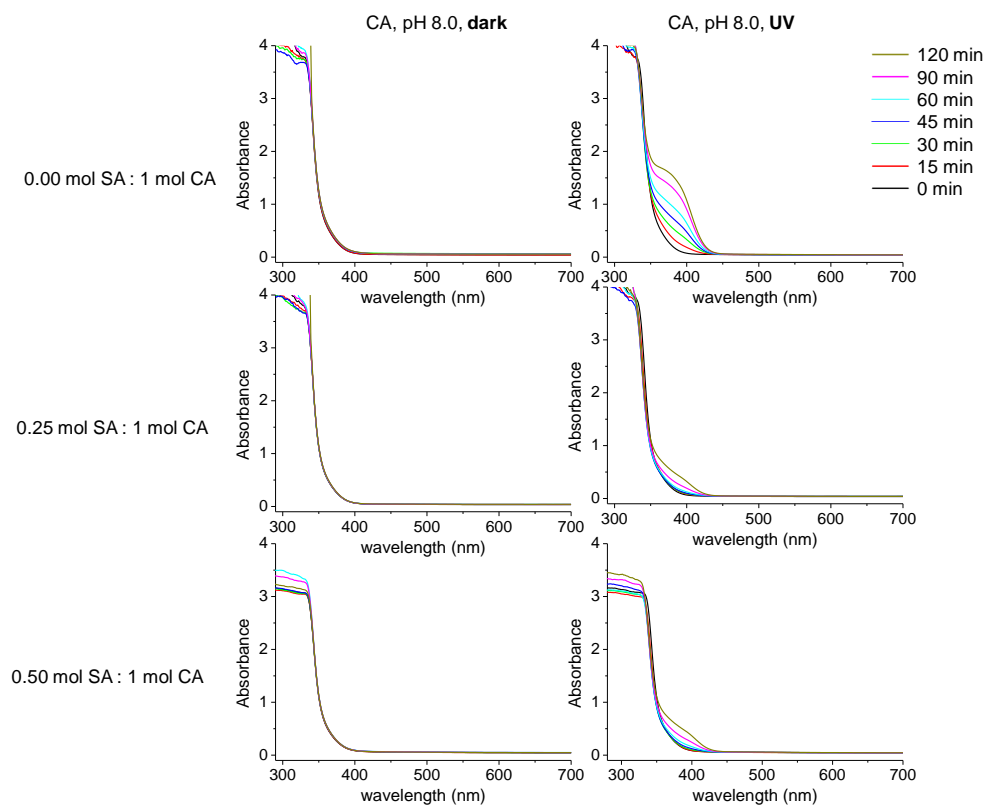


Figure S 9.12 UV-vis spectra of CA solution (0.2 mg/mL) at phosphate buffer 5 mmol/L at pH 8.0, stored in dark environment (left) and after UV irradiation (right) containing SA measured at different time intervals.²³

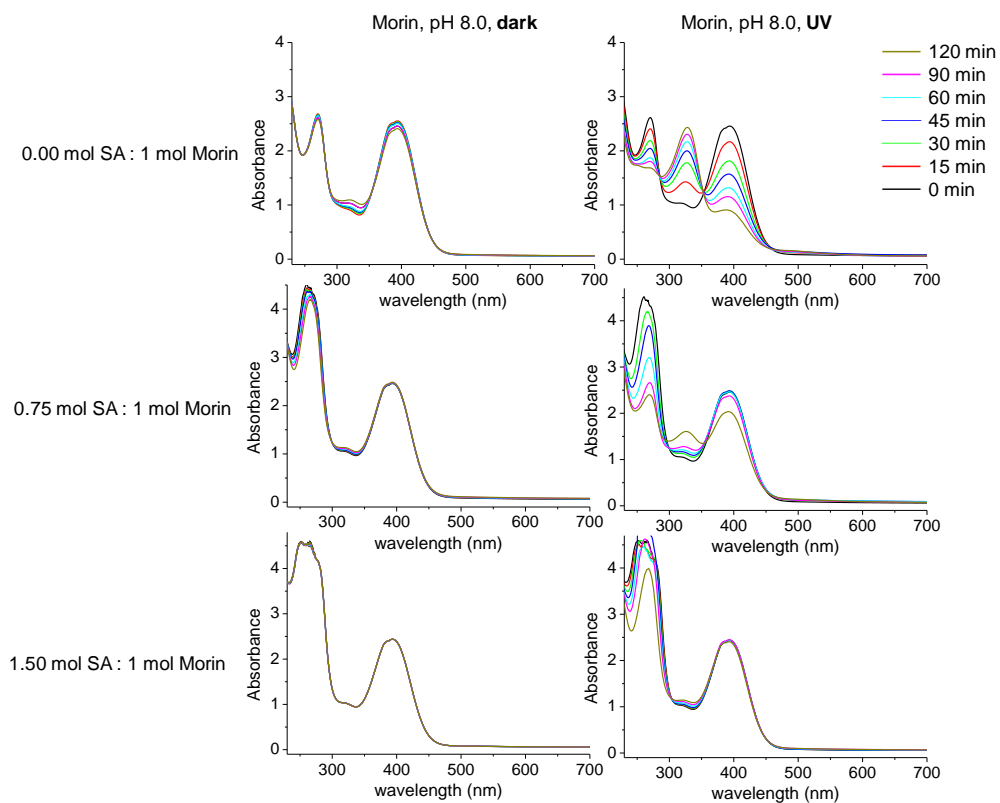


Figure S 9.13 UV-vis spectra of morin solution (0.2 mg/mL) at phosphate buffer 5 mmol/L at pH 8.0, stored in dark environment (left) and after UV irradiation (right) containing SA measured at different time intervals.²³

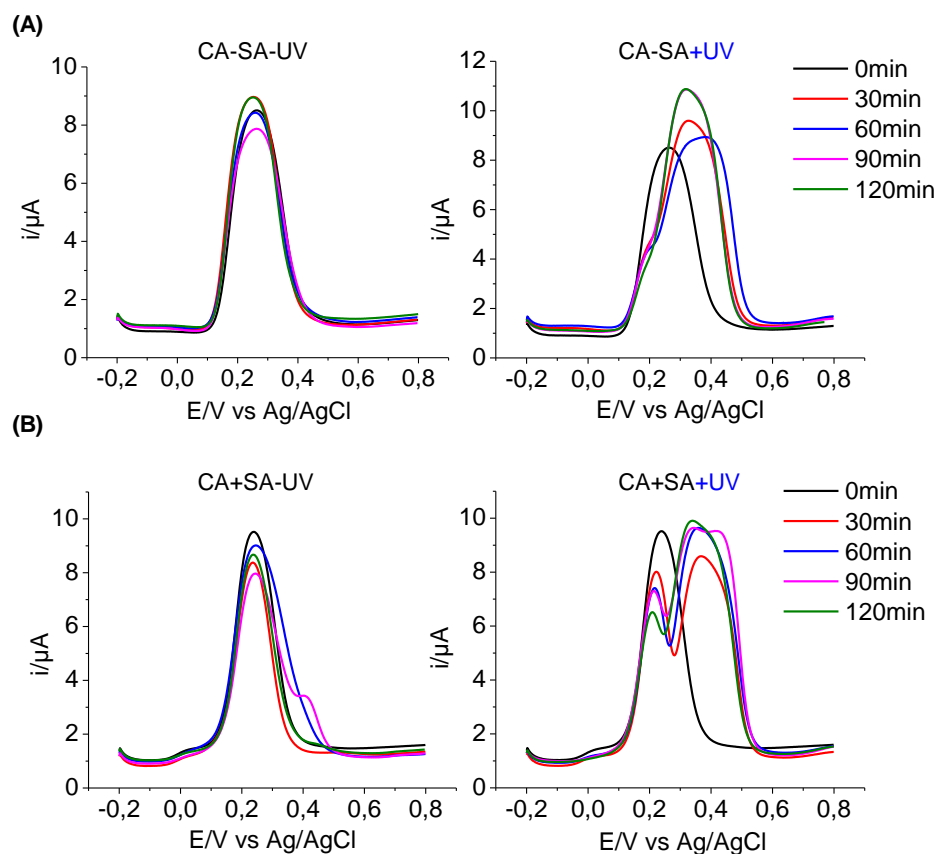


Figure S 9.14 Differential pulse voltammetry (DPV) in phosphate buffer (5 mmol/L, pH 8.0) at activated glassy carbon disk electrodes for (A) CA solution (1.58 mmol/L CA in phosphate buffer, 5 mmol/L, pH 8.0) stored in dark (left) or under UV irradiation (right) for 2h and (B) SA-CA solution (1.58 mmol/L CA in phosphate buffer, 5 mmol/L, pH 8.0; 0.5:1, SA:CA molar ratio) stored in dark (left) or under UV irradiation (right) for 2h.²³

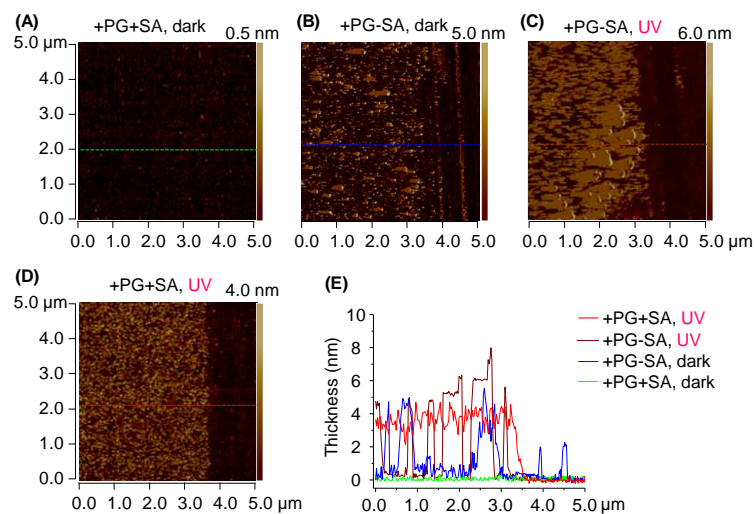


Figure S 9.15 AFM on silicon surfaces exposed to PG solution at pH 8.0 (5 mmol/L) with SA in dark (A), without SA in dark (B), without SA under UV irradiation (C), and with SA under UV irradiation (D) for 30 min. The obtained images indicate a more homogeneous phenolic layer is deposited on the surface in the presence of SA after 30 min UV irradiation at pH 8.0. Surface topographies measured along the dashed line are shown in the graph (E).²³

Appendix C: Supplementary information for Chapter 4^a

^a This chapter is adapted from Ref.¹¹⁴

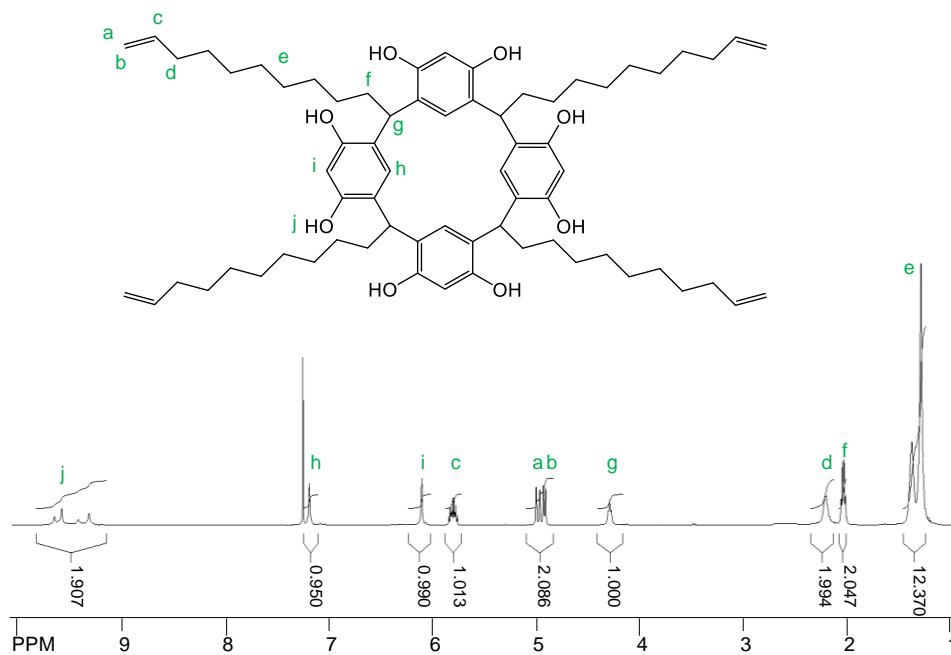


Figure S 10.1 Nuclear magnetic resonance (^1H NMR, 500 MHz, CDCl_3) spectrum of *C*-dec-9-enylresorcin[4]arene (**3**).¹¹⁴

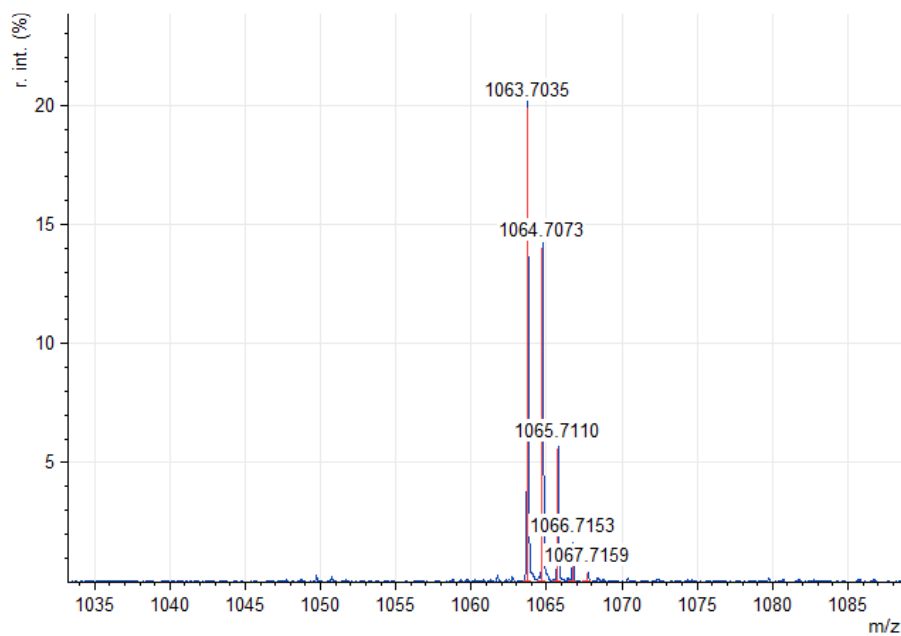


Figure S 10.2 Mass spectrometry (ESI-MS, positive mode) spectrum of *C*-dec-9-enylresorcin[4]arene (**3**). ESI-MS (positive mode, m/z): $[\text{M}+\text{Na}]^+_{\text{theor.}}=1063.6991$, $[\text{M}+\text{Na}]^+_{\text{exp.}}=1063.7035$.¹¹⁴

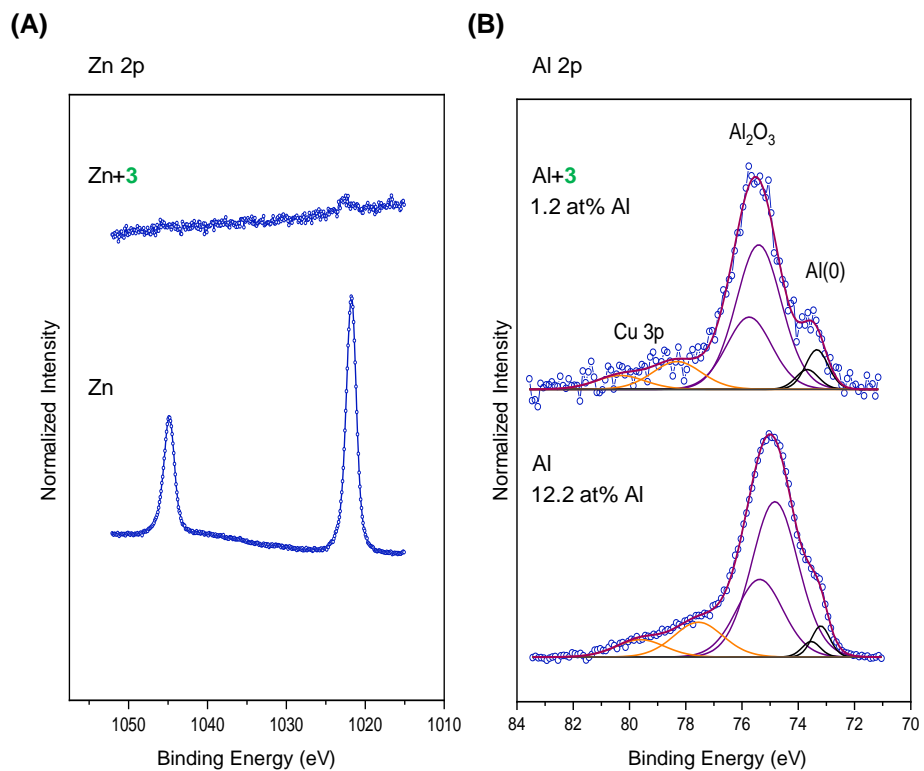


Figure S 10.3 (A) Detailed Zn 2p and (B) Al 2p XPS spectra of Zinc copper alloy (Zn) and aluminum (Al) substrates before and after modification with *C*-dec-9-enylresorcin[4]arene (**3**). The signal intensities for Al 2p were normalized to the maximum of intensity.¹¹⁴

Curriculum Vitae

Curriculum Vitae (Academic CV)
Farid Behboodi-Sadabad

Email: farid.sadabad@kit.edu

Web: www.linkedin.com/in/farid-sadabad



Education

- **University of California Berkeley, Berkeley, USA** 2017-2018
 - *Material Science and Engineering, Visiting Researcher*
 - Group of Bioinspired Materials (Prof. Dr. Phillip B. Messersmith)
- **Karlsruhe Institute of Technology (KIT), Karlsruhe, Germany** 2015-2018
 - *Chemistry, Ph.D.*
 - Group of Biofunctional Materials (Priv.-Doz. Dr. Pavel A. Levkin)
- **AmirKabir University of Technology, Tehran, Iran** 2008-2011
 - *Polymer Engineering, M.Sc.*
 - Group of Polymerization Reaction Engineering (Prof. Dr. Vahid Haddadi-Asl)
- **AmirKabir University of Technology, Tehran, Iran** 2004-2008
 - *Polymer Engineering, B.Sc.*
 - Electrospinning of Polymeric Nanofibers for Biomedical Applications

Publications in peer-reviewed journals

14. High Throughput Screening (HTS) of Coating and Anti-bacterial Properties of Natural Polyphenols and Their Combinations

F. Behboodi-Sadabad, P. Messersmith, P.A. Levkin.

Manuscript under preparation.

13. Surface Functionalization and Patterning by Multifunctional Resorcinarenes

F. Behboodi-Sadabad, V. Trouillet, A. Welle, P. Messersmith, P.A. Levkin.

ACS Applied Materials & Interfaces **2018**, 10, 39268–39278.

12. Repairable Superhydrophobic Surface with Hidden Reactivity, Its Photofunctionalization and Photopatterning

X. Du, M. Wang, A. Welle, F. Behboodi-Sadabad, P.A. Levkin, Z. Gu.

Advanced Functional Materials **2018**, DOI: 10.1002/adfm.20180376.

11. Bioinspired Strategy for Controlled Polymerization and Photopatterning of Plant Polyphenols

F. Behboodi-Sadabad, H. Zhang, V. Trouillet, A. Welle, N. Plumeré, P.A. Levkin.

Chemistry of Materials **2018**, 30, 1937-1946.

10. UV-Triggered Polymerization, Deposition and Patterning of Plant Phenolic Compounds

F. Behboodi-Sadabad, H. Zhang, V. Trouillet, A. Welle, N. Plumeré, P.A. Levkin.

Advanced Functional Materials **2017**, 27, DOI: 10.1002/adfm.201700127.

9. Bio-inspired Strategy for Controlled Dopamine Polymerization in Basic Solutions

X. Du, L. Li, F. Behboodi-Sadabad, A. Welle, J. Li, S. Heissler, H. Zhang, N. Plumeré, P.A. Levkin.

Polymer Chemistry **2017**, 8, 2145-2151.

8. Effect of Loading and Surface Modification of Nanoparticles on the Properties of PMMA/Silica Nanocomposites Prepared via In-Situ Free Radical Polymerization

Salami-Kalajahi, M.; Haddadi-Asl, V.; Rahimi-Razin, S.; Behboodi-Sadabad, F.; Roghani-Mamaqani, H.; Najafi, M.

International Journal of Polymeric Materials and Polymeric Biomaterials **2013**, 62, 336-344.

7. A study on the properties of PMMA/silica nanocomposites prepared via RAFT polymerization

Salami-Kalajahi, M.; Haddadi-Asl, V.; Rahimi-Razin, S.; Behboodi-Sadabad, F.; Najafi, M.; Roghani-Mamaqani, H.

Journal of Polymer Research **2012**, 19, DOI 10.1007/s10965-011-9793-1.

6. Effect of Carbon Nanotubes on the Kinetics of in Situ Polymerization of Methyl Methacrylate

Salami-Kalajahi, M.; Haddadi-Asl, V.; Behboodi-Sadabad, F.; Rahimi-Razin, S.; Roghani-Mamaqani, H.; Hemmati, M.

Nano **2012**, 7, DOI: 10.1142/S1793292012500038.

5. Effect of silica nanoparticle loading and surface modification on the kinetics of RAFT polymerization

Salami-Kalajahi, M.; Haddadi-Asl, V.; Behboodi-Sadabad, F.; Rahimi-Razin, S.; Roghani-Mamaqani, H.

Journal of Polymer Engineering **2012**, 32, 13-22.

4. Properties of PMMA/Carbon nanotubes nanocomposites prepared by "grafting through" method

Salami-Kalajahi, M.; Haddadi-Asl, V.; Behboodi-Sadabad, F.; Rahimi-Razin, S.; Roghani-Mamaqani, H.

Polymer Composites **2012**, 33, 215-224.

3. Matrix-grafted multiwalled carbon nanotubes/poly(methyl methacrylate) nanocomposites synthesized by in situ RAFT polymerization: A kinetic study

Rahimi-Razin, S.; Haddadi-Asl, V.; Salami-Kalajahi, M.; Behboodi-Sadabad, F.; Roghani-Mamaqani, H.

International Journal of Chemical Kinetics **2012**, 44, 555-569.

2. Properties of matrix-grafted multi-walled carbon nanotube/poly(methyl methacrylate) nanocomposites synthesized by in situ reversible addition-fragmentation chain transfer polymerization

Rahimi-Razin, S.; Haddadi-Asl, V.; Salami-Kalajahi, M.; Behboodi-Sadabad, F.; Roghani-Mamaqani, H.

Journal of the Iranian Chemical Society **2012**, 9, 877-887.

1. Investigating the effect of pristine and modified silica nanoparticles on the kinetics of methyl methacrylate polymerization

Salami-Kalajahi, M.; Haddadi-Asl, V.; Rahimi-Razin, S.; Behboodi-Sadabad, F.; Roghani-Mamaqani, H.; Hemmati, M.

Chemical Engineering Journal **2011**, 174, 368-375.

Honors & Awards

- **Awarded with Networking Grant** 06/2018
By Karlsruhe House of Young Scientists (KHYS), Karlsruhe, Germany.
- **Awarded with Research Travel Grant** 05/2017
By Karlsruhe House of Young Scientists (KHYS), Karlsruhe, Germany.
- **Wilhelm and Else Heraeus Foundation Financial Support** 04/2017
To attend the 644. WE-Heraeus-Seminar, Bad Honnef, Germany.
- **Winner of Best Research Spotlight and Conference Contest Prize** 2016-2018
For three years, BioInterfaces International Graduate School, Karlsruhe, Germany.
- **Awarded with Master Program Scholarship** 2008-2011
For a two years master program, AmirKabir University of Technology, Tehran, Iran.
- **Awarded with Bachelor Program Scholarship** 2004-2008
For a four years undergraduate study, AmirKabir University of Technology, Tehran, Iran.
- **Graduation within top students** 2004-2011
Within the top students in “Department of Polymer Engineering & Color Technology” during both M.Sc. and B.Sc. studies, Tehran, Iran.
- **Graduation in 1st place** 2000-2004
for four years in high school and pre-university, Iran.

Teaching and Mentorship Experience

- **Lecturer at University** 2012-2013
Fluid mechanics, Heat transfer, Numerical Calculations, Aspen plus, and MATLAB courses.
Chemical Engineering Department, Yasuj National University, Iran.
- **Mentoring Graduate and Undergraduate Students** 2016-2017
At KIT, Karlsruhe, Germany and at UC, Berkeley, USA.
- **Supervision of undergraduate students in practical course** 12/2016
Synthesis of a Small Combinatorial Library of Cell Penetrating Peptoids,
Institute of Organic Chemistry (IOC), KIT, Germany.

Last update of the CV: Nov. 2018.